NEW PROCESSING TECHNIQUES FOR THREE-COMPONENT SEISMIC REFLECTION AND VSP DATA

Mohamed BOULFOUL (Ingenieur d'Etat)

A thesis submitted for the degree of Doctor of Philosophy at the Department of Geology & Applied Geology, University of Glasgow. December, 1992.

Dedicated to my Father, to the memory of my Mother and to the Martyrs of Algeria

DECLARATION

The material presented herein is the result of my independent research undertaken between Octotober 1988 and December 1992 in the Department of Geology & Applied Geology, University of Glasgow. It has not previously been submitted for any degree.

Any published or unpublished results of other workers have been given full acknowledgement in the text.

Mohamed Boulfoul.

ACKNOWLEDGMENTS

My primary acknowledgement is to the **Martyrs of Algeria**. Without their sacrifice I would have never done this project; to every Algerian, who has been sincerely dedicated to be useful to his community.

My sincere acknowledgement to my supervisor Dr. Doyle R. Watts for his meticulous interest, his guidance in the execution of this project and the many fruitful discussions, critics and comments. He was always ready to spend as much time as I wanted for the progress of this project. The enormous efforts he spent during field work and in helping to add new processors to the SierraSeis package are also gratefully acknowledged.

Professor Dave K. Smythe and Dr. J. J. Doody are acknowledged with thanks for the many discussions, comments and criticisms I benefited from. Professor D. K. Smythe is also gratefully acknowledged for his help in connecting me to the British Geological Survey (BGS) at Edinburgh for the computation of the anisotropic models.

My thanks are due to Li Xiang Yuang who helped in computing synthetic data at BGS and to Professor S. Crampin who allowed me to use the ANISEIS Package. My sincere thanks to Professor M. J. Russel for his sympathy and friendship. All the technical staff of the Department of Geology and Applied Geology are acknowledged with thanks including, Eddy Spiers; Kenny Roberts; Alex Russel; John Young and George Gordon. They worked very hard in drilling holes and stretching geophone cables, during rain and cold winds. Bob Cumberland and Roddy Morrison were always helpful and ready for supplying maps and other materials.

This project has benefited much from the comments and suggestions of many research students at this Department, particularly Fawzi Ahmed; Zayed Kamaldin; A. Boumezber; Fathi Ghrouda; Mohamed Salah; Ali Alsogheir; and others. They are all acknowledged with thanks.

Many thanks to British Institution Reflection Profiling Syndicate (BIRPS) and to British Petroleum of Amercia for supplying three-component reflection and VSP seismic data

I am deeply indebted to my parents and to every member of my family, particularly my brother Azedine, to my parents in law and to my sons Sebstian Mohamed (Nadir) and Tarek Iskander, and my wife, with whom I spent very little time during this project.

LIST OF CONTENTS

LIST OF FIGURES

SUMMARY

In order to test new three-component seismic attributes and processing techniques, model shear wave data were generated using the ANISEIS Package. The models utilized both isotropic and anisotropic media simulating a sedimentary basin. A number of models were used with varying crack orientations, crack densities, layer thicknesses and shear source orientations to generate test data.

New seismic attributes have been defined relating to anisotropy and shear wave polarization: The apparent azimuth, the eccentricity of the total wave field vector and the coordinates of the poynting vector with its apparent azimuth and the eccentricity. The analysis of the attributes from the wave field vector has shown that the azimuth angle may be used to determine the direction of anisotropy axes and the eccentricity can be used to either design a filter called the P-wave filter (PWF) to cancel P-wave energy from the horizontal components, or possibly to determine the tilt angle of the crack plane from the vertical axis .

A new technique for either determining the direction of particle motion or the direction of crack strike (tested on a uniformly cracked medium) is presented in Chapters 4 and 5 based on the computation of the maximum energy of the trace. The energy of the trace is computed over a window containing a reflected waveform, each time the horizontal components are rotated clockwise by an increment of 5°, from 0° to 180°.

It is found that the direction given by the maximum value of the energy of the rotated radial component for the considered three offsets:

i) is the direction of the shear source, if the medium is isotropic.

ii) this direction deviates from the shear source orientation and the deviation is offset dependent, if the waveform within the window is reflected from the lower interface of an azimuthally isotropic medium.

iii) this direction is either the polarization direction of the fast shear wave or that of the slower one, depending on which has the highest energy.

It is demonstrated that the square roots of the maximum and the minimum energy values of the rotated waveform are directly proportional to the major and the minor axes of the ellipse, respectively, describing the particle motion within the window

containing the waveform.

The new technique has been automated by computing the maximum, the minimum values and their corresponding angles over a window which advances through the horizontal seismogrammes. This has led to the definition of new seismic attributes. The instantaneous maximum energy; the instantaneous minimum energy and the instantaneous polarization angle. These three attributes, when combined together are a useful tool in monitoring anisotropy and shear polarization, as is demonstrated in the examination of test data.

A new filter called the energy filter has been designed to automatically separate split shear waves and enhance polarized shear waves. Each sample of the horizontal component is rotated by its corresponding instantaneous polarization angle then multiplied by its corresponding value of the energy function. It is found that the data has to be shifted by the length of the moving window. The window must be greater than or equal to the combined length of the two split shear waves.

The covariance matrix method restricted to the horizontal plane is used to compute the following attributes: the instantaneous largest and second largest eigenvalues and the instantaneous polarization angle. It is found that the two former attributes are similar to the maximum and the minimum energies, respectively; and the instantaneous polarization angle can be found from the direction of the eigenvector corresponding to the largest eingenvalue and can be restricted to vary between 0° and 180° in a clockwise direction. Consequently, the energy filter can be computed by using the covariance matrix. This results in increasing the computation speed by more than 40 times, and the split shear waves are separated irrespective of the length of the moving window and the amplitude of the fast shear wave.

A comparison has been done between the energy filter and the polarization filter (Montalbetti & Kanasewich, 1970). It has been found that the energy filter is more appropriate in the presence of anisotropy, since it can separate the split shear waves and does not distort the signal of the reflected wave.

The methods have been tested on three-component reflection and VSP data. Reflection data were acquired using either dynamite (data supplied by BIRPS, the British Institution Reflection Profiling Syndicate) or vibroseis (recorded by the Department of Geology & Applied Geology of Glasgow University in Kola region, Russia); VSP data were acquired using a multisource, multireceiver technique by British Petroleum of America.

The results show that the application of the energy filter does improve the coherency and the resolution of shear wave data, as a result of the separation of the split shear waves irrespective of the type of source used. The instantaneous attributes computed from VSP data are in good agreement with theory.

INTRODUCTION

Longitudinal waves have been used worldwide in exploration seismology for imaging subsurface and locating hydrocarbon reservoirs. New interest in using combined longitudinal and shear waves has developed in the last decade, since their use may lead to more information about the nature of the rocks investigated by those waves.

Shear waves are sensitive to the presence of anisotropy within the rocks and may be used for discriminating rock types (Dominico, 1984), detecting fractures and permeability trends. In shale, which is known as a transverse isotropic medium with vertical axis of symmetry, the velocity of the horizontally polarized shear wave when travelling horizontally is much bigger than that of when travelling vertically. Cracked media are known to be azimuthally anisotropic with horizontal axis of symmetry and it is well known that subsurface microcracks can be formed by the regional tectonic stress; differential stress can also cause significant cracking (Brace et al, 1966) with preferred orientation parallel to the maximum principal stress direction. The presence of a cracked medium is related to shear wave splitting and to the variation of the reflection coefficients with the azimuth. Evidence of azimuthally dependent reflection coefficients is considered indicative of azimuthally anisotropic media (Crampin, 1978; Thomsen,1988). Lithology can be investigated using the variation of Vp/Vs or the time ratio Tp/Ts (Erickson et al, 1968; Polskov et al, 1980).

To investigate crack orientation, crack density and Poisson's Ratio, hence characterizing an oil field reservoir, imaging the subsurface by both P-and S-waves is necessary. However, shear waves recorded at the surface have usually been of bad quality compared to P-waves. This is commenly due to the effect of the weathering layer, shear wave splitting, mode conversion and in general because most shear data recordings are done without taking into consideration the shear wave window. Also the generation of shear waves at the near surface using either a horizontal vibrator or an explosive source generates surface waves; including Love waves which have the same characteristics as horizontally polarized shear wave. Hence, it is difficult to remove the effect of this type of wave.

The objectives of this project are

i) Recording shear data with a better signal to noise ratio at near-zero offset and study the variation of the reflection coefficients with azimuth, which could be diagnostic of anisotropy. For this

purpose a circular receiver array characterized by a symmetrical distribution of three-component geophones was designed; the source point was located at the center.

ii) Computation of new seismic attributes to be used in characterizing and recognizing anisotropy, azimuthal isotropy and azimuthal anisotropy.

iii) Improving shear data imaging by designing new processing techniques.

CHAPTER 1

Shear waves: Review of theory and applications

1.1.INTRODUCTION

Most crustal and sedimentary rocks are found to be seismically anisotropic. The physical causes of anisotropy in sedimentary rocks are in general tought to be due to preferred orientation of anisotropic mineral grains; preferred orientation of cracks or thin bedding of isotropic or anisotropic layers (Jolly, 1956; Backus, 1962 and 1965; Brace et al, 1966; Keith & Crampin, 1977c; Crampin, 1978; Winterstein, 1986; Obolentseva, 1987; and others). Most sedimentary rocks are only weakly anisotropic (Thomsen, 1986), not exceeding 20%, even though many of their constituent minerals are highly anisotropic.

The two simplest cases in geophysical applications are transverse isotropy with vertical axis of symmetry or azimuthal isotropy, and transverse isotropy with horizontal axis of symmetry or azimuthal anisotropy. White & Agona (1955) and Postma (1955), have shown that a stratified section composed of alternating layers of different elastic materials (isotropic or not) may be considered as a single homogeneous transversely isotropic layer having a vertical axis of symmetry, provided that the wavelengths being propagated are large in comparison with the individual layer thicknesses. The outstanding feature of wave propagation in such a medium is that velocities of elastic waves travelling in the medium vary with angle measured from the axis of symmetry. For example, horizontal S-wave velocity is greater than vertical S-wave velocity in the medium having a vertical axis of symmetry.

Azimuthal anisotropy is most likely due to the presence of vertically aligned fluid filled cracks, particularly at greater depths where the vertical stress is larger than the minimum horizontal stress. In this situation the cracks and fractures tend to be

vertical, striking perpendicular to the direction of minimum horizontal stress or parallel to the maximum horizontal stress (Crampin,1989).

This chapter is a review of the theoretical background necessary for understanding anisotropy, and the use of shear waves in exploration seismology. Acquisition, generation and processing techniques for shear waves are also considered.

1.2. AZIMUTHAL ISOTROPY

For sediments deposited in horizontal layers or for rocks compressed by the increasing weight of later sediments, all properties may be expected to show symmetry about the vertical axis (White,1983) . A material with such an axis of symmetry is called transversely isotropic or PTL (from Periodic Thin Layers). Stonely (1949), was the first to investigate plane waves in such a medium.

For a transversely isotropic medium, five independent elastic constants are required to express the generalized Hoock's law. Consequently, the elastic modulus matrix has five independent components among twelve nonzero components (Crampin, 1984) giving the elastic modulus matrix the form

$$\begin{bmatrix} c_{11} & c_{12} & c_{13} & 0 & 0 & 0 \\ & c_{11} & c_{13} & 0 & 0 & 0 \\ & & c_{33} & 0 & 0 & 0 \\ & & & c_{44} & 0 & 0 \\ & & & & c_{44} & \\ & & & & & c_{66} \end{bmatrix} \qquad (1.1)$$

with $c_{12} = (c_{11} - 2.\, c_{66})$

The Voigt notation of the elastic constants is used here and the modulus matrix is symmetric.

The stress-strain relations for this medium (White, 1983) are

$$\begin{aligned}
\sigma_{xx} &= c_{11}\, e_{xx} + (c_{11} - 2c_{66})\, e_{yy} + c_{13} e_{zz} \\
\sigma_{yy} &= (c_{11} - 2c_{66})\, e_{xx} + c_{11} e_{yy} + c_{13} e_{zz} \\
\sigma_{zz} &= c_{13} e_{xx} + c_{13} e_{yy} + c_{33} e_{zz} \\
\sigma_{xy} &= c_{66} e_{xy} \\
\sigma_{yz} &= c_{44} e_{yz} \\
\sigma_{zx} &= c_{44} e_{zx}
\end{aligned} \qquad (1.2)$$

Where x, y, z are the spatial coordinates with the z- axis directed vertically downward.

σ_{ij} and e_{ij} (i, j = x, y, z) are the elements of the second rank tensors of the stress and the strain, respectively.

Stoneley (1949) initially solved the equation of motion for such a medium: the above expressions (1.2) were reproduced in the equation of motion for an anisotropic medium, and it is found that three types of waves propagate in such a medium, a quasi P-wave and two quasi S-waves, all three with mutually orthogonal polarizations. Their velocities are related to the elastic constants and to the direction of propagation by the following equations (Levin, 1979).

For SH-wave type

$$V^2_{SH} = (c_{66} / \rho)\sin^2\theta + (c_{44} / \rho)\cos^2\theta \qquad (1.3)$$

For SV- and P-wave types

$$\begin{aligned}
2\rho V^2 = {} & c_{11}\sin^2\theta + c_{33}\cos^2\theta + c_{44} \pm \{[(c_{11} - c_{44})\sin^2\theta - \\
& - (c_{33} - c_{44})\cos^2\theta]^2 + (c_{13} + c_{44})^2 \sin^2 2\theta\}^{1/2}
\end{aligned} \qquad (1.4)$$

where the quasi P-wave velocity corresponds to the plus sign before the radical and the quasi SV-wave velocity is given by the

minus sign. θ is the angle measured relative to the vertical axis, giving the direction of propagation of the incident wave.
For $\theta = \pi/2$, i.e. a wave travelling horizontally, we have

$$v_{SH} = (c_{66}/\rho)^{1/2};\ v_{SV} = (c_{44}/\rho)^{1/2};\ v_p = (c_{11}/\rho)^{1/2} \qquad (1.5)$$

where ρ is the density of the medium.

For $\theta = 0$, a wave travelling vertically

$$v_{SH} = V_{SV} = (c_{44}/\rho)^{1/2};\ v_p = (c_{33}/\rho)^{1/2} \qquad (1.6)$$

It is seen that the vertical SH-wave velocity, the vertical SV-wave velocity and the horizontal SV-wave velocity are identical.

Levin (1979) modelled a PTL medium consisting of three layers made of sandstone, shale and limestone. He found that

i) The SH-wave surface, which is the locus of points reached in unit time by a wave disturbance arising at the origin at time t=0, is an ellipsoid with horizontal velocity greater than the vertical velocity and neither the SV-wave surface nor the P-wave surface are ellipsoids. Only at a very near vertical (near zero-offset) is the P-wave surface approximately ellipsoid (see also Krey & Helbig, 1956). This is equivalent to showing that P-wave anisotropy is negligible near the vertical.

ii) Regardless of the amount of anisotropy and the length of the geophone spread, velocity analysis of surface SH-wave data gives the velocity for travel in the horizontal direction and the $t^2 - x^2$ plots are straight lines.

iii) Even for fairly small amount of anisotropy, the SV-wave $t^2 - x^2$ plots deviate from straight lines. As anisotropy increases, the SV-wave surface becomes distorted and for very large amount of anisotropy forms cusps.

1.3. WAVE VECTOR AND RAY VECTOR

When a plane P-wave propagates in an anisotropic medium, it is well known (Auld, 1973) that the wave vector **k**, the ray vector **R**, along which energy propagates, and the polarization vector **u** defining the direction of particle motion all deviate from a given axis by angles θ, ϕ and ψ, respectively.

For a plane wave propagating in a vertical plane of incidence in a transversely isotropic medium, the three vectors may be rewritten (Daley & Hron, 1977; Berryman, 1979) as

$$\begin{aligned} \mathbf{k} &= k(\sin\theta\mathbf{x} + \cos\theta\mathbf{z}) \\ \mathbf{u} &= u(\sin\psi\mathbf{x} + \cos\psi\mathbf{z}) \\ \mathbf{R} &= R(\sin\phi\mathbf{x} + \cos\phi\mathbf{z}) \end{aligned} \qquad (1.7)$$

They also, demonstrated that for a P-plane wave the departure of the wave vector from the polarization vector is very small and may be negligible in case of weak anisotropy. Thomsen (1986) also derived mathematical relations in case of weak anisotropy relating the group angle ϕ to the phase angle θ. He also showed that for P-waves moveout velocity of such a medium is neither the vertical velocity nor the horizontal one.

1.4. AZIMUTHAL ANISOTROPY

Anisotropy or azimuthal anisotropy are used to describe symmetries with azimuthal variation of properties. Most of the effects of azimuthal anisotropy on seismic waves have been published only in earthquake seismology literature. Anisotropy in exploration seismology has generally been restricted to transverse isotropy with a vertical axis of symmetry.

Transverse isotropy with vertical axis of symmetry (or vertical transverse isotropy) is an exceptional form of anisotropy where there are no azimuthal variation and the shear wave source split

into SV- and SH-wave types. Consequently, the geological media having this type of anisotropy are called azimuthal isotropic media (Thomsen, 1988).

Another type of transverse isotropy, called horizontal transverse isotropy, has a horizontal axis of symmetry in which the anisotropy is due to a single set of aligned, vertical, circular flat cracks. It seems likely (Crampin, 1977) that forces orienting crystals in the upper mantle would result in the anisotropy having a horizontal plane of symmetry; and all the models used for the numerical calculations have a plane of elastic symmetry parallel to the interface.

When the wave propagates along the symmetry axis, there are two degenerate shear waves with polarizations normal to the direction of propagation having the same velocity. In a synthetic seismogram, the arrival time of the pulses are equal. Since the vertical plane is a plane of mirror symmetry the horizontal axis of symmetry is a direction of saggital symmetry.

Garbin & Knopoff (1975) examined the scattering of elastic waves by a thin circular crack and determined the following expressions for the velocity variation of body waves propagating through a dilute concentration of dry parallel penny-shaped cracks in an isotropic matrix:

$$v_p^2 = v_{p0}^2 \,/\, \{1+ \tfrac{8}{3}\varepsilon\left(\tfrac{8}{7}(c^2 - c^4) + [\tfrac{(1+2c^2)^2}{4}]\right)\} \qquad (1.8)$$

for longitudinal waves and

$$v_s^2 = v_{s0}^2 / \{1 + 16\varepsilon\left(\tfrac{c^2\cos^2\phi}{7} + \tfrac{(1-2c^2)}{7}\sin^2\phi\right) + \left[[\tfrac{(c^2-c^4)}{4}\sin^2\phi]\right]\} \qquad (1.9)$$

for shear waves.

v_{p0} and v_{s0} are the longitidunal and shear velocities in the undeformed matrix. $\varepsilon = (Na^3 / V)$ is the crack density; N is the number of craks with radius a, in volume V; $c = \cos\theta$, where θ, is the angle of the ray path to the crack normal and ϕ is the angle of the polarization of the shear wave to the normal of the plane of incidence. The terms in double brackets are to be omitted to obtain corresponding expressions for liquid filled cracks.

Crampin (1977) considered the variation of the velocity of the three body waves over the plane Z=0, which is a plane of symmetry, in a weakly anisotropic solid with elastic constants c_{ijlm} referred to the x, y, z coordinate system, where x, y, z are not necessarily principal axes of anisotropy. When the direction of propagation is measured from the horizontal axis of symmetry x, which is a direction of saggital symmetry; he showed that velocities vary as :

$$\begin{aligned} \rho v_p^2 &= A + B\cos 2\theta + C\cos 4\theta \\ \rho v_{SP}^2 &= D + E\cos 4\theta \\ \rho v_{SR}^2 &= F + G\cos\theta \end{aligned} \qquad (1.10)$$

$$\begin{aligned} A &= \{3(c_{1111} + c_{2222}) + 2(c_{1122} + 2c_{1212})\} / 8 \\ B &= (c_{1111} - c_{2222}) / 2 \\ C &= \{c_{1111} + c_{2222} - 2(c_{1122} + 2c_{1212})\} / 8 \\ D &= \{c_{1111} + c_{2222} - 2(c_{1122} - 2c_{1212})\} / 8 \\ E &= -D \\ F &= (c_{1313} + c_{2323}) / 2 \\ G &= (c_{1313} - c_{2323}) / 2 \end{aligned} \qquad (1.11)$$

where ρ is the density and v_P, v_{SP} and v_{SR} are the velocities of the quasi-longitidunal wave qP and the two quasi-shear waves, qSP and qSR. The qSP is specified as the quasi-shear wave with polarization parallel to the plane of incidence and the qSR polarization is perpendicular to it. These are Crampin's notations.

Hudson (1981) derived expressions for the computation of the

velocities of the two waves of shear type in both dry and fluid filled cracks. One shear wave, qS1, polarized parallel to the crack-plane and the other, qS2, polarized parallel to the plane formed by the propagation vector **k** and the z axis. For waves propagating vertically downward in a cracked medium, where the crack-planes are vertical, Hudson's equations for fluid filled cracks reduce to

$$V_{qS1}^{2} = \beta = \left(\frac{\mu}{\rho}\right)^{1/2} \tag{1.12}$$

for shear type polarized parallel to the crack-plane, and

$$V_{qS2}^{2} = \beta^{2}\left[1 - \frac{16}{3}(Na^{3})\left(\frac{\lambda + 2\mu}{3\lambda + 4\mu}\right)\right] \tag{1.13}$$

for shear waves polarized normal to the crack plane.

where (λ, μ) and ρ are Lame's constants and density of the medium, respectively.

N, a, are the number of cracks per unit volume and the mean radius of the cracks, respectively.

Comparing Hudson's equations to Garbin-Knopoff equations, although they agree (Crampin, 1984) with each other, the wave speeds are independent of the polarization of the shear source.

It is seen from relation (1.13) that with increasing crack density the velocity of the shear type polarized normal to the crack-plane decreases. The wave with polarization direction perpendicular to the crack can deform the rock easily because of the favourable orientation of the zones of weakness. Hence, this wave experiences a low (compliant) effective rigidity and its velocity V_{qS2} is slow. By contrast, the wave having a polarization direction parallel to the crack-plane cannot take advantage of the zones of weakness, but must deform the uncracked rock. Hence this wave experiences a

high (stiff) effective rigidity and its velocity V_{qs1} is higher ($V_{qS1} > V_{qS2}$) (Thomsen,1988). The wave with polarization parallel to the crack-plane advances faster than the wave with perpendicular polarization, as each one propagates vertically. The directions parallel and normal to to crack-plane are called principal axes of anisotropy; the parallel direction is also called fracture strike.

1.5. ANISOTROPY EFFECTS ON WAVE PROPAGATION

A fundamental property of wave propagation in anisotropic media is that for propagation in any direction there are always three body waves with mutually orthogonal polarizations. Such body waves are called quasi-longitudinal (qP) and quasi-shear (qS1 and qS2). In isotropic media the polarization vectors of the quasi-S-waves can be in any two orthogonal transverse directions. In anisotropic media this degeneracy is removed and the polarization vectors are mutually orthogonal and fixed in the medium, depending only on the direction of propagation (Crampin, 1977).

Crampin (1976) modelled wave propagation in the three orthogonal planes of symmetry of transverse isotropic olivine, which is likely to be the configuration in the oceanic upper mantle. Keith and Crampin (1977) computed the reflected and transmitted energy for an incident wave at interface separating an isotropic and an anisotropic half space, the orthorhombic olivine. The continuity of displacements and the stresses at interface separating either isotropic and anisotropic medium or two anisotropic media imposes the coupling of three waves. An incident P-wave propagating at an angle θ from the vertical will decompose at the interface into three reflected waves (qP^R, qS_1^R, qS_2^R) and into three transmitted waves (qP^T, qS_1^T, qS_2^T); one quasi-longitidunal and two quasi-shear with mutual orthogonal polarization directions. The computed results, amplitude (square-root energy) versus angle of incidence of an incident plane wave of

SH-type are shown in Figure 1.1 for various orientation of the anisotropic material, i.e. the plane of incidence was oriented at 0°, 30°, 45°, 60° and 90° measured from plane (100) towards plane (010). Planes oriented at 0° and 90° are coincident with symmetry planes of the anisotropic olivine. From this Figure the effect of the presence of anisotropy is clearly evident. There is an azimuthal variation of the reflection properties and an SH-wave is coupled to a quasi-P-wave and quasi-SV-wave when the plane of incidence is off the plane of symmetry. Thus, for incident planes (0° and 90°) parallel to an anisotropic plane of symmetry, no qP-wave nor qSV-waves are generated.

Thomsen (1988) also computed the reflection coefficients for incident P-waves and SH-waves at the interface separating an isotropic and an anisotropic rock (cracked sandstone), where the anisotropy is due to vertically aligned fractures. The results are shown in Figure 1.2, showing reflection coefficients versus azimuth (survey line to fracture strike). It is seen from this figure that P-wave amplitudes are independent of azimuth. By contrast, SH-reflectivity shows a strong azimuthal dependence at all angles of incidence. This strong azimuthal dependence may be used in the detection of anisotropy from recording at the surface.

Also, in anisotropic media the group velocity of plane waves is not parallel to the propagation vector and the group vector will be out of the incident plane, unless this plane is a plane of elastic symmetry. Keith and Crampin (1977) showed that for non symmetry planes of incidence the propagation of energy diverges out of the incident plane by up to 20° for some orientations of orthorhombic olivine. The projection of the group vector on the plane of incidence always deviates from the propagation vector and this deviation is dependent on the angle of incidence. However, those two anomalies are difficult to observe in a weakly anisotropic medium and considered small enough to be neglected in an azimuthally isotropic medium of sedimentary rocks (Berrymann, 1979 ; Thomsen, 1986).

1.6. SHEAR WAVES IN EXPLORATION SEISMOLOGY

1.6.1. Previous work

Most of the work in exploration seismology using shear waves has been done by the oil industry and only few works have been published so far (Alford, 1986; Lynn & Thomsen, 1986; Mueller, 1992). Nowadays, the use of shear wave VSP data (Vertical Seismic Profiling) is highly promising in characterizing hydrocarbon reservoirs (Crampin, 1985; Naville, 1986; Johnston, 1986; Ahmed, 1990; Queen & Rizer, 1990; Winterstein & Meadows, 1991a, b).

The first thorough experimental study on the use of shear waves in exploration was done by Jolly (1956). His experimental test was confined to a site where there is a fairly thick, uniform section of shale near the surface. To generate shear waves he used a recoil device shaped like a gun. His work, based on refraction profiles and some subsurface data, demonstrated that shear waves are sensitive to an anisotropic medium, since the shapes of the theoretical and experimental time-distance curves are entirely different. The theoretical curves were computed assuming an isotropic medium. Theoretical curves computed assuming a transversely isotropic medium fitted the experimental data points well.

The first attempt in recording SH-waves using continuous signal methods was done by Cherry & Watters (1968, part 1). They found that in order to attenuate horizontally travelling waves (refraction and surface waves) and to obtain shear wave data with the same quality as the P-wave reflection, more geophones and larger patterns of sources and receivers were needed. They also demonstrated:

i) Most of shear energy is lost within the weathering layer, due to high impedance contrast between this layer and the layer just below it because of the velocity contrast; and this layer contributes to the degradation of the quality of an SH-reflection.

ii) The horizontally polarized surface waves (Love waves) are well cancelled by using a well-designed in-line pattern of

geophones and vibrator positions.
Using eight hundred feet of in-line pattern coverage at both source and receiver, near Kingfisher, Oklahoma, they obtained the first interpretable SH-seismic section, which is seen in Figure 1.3. However, they could not establish an absolute correlation between Vs/Vp and lithology.

Seismic studies conducted in Tataria, USSR, by Polskov et al (1980) used combined longitudinal and transverse waves to derive lithological information. The shear waves were recorded by cross-line receivers.

For recording S-waves, an in-line receiver array of 24 cross-line receivers, with a group interval of 40 m, was used with a large offset of 800 m. Plane shear waves were generated by means of specially designed pairs of polarized shots. Those pair of shots were generally assumed to generate two shear waves of opposite polarization directions normal to the survey line; the data recorded from both shots was subtracted so that P-waves generated by those shots and recorded on the cross-line components are cancelled and S-waves enhanced. Also, a coefficient D was computed for estimating the generation of shear waves and their polarity. Theoretically, D tends to infinity if the two shots generate shear waves with exactly opposite polarization directions, or to zero when the shear waves have the same polarization direction. In their experimental work the value of the coefficient D has never exceeded 5.0 and computed values were below 0.5. This suggest that the two opposite pair of shots may not generate shear waves with exactly opposite polarization direction and that the polarization direction of the explosive shear source varies with depth and offset, as it will be seen in chapter 6 when processing BIRPS data.

Dohr and Janel (1982) recorded and processed P- and converted pS waves by reflections at the free surface or the base of the weathering layer in order to obtain the shear wave velocity and the Vp/Vs ratio. The processing of pS-waves was based on the

knowledge of the velocity of P-waves, which were determined by a conventional velocity analysis.

Ensley (1984, 1985) used combined P-and S-wave seismic sections for detecting hydrocarbon reservoirs. Direct Hydrocarbon Indicators on stacked data, such as bright/dim spots, flat spots, shadow zones, low frequency, are often found in seismic sections are either associated with hydrocarbon reservoirs or are caused by low velocity rocks, changes in stratigraphy and beds. The use of a combined interpretation of P-and S-waves may allow discrimination between direct hydrocarbon indicators (DHI) associated with gas and those associated with lithological phenomena. Winterstein (1986) demonstrated that the anisotropy of a subsurface layer may be taken as the ratio of the thickness computed using SH-interval velocity and correlated it to lithology. P- and S- wave interval velocities were computed using the well known Dix's formula. His studies showed that layer thicknesses calculated from S-wave are not significantly different from the P-wave, when the layer consists of interbeded sandstone and shale. However, where well logs indicated a transition zone from sandstone to shale the discrepancies become evident. So using interval velocities of both P-and S-waves, it was possible to investigate intrinsic anisotropy.

Recent surveys have shown that azimuthal anisotropy, due most plausibly to aligned fractures, is widespread but not universal and has an important effect on shear waves. Lynn & Thomsen (1986) collected for the first time P- and SH-reflection, i.e. cross-line source and cross-line receivers were used, along two lines, lying approximately parallel and perpendicular to a major oriented vertical fracture set, so that the effect of shear wave splitting (Crampin, 1985) are minimized. The processed data as seen in Figure 1.4, evidenced a mis-tie between the SH-wave lines, which is time variant, and a difference in reflection amplitudes (Figure 1.5). These two features characterize the existence of fracture sets. Intersection of P-wave lines have shown that P-wave

reflection tie well to within seismic reflection method.

Shear wave splitting is another factor which accounts for erratic data quality attributed to shear data recorded over azimuthally anisotropic media. It is well known that a conventional SH-survey in exploration seismology is often run at an angle oblique to the fracture strike. This type of survey has a cross-line source, generally generated by a vibrator and cross-line receivers, i.e., oriented parallel to the shear source motion.

The equation of wave propagation in an anisotropic medium (Crampin, 1981) asserts that a shear wave entering this medium will split into two shear components with mutual orthogonal polarization propagating with different speeds. When the wave propagates vertically down and up, i.e. recording reflections at near zero-offset, the two shear waves will have polarizations parallel to the fracture strike and perpendicular to it. Hence, recording at near zero-offset is a good approximation to the theoretical model, if the cracks are vertical. This effect was demonstrated by Alford (1986) on shear data, cross-line source and cross-line receiver acquired at Delly, Texas. Contrary to Lynn and Thomsen's work, the acquisition line were off the principal axes of anisotropy and the processed data exhibited very poor lateral continuity. Alford, 1986 derived a simple mathematical operation for rotating the data to the principal axes of anisotropy and the data quality greatly improved. The rotation angle is the angle between the acquisition line and the direction of strike.

Thomsen (1988) derived similar formulas for rotating the data with a criterion control on the recorded data whether it fits the model or not, and presented a thorough study of the possibility of determining an azimuthally anisotropic medium by studying the reflection coefficients of an acquired shear data.

It is seen from the previous review on shear data recording that most of the shear data was acquired at large offsets without taking into consideration the shear-window, which is defined as the critical angle given by $\sin^{-1}(v_s / v_p)$, Crampin (1987). Outside

this window shear data quality deteriorates and polarization diagrams or hodograms become uninterpretable (Crampin,1981). Few work on recording S-wave reflection using a near zero-offset has been done (Becker et al, 1989; Murtha et al, 1989 and Beckham & Glassman, 1989; and others) which might be of importance in detecting fractured reservoirs, thus reducing drilling costs. Most of the studies have been carried out on VSP data to characterize fractured reservoirs (Winterstein & Meadow, 1991a, b; Shuck, 1991; Cliet et al, 1991; Lefeuvre et al , 1992). A seismic array for recording reflection data at near zero offset and studying the reflection coefficients with azimuth is presented in Chapter 2.

1.7. GENERATION OF SHEAR WAVES

Shear waves are generated either by explosive sources or by horizontally mechanical forces applied at the free surface. Jolly (1956) used a recoil device, which is like a gun. It consists essentially of a thick-walled tube and coupled to the ground by steel pegs. The detonation of an appropriate explosive charge gave a horizontal recoil, which provided a horizontal force. However this device generated shear waves with very small energy and their penetration was limited only to very shallow depths.

Geyer & Martner (1969) concluded that SH-waves from explosive sources are common. They have been identified in almost any area where three component geophones were used. Their study also showed that strong SH-motions are produced when the shot is either in the limestone or near the interface separating the shale having a low velocity and the limestone having a high velocity, giving a high impedance contrast.

The camouflets produced by underground explosion when studied by Wright & Carpenter (1962) showed that in addition to the formation of cracks, assymmetries associated with an explosion in the soil may be mechanisms of generating SH-motion. Knowing that explosive sources generate SH-waves, Brodov in 1968 developed a

technique, which was used in a joint cooperation project between French and Russian scientists, for an exploration survey using combined P- and S-waves (Polskov et al, 1982). This is the three hole technique, based on the creation of assymmetric boundary conditions to generate SH-motion. It consists of drilling three shotholes, 1m apart, in the chosen direction of polarization. The central hole is detonated first, creating an assymmetric cavity or camouflet, and cracks and providing a conventional P-wave source. Each of the two remaining holes will be detonated in turn creating a shear source polarized in the direction of the line joining the central cavity to the detonated hole. The two seismic traces recorded by the same geophone from those opposite shots will be of reversed polarity, because of the opposite directions of polarization generated by the opposite shots.

For the efficiency of the technique and to create plane waves, Polskov et al, 1982 replaced each of the three holes by equidistant holes aligned parallel to the survey line, making three lines of holes of 16 m long. The interval distance separating the holes and the lines was of the order of 1m. This technique proved to be successful in most shot points, but sometimes geological media imposed their own conditions and the directions of polarization from the opposite shots may become random. shear reflections polarized normal to survey line or SH-motions, are severely blended with P-wave reflections when using explosive sources; and the aim of the technique is to produce high shear energy and to cancel recorded longitudinal waves by the transverse geophones, hence enhancing SH-motion.

This technique of three holes was also used in England by BIRPS, in 1988, in its program of deep seismic data acquisition and proved to be unsuccessful as it will be demonstrated later in chapter 6.

Wright & Johnston, 1982, used a sliding weight for generating P- and SH-motions in a crystalline rock body at Chalk-River, Ontario. The source consists of a 700kg weight that could be dropped vertically (Figure 1.6.a) guided by two rails, onto a steel baseplate

to produce P-waves. For SH-waves the tower was allowed to tilt 45° either side (Figure1.6.b, 1.6.c). The weight then slides down a rail. The tower is then tilted to the opposite side to produce an SH-motion with opposite polarity to the first and keeping P-wave phase constant. Subtracting the shear data of the opposite shots allows the removal of P-wave from the horizontal component. This technique has been used by Turpening et al (1980) in his investigation of fracturing techniques using three-component zero-offset VSP data.

1.8. A SUGGESTED TECHNIQUE

The technique of three holes for generating SH-energy resulted in the creation of a horizontal assymmetry created by the explosion of the central shot. It would be worth also to try the following technique for creating a strong vertical assymmetry, which could be of importance in the generation of SH-energy. Three explosive charges should be put at different levels in each of the three holes. The central hole is first shot, creating a cavity with a vertical assymmetry. This cavity may focus the energy from the central charge of the two other holes to propagate horizontally and creating a strong polarization in the horizontal direction.

Generating SH-motions by mean of explosive sources at a certain depth is a mean of cancelling Love wave and using simple receiver array, hence reducing considerably survey costs. Also shooting beneath the weathering zone will increase the depth of penetration, since the travel time of the wave within this zone is reduced by half. Consequently, diminishing the absorption by a factor of 10 (Cherry & Waters, 1968). Because of the high impedance contrast between the weathering zone and the overlying medium, shooting near the interface separating them will contribute to the generation of strong SH-motion (Geyer & Martner, 1968). However the depth of the hole should be appropriate to avoid generating Love waves.

1.9. NEAR-ZERO OFFSET DATA ACQUISITION

Shear data quality recorded conventionally in exploration seismology has always been a problem and are still expensive compared to P-wave. Good quality S-wave data is essential for an appreciable correlation between the seimic horizons obtained by the two type of waves. By recording at near zero-offset S-wave data quality may be improved, since:

i) The signal of the reflected event is recorded within the shear wave window, so that further distortions of the signal are avoided or minimized.

ii) The noise from mode conversion is highly reduced, attenuation minimized and the deviation angle of the particle motion of the reflected longitudinal wave, recorded by the transverse geophone when an explosive source is used, from the vertical plane containing the axis of the transverse receiver will be small, so that at near zero offset their effect is minimized. Consequently, reflection coming from deep interfaces and recorded by the transverse components may only be of S-wave type.

ii) The interference of surface waves with reflected S-waves may only be confined to very shallow data if a shallow explosive source is used. However, the best way of attenuating Love waves when an explosive source is used is to shoot deeper, because the greater the depth of the explosive source, the more the amplitude of the surface waves is reduced (Kisslinger, Mateker & Evilly,1961). The shooting depth may be determined by tests. The second possibility when either a horizontal vibrator or a shallow explosive source is used is to choose an optimum length spread so that surface waves strike the horizontal component before any S-wave reflection coming from deeper interfaces. In this case, only very shallow data will be mixed with surface waves.

1.10. SPLITTING OF SHEAR WAVES

In exploration seismology SH-wave types are defined as shear waves with polarization direction normal to the plane of incidence and SV-wave types are defined as shear waves with direction of polarization parallel to the plane of incidence. When the plane of incidence is a plane of symmetry, either the SH-or the SV-waves are pure shear and there is no splitting phenomenon. When the plane of incidence is not a plane of symmetry, which is usually the case in exploration seismology, the generated S-wave, either of SH- or SV-type will split into two shear components, whose polarization directions are fixed in the media with crack anisotropy (Crampin, 1978). Figure 1.7 shows the splitting of an SH-wave in a cracked medium. The cracks are vertical; the normal to the crack-plane, which is a plane of symmetry makes an angle θ with the survey line. The plane of incidence (P) and the plane of symmetry make and angle equal to $(\frac{\pi}{2} - \theta)$. Consider an incident SH-wave type travelling vertically; just as it enters the cracked medium it splits into two components $S_{\perp}$ and $S_{\parallel}$ (Thomsen's notation, 1988). One with polarization direction normal to the plane of symmetry travelling with a lower velocity ($v_{\perp}$) and the other polarized parallel to the plane of symmetry and propagating with a faster velocity ($V_{\parallel}$). Both of them will be travelling vertically and will be recorded by the transverse and the radial geophones; but one will be delayed from the other because of their different velocities. The recorded wavelet is the result of the superposition of the two wavelets, the fast and the slow one, respectively; this results in the deterioration of the reflected signal.

The time delay between the two split waves is dependent on the crack orientation, the thickness of the medium traversed by the two waves and the crack densities. Both, crack orientation and small values of crack densities can cancel wave splitting. However with large crack densities, the split shear pulses separate (Crampin, 1978).

The most distinctive phenomena associated with the presence of anisotropy are anomalies in polarization and the degree of anisotropy may be seen from the variation of amplitudes in the polarization anomalies (Crampin, 1978). Thomsen (1988) in studying shear wave reflection data acquired over fractured rocks concluded that the difference in amplitude of the separated time series of the two split shear waves constitutes a detection from the surface of intensely fractured beds at depth.

The problem is to use the delay between those split waves and the variation of their amplitudes and to produce a model of anisotropy.

The delay Δt between the fast and the slow waves is

$$\Delta t = (t_{\perp} - t_{\parallel}) = t_{\parallel}\left(\frac{t_{\perp}}{t_{\parallel}} - 1\right) \tag{1.17}$$

Since travel time is inversely proportional to the velocity, we have

$$\Delta t = t_{\parallel}\left(\frac{v_{\parallel}}{v_{\perp}} - 1\right) \tag{1.18}$$

The anisotropy factor for such a cracked medium is defined as

$$\frac{v_{\parallel} - v_{\perp}}{v_{\perp}} = \frac{t_{\perp} - t_{\parallel}}{t_{\parallel}} = \gamma \tag{1.19}$$

Hence,

$$\Delta t = \gamma t_{\parallel} \tag{1.20}$$

It is seen that the more $t_{\parallel}$ increases, the more Δt increases, the deeper the seismic reflector .

The P- and SH-field data collected along two lines (Lynn and Thomsen, 1986) lying approximately parallel and perpendicular to

a major oriented vertical fracture set demostrated that one line shows progressive time delays of the shear wave reflection arrivals relative to the corresponding arrivals on the other line and this time delay is increasing with depth. Some reflections displayed a marked difference in shear wave reflection amplitudes on the two lines (see Figures 1.4 and 1.5). S-wave zero-offset VSP data from sources polarized parallel and normal to fracture orientation recorded using three component geophones (Johnston, 1986), in the Marcelina Creek field, Wilson County, Texas, about 30 miles South of San Antonio, documented significant S-wave velocity anisotropy of 27.5 % associated with preferentially aligned vertical fractures in the Austin Chalk sediments. Figure1.8 shows VSP derived interval velocities for S-waves polarized parallel and perpendicular to fracture orientation (Johnston, 1986). The separation of the two curves is evident within the fractured medium, where it is a maximum. Fracture orientation and shear wave splitting in the Austin were also demonstrated by Becker et al (1986) using polarization diagrams. The polarization diagram is a plot of the particle velocity in orthogonal coordinates, as a function of time over a limited time window.

Crampin (1978) showed with synthetic seismograms recorded over a cracked medium simulating a dilatant zone that the polarization diagrams in the window covering the shear motion display a characteristic cruciform pattern showing the separate arrival of the two split shear waves with orthogonal polarizations and if the two shear pulses are not completely separated, elliptical motion links the two orthogonal sections.

Using polarization diagrams it is possible to identify the splitting phenomenon when a complete measure of the elastic wave field is made utilizing three component detectors. However, with real data it is difficult to do so, due to the complicated time series recorded resulting from interference with other wave types. This stimulates the search for new techniques to detect shear wave splitting.

1.11. PROCESSING OF SHEAR WAVE DATA

Before the effect of azimuthally anisotropic media on shear waves was recognised, most bad quality of shear data was attributed to the weathering zone or Low Velocity Layer (Erickson et al, 1968). Cherry & Waters (1968) showed that the ratio of v_p / v_s for consolidated sedimentary sections penetrated was close to 0.5, and a time compression of the SH-records facilitated the comparison of SH- and P-wave reflection records. Tatham & Goolsbee (1984) used processing techniques in the tau-p domain to separate P-waves and mode converted S-waves recorded in a marine environment. For an initial estimates of the SV-wave NMO velocity limits, those authors started by taking one-half of the P-wave velocity value, assigning it twice the reflection time associated with P-wave value. Further, limits in angle of incidence of 0°-15° for P-wave energy and 15°-60° for S-wave energy were applied by limiting the range in the slowness p-values during the tau-p transform. The tau-p processing consisted of a forward transform, applying the NMO velocity values, followed by an inverse tau-p transform back to the record space. However, the seismic section with predominantly S-wave energy showed no continuity of reflections compared to P-wave seismic section, particularly at deeper horizons.

In recording shear waves at longer offsets those authors ignored the effect of shear wave window on the distortion of the signal and the effect of anisotropy, particularly the splitting phenomenon, where two S-waves with mutually orthogonal polarizations having different velocities travelling within an anisotropic medium.

Fertig & Hentschke (1987) processed converted pS-waves generated by reflection at the free surface and recorded by an in-line receiver. They designed a filter called the geometrical-mean balancing filter to balance the spectra of the individual traces within a shot gather to have approximately the same spectrum to

compensate for the filtering effect of the weathering zone on such waves. The stacked data with spectral balancing showed an improvement over stacked data processed conventionally.

Stacking is generally done on the assumption that the time distance curve is hyperbolic. However, this is not the case for converted PS-waves (not to be confused with pS-waves), from the subsurface as shown by Dohr & Janel (1980).

In recent years, azimuthal anisotropy has been evidenced in many exploration surveys (Lynn & Thomsen, 1986; Becker & Perlberg, 1986; Navill, 1986). These recent studies demonstrated that reflection shear data acquired at an angle to one of the principal axes of an azimuthally anisotropic medium may be improved if the data are rotated by an appropriate angle toward the direction of crack-strike or the normal to it. A common approach for processing shear data is to rotate the recorded horizontal components about the vertical axis, and search for angles at which some form of discriminant function is optimum. Discriminants may consists of calculation of maximum vectorial displacement (Igel & Crampin, 1990) or maximum energy of the rotated radial trace (Boulfoul & Watts, 1991).

Alford (1986) linearly combined two shear sources with mutually orthogonal polarization directions and rotated in synchronism both the source and the receiver. This is equivalent to rotating the medium whilst the original source and geophone orientations are maintained. The rotation angles which both minimize the reflected energy detected on the seismograms constituting the off-diagonal stacks (in-line source recorded on cross-line receivers, and vice versa), and focus energy on to the principal diagonal stacks (in-line source in-line receivers; and cross-line source cross-line receivers), are the optimal positions. The rotation procedure is done on stacked data; this has a drawback, since stacking geophone components containing shear waves, which have not been rotated to separate the split shear waves, can seriously degrade the information in the shear

wavetrain (Li & Crampin, 1989). Obolentseva et al (1987) developed a method for the separation of direct waves (VSP data) based on the similarity of the record patterns. The similarity of pulse shape was established by computing the cross-correlation function between the components for different coordinate systems. The solution was the coordinate system for which the cross-correlation function attained its maximum. However, the cross-correlation function is insufficient for recognizing the similarity of the record patterns, and amplitude spectra were also used. This makes the technique sensitive to noise, since it operates in the frequency domain. MacBeth & Yardley (1992) formulated the non uniqueness of fracture orientation, but did not solve the problem of extracting the crack strike, as it changes with depth, from one medium to another. The 2x2 data matrix from both reflection and VSP data may not be symmetric due to the change in the crack-strike within the medium (Winterstein & Meadow,1991b). Layer stripping method (Winterstein & Meadow, 1991a) and the propagator matrix method (Lefeuvre et al, 1992) are useful techniques in processing VSP data when the fracture strike changes discontinuously with depth. The energy filter presented in Chapter 5 acts as a time varying rotation process along the horizontal seismograms. Therefore it has the potential to deal with multiple splitting, particularly for reflection data where sufficient time delay may exist between the two split S-waves.

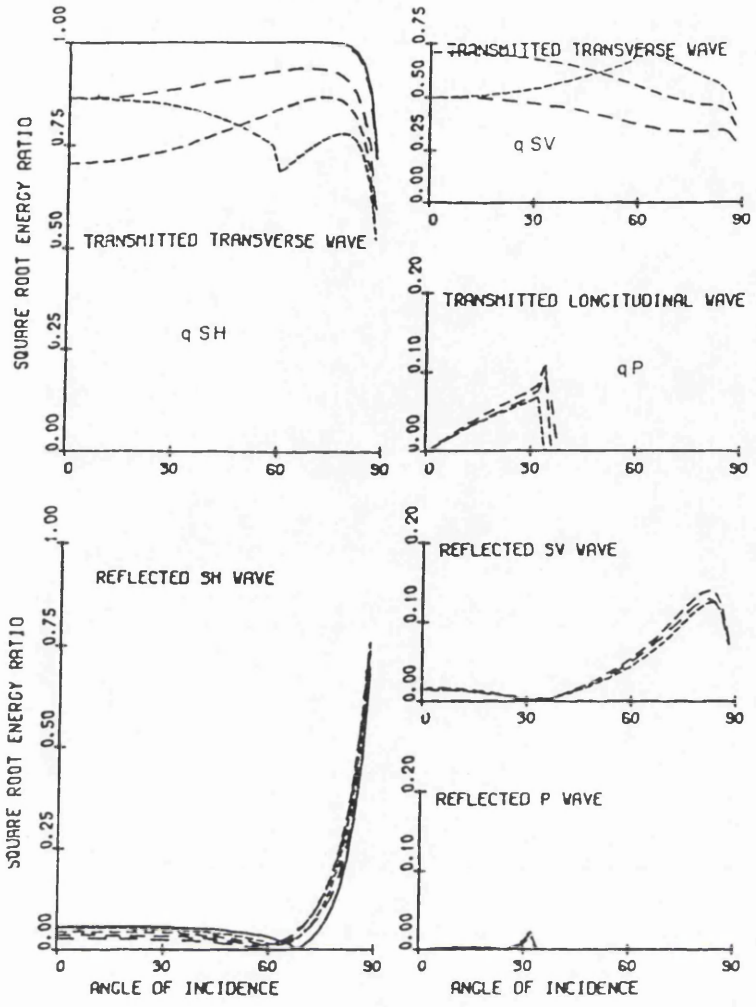

Figure 1.1. Square-root energy ratios for incident SH-waves, for waves generated at interface between an isotropic half-space and a transversely isotropic half-space with horizontal axis of symmetry. The orientations of the incident planes on the anisotropic half-space are at 0°, 30°, 45°, 60° and 90°, measured from the axis of symmetry. After C. Keith and S. Crampin, 1977.

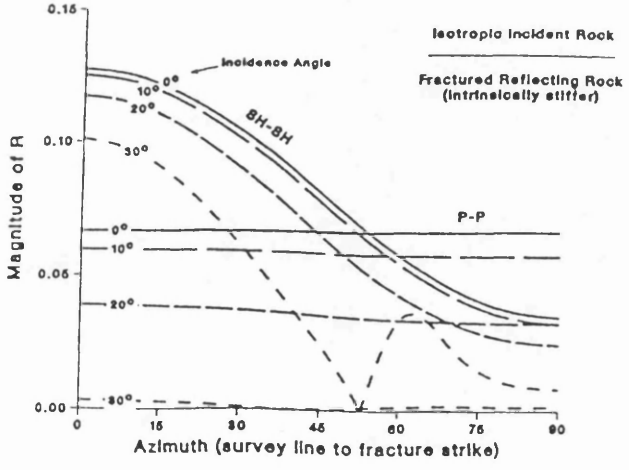

Figure 1.2. Plane-wave reflection coefficients: dependence on azimuthal and incidence angles. After Thomsen, 1988.

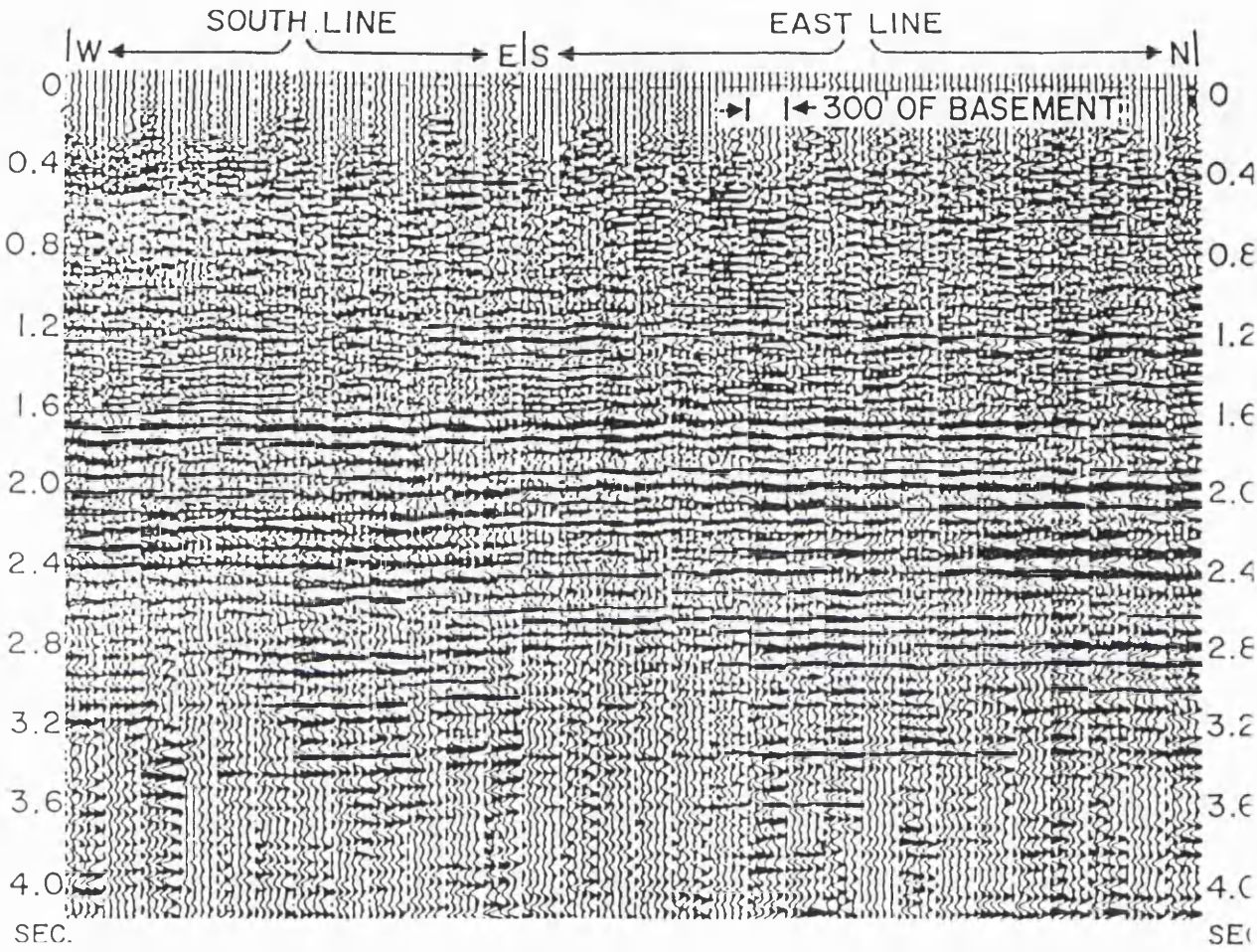

Figure 1.3. Two tied SH-reflection lines, the North-South and the East-West lines recorded near Kingfisher County, Oklahoma. conventional processing steps had been carried out. Splitting phenomenon were not known at that time, i.e. azimuthal anisotropy had not been taken into consideration. After E. L. Erickson, D. E. Miller & K. H. Waters, 1968.

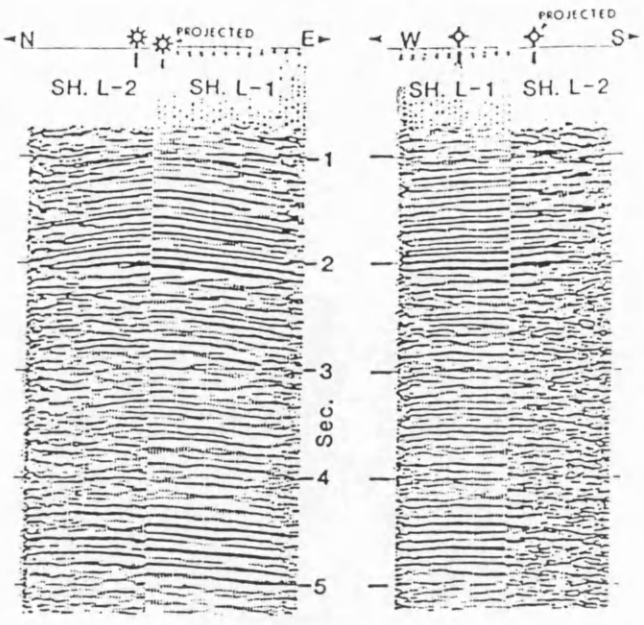

Figure 1.4. Intersection of two SH-wave lines with time zero aligned. Reflections do not exhibit same travel time at tie points compared to P-wave reflections; reflections on line 1 have progressively greater travel time than same reflections on line 2. This demonstrates that shear velocity East-West is slower than North-South, evidencing that the area surveyed is azimuthally anisotropic. After H. B. Lynn & L. Thomsen, 1986.

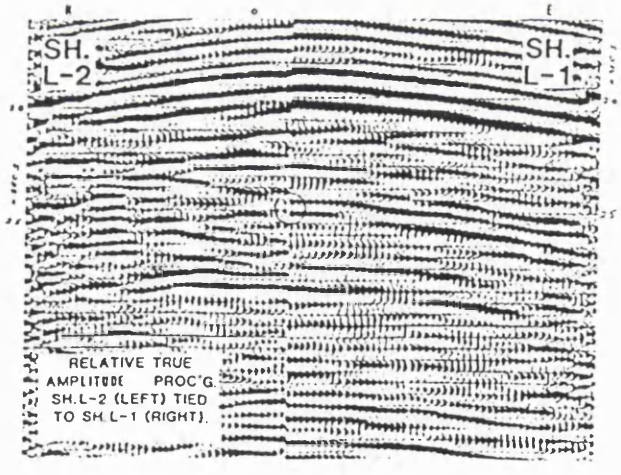

Figure 1.5. Enlargement of intersection of shear lines 1 and 2 of Figure 1.4; zone of interest circled (2,4 sec.). Weak reflections on line 2 (North-South) is attributed to the presence of North-South fractures, associated with production, which decreased velocity contrast between overlying shale and reservoir sandstone on North-South line. After H. B. Lynn & L. Thomsen, 1986.

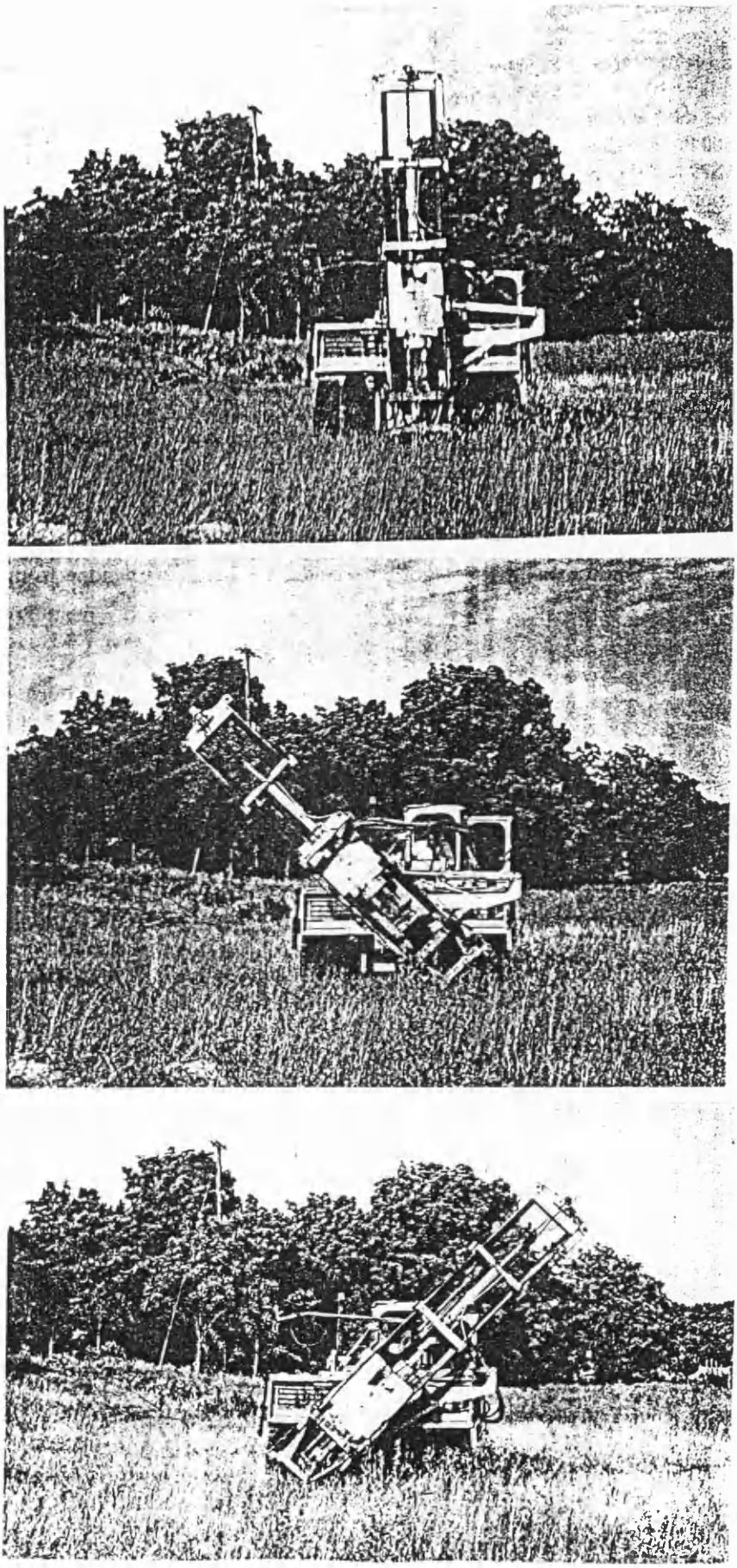

c

Figure 1.6. Sliding weight longitudinal and shear wave source. The dropping mass is of 700 Kg. (a) is the vertical orientation of the source; (b) and (c) the two shear wave configurations (opposite polarities). courtsey shear wave technology corporation.

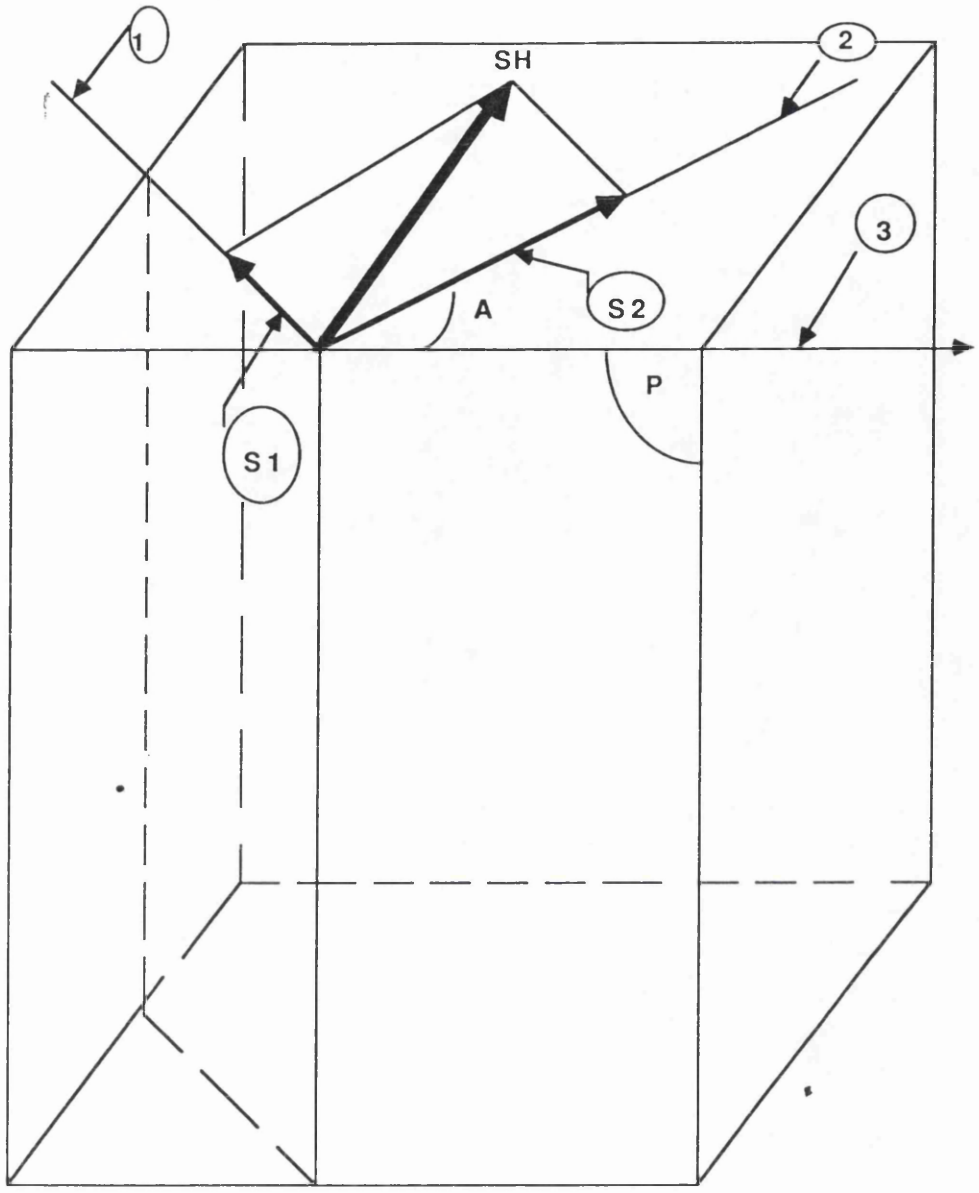

Figure 1.7. Schematic representation of the splitting of a cross-line shear source along the principal axes of an azimuthally anisotropic medium. (1) is the crack strike parallel to the crack plane; (2) the normal to the crack plane and (3) the direction of the survey line.(P) and A are the plane of incidence and the angle between the survey line and the crack strike respectively. S1 and S2 are the polarization vectors of the fast and the slow shear waves, respectively. After Thomsen, 1988.

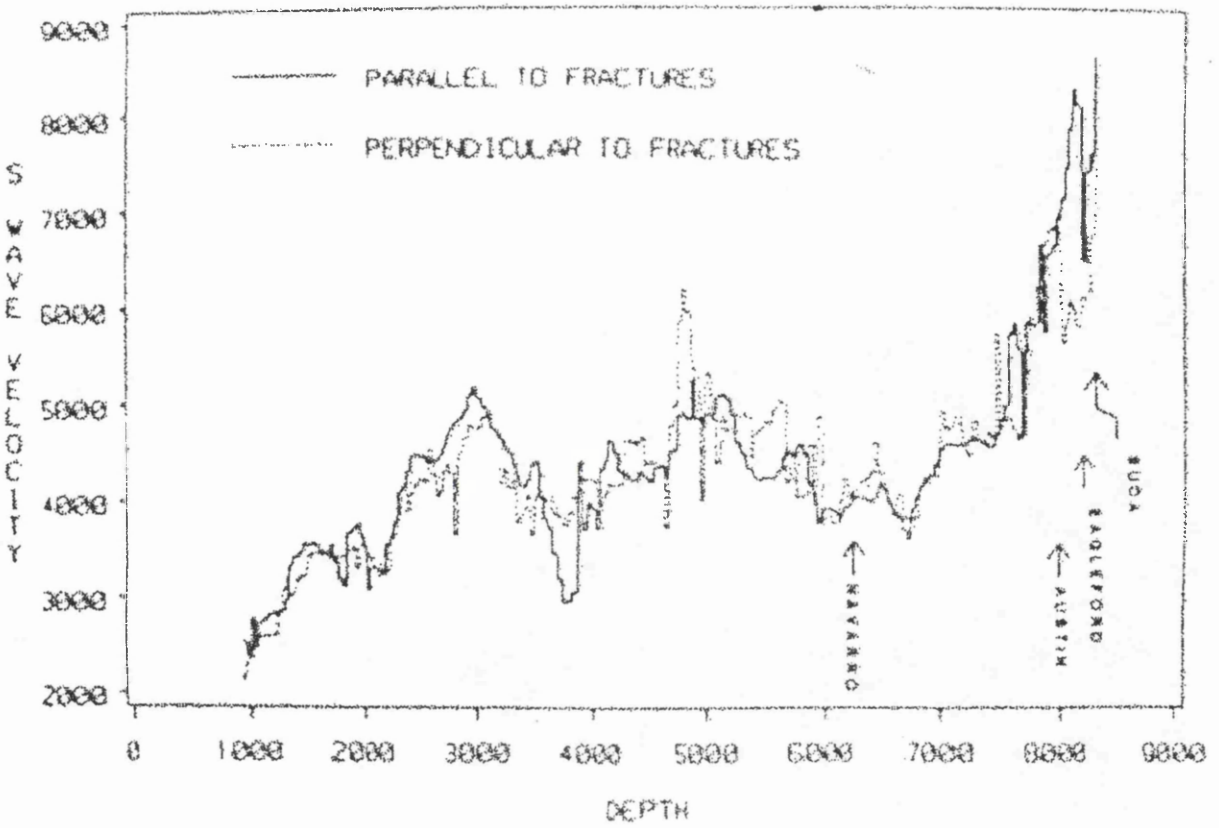

Figure 1.8. A comparison of VSP-derived interval velocities for S-waves polarized parallel and perpendicular to fracture orientation. After Johnston, 1986.

CHAPTER 2

Synthetic Modelling of Shear Waves in an anisotropic sedimentary basin.

2.1. INTRODUCTION

Geological models representing an azimuthally isotropic medium on top of two azimuthally anisotropic media having the same crack orientation but with different crack densities, simulating a sedimentary basin, are investigated in this chapter. The synthetic data is recorded at near-zero offset using three component receivers equidistantly distributed along three concentric circles, to investigate the behavior of shear waves as the ray path deviates from the vertical axis. Even for small offsets, say 300 m, SH- and SV-waves may arrive at slightly different times at the first interface.

The seismograms recorded by the three-component detectors, i.e., computed using the ANISEIS Package, have been, first analysed. They showed that recording at near-zero-offset might be most appropriate for obtaining shear data of better quality, as the signal should be less distorted.

2.2. OPTIMUM NEAR-ZERO OFFSET

For Love waves to interfere only with very shallow shear-data when using a horizontal mechanical force or shooting at shallow depth for generating shear waves, t_L , the arrival time of this wave must be less than t_s, the arrival time of a reflected S-wave from an interface at depth H.

Consider a horizontal layer having an interface at depth H, and x, be the near zero-offset, the distance between the source and the receiver, since a Love wave is a horizontally travelling wave (also, horizontally polarized) with velocity v_L, we have

$$x = v_L t_L \tag{2.1}$$

For S-wave reflections coming from depth H recorded by a receiver at distance x, we have the well known hyperbolic equation relating x, H and V, the S-wave medium velocity.

$$\left[\frac{x}{2}\right]^2 + H^2 = \left[\frac{t \cdot v}{2}\right]^2 \Rightarrow t^2 = \frac{4.H^2}{v^2} + \frac{x^2}{v^2} \tag{2.2}$$

We need an offset x so that , hence

$$\frac{x^2}{v_L^2} < \frac{4.H^2}{v^2} + \frac{x^2}{v^2} \Leftrightarrow x < \frac{2.H}{\left[\left(\frac{v}{v_L}\right)^2 - 1\right]^{1/2}} \tag{2.3}$$

For example, a Love wave having a velocity v_L =350 m/sec and an S-wave medium velocity V=1000 m/sec all geophones laid out at an offset x less than 74m record traces of Love waves followed separately by S-wave reflections coming from interfaces lower than 100 m (H=100 m). For S- wave reflections coming from upper interfaces, having a depth less than 100 m will probably be mixed with Love waves.

From this simple example, we conclude that, the optimum near zero-offset may be determined by field test and to what extend shallow S-wave deteriorated data is acceptable.

2.3. RECEIVER ARRAY

To investigate anisotropy by studying the azimuthal variation of the reflection amplitudes and possibly recording shear data of better quality a circular receiver array characterized by a symmetrical distribution of three component receivers was

designed. Eight three component receivers are set along a circle, each 45°, sampling the whole azimuth (360°). The two horizontal components are oriented North and East, respectively. The shot point was situated at the centre of the circular array with a shear source. To cancel random noise coming from all directions and enhance signal to noise ratio by a factor of 2, every receiver station was comprised of 3 three components seismometers. All the geophones of the same type are connected in series, giving three channels for every recording station. However, this array has not been yet tested in the field. It has only been used for the computation of synthetic seismograms with the horizontal components oriented parallel and normal to the survey line.

2.4. GEOLOGICAL MODELS

The geological models used for this project are based on the assumption that the sequence of layers at shallow depth in sedimentary basins are most likely to be transverse isotropic with vertical axis of symmetry (Jolly, 1956; Levin, 1979 and Thomsen, 1986), and that at an appropriate depth, when the minimum horizontal stress as mentioned in the first chapter is horizontal. The sedimentary layers below this depth are likely dominated by vertically aligned-fluid-filled-cracks, and preferentially oriented pore-spaces (Crampin,1989).

In order to investigate the two types of anisotropy using shear-wave sources with different polarization directions, a geological model representing a homogeneous anisotropic medium, simulating a sedimentary basin with shale overlying two cracked media, sandstone and limestone, having the same crack orientation but different crack densities, above an isotropic granite half-space. The azimuthal isotropic layer has a thickness of 800 m and that of the two anisotropic layers is 1000 m (Figure 2.1).

The shale material has a velocity anisotropy of 30%, a density of 2.38 g/cm^3, an isotropic P-wave velocity of 2.5 km/s and a

horizontal S-wave velocity of 1.5 km/s.The velocity anisotropy has been taken to be the percentage by which the minimum vertical velocity (Levin, 1979) is less than the maximum horizontal velocity.

$$\frac{V_h - V_v}{V_h} \times 100 \qquad (2.4)$$

is the anisotropy percentage, where and are the horizontal and the vertical velocities, respectively.

The sandstone and limestone have an isotropic P-wave velocity of 3.5 km/s and 4.5 km/s; a density of 2.3 g/cm^3 and 2.25 g/cm^3 with a Poisson's ratio of 0.32 and 0.28, respectively; both have an aspect ratio of 0.001 and the same orientation of the principal axes of anisotropy and a thickness of 1000 m. The direction of the strike is oriented 30° toward North from West-East orientation, N60E.

To see how the time delay between the two split shear waves is affected by the crack density, by the crack orientation and by the presence of fluids within the cracks, 5 geological models have been used (figure 2.1). Model 2 and model 3 are for anisotropic media with dry-cracks but having different crack-densities. Model 5 and model 6 are for saturated cracks. Model 7 has the same geological material as Model 3, but for this case the three component-receivers are fixed in the direction of the survey line, and the direction of the strike, which is parallel to the crack-plane is varied so that the relation between the crack-orientation and the extrema of the energy of the trace is investigated. The energy of the trace is computed within a time window containing the reflected event from each interface for each crack orientation and its maximum or minimum value is related to the strike orientation. This technique proved to be efficient in the determination of crack-orientation or the polarization direction of the reflected waveform as it will be demonstrated later in chapter 4.

Changing the direction of the strike is simply obtained by rotating the initial elastic tensor about the axis of symmetry by

the appropriate angle to obtain the new anisotropic medium with the desired crack orientation (Auld,1973).
All models are illustrated in Figure 2.1. Model 1 is for an isotropic medium made of uncracked sandstone, uncracked limestone and isotropic shale. No splitting is to be expected within this medium. The two excited shear waves with mutual orthogonal polarizations are degenerate, i.e. travelling in the isotropic medium with the same velocity whatever the direction of propagation.

In model 4, a thin layer with a horizontal axis of symmetry was introduced to investigate the efficiency of the energy attributes in the determination of small time delays of the order of the sample rate.

A rectangular cartesian coordinate system (x, y, z), corresponding to West-East, South-North and Vertical has been set, respectively. Coordinate axes do not coincide with the principal axes of anisotropy.

2.5. ZERO OFFSET SYNTHETIC SEISMOGRAMS.

For this experiment a circular receiver array was designed where 8 three-component-geophones are equidistantly distributed over a circle. Since the shot point will be at the center of the circle and the receiver array is symmetrical about the center, half of the array has only been used for recording synthetic data. This array is also designed so that azimuthal variation of the recorded data is investigated. Thomsen, 1988, showed that if the medium is anisotropic and a shear source polarized normal to survey line is used, the reflection coefficients vary as functions of azimuth even at a vertical angle of incidence. The azimuth is the angle between the survey line and the crack-strike.

Vertically propagating S-waves are modelled using three offsets with radii of 75 m, 150 m, 300 m, making a receiver array of three concentric circles. This is also for optimizing the appropriate offset, so that SV- and SH- waves propagate vertically, near the

axis of symmetry, in the shale to become degenerate and arrive at the same time at the shale/sandstone interface to avoid a successive splitting at this interface, since the velocities of those two waves are dependent on the angle of incidence and the time delay increases with increasing offset. Converted energy on the horizontal components is also minimized at zero offset. Figure 2.2 illustrates the half circular array.

Two shear sources with mutual orthogonal polarizations have been used at the center of the receiver array. One oriented West-East, corresponding to line 1 in Figure 2.2 and the other oriented South-North normal to it. This enables us to see the effect of the source orientation on the seismograms for both anisotropic and isotropic media. Also, as it will be demonstrated later that, if the medium on which the shear source is generated, (say shale for our case), is transverse isotropic with vertical axis of symmetry, the maximum value of the energy of the rotated trace computed within the time window containing the reflected event from this medium is coincident with the polarization direction of the shear source if the offset is less than 150 m. However, if this medium is azimuthally anisotropic, the maximum and the minimum value of the energy of the trace computed within the time window containing the reflected waveform from the interface of any cracked medium gives the direction of the principal axes of anisotropy of this medium.

The synthetic seismograms for the models, which have been just mentioned were computed using the ANISEIS modelling package at BGS (British Geological Survey) at Edinburgh. This package allows the calculation of the synthetic seismograms in horizontally stratified isotropic or anisotropic structures, based on the reflectivity technique on isotropic and anisotropic media (Fuchs, 1971; Booth and Crampin, 1983a, b).

The radial and the transverse components are set so that their axes are parallel and normal to each survey line, respectively.

To generate shear synthetic data, the medium is excited by a

surface horizontally polarized shear source directed along a desired orientation with a dominant frequency of 25 Hz. This generates a vertically propagating linearly polarized plane wave, travelling through the medium and reflected back to the surface from each interface.

The most commonly used formulas for the computation of the phase velocities of the three body waves propagating in the symmetry planes of a cracked solid have been provided by Hudson,1981; and to estimate the elastic constants of such a cracked medium the reduced equations derived by Crampin (1977) are equated to the numerical values of the velocities given by Hudson's formulas and solved for elastic constants.

The software is designed so that a trace length cannot exceed 1024 samples, when it is recorded using a sample interval of 4 msec. However it is possible to extend trace length by choosing a greater sampling frequency as long as it is greater than twice the highest frequency component in the the waveform to be sampled.

2.6. ANALYZING DATA FROM MODEL 2.

Figure 2.3 shows 9 synthetic seismograms obtained using a shear source making 45° with the survey line, (line 2' in Figure 2.2) and three three-component-receivers at offsets of 75 m, 150 m and 300 m. Traces 1, 2 and 3 are the radial, the transverse and the vertical, respectively corresponding to 75 m offset. Traces 4, 5 and 6 similarly correspond to a 150 m offset; and 7, 8 and 9 are for 300 m offset. The two split shear waves are clearly seen on both the radial and the transverse component seismograms, reflected from the cracked media, sandstone and limestone. Also the delay between the two split shear waves is increasing with depth, since one shear mode is travelling faster than the other.

On the vertical component, we can see the arrival of a P-wave at 830 msec, a converted shear-wave at 1100 msec, where its amplitude has slightly increased at 300 m offset, as the particle

motion of the SV-wave tends to deviate from the horizontal motion as the propagation direction moves away from the vertical direction, and a reflected S-wave arriving at 1340 msec. Hence the incident shear wave has been coupled to another shear wave and a P-wave, all three having mutual orthogonal polarizations fixed with the direction of propagation. This is characteristic of anisotropic media (Crampin, 1977).

Two reflected shear events from the interface separating shale and sandstone are recorded by the radial and the transverse components, for offsets 75 m and 300 m, corresponding to angles of incidence of 2.7° and 5.35°, respectively, have the same arrival time, since for those offsets the wave is travelling (nearly) vertically along the axis of symmetry. The two shear waves are said to be degenerate. Consequently the two shear velocities are equal.

For offset 300 m, corresponding to an angle of incidence of 10.6° the two shear waves arrive at slightly different times; the time difference is of the order of 3 to 5 msec. This is due to the fact that at this angle of incidence, for such an anisotropic shale the SV-surface wave velocity exceeds that of the SH-surface wave velocity as it is illustrated schematically in Figure 2.4 (Kelvin,1979).

As the angle of incidence increases, the two surface waves might well separate, first with the SV-surface wave above the SH-surface wave. At a certain angle of incidence the two surface waves intersect again and from the point of intersection the SH-surface wave will be above the SV-surface wave. Because of this the velocity difference increases, the length of the ray path increases with increasing offset. Consequently, the time delay between the SV- and SH-waves increases.

In the case of our experiment the time delay, of the order of 3 to 5 msec, is too small. Hence the SV- and SH- waves split simultaneously as if only the original shear polarization has just split at the interface separating shale and sandstone. This simple

result demonstrates the important fact that reflected shear signals recorded at longer offsets in the presence of anisotropy will be distorted. Consequently, at zero-offset this distortion is minimized by avoiding the phenomenon described just before.

When the source polarization has the same direction as the radial component (in-line source), the transverse one records a reflected event having a very small amplitude coming from the interface of the anisotropic shale-anisotropic sandstone. When the polarization source is parallel to the transverse component (cross-line source), it is the radial component, which records a very small amplitude coming from the same interface mentioned just before. This slight energy on the mismatched components is due to the small deviation of the ray path from the vertical axis of symmetry.

2.7. PROCESSING SYNTHETIC DATA

2.7.1. Separation of the two split shear waves

As it is shown in the previous section, the radial and the transverse components record two seismic traces, R(t) and T(t), each one containing two split shear waves coming from each reflector separating two anisotropic media. Alford (1986) derived mathematical formulas for the separation of the two split shear modes by synchronous rotation of the two orthogonal shear sources and the recorded data of the horizontal components to conform with the principal axes of anisotropy. This rotation by the angle separating the survey line and the direction of the strike leads to two synthesized seismic sections, one made of seismic traces of the faster shear waves and the other made of slower ones. Thomsen (1988) derived an algorithm for the separation of the two split shear waves, identical to that of Alford with an additional criterion control of the recorded data, if it fits the the azimuthal anisotropic model.

For example, given a shear source with polarization direction making 45° with the survey line, the horizontal receivers will

record the projection of the particle motion vectors of the two split shear modes. Consequently, it can be demonstrated (Thomsen, 1988) from simple geometrical constuction (as shown in Figure 2.5)

$$T(t) = Cos(\varphi - \theta)\,Sin\theta \cdot FS(t) + Sin(\varphi - \theta)\,Cos\theta \cdot SS(t)$$
$$R(t) = Cos(\varphi - \theta)\,Cos\theta \cdot FS(t) - Sin(\varphi - \theta)\sin\theta \cdot SS(t) \qquad (2.5)$$

Where FS(t) and SS(t) are the time series of the faster and the slower modes, respectively. Each one is the result of a convolution between the input impulse and the medium filter which is different for each mode, since they have different polarization directions. However, in sedimentary basins where the anisotropy is considered to be weak, of the order of 5%, the two filters are approximately the same (Thomsen,1986).

θ and φ are the angles between the fracture strike and the survey line, and the angle between the direction of the polarization source and the survey line, respectively. From Figure 2.5, rotating the horizontal components toward the anisotropic axes will directly separate the two split shear waves into the fast and the slow one giving two new seismic traces. In Chapter 5, the values of the new attribute, instantaneous polarization angle, are used to automatically separate the two split shear waves by instantaneously rotating each sample of the recorded data toward the direction of maximum energy computed within a moving window each time it slides down by a sample rate over the horizontal components.

The resulting seismograms of the two separated time series for a West-East oriented shear source are shown in Figures 2.6, and 2.7 corresponding to models 2, 3, respectively. Each figure shows the time series of the faster and the slower modes derived using a simple rotation of the horizontal components toward the anisotropic axes. Traces numbered 1 to 5 are the faster modes

derived from the receivers 1 to 5 equidistantly distributed along the half circle; traces numbered 6 to 10 are their corresponding slower ones.

Two common features may be seen in all figures:

i) The faster modes are in phase with one another, as are the slower ones due to near vertical incidence and the horizontal layer model.

ii) The arrival time of the reflected fast shear modes coming either from the interface separating sandstone and limestone or the interface separating limestone and granite is the same for all the models, corresponding to 2440 msec for the former interface and to approximately 3260 msec for the latter one. This is due to the fact that, for vertically cracked media there is no variation of the velocity with the azimuth, as it is stated in the Hudson's formulas. For vertically travelling shear waves, the velocity of the faster one is only dependent on the Lame's constant μ and the density ρ

$$v_f = \left(\frac{\mu}{\rho}\right)^{1/2} \tag{2.6}$$

characterizing the uncracked medium, i.e. the velocity is that of the uncracked medium.

The velocity anisotropy in the sandstone due to a crack-density of 0.06 (model 2) is of the order 6% ; for a crack-density of 0.1 (model 3) it is equal to 10%. The velocity anisotropy is defined as:

$$\frac{v_f - v_{sl}}{v_f} \times 100 \tag{2.7}$$

Where v_f and v_{sl} are the velocities of the faster shear travelling within the uncracked medium and the slower one, respectively.
The velocity anisotropy in the limestone due to crack-density of 0.04 (model 2) and 0.06 (model 3) are 4.3% and 6.4%, respectively. Model 5 and model 6 show the same results as models 2 and 3.

Consequently, shear waves travelling vertically are not sensitive to the presence of fluids filling the cracks. All the results are summarized in table 2.1.

2.8. CONCLUSION

The previous studies have shown that anisotropy should be taken into consideration when exploring sedimentary basins by shear waves. The crack density may be estimated from the anisotropy percentage if the model is azimuthally anisotropic. Increasing density will increase the time dealy between the two split shear waves. The variation of the time delay may be monitored by the energy attributes as it will be demonstrated later in chapter 6.

Shear waves could be seriously degraded if recorded at long offsets, particularly when the upper medium is strongly azimuthal anisotropic or at offsets beyond the shear wave window.

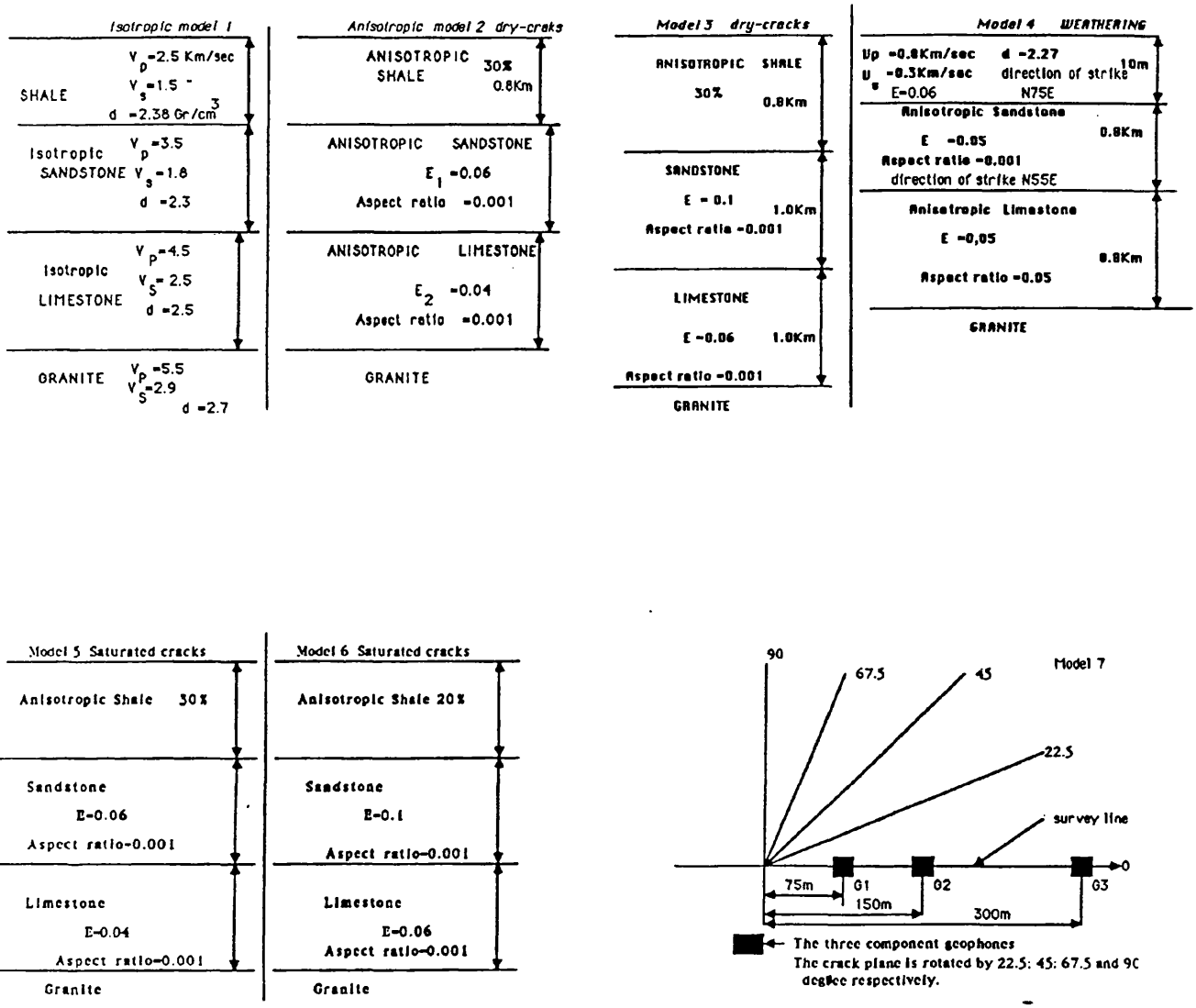

Figure 2.1. 7 Geological models. Isotropic model 1; anisotropic models 2, 3 and 4 with dry-cracks; anisotropic models 5 and 6 with saturated cracks; model 7 has the same materials as model 3 but the crack-plane has been rotated by 0°, 22.5°, 45°, 67.5° and 90°, respectively.

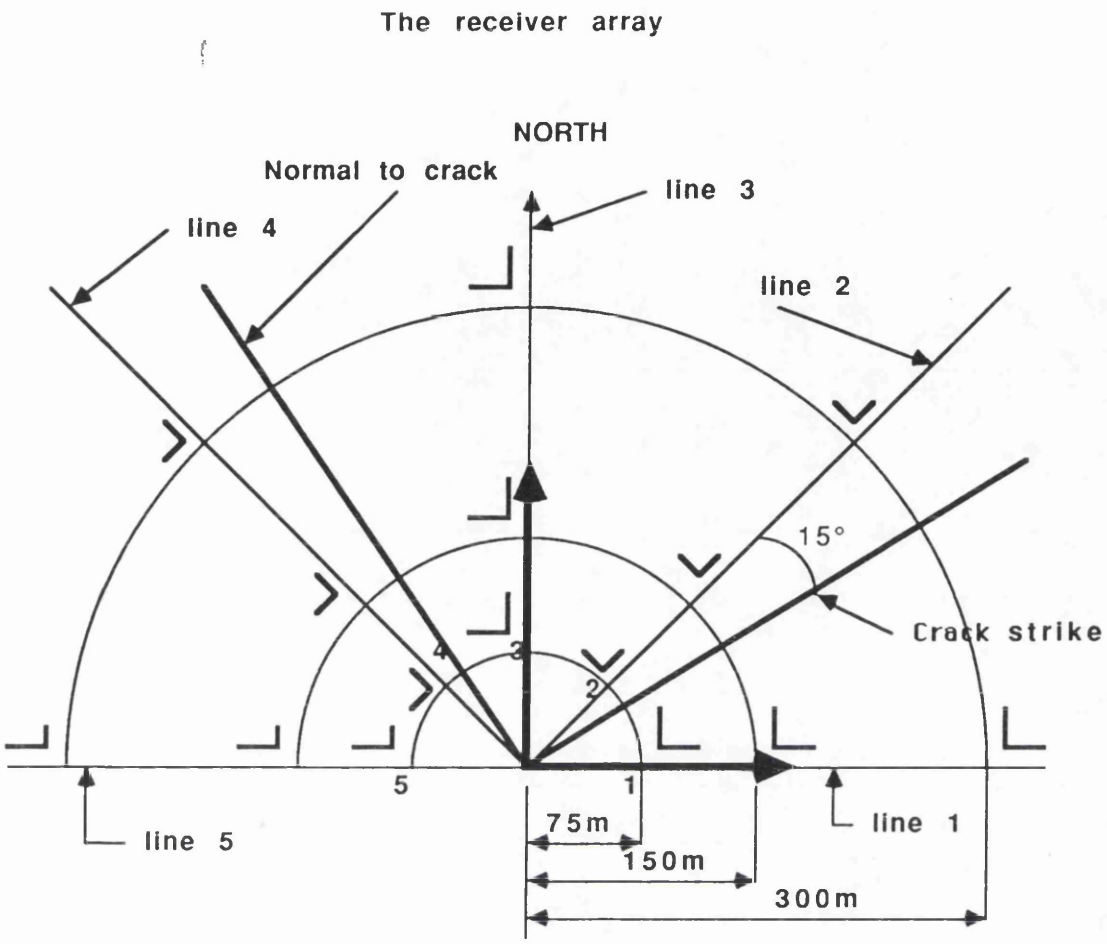

Figure 2.2. The receiver array. The stations numbered are three-components receivers. Each line joining three aligned stations is the survey line. All the receivers are distributed over three-concentric circles with radii 75 m, 150 m and 300 m. The shear source is at the center of the circle and the distance between the point source and the receiver is the offset. Line 1 is oriented East-West and line 3 South-North. The symbol **L** represents the orientation of the horizontal components.

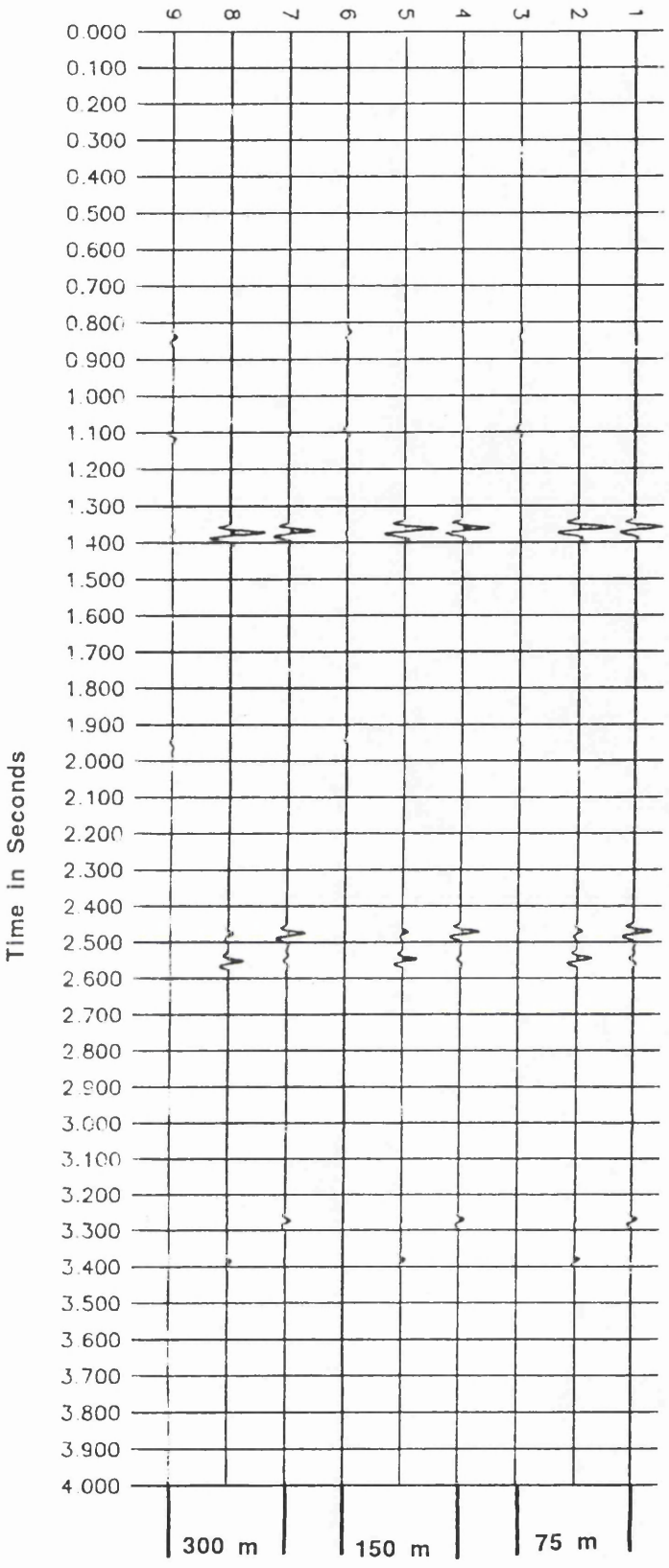

Figure 2.3. 9 Seismograms obtained using a shear source oriented parallel to survey line 1 and three component receivers with 75 m, 150 m and 300 m offset aligned with survey line 2. Traces 1, 2 and 3 are the radial, the transverse and the vertical, respectively, corresponding to 75 m offset.

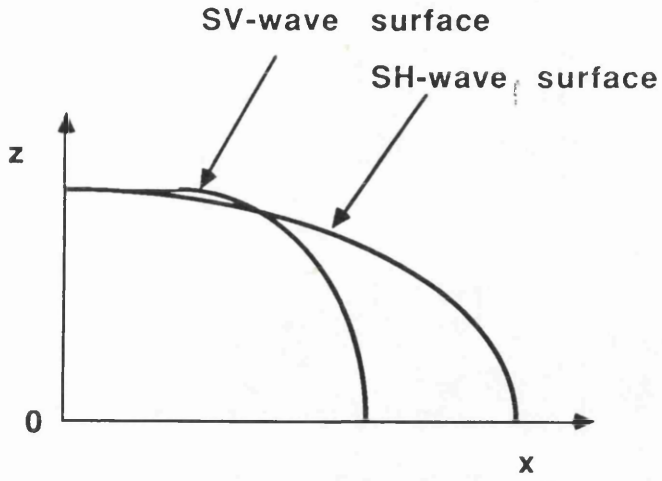

Figure 2.4. Schematic representation of the wave surface velocities of SV- and SH- waves for the anisotropic shale of the models considered.

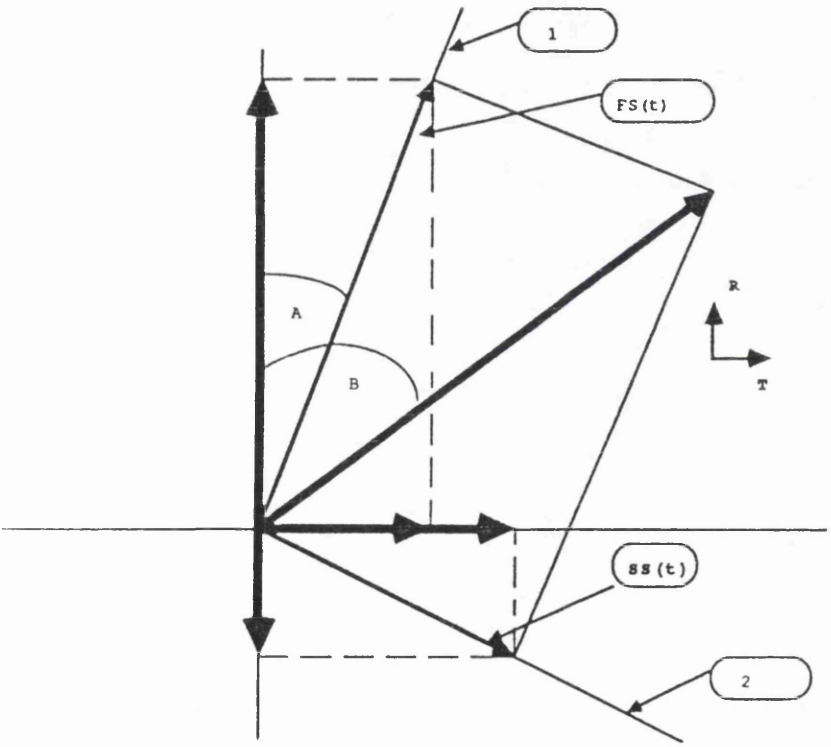

Figure 2.5. Computation of the split shear waves. FS(t) and SS(t) are the faster and the slower shear waves, respectively. Axes 1 and 2 are the direction of maximum and minimum horizontal stresses. Angles A and B are the angle of the strike and the angle of polarization of the shear source, respectively. The arrows are the projections of the polarizations of the split wavelets onto the axes of the radial and the transverse geophone axes given by the vectors **R** and **T**, respectively.

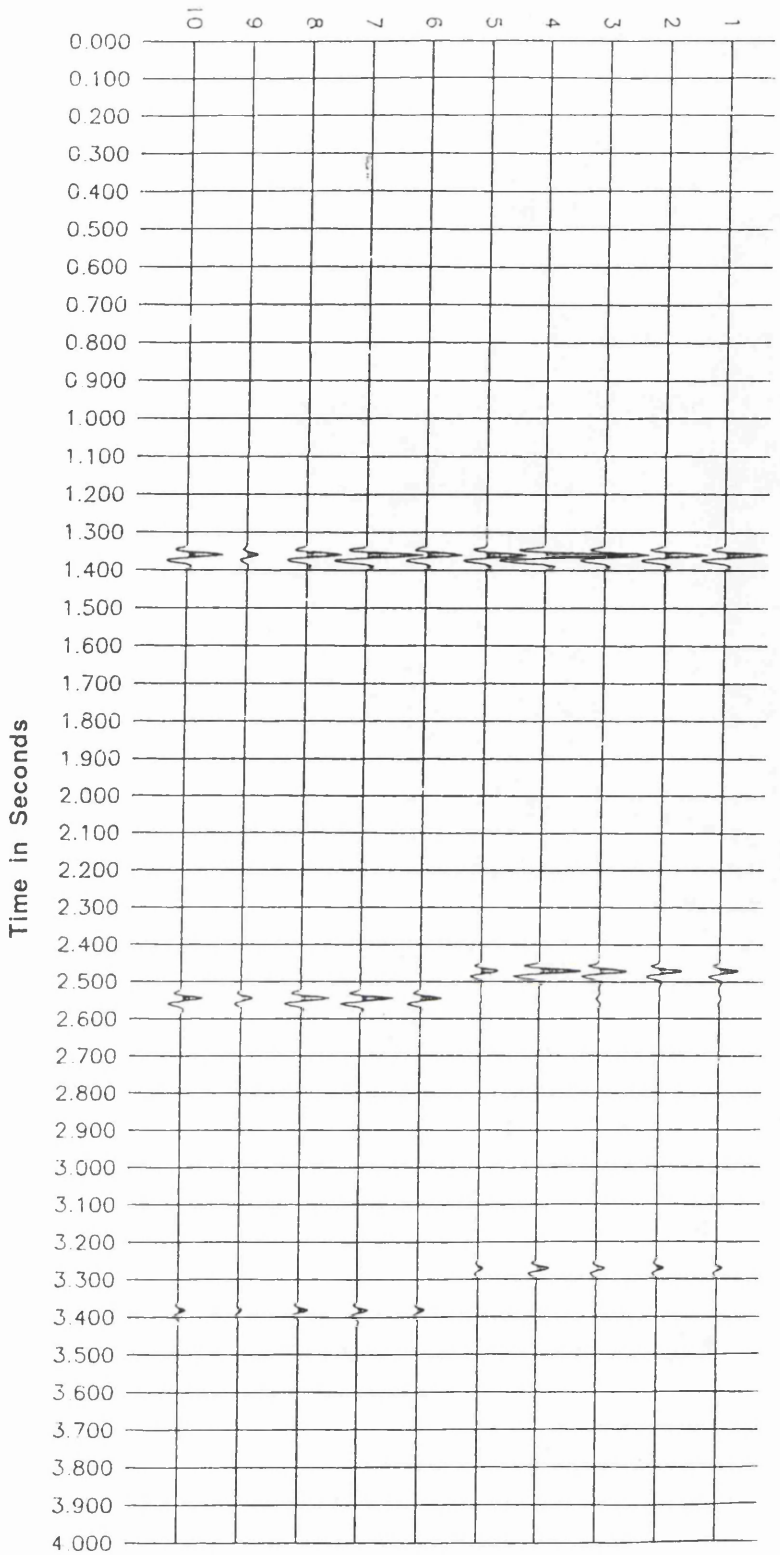

Figure 2.6. The seismograms of the faster and the slow wave separated by a simple rotation of the horizontal components toward the direction of anisotropic axes, recorded by the half-circular array of radius 75 m, i.e. three-component receivers numbered 1 to 5 in Figure 2.2, over model 2 having a crack density of 0.06 and 0.04 in Sandstone and Limestone, respectively. Traces numbered 1 to 5 are the faster modes and traces numbered 6 to 10 are their corresponding slower ones, respectively. A shear source polarized parallel to survey line 3 has been used.

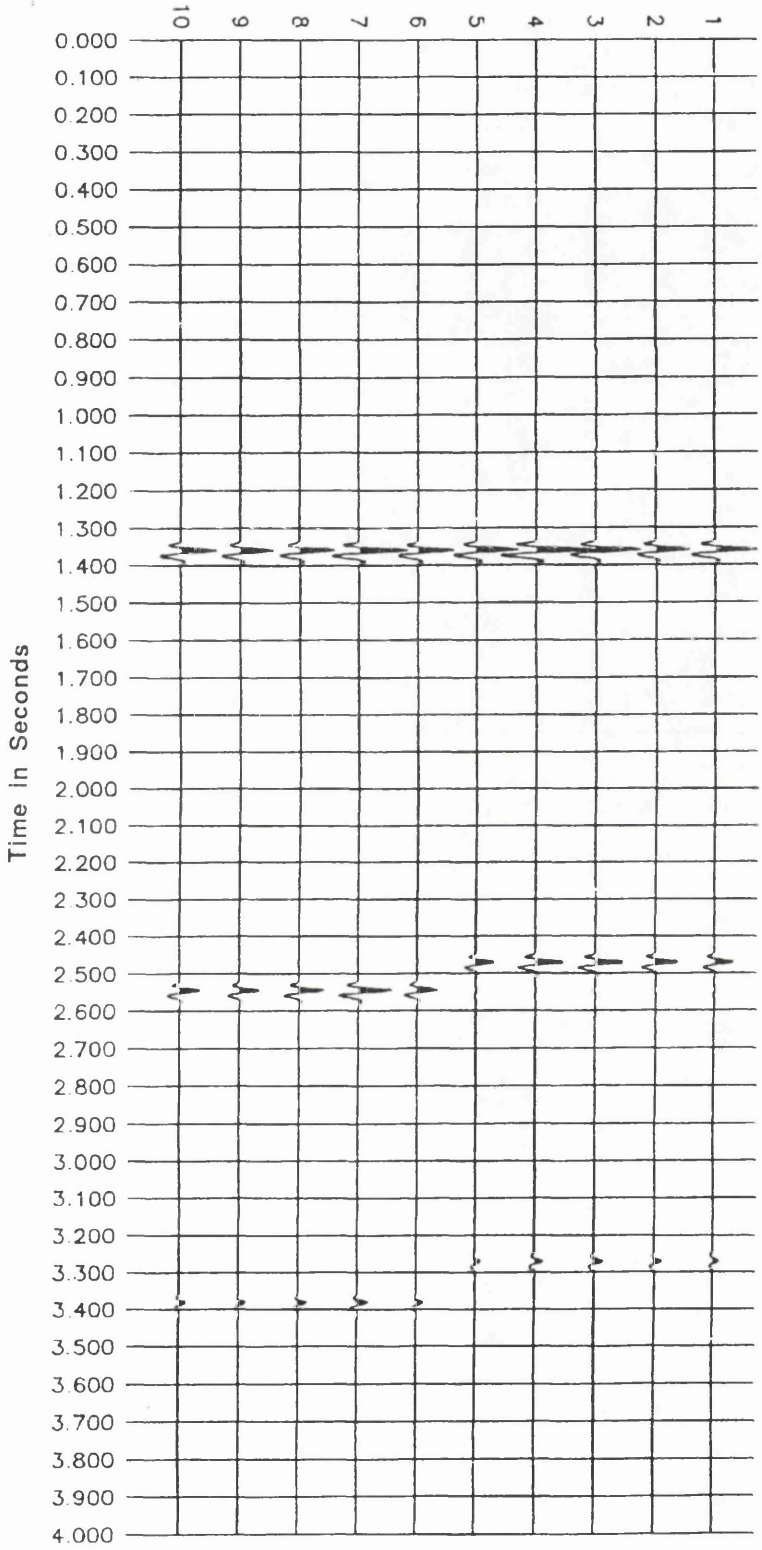

Figure 2.7. Similar to Figure 2.6 and corresponds to model 5 having the same crack-densities but are fluid filled. Note that fluid-filled-cracks have no effects on the delay between the split shear waves travelling vertically.

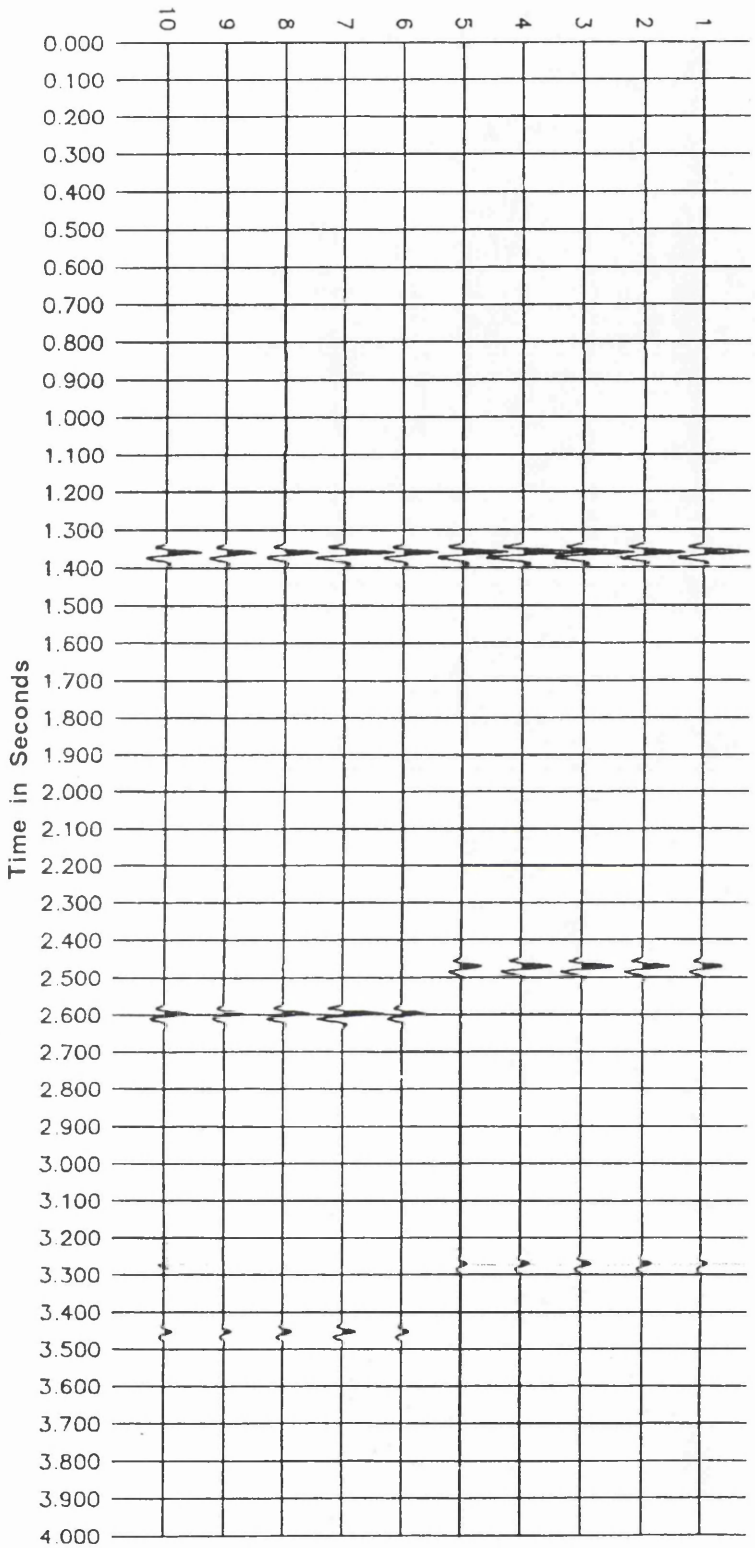

Figure 2.8. Similar to Figure 2.6 and corresponds to model 3 having larger crack-densities than model 2. Note that increasing crack-density increases the time delay between the split wavelets.

Table 2.1

	SANDSTONE Models		LIMESTONE MODELS	
	2 and 5	3 and 6	2 and 5	3 and 6
v_f (m/sec)	1800	1800	2500	2500
Δt (msec)	1180	1235	845	855
$t_{sl} - t_f$ (msec)	70	125	110	175
v_{sl} (m/sec)	1700	1620	2370	2340
$\frac{v_f - v_{sl}}{v_f} \times 100$	5.5%	10%	5.2%	6.4%
Crack density	0.06	0.1	0.04	0.04

v_f and v_{sl} are the velocities of the fast and the slow shear wave, respectively.

Δt is the difference in travel time between two successive horizons

$t_{sl} - t_f$ is the time differnce between the slower and the faster shear modes

CHAPTER 3

Seismic attributes in isotropic and anisotropic media from three component synthetic data.

3.1. INTRODUCTION

The seismograms recorded by a three component detector may be considered as the projection of a wavefield vector (Kanasewich, 1981) onto the geophone axes. This leads to the investigation of new seismic attributes in the presence of anisotropy, such as the apparent azimuth angle, the eccentricity and, the components of the poynting vector corresponding to the wavefield vector. The variation of those attributes in isotropic and anisotropic media are investigated in this chapter. Attributes of the complex traces of the horizontal components are also computed using The Hilbert Transform and investigated. Two shear sources mutually orthogonal have been tested and the attributes are computed for each source orientation.

In this Chapter we will show that the apparent azimuth gives the direction of principal axes of anisotropy if the medium is azimuthally anisotropic; or the shear source orientation if the medium is isotropic or azimuthally isotropic. The eccentricity may be useful in controlling the deviation of the polarization of the reflected waveform from the horizontal plane and may be used to design a new filter called the P- Wave Filter (PWF) for attenuating P-waves recorded by the horizontal components.

3.2. BASIC DEFINITIONS

The three component receiver may be considered to record the instantaneous components of an instantaneous vector

$$\mathbf{V(t)} = x(t)\mathbf{i} + y(t)\mathbf{j} + z(t)\mathbf{k} \qquad (3.1)$$

This gives a three-dimensional picture of particle motion. x(t); y(t) and z(t) are the instantaneous displacement vectors recorded by the radial, the transverse and the vertical receivers, respectively. The geophone axes form a rectangular cartesian coordinate as seen in Figure 3.1. Benhama et al (1988) used this representation to design a spatial directional filter to cancel waves with undue polarization and enhance signal-to-noise ratio by selecting polarization in a given direction, the radial, the transverse or the vertical direction.
v(t) is called the instantaneous wave vector and the modulus **|v(t)|** is called the total reflection strength.

w(t) = x(t)**i** + y(t)**j** is the projection of the wave vector onto the horizontal plane

$$w(t) = \left[x(t)^2 + y(t)^2\right]^{1/2} \qquad (3.2)$$

is called the horizontal reflection strength of the wave vector
The two following instantaneous attributes $\varphi(t)$ and $\theta(t)$ are needed to define the instantaneous wave vector in a spherical coordinate system (Kanasewich, 1981).

$$\varphi(t) = \tan^{-1}\left(\frac{y(t)}{x(t)}\right)$$

$$\theta(t) = \cos^{-1}\left(\frac{z(t)}{|v(t)|}\right) \qquad (3.3)$$

or

$$\theta(t) = \frac{\pi}{2} - \tan^{-1}\left(\frac{z(t)}{w(t)}\right)$$

$\varphi(t)$ and $\theta(t)$ are the two seismic attributes which are investigated in case of isotropy and anisotropy due to induced cracks. The variation of those attributes with source orientation is also examined.

$\varphi(t)$ and $\theta(t)$ are called the apparent horizontal azimuth and the eccentricity, respectively. Those two attributes have been used to design (Kanasewich, 1981) a filter which discriminates between surface waves, the Rayleigh and the Love waves based on their motion within the vertical and the horizontal plane, respectively.

3.3. ISOTROPIC MEDIUM AND THE ATTRIBUTES

As mentioned before, the isotropic model is made of three layers: isotropic shale, isotropic sandstone and limestone. Three aligned three-component geophones have been used to record synthetic seismograms, having 75m, 150 m and 300 m, respectively. Two shear sources polarized parallel and normal to the survey line were utilized for generating shear energy. The half circular array has not been used because of the isotropic properties of the medium. The seismic properties do not vary with the azimuth.

3.3.1. Cross-line and In-line source

When the polarization direction is normal to the survey line, i.e. parallel to the transverse geophone, only SH-waves are generated and recorded. No mode conversions are excited by the interface separating two isotropic media. Hence, the radial and the vertical will record no seismic motion, i.e. x(t) and z(t) are set equal to zero, and the instantaneous phase angles become:

$$\varphi(t) = \tan^{-1}\left(\frac{y(t)}{x(t)}\right) = \frac{\pi}{2}$$

$$\theta(t) = \frac{\pi}{2} - \tan^{-1}\left(\frac{z(t)}{y(t)}\right) = \frac{\pi}{2} \qquad (3.4)$$

With the polarization direction parallel to the survey line SV-waves are generated and conversion modes occur at interfaces separating isotropic media. SV-waves generate P-waves and vice versa, but no SH-motion is converted at the interface. Hence, the transverse component records no seismic motion and y(t) is set equal to zero.

For this source orientation the instantaneous attributes become:

$$\varphi(t) = 0$$
$$\text{and} \qquad \theta(t) = \frac{\pi}{2} - \tan^{-1}\left(\frac{z(t)}{x(t)}\right) \qquad (3.5)$$

At 75 m offset, a near-zero offset, mode conversions are highly attenuated. Consequently, Z(t) tends towards 0.0 and $\theta(t)$ tends to $\pi / 2$

3.4. ANISOTROPIC MEDIUM AND SEISMIC ATTRIBUTES

All the synthetic data used for this experiment are derived from model 2 using the half circular receiver array, where 5 three-component geophones are equidistantly distributed along the circle, having a radius of 75 m, i.e. 75 m offset (see Figure 2.2). A shear source parallel to survey line 3 has been used. The problem is to study the seismic attributes and their variations as source orientation varies, i.e, the direction of the survey line changes and the source orientation is kept fixed.

It is well known that, whatever the type of source is used, three body waves are always coupled when a type of wave is travelling in an anisotropic medium (Keith & Crampin, 1977). Three reflected and three transmitted waves are generated at the interface separating two anisotropic media or isotropic-anisotropic media, when an incident wave is impinged on it and travelling off the

symmetry plane. Hence each component will record a seismic trace. Consequently the azimuth angle and the eccentricity will differ from the ones of the isotropic case. Figure 3.2a, b shows the apparent azimuth $\phi(t)$ computed within the windows 1300-1440 msec and 2400-2640 msec, respectively. The former window contains the reflected wavelet from the shale/sandstone interface and the latter one from the sandstone/limestone interface. Each Figure contains 5 traces, each one computed from each of the 5 equi-spaced three-components of the circular receiver array, for investigating the variation of this attribute with source orientation. Traces 1 to 5 are from stations 1 to 5 (see Figure 2.2). A larger scale has been chosen for an appropriate reading of the values of those attributes. Taner et al., 1979, used color display for a better quantification of the instantaneous phase angle. The variations of $\phi(t)$ within each anisotropic medium are different as seen from the Figure. Because of the vertical incidence, $\phi(t)$ is constant and equal to zero within the first window for a in-line source (trace 3 Figure 3.2a); equal to 90° for an cross-line source (trace 1 Figure 3.2a), giving the direction of the shear source in an azimuthally isotropic medium.

Figure 3.2b shows the azimuth angle computed for each survey line (Lines 1, 2, 3, 4 and 5) within the window containing the waveforms of the fast and the slow shear. The azimuth angle is measured from the survey line. Within the window containing the fast shear wave it is constant and gives the direction of the crack strike; within the slow shear it also constant and gives the direction of the crack-strike normal. For example, when considering survey line 1, the apparent azimuth numbered by 1 in Figure 3.2b is constant and equal to 30°, then changes to 60°, within the fast and the slow shear, respectively. For line 2 (numbered by 2 in Figure 3.2.b), it varies from 15° to 75°, giving the direction of crack strike and the normal to it , respectively, relative to the survey line. (All angles are measured in radians, and in terms of a degree, 1mm corresponds to 10°). Consequently, if

there is any splitting the azimuth angle may be used as an attribute to identify the direction of principal axes of anisotropy. However, it is more efficient as it will be demonstrated later in Chapter 5 that anisotropy may be better assessed and quantified by the instantaneous polarization angle and the energy attributes, when combined together.

The variation of eccentricity $\theta(t)$ within the considered windows are seen in Figures 3.3a, b. Those Figures show that $\theta(t)$ is constant and nearly equal to 90°, showing that the particle motion occurs in the horizontal plane whether there is a splitting or not. Consequently, this angle may be used to control the behavior of a horizontally polarized shear wave whether it remains in the horizontal plane or not, particularly in the presence of a tilted crack plane about the vertical axis of symmetry. Liu & Crampin, 1991, reported strong coupled energy on vertical and radial components from a transverse horizontal shear source, indicating the presence of non vertical cracks in the rockmass, i.e., inclined from the vertical axis.

If a wave from a horizontal shear source splits along the principal axes of anisotropy in a non-vertical crack geometry, then the angle between the normal to the crack-strike and the horizontal plane is equal to the tilt angle. Consequently, the polarization direction of the slower shear is off the horizontal plane by the tilt angle, as it is polarized along the crack-strike normal. The eccentricity may be then defined as the angle between the eigenvector corresponding to the largest eigenvalue and the vertical axis, giving the direction of polarization, computed from the covariance matrix within a window of N samples. Hence, if the window contains the slower shear wave, then the eccentricity is the complement of the tilt angle. Winterstein & Meadows,1991, found that some Lost Hills (in southern San Joacquin Valley of California) rocks have non-vertical crack geometry and modelled them to extract the tilt angle. Unfortunately, no synthetic nor real data was available to experiment with the use of such attributes in

extracting information about the the tilt angle.

The eccentricity may have another important practical use, if the recorded three component data are generated by an explosive source, in attenuating reflected P-waves recorded by the horizontal components. The reflected P-wave energy is expected to be polarized in all directions, within a cone with its axis the axis of the vertical component.

Shear waves are expected to be polarized horizontally or nearly horizontally, but neither radially nor transversely because of the presence of azimuthal anisotropy in sedimentary rocks, and even in isotropic media the shear source rotates as offset increases (Liu & Crampin 1990). Consequently, $\theta(t)$ may be defined, as mentioned just above, as the angle between the eigenvector corresponding to the largest eigenvalue and the vertical axis to design a filter. The filtered seismograms may be expressed as:

$$\begin{aligned} X_f(t) &= RL(t).\sin^2\theta(t) \\ Y_f(t) &= RL(t).\sin^2\theta(t) \end{aligned} \qquad (3.6)$$

Where RL(t) is the rectilinearity function (Montalbetti & Kanasewich, 1970). Relation (3.6) shows that linearily polarized waves near the horizontal plane (the role of $\theta(t)$) are expected to be enhanced within the horizontal components. This new filter is called P Wave Filter (PWF), as it can attenuate P-wave energy from the horizontal components

3.5.THE POYNTING VECTOR AND ITS ATTRIBUTES

3.5.1. Definition

The acoustic poynting vector **p** is defined as the dot product of the particle velocity displacement **v** and the stress **T** applied to the considered medium (Auld, 1973).

$$\mathbf{p} = \mathbf{v}.\mathbf{T} \tag{3.7}$$

$$\mathbf{P}\ (\mathbf{t}) = Px(t)\mathbf{i} + Py(t)\mathbf{j} + Pz(t)\mathbf{k} \tag{3.8}$$

v and **T** are first and second rank tensors,respectively with **v** in m/sec and **T** in $newton/\ m^2$; the acoustic poynting vector has the appropriate dimension $watt/\ m^2$. Hence the power flow through a surface may be computed as the flux of this vector, which is

$$\int_s p.\ nds \tag{3.9}$$

Where **n** is the normal to the surface ds
In matrix form relation (3.9) becomes

$$\begin{bmatrix} p_x \\ p_y \\ p_z \end{bmatrix} = \begin{bmatrix} v_x \\ v_y \\ v_z \end{bmatrix} \begin{bmatrix} T_{xx} & T_{xy} & T_{xz} \\ T_{yx} & T_{yy} & T_{yz} \\ T_{zx} & T_{zy} & T_{zz} \end{bmatrix} \tag{3.10}$$

$T_{ij}(i, j = x, y, z)$ are the stress components

The three components of the poynting vector are time variant and may be strictly expressed in terms of particle velocity components as

$$\begin{aligned} p_x(t) &= y(t) \cdot z^*(t) - z(t) \cdot y^*(t) \\ p_y(t) &= z(t) \cdot x^*(t) - x(t) \cdot z^*(t) \\ p_z(t) &= x(t) \cdot y^*(t) - y(t) \cdot x^*(t) \end{aligned} \tag{3.11}$$

These are also called the instantaneous components of the acoustic

poynting vector.

In exploration seismology x(t), y(t), z(t) will be the velocity displacements of the three-component geophones, the radial, the transverse and the vertical, respectively; $x^*(t)$, $y^*(t)$, $z^*(t)$ are their imaginary parts, which can be computed using Hilbert transform (see paragraph 3.6).

The module

$$|p(t)| = \left[p_x^2 + p_y^2 + p_z^2 \right]^{1/2} \tag{3.12}$$

is called the instantaneous reflection strength of the poynting vector

Also as we have defined the instantaneous phases for the total seismic vector; the same definitions can be used so as the poynting vector is represented in a spherical coordinate system.

$$\varphi_p(t) = \tan^{-1}\left[\frac{p_y(t)}{p_x(t)} \right]$$

$$\theta_p(t) = \frac{\pi}{2} - \tan^{-1}\left[\frac{p_z(t)}{|p_{xy}(t)|} \right] \tag{3.13}$$

where $p_{xy}(t)$ is the projection of the poynting vector into the horizontal plane.

The variation of those attributes with the polarization direction and the azimuth are investigated whether the medium is isotropic or anisotropic.

3.5.2. Isotropic medium and the poynting vector

3.5.2.1. In-line and cross-line source

In the case of an in-line source there is no coupling to the horizontally polarized shear wave. Only SV-wave and converted

modes, SV- to P-wave and P-wave to SV-wave are excited. Hence, only the radial and the vertical components will record those types of waves; the horizontal component records a null trace.
Since y(t), the trace recorded by the transverse is null its complex conjugate y*(t) is also null and the components of the poynting vector are:

$$p_x = y \cdot z^* - z \cdot y^* \equiv o$$
$$p_y = z \cdot x^* - x \cdot z^*$$
$$p_z = x \cdot y^* - y \cdot x^* \equiv 0 \qquad (3.14)$$

$$|p(t)| = |p_y(t)|$$

is the instantaneous reflection strength of the poynting vector.
The instantaneous phases $\varphi_p(t)$ and $\theta_p(t)$ are identical

$$\varphi_p(t) \equiv \theta_p(t) = 0 \qquad (3.15)$$

So those two phases are the same as that of the total seismic wave vector in the case of a polarization direction parallel to the survey line.
Using a cross-line, only reflected SH-waves are recorded, so that we have

$$x(t) \equiv z(t) \equiv 0$$
$$p_x(t) \equiv p_y(t) \equiv p_z(t) \equiv 0 \qquad (3.16)$$

$\varphi_p(t)$ and $\theta_p(t)$ become undefined for this case.

3.5.3. Anisotropy and the poynting vector

For the anisotropic case, whatever the polarization direction (except for, when it is normal or parallel to a plane of symmetry), all the three-components traces are non null traces, as are $p_x(t)$, $p_y(t)$, $p_z(t)$.
Figure 3.4a, b, and c show those attributes, respectively, obtained using seismograms recorded from model 2 with 75 m offset and a

shear source oriented South-North, parallel to line 3 (see Figure 2.2). each Figure contains 5 traces computed from each of the 5 three-component stations distributed over the semi-circle. Each trace reproduces the reflected events coming from each interface. Mode conversions are easily evidenced, particularly in trace 3 of Figure 3.4b. However they are highly attenuated in trace 3 of Figure 3.4a. and completely extinguished in Figure 34c.

Whether a cross-line or an in-line source is used, traces 1 and 3 in Figure 3.4c. representing $p_z(t)$ do not have P-wave and SV- to P-wave converted modes (trace 1 is computed from a cross-line source and trace 3 is from an in-line source). This situation corresponds to when one of the the axis of the horizontal receivers is parallel to the source orientation.

The computed reflected signal of $p_z(t)$ from the shale/sandstone interface is distorted compared to the original one from the seismogram; the split wavelets in $p_z(t)$ are highly enhanced for a shear source polarized parallel to survey line (trace 3 of $p_z(t)$).

Figure 3.5a, b shows the apparent phase azimuth of the poynting vector and its eccentricity, respectively. From those, attributes information about anisotropy is difficult to be extracted.

3.6 COMPLEX TRACE ANALYSIS

A seismic trace $f(t)$ is considered as the real part of an analytical signal or complex trace defined as

$$F(t) = f(t) + j\, f^*(t) \qquad (3.17)$$

$f^*(t)$ is called conjugate or imaginary component and j is the complex number.

$f^*(t)$ may be computed using the discrete form of Hilbert transform

$$f^*(t) = \sum_{-\infty}^{=\infty} f(t - n\Delta t)\frac{1 - e^{i\pi n}}{n} \qquad (3.18)$$

Where Δt is the sample interval and $f(t)$ is the real part.
(Taner et al., 1979) used this definition and computed the following attributes for conventional P-waves seismic data.

$$|F(t)| = \left[f^2(t) + f^{*2}(t)\right]^{1/2}$$
$$\theta(t) = \tan^{-1}\left[\frac{f^*(t)}{f(t)}\right] \qquad (3.19)$$

Equations 3.18 are the reflection strength and the instantaneous phase, respectively. These attributes have been computed and their plots displayed in a color-encoded manner by Taner et al, 1979, which helps an interpreter see their interrelationships and spatial changes. For example, high reflection strength is often associated with major lithological changes between adjacent rock layers. Lateral variation in bed thicknesses produce gradual changes in reflection strength. High reflection strength is also associated with gas accumulation.

Instantaneous phase often makes weak coherent events clearer; also phase displays are effective in showing discontinuities, faults, pinchout and events with different dip attitudes, which interfere with each other. (Taner et al., 1979).
The complex seismic trace and its attributes of either the radial or the transverse components may be computed in the same manner as, Taner, may help in correlating between SH-events and their P-waves counterparts, since this task has always proved doubtful and difficult.
In the past (Winterstein, 1986) only processing steps such as band-pass filtering have been used to enhance similarities between P-waves and SH-wave sections. The same author also used the ratio v_p / v_s for establishing event correlations. Using both P- and SH-

wave attributes may be of real importance in the contribution of identifying the same events or features on each separate seismic section.

Figure 3.6a shows the radial and the transverse components (traces 1 and 2) with their imaginary parts, (traces 3 and 4), respectively. Figure 3.6b represents the instantaneous phases of the complex radial and transverse, respectively. The real traces and their imaginary parts are similar, except for the scale. Imaginary parts present lower amplitudes. Consequently, the instantaneous phases are expected to be different (they are similar within the reflected waveforms) from each other and different from the azimuth angle, so they may not be appropriate in assessing anisotropy.

3.7. DISCUSSION AND CONCLUSION

The assessment of anisotropy from the new seismic attributes is possible, specifically, the azimuth angle may be used to identify the principal axes of anisotropy where the experimental results have shown that this angle varies in a constant form from the direction of the crack strike (relative to the survey line) to the direction of the normal to crack strike when it is evaluated within the composite wavelet containing the two split shear waves. Color codes should be used to facilitate reading the apparent phase azimuth angle and correlating events with the same polarization direction (Taner et al., 1979). However, for more stability, as it is shown in Chapter 5, the covariance matrix should be used to compute the azimuth angle and the eccentricity.

By using equations (3.6) it is possible to construct a filter which will attenuates P-wave energy in the horizontal components. This filter can be implimented for practical use in the processing of three-component data generated by explosive or vibroseis sources.

The instantaneous phase angle and the instantaneous reflection strength of the horizontal components may be useful for correlating seismic events present in both P-wave and S-wave

selsmic sections, but the shear data should be processed (separation of the split shear waves) prior to any correlation. Attributes computed from the poynting vector have shown no practical use, and even more expensive to compute, as convolution is needed to compute the imaginary parts of the horizontal components through Hilbet transform.

Figure 3.1. The wave vector in a spherical coordinate system. φ is the apparent azimuth and θ is the eccentricity. x(t), y(t) and z(t) are the velocity displacements recorded by the radial, the transverse and thevertical components, respectively. After Benhama et al, 1988.

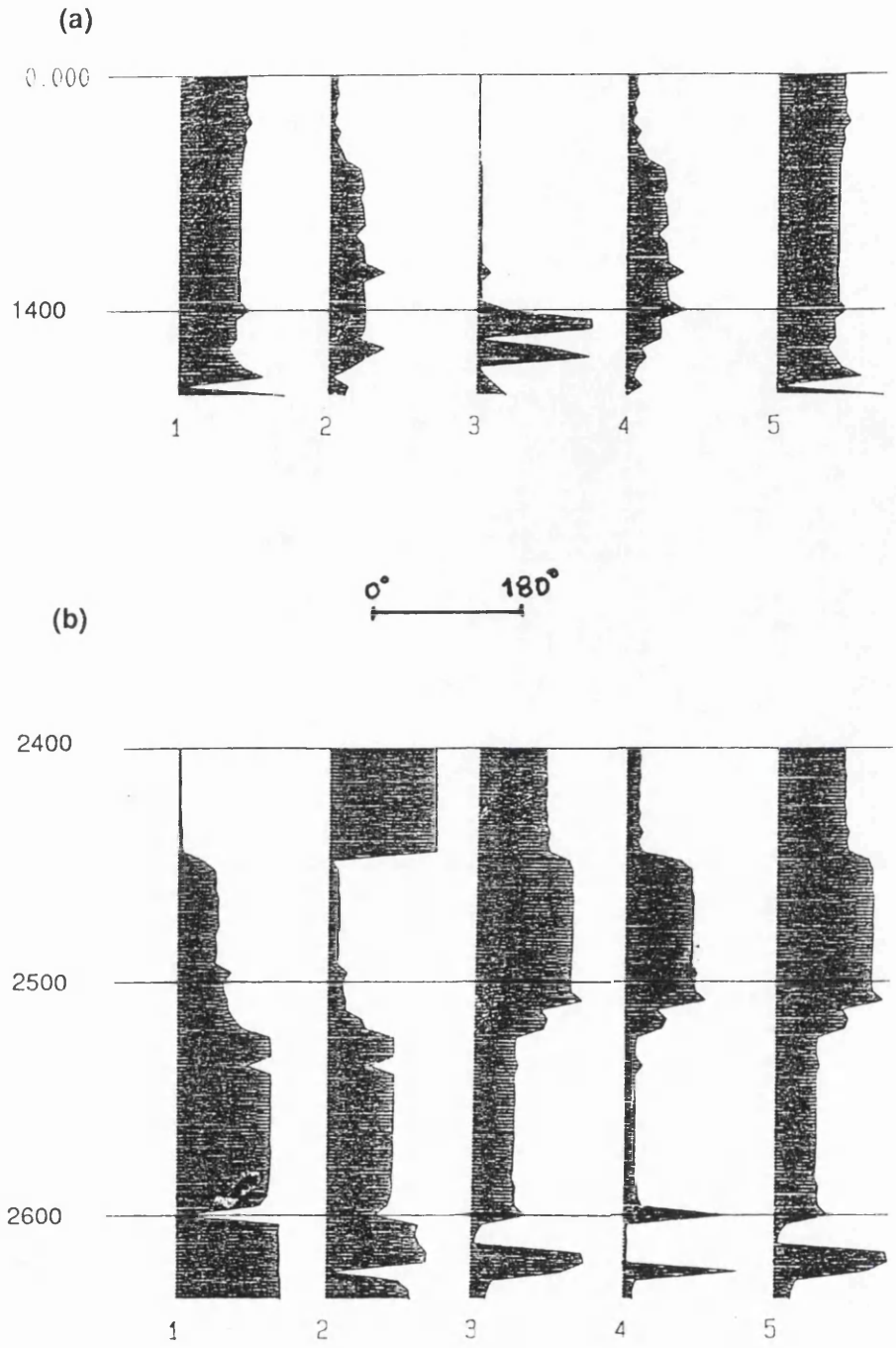

Figure 3.2. (a) and (b) are the apparent azimuth computed within windows 1300-1440 msec. and 2400-2640 msec, respectively, using a shear source parallel to survey line 3. The former window contains the reflected wavelet from shale/sandstone interface and the latter one from the sandstone/Limestone interface. Each Figure contains 5 traces, each one computed from each of the 5 equi-spaced three-components of the circular receiver array for investigating the variation of this attribute with source orientation. Traces 1 to 5 are from stations 1 to 5 (see Figure 2.2). The azimuth angle gives the direction of anisotropy axes relative to the survey line and 1mm corresponds 10 degrees

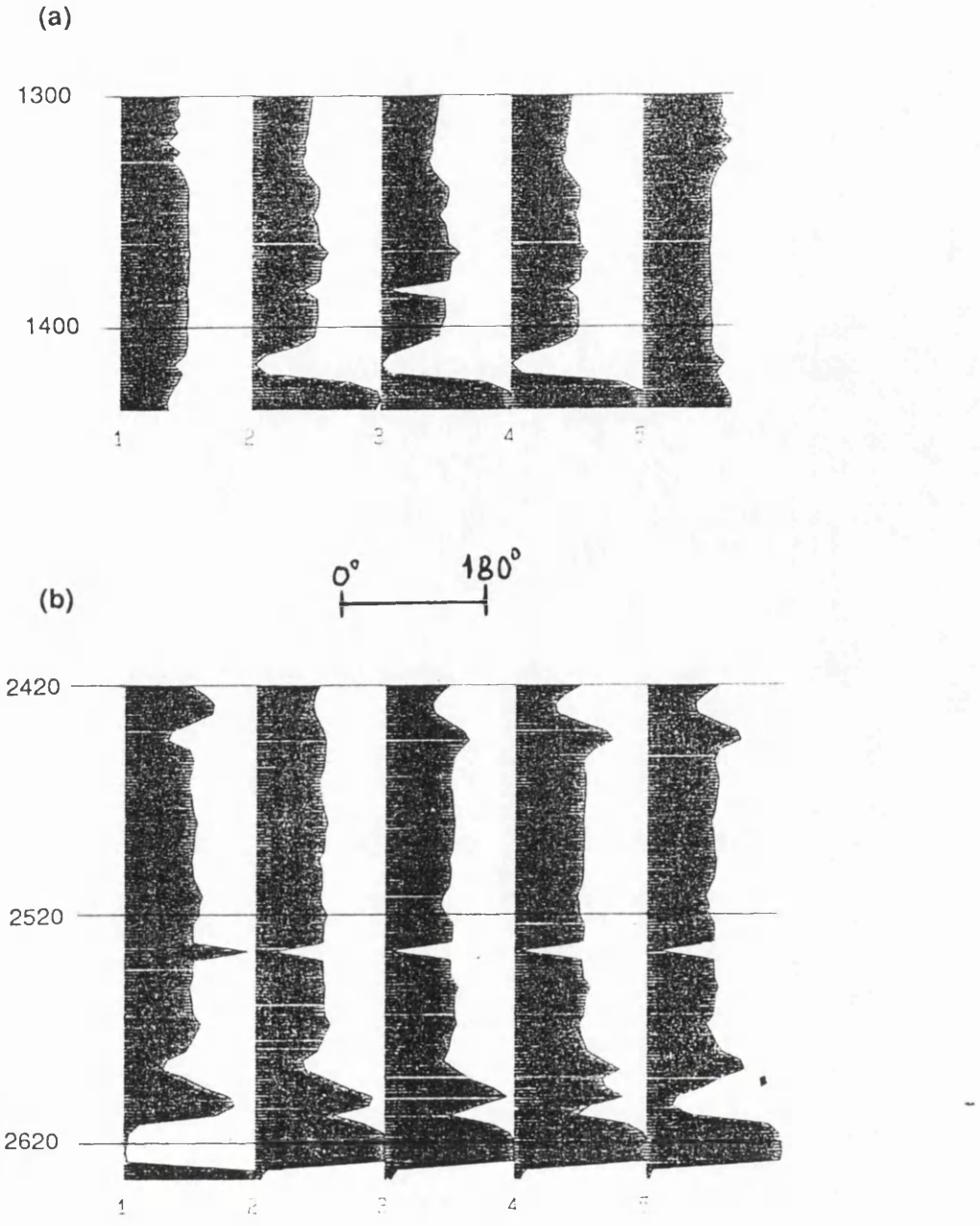

Figure 3.3. (a) and (b) is the eccentricity computed within the windows 1300-1440 msec. and 2420-2460 msec, respectively. This Figure is obtained in the same way as Figure 3.2.

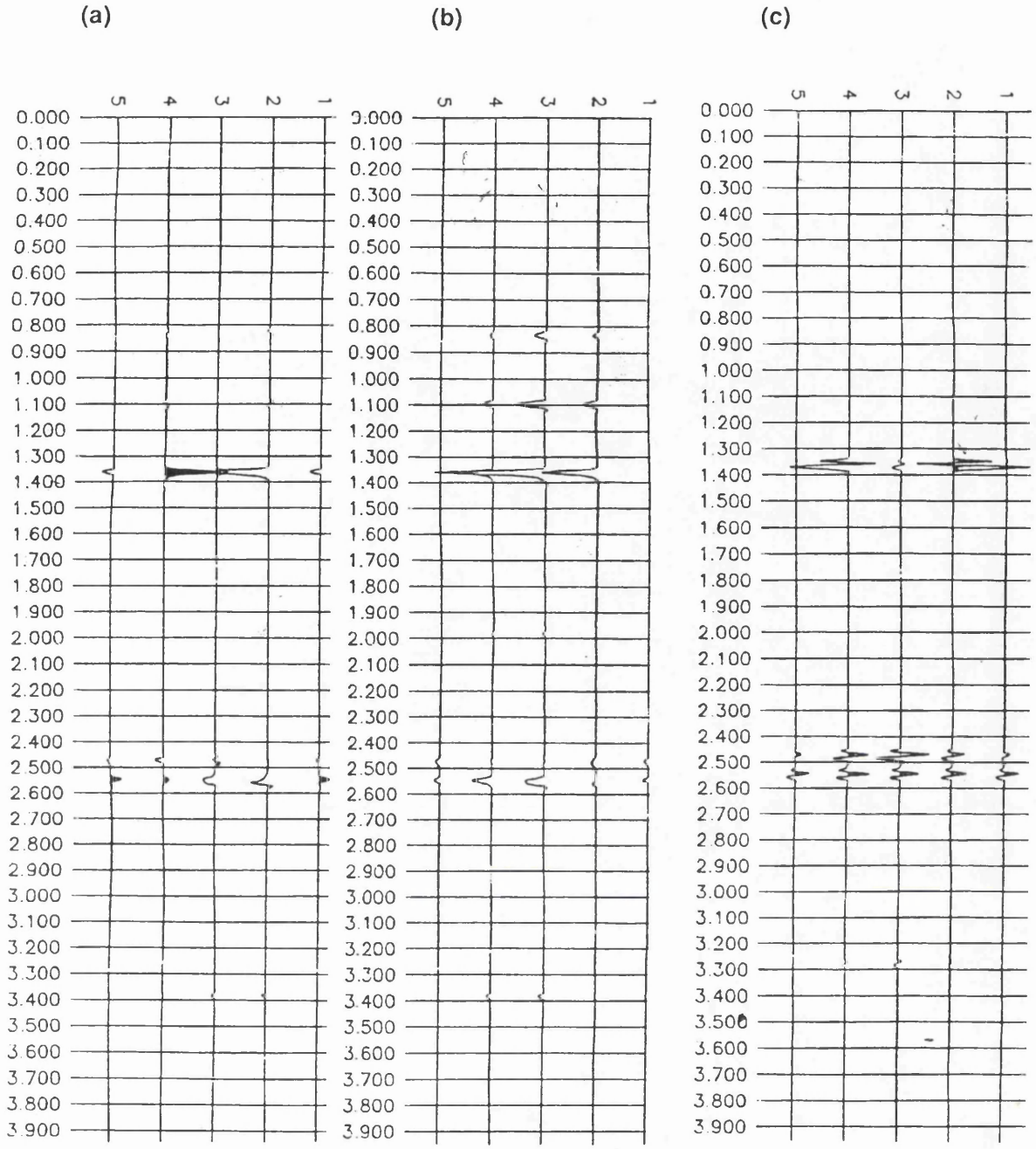

Figure 3.4. (a), (b) and (c) are the components of the poynting vector Px(t), Py(t) and Pz(t), respectively. These are computed from seismograms recorded from model 2. A shear source oriented parallel to line 3 has been used. Each Figure contains 5 traces, each one is computed from each of the 5 three-component receivers of the half-circular array of radius 75 m.

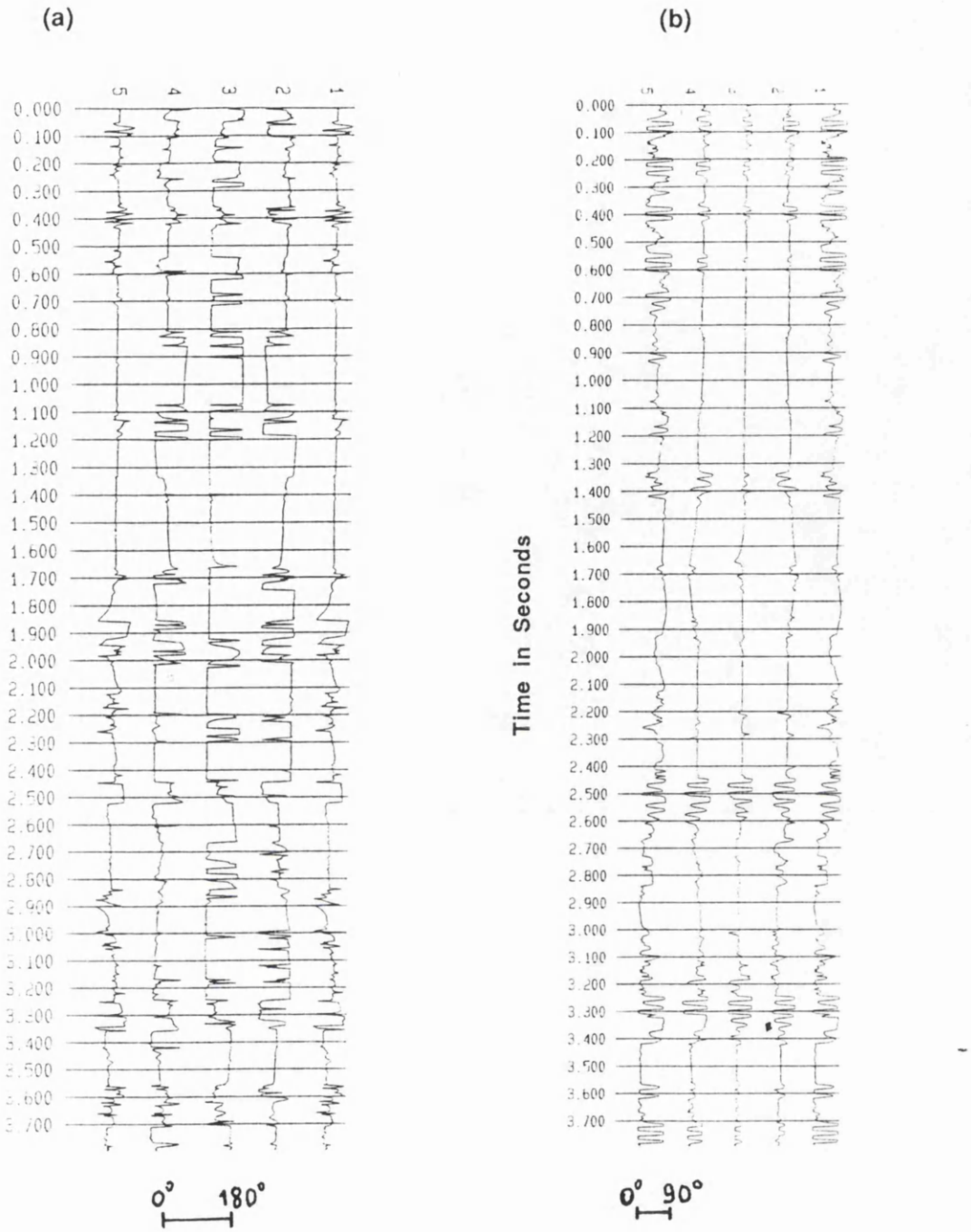

Figure 3.5. (a) apparent phase azimuth, and (b) the eccentricity of the poynting vector. This Figure is obtained in the same way as Figure 3.2., except for, the attributes are computed over the whole trace. It is difficult to extract any information about anisotropy from those attributes.

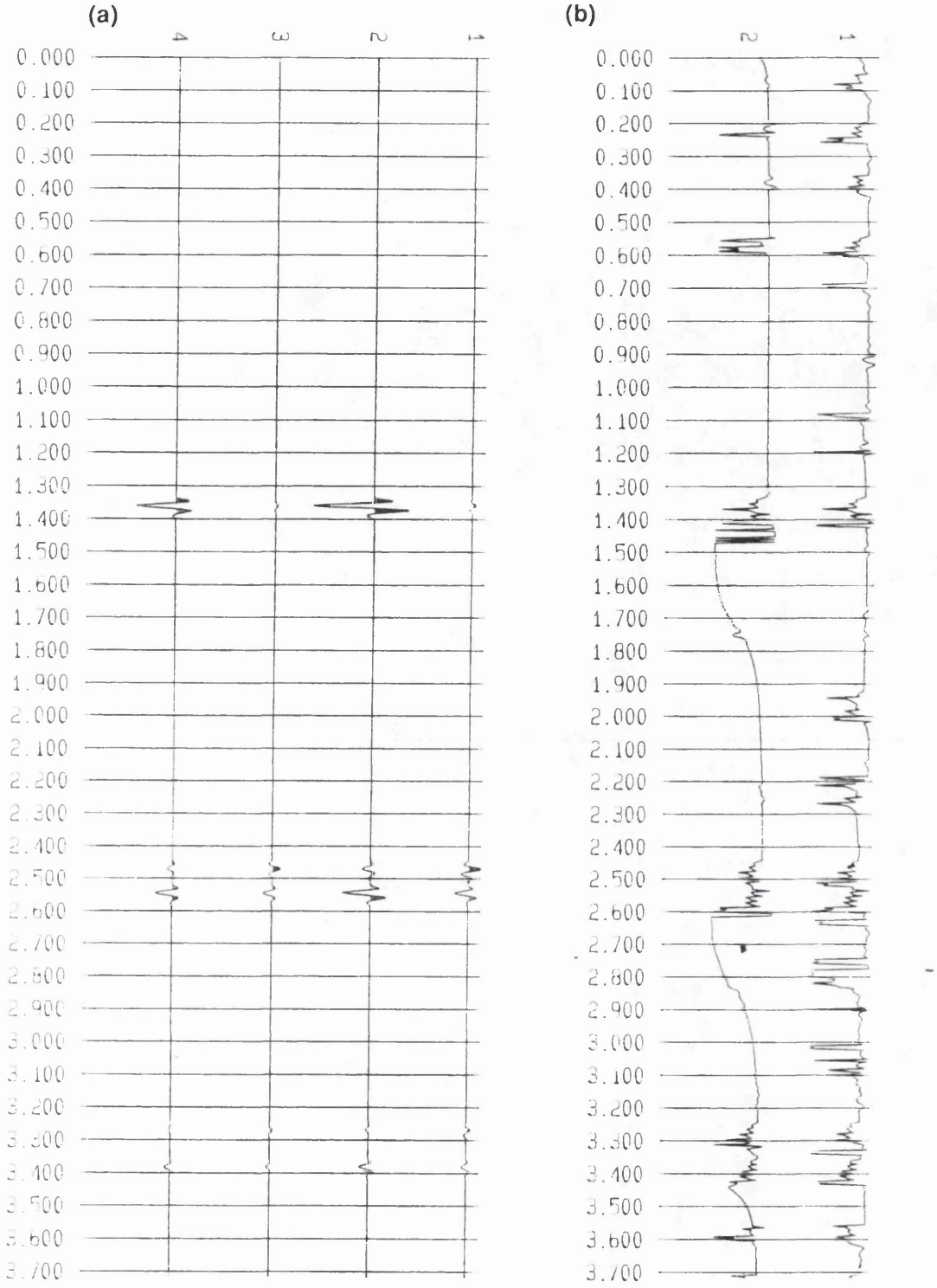

Figure 3.6. (a) 4 traces: (1) and (2), are the radial and the transverse components recorded at 75 m offset computed from a cross-line source oriented in the direction of survey line 3. (3) and (4), are their imaginary parts, respectively. (b) plots of the instantaneous phases of the complex radial and the complex transverse, respectively

CHAPTER 4

Energy of the trace and Anisotropy: Synthetic modelling.

SUMMARY

The horizontal components from three-component seismic reflection data are rotated about the vertical axis by small angular increments to simulate the trace of a radial geophone directed an angle θ from the survey line. The energy of this trace is computed using a zero lag auto-correlation function over an appropriate window after each rotation increment. The extrema of the energy as a function of rotation angle will coincide with the axis of anisotropy if the shear wave data are split. Otherwise the extrema will coincide with the direction of polarization of the source. Theoretical considerations of the technique are presented testing various source orientations and offsets using synthetic seismograms; demonstrating the possible use of this method in investigating anisotropy. The fully automated technique with new anisotropy attributes is presented in Chapter 5.

4.1. INTRODUCTION

The recent studies have shown that azimuthal anisotropy may have important effects on seismic shear wave data. Such effects are discussed for VSP data by Crampin (1985), and reflection shear wave data acquired at an angle to one of the principal axis of an azimuthally anisotropic medium may be improved if the data are rotated by an appropriate angle toward the direction of the crack strike or the normal to it. This angle is defined as the angle between the direction of the crack strike defining the crack plane orientation and the survey line. Alford (1986) and Thomsen (1988) derived similar formulas for the computation of this angle using

shear-wave data recorded from two orthogonal shear sources at the same shotpoint, one polarized in-line and the other polarized normal to the survey line. Also, Igel & Crampin (1990), used different source orientations for extracting shear wave polarizations. Other methods for determining the principal directions of anisotropy apply to earthquake data or to vertical seismic profiling (VSP) data (see Macbeth & Crampin, 1991 for a review).

In this chapter a new technique is presented by the author based on the computation of the energy of a rotated trace using data from only one shear source, is investigated. The method is tested using different source orientations, offsets and crack strike directions from synthetic data as described below. The automation of the technique is presented in chapter 5.

4.2. EXTREMA OF THE ENERGY OF THE TRACE

Alford's method is the most commonly used technique in processing shear wave data, particularly in VSP surveys, (Winterstein & Meadow, 1991a, b). The method involves the use of stacked data recorded from two shear sources with mutual orthogonal polarizations. The rotation angle which minimizes the energy detected on the seismograms constituting the off-diagonal stacks (in-line source recorded on cross-line receivers, and vice versa), and focuses energy onto the principal diagonal stacks, is considered the optimum position.

The technique we are presenting, may be used to automatically separate the split shear waves and to extract the polarization direction of the leading shear wave, i.e., the angle between the crack strike and the survey line, and the time delay, as it will be demonstrated in this chapter and Chapter 5 .

The method described here involves a simple rotation of the horizontal components about the vertical axis to simulate the traces recorded by a radial component geophone directed at an

angle θ_r from the seismic line. The technique may be illustrated by considering an in-line shear source consisting of a unit impulse over an anisotropic medium in which the principal axis or crack strike makes an angle θ_c with respect to the source orientation as illustrated in Figure 4.1.

For a unit shear impulse with an orientation parallel to the x axis of Figure 4.1 and travelling through the anisotropic medium, the radial and the transverse component of the fast (R_f, T_f) and slow (R_s, T_s) waves will be:

$$\begin{bmatrix} R_f \\ T_s \end{bmatrix} = \begin{bmatrix} \cos^2 \theta_c \\ \cos \theta_c \sin \theta_c \end{bmatrix} \tag{4.1}$$

and

$$\begin{bmatrix} R_s \\ T_s \end{bmatrix} = \begin{bmatrix} \sin^2 \theta_c \\ -\cos \theta_c \sin \theta_c \end{bmatrix} \tag{4.2}$$

Where θ_c is the angle between the axis or between the unit shear impulse orientation and the crack strike. We can apply a counter-clockwise rotation by an angle θ_r to both horizontal components about the vertical axis, as follows:

$$\begin{bmatrix} R_f' \\ T_f' \end{bmatrix} = \begin{bmatrix} \cos\theta_r & \sin\theta_r \\ -\sin\theta_r & \cos\theta_r \end{bmatrix} \begin{bmatrix} \cos^2 \theta_c \\ \cos\theta_c \sin\theta_c \end{bmatrix} \tag{4.3}$$

and

$$\begin{bmatrix} R_s' \\ T_s' \end{bmatrix} = \begin{bmatrix} \cos \theta_r & \sin \theta_r \\ -\sin \theta_r & \cos \theta_r \end{bmatrix} \begin{bmatrix} \sin^2 \theta_c \\ -\cos \theta_c \sin \theta_c \end{bmatrix} \tag{4.4}$$

The energy of the rotated radial component is defined as:

$$E_r = [R_f']^2 + [R_s']^2 \qquad (4.5)$$

and is found over a window containing the fast and the slow components. The energy may be calculated from the above equations as a function of θ_r and θ_c as:

$$E_r = \cos^2 \theta_c \cos^2(\theta_c - \theta_r) + \sin^2 \theta_c \sin^2(\theta_c - \theta_r) \qquad (4.6)$$

Computing the derivative with respect to θ_r, to find where the function has its extrema we get:

$$\frac{dE_r}{d\theta_r} = (\cos^2 \theta_c - \sin^2 \theta_c)[2\cos(\theta_c - \theta_r)\sin(\theta_c - \theta_r)] \qquad (4.7)$$

It is seen that

$$\frac{dE_r}{d\theta_r} = 0, \text{ if } \theta_r = \theta_c;\ \theta_r = \theta_c - \pi/2;\ \theta_r = \theta_c - \pi;\ \theta_c - 3\pi/2, \text{ etc...}$$

or $\cos^2 \theta_c = \sin^2 \theta_c \Rightarrow \theta_c = \pi/4$

When the energy of the rotated radial is found over a window containing only one of the split shear waves, for example the waveform of the fast shear, it can be written as:

$$E_r = (R_f')^2 = (\cos \theta_r \cos^2 \theta_c + \sin \theta_r \cos \theta_c \sin \theta_c)^2 \qquad (4.8)$$

Computing again its derivative with respect to θ_r as before to find its extrema, we get.

$$\frac{dE}{d\theta_r} = \sin 2(\theta_c - \theta_r) \qquad (4.9)$$

If $\theta_r = \theta_c$ then $\frac{dE}{d\theta_r} = 0$ (4.10)

Hence, the function E_r will in both cases have extrema when θ_r coincide with an axis of anisotropy. However, if the window chosen contains the two split shear waveforms, as it might always be the case, since the delay between the fast and the slow one could be very small, the condition $(\cos^2 \theta_c = \sin^2 \theta_c)$ shows that the method will not work in the special case where $\theta_c = \pi / 4$.

4.3. CALCULATION OF THE ENERGY OF THE TRACE

It is well known that the cross-correlation function of the function $f(t)$ and $g(t)$ is given by

$$\phi_{12}(\tau) = \int_{-\infty}^{+\infty} f(t) g(t + \tau) dt \quad (4.11)$$

When the cross-correlation becomes the autocorrelation of, that is

$$\phi_{11}(\tau) = \int_{-\infty}^{+\infty} f(t) f(t + \tau) dt \quad (4.12)$$

When $\tau = 0$ the equation becomes

$$\phi_{11}(0) = \int_{-\infty}^{+\infty} |f(t)|^2 dt \quad (4.13)$$

$\phi_{11}(0)$ is the zero-lag autocorrelation function and, in this case it is identical to E_r, $(\phi_{11}(0) = E_r)$.

In practice the signal will not be an impulse but a split wavelet, rotated into a trace f(t). The energy of the trace E_r, is computed

from the zero-lag auto-correlation function, which is written in the following discrete form:

$$E_T = \sum_{t=m}^{n} |f_t|^2 \qquad (4.14)$$

where t is the summation index from the start of the window on to the end n.

In exploration seismology f(t) represents the particle displacement velocity, recorded either by the vertical or the horizontal components, so that $|f(t)|^2$ is proportional to the energy. Hence, E_T is called the energy of f(t) or the energy of the trace. In the experimental work described below, the quantity (4.14) has been computed within the windows considered (m,n) after each increment (5° being the increment used for search) of rotation of the data for a given shear source of known orientation.

The total energy E_T is defined as

$$E_T = \sum_{i=1}^{3} e_i \quad , \quad i = 1, 2, 3 \text{ or, } i=1, 2. \qquad (4.15)$$

depending whether using data from three components or the data from two only..

where e_i, is the energy of the trace of each of the orthogonal unrotated components over the appropriate window. The energy percentage is computed as the ratio of the energy of the corresponding rotated component to the total energy multiplied by 100%, i.e. $(E_T / E_T) \times 100\%$. E_T is a constant value, i.e. does not depend upon the rotation angle. In the following, the total energy is computed using data from the horizontal components.

4.4. ENERGY PERCENTAGE AND PARTICLE MOTION

Consider two samples R_i and T_i from the horizontal components,

the radial and the transverse, respectively. Their corresponding amplitudes A_r are A_T and . Rotating the axes of the horizontal components so that the rotated radial axis coincides with the direction of maximum energy. The amplitudes of the samples become A_R and A_T, where R and T indicate the new rotated axes. The maximum E_{max} and the minimum E_{min} values of the energy of the rotated traces are directly proportional to the square of A_R and A_T , respectively.

In terms of energy percentage, E_{max} and E_{min} may be expressed as

$$E_{max} + E_{min} = 1 \tag{4.16}$$

Considering the rotated amplitudes, equation (4.16) may be rewritten as

$$A_R^2 + A_T^2 = 1 \tag{4.17}$$

Equation (4.17) is that of an ellipse with the major and the minor axes oriented toward the direction of maximum and minimum energy. Consequently, the root of maximum and minimum energy may be taken as directly proportional to the length of the major and the minor axes of the ellipse, respectively.

From either equation (4.16) or (4.17) it is seen that if the minimum energy is zero the motion is rectilinear along the direction of maximum energy; it is circular if $E_{max} = E_{min}$.

4.5. MODEL

The geological model is model 2 shown in Figure 2.1, representing a homogeneous anisotropic medium, simulating a sedimentary basin, with shale overlying two cracked media, sandstone and limestone, having the same crack orientation but different crack densities, above an isotropic granite half-space. The idea of the maximum

value of the energy of the rotated trace and its relation to the shear source orientation is applied to this model.

To generate synthetic data, the medium is excited by a horizontally polarized surface shear source directed along a desired orientation and having a dominant frequency of 25Hz. This generates a vertically propagating, linearly polarized plane wave, travelling through the medium and reflected back to the surface from each interface. The seismograms have been computed using the ANISEIS Package (see Chapter2). The record length of each seismogram is 4.0 sec, with three events coming from the interfaces separating the four media. The windows are at 1.3-1.5 sec, 2.4-2.7 sec and 3.2-3.5 sec. (Figure 2.3), each containing the waveform of a reflected event. The first window represents the reflected event from the shale/sandstone interface, the second from the sandstone/limestone interface and the third from the limestone/granite interface. Both last waveforms are composed of two split shear wavelets, the fast and the slow ones.

Three source orientations have been tested (Figure 4.2). These include a shear source polarized at 45° to the survey line (line 2), an in-line source, parallel to the survey line (line 1), and a cross-line source normal to line 1 (parallel to line 3) . Three offsets, 75 m, 150 m and 300 m have been used to investigate their effect on the energy of the trace relative to the source orientation and to the direction of the crack strike.

4.6. SYNTHETIC MODEL-RESULTS

4.6.1. Source polarized at 45° to the survey line

Survey line 2 (Figure 4.2) is 15° from the crack strike. The shear source orientation is in-line with line 1, i.e., at 45° to the the survey line and 30° to the crack strike. Beginning with a 75 m offset, the energy of the trace is computed as a function of rotation angle (Figure 4.3a) for the first window representing a PTL medium. The maximum is attained after a clockwise rotation by an

angle of 55° corresponding to a deviation of 10° from the source orientation and its energy percentage is 99.78%, $[(E_r / E_T) \times 100\%]$. The energy percentage in the rotated transverse component corresponding to the minimum value is 0.22%. It is seen from those values that there is no shear energy on the rotated transverse, since all the energy is transferred by the rotation process to the radial. This reveals a shear wave linearly polarized along the direction given by the maximum energy, i.e., 10° away from the source orientation. Note that only the un-normalized energy of the trace is displayed in the figures showing a polar plot of energy of the trace versus angle of rotation.

Considering the second window containing the event coming from the interface between sandstone and limestone, the maximum value of the energy of the trace is attained when the angle of a clockwise rotation is equal to 20°, as in Figure 4.3b. At this angle of rotation, the rotated axis of the radial geophone deviates only by 5° from the direction of the principal axis of anisotropy called the crack strike. The energy percentage of the maximum and the minimum values correspond to 61.74% and to 38.26%, respectively. The increase of the minimum value relative to the first window, where there are no cracks, is due to the splitting of energy along the anisotropic axes. Similar results have been obtained for the third window containing the event reflected from the interface separating cracked limestone and the granite as half-space (Figure 4.3c). The similarity of those results is obvious, since the two layers, sandstone and limestone have the same anisotropic axes.

The maximum value of the energy of the trace for the first window corresponding to 300 m offset (Figure 4.3d) is attained when the angle of rotation is 60° and the energy percentage of the maximum and the minimum values are 81.17% and 18.83%, respectively. The results are significantly different from those obtained from the 75 m offset. The energy percentage of the maximum value has decreased from 99.78% to 81.17%, and that of the minimum has increased from 0.22 to 18.83%. This is related to

the larger angle of incidence of the wave, so that the coupling between SH- and SV- waves increases at greater offset for this source orientation, leading to an increase of ellipticity due to the presence of two shear waves orthogonally polarized, as it is clearly seen by comparing Figure 4.3a to Figure 4.3d.

The deviation of the maximum value of the energy from the source direction is the result of the rotation of the direction of polarization with offset as a result of varying amplitude reflection coefficients, from the shale/sandstone interface, with increasing angle of incidence (Liu & Crampin, 1990), for any incident source polarization that is not pure SV or pure SH. However, as it is expected, except for this source orientation, this deviation for a cross-line or an in-line is never larger than a single increment of 5°, as it is demonstrated in the following examples.

For the remaining two windows (Fig. 4.3e, f), the results are the same whether using a 75 m, 150 m or 300 m offset. The deviation of the maximum value by 5° from the the direction of the crack strike is simply due to the increment used for search.

4.6.2. In-line source.

In this experiment, the crack strike and the survey line, line 1 (Figure 4.2), are 30° away from each other. For the first window the maximum value of the energy of the trace is achieved when the rotated axis of the radial component makes an angle of 5° with the source direction (Fig. 4.4a) and its energy percentage is 99.99% while that of the minimum value is nearly 0.01%, evidencing a linearly polarized shear wave along that direction.

The maximum and the minimum value of the energy of the trace for the remaining two windows (Figure 4.4b, c) are achieved after both axes of the horizontal components have been rotated counter-clockwise by 35°. Hence, again the maximum value of the energy of the trace is attained when the axis of the radial deviates by 5° from the crack strike and its energy percentage is 70.56% , while

that of the minimum is 29.44% evidencing an elliptical motion due the presence of both split shear waves

Using a 300 m offset with the same source orientation, the results obtained are identical to those for 75 m offset for each window considered (Figure 4.4d, e, f).

4.6.3. Cross-line source.

The survey line is line 1, and the source orientation is coincident with line 3 in Figure 4.2. For all offsets, the maximum value of the energy of the trace corresponding to the first window is achieved when the rotated axis of the radial component has been rotated counter-clockwise by 85°, i.e. the angle between the axis of the radial and the source orientation is reduced to 5° as shown in Figure 4.5a. Also the energy percentage of its maximum and minimum values are 99.93% and 0.07%, respectively. This means that for this type of anisotropy nearly all the energy is recorded by the transverse component when a cross-line source is used. The coupling between the two shear waves is not significant at zero offset and the motion is linear. For the remaining two windows the data have been rotated counterclockwise and the maximum value is found when the rotated axis of the radial deviates by 5° from the normal to the crack strike, corresponding to an angle of rotation of 115°, (Figure 4.5b, c, d, e, f). Their corresponding energy percentages are 76.85% and 23.15%, respectively showing an elliptical motion.

4.7. ENERGY OF THE TRACE AND CRACK ORIENTATION

The crack-plane of model 2 has been rotated counterclockwise from East to North by 0°, 22,5°, 45°, 67.5° and 90°, respectively. The calculation is carried out only for the record time window 2.4-2.7 sec, since the sandstone and limestone may be considered as a single layer having the same crack orientation, although having

different crack densities. Three three-component stations with 75 m, 150 m and 300 m have been set along a survey line oriented East-West, as seen in Figure 4.6. Two mutually orthogonal shear sources, are tested, one oriented East-West (in-line) and the other North-South (cross-line).

When the source orientation is normal to the crack-plane or parallel to it there is no splitting, and the shear wave generated is either a pure SH- or a pure SV-wave. Consequently, when the crack strike is coincident with the source orientation and is taken as the survey line, a pure SV-wave is generated with no coupling between it and the other shear wave, so only mode conversions occur. Hence, no motion is recorded by the transverse component and the radial component records the faster shear wave. However, when the crack strike is normal to the source orientation, the transverse component records the slower one. These two situations correspond to 0° (Figure 4.6) and 90° (Figure 4.7) of the crack-plane orientation, respectively and the maximum value of the energy of the trace is computed when the axis of the radial is rotated so as to coincide with the source orientation.

When the source orientation is away from the crack strike, say by 22.5° and 67.5°, we fall into the situations described earlier. The maximum value of the energy of the trace is attained when the rotated axis of the radial deviates by only a few degrees (less than or equal to 5°) from the crack strike or the normal to it, as illustrated in (Figure 4.6) and (Figure 4.7). Only when the shear source orientation is away from the crack strike by 45° does the maximum value deviate considerably from the crack strike or its normal. However, this is to be expected, as seen from the discussion in Section 4.2.

4.8. ENERGY PERCENTAGE AND PARTICLE MOTION

If the energy of the rotated trace is computed within a window containing, for example, the waveform of the fast shear, the

maximum value of the energy (or the minimum of it) is attained when the rotated radial axis coincides exactly with the direction of the crack strike (or the normal to it). The energy percentage corresponding to the maximum and the minimum values becomes equal to 100% and 0.0%, respectively. this is to be expected as it is seen from section 4.2.

Figure 4.8 shows a polar plot, energy of the trace versus angle of rotation in case of an in-line source (Figures 4.8a, b, c.)with survey line 1 and a source polarized 45° to survey line 2 (Figures 4.8d, e, f.). The energy is computed within three windows, with data being rotated clockwise. A window containing two split shear waves and the two others contain the fast and the slower one, respectively.

From the polar plot Figures and the values of the energy percentages computed before, it becomes evident that the type of motion within any time window of a seismic trace may be easily described by the maximum and the minimum energy. The major and the minor axis of the ellipse may be taken as directly proportional to the square root of the two energy attributes. This is clearly seen that when the minimum correspond to 0.0% and the maximum is 100% the motion is linear; similarly, when both attributes are equal the motion is circular. The motion in Figure 4.8a is less elliptical than the motion in Figure 4.8b, as evidenced by the plots and their corresponding energy values.

4.9. SOURCE ORIENTATION AND ENERGY OF THE TRACE

The last results showed that, if there is a splitting the maximum energy of the rotated trace computed over a window containing the two waveforms gives either the direction of the fast or the slow shear wave; when there is no splitting, i.e., the generated shear energy is travelling (vertically) within an isotropic or azimuthally isotropic medium, the polarization direction given by the maximum value of the energy of the rotated trace may be that of the shear

source.

In this experiment, the computation of the energy of the trace over a window has been extended to the entire data length, the whole trace. Three shear sources have been tested. An in-line, a cross-line and the third one is oriented 45° to the survey line. The energy of the trace is computed over the entire trace for each shear source and every offset, 75 m, 150 m, 300 m. Figures 4.9, 4.10 and 4.11 show the graphical results. In the case of an in-line source the maximum value of the energy of the trace is attained when the angle of rotation deviates only by 10° from the polarization direction and the deviation is not offset dependent; for the cross-line source this maximum is attained when the axis of the rotated component coincides with the polarization direction of the shear source and there is no deviation for the considered offsets; for the shear source polarized 45° to the survey line the deviation is offset dependent.

When computing the energy of the trace after each rotation there is a transfer of energy from the fast to the slow shear wave or vice-versa so that, the energy of the trace containing those split shear waves remains constant for all rotations. Only the amplitude of the unsplit shear event increases or decreases as shown in Figure 4.12. This Figure shows trace 1 recorded by the transverse component using a shear source polarized 45° to the survey line, rotated 9 times (traces 2 to 10) by 10° increment. The amplitude of the event within the window 1.3-1.5 sec. decreases until a minimum and then increases again by reversing it polarity. This minimum is attained when the axis of the rotated transverse component deviates by 5° from the normal to the polarization direction of the shear source for 75 m offset.

From those experimental results an attempt has been made to estimate the shear energy released by an explosive source and possibly its polarization direction, especially the polarization directions given by the opposite shots of the technique of three holes. The case of BIRPS data has been studied in chapter 6.

4.10. DISCUSSION

When an in-line source is used, the maximum value of the energy of the trace for two windows representing a cracked medium is found when the rotated radial axis is parallel to the crack strike . Conversely, when a cross-line source is used, this maximum value is found when the rotated radial axis is normal to the crack strike. This is related to the position of the crack strike relative to the source orientation. The maximum of the energy of the trace will indicate either the crack strike direction or the normal to this direction, depending on which direction makes the smaller angle with the source orientation. So, we can say that whenever an in-line or a cross-line source is used it is possible to recover the anisotropic axes using the energy of the rotated trace, but the identification of fast and slow axes may be ambiguous. However, this ambiguity can be resolved after plotting the anisotropy attributes or automatically separating the split shear waves (Chapter 5).

The results obtained from this experiment are based on a model that is a mixture of two type of anisotropy: azimuthal isotropy (PTL) and azimuthal anisotropy (EDA-cracks). It is most likely that in the real earth PTL dominates near the surface, since at the free surface, the vertical stress is small, and hence the fractures at shallow depth are likely to be horizontal, behaving as a PTL medium. At greater depths, the vertical stress is larger than the minimum horizontal stress, so the cracks and the fractures tend to be vertical, striking perpendicular to the direction of minimum horizontal stress, to give an EDA type anisotropy.

Those results are obtained using noise free synthetic data. Real data are always contaminated by noise of different types. However this technique is based on squaring the amplitudes of both signal and noise. Consequently, if seismic data is of good quality, having a reasonable signal to noise ratio, the noise may not undermine the

robustness of the technique, as a better signal to noise ratio is obtained by weighting each sample by its energy. Multiples in case of of surface recorded data might be a problem, but they can be attenuated at the early stage of processing if recognized.

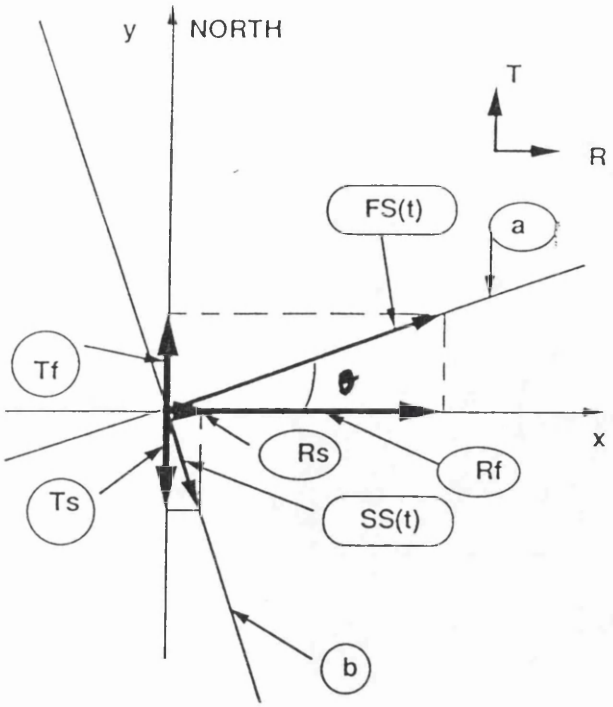

Figure 4.1. The axes (a) and (b) are the anisotropic axes; FS(t) and SS(t) are the two split shear waves, the fast and the slow , respectively, of the unit impulse (parallel to axis x); angle θ is the angle of the crack strike, i.e. the angle between the survey line (direction x) and axis (a), defining the crack strike; Rf, Tf, Rs and Ts represent the projections of the two split shear waves on both the radial and the transverse geophone; the arrows R and T give the direction of the radial and the transverse geophone, respectively.

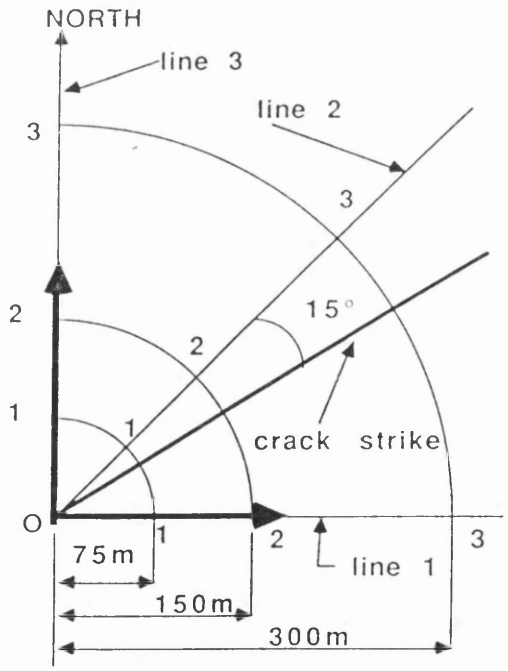

Figure 4.2. (a) Line and source polarization configuration for which the models were computed. The stations numbered are three component receivers. All the receivers are equidistantly distributed over the three concentric circles with radii 75 m, 150 m and 300 m. The shear source is at the centre of the circle (point O). Line 1 is oriented East-West and line 3 South-North. The large arrows indicate the source orientations.

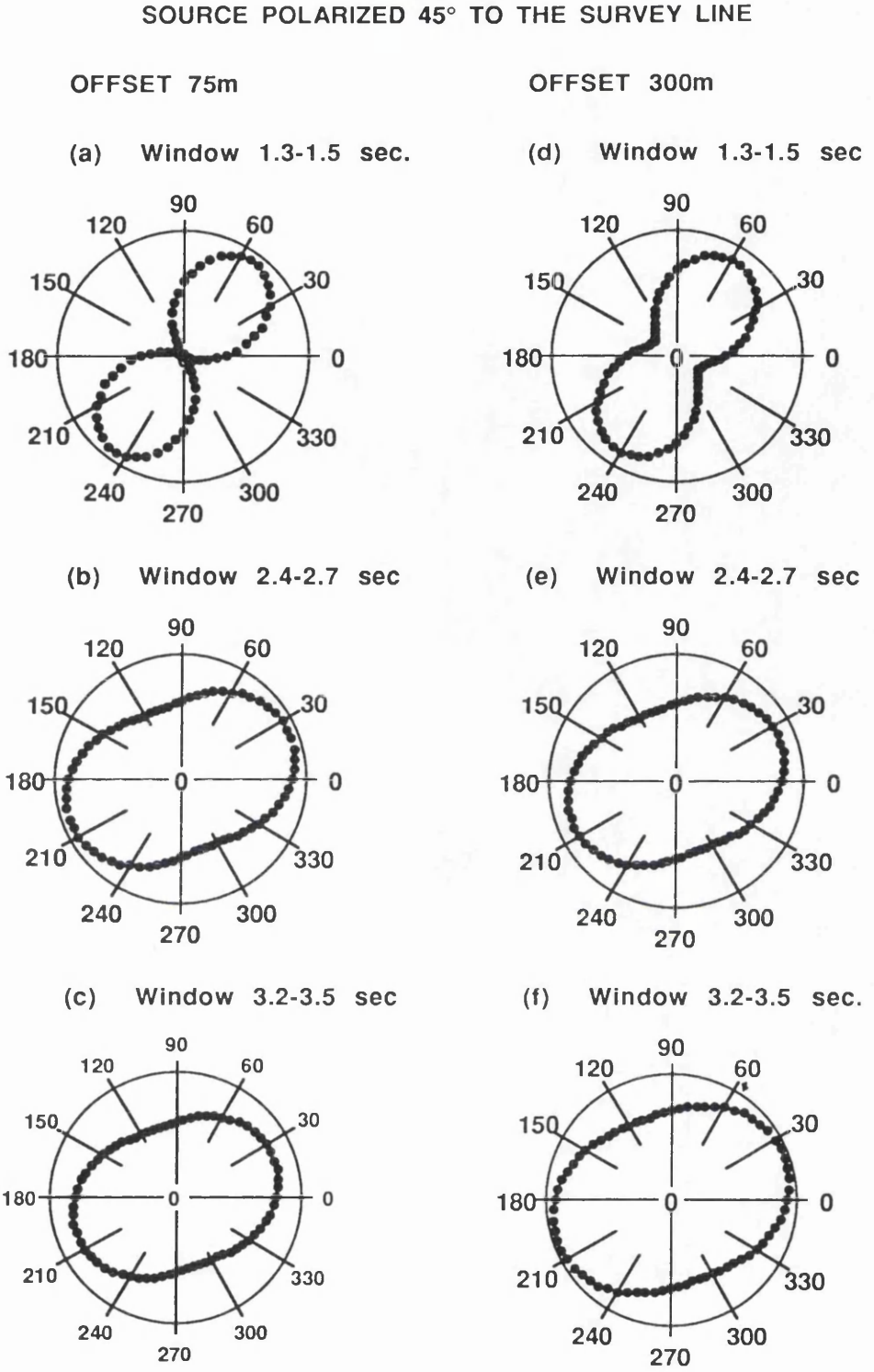

Figure 4.3. Energy of the rotated trace versus angle of rotation obtained using a shear source polarized at 45° to the survey line and with crack strike at 15° to the survey line. a), b) and c) are from 75 m offset corresponding to windows1.3-1.5 sec, 2.4-2.7 and 3.2-3.5 sec, respectively; d), e) and f) obtained from 300 m offset and for the same windows. In all the Figures showing the energy of the trace versus angle of rotation, the values shown on the vertical axis are not normalized. They are a scaled version of the computed values of the energy of the trace.

IN-LINE SOURCE

OFFSET 75m

(a) Window 1.3-1.5 sec.

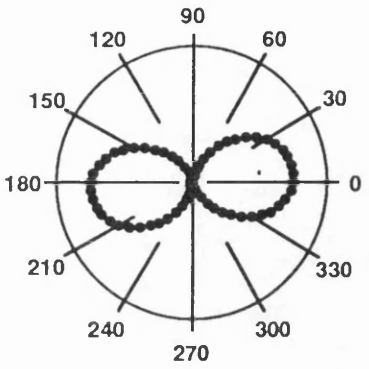

(b) Window 2.4-2.7 sec.

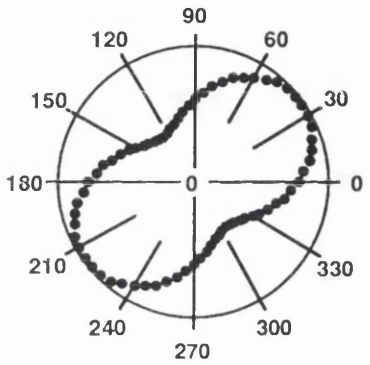

(c) Window 3.2-3.7 sec

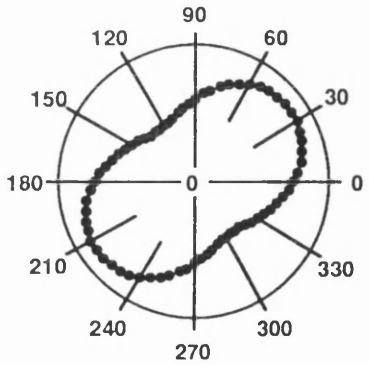

OFFSET 300m

(d) Window 1.3-1.5 sec.

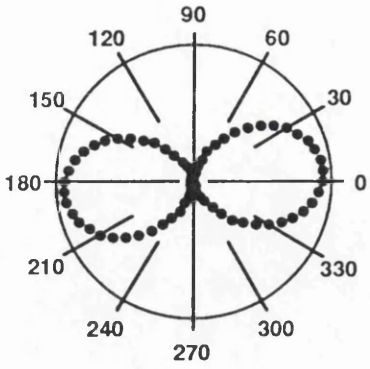

(e) Window 2.4-2.7 sec.

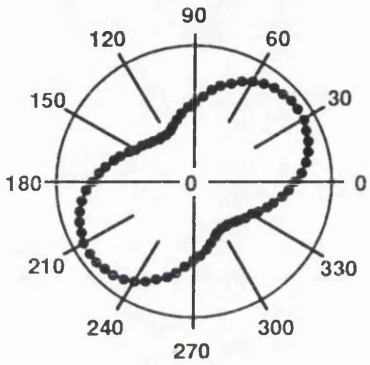

(f) Window 3.2-3.5 sec.

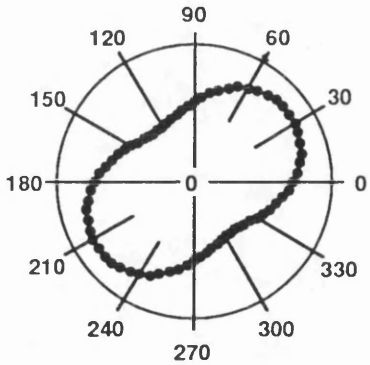

Figure 4.4. Similar to Figure 4.3., but an in-line shear source has been used for this case.

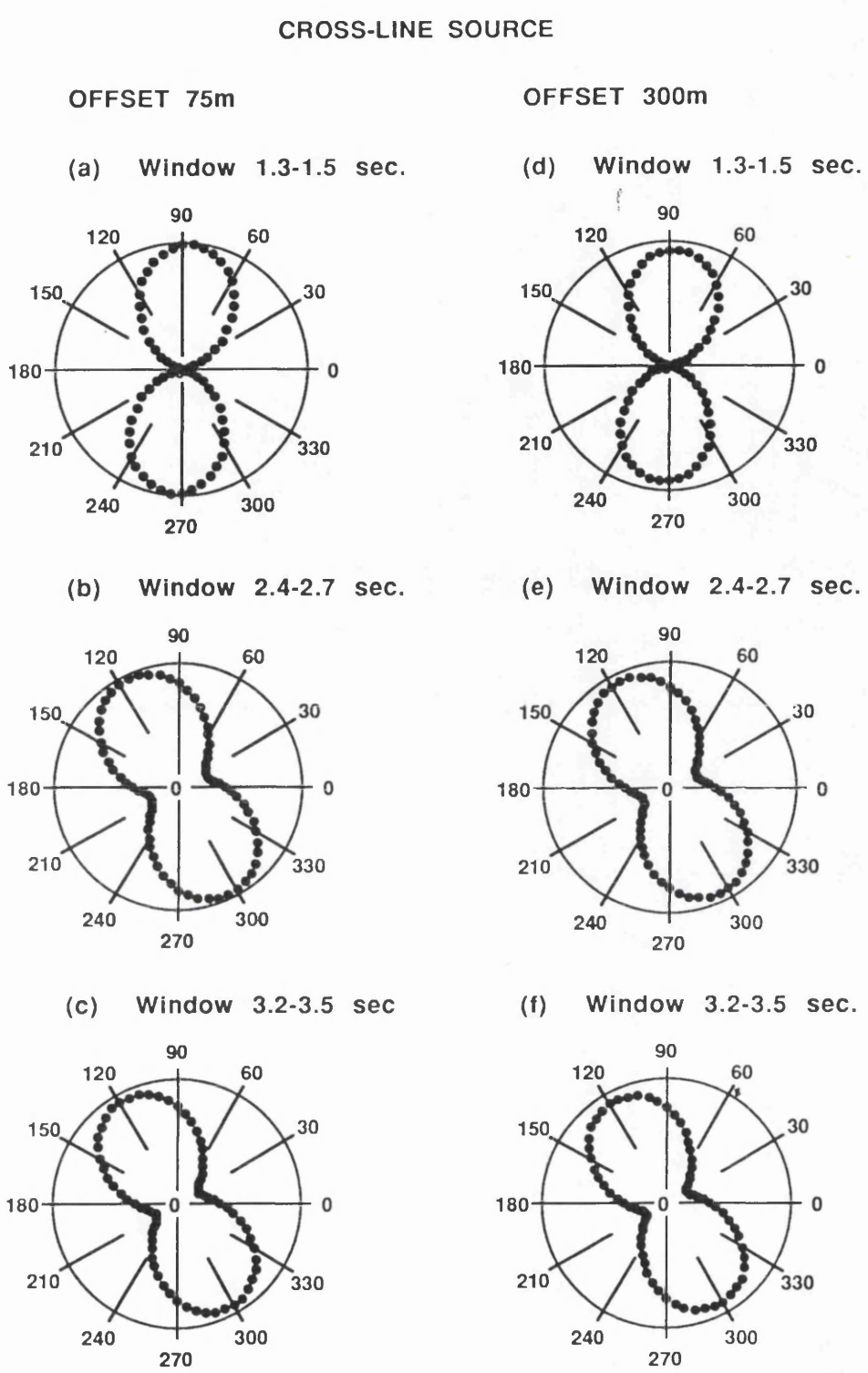

Figure 4.5. Similar to Figure 4.3., but a cross-line shear source has been used. The maximum value of the energy of the trace indicates the normal to the strike.

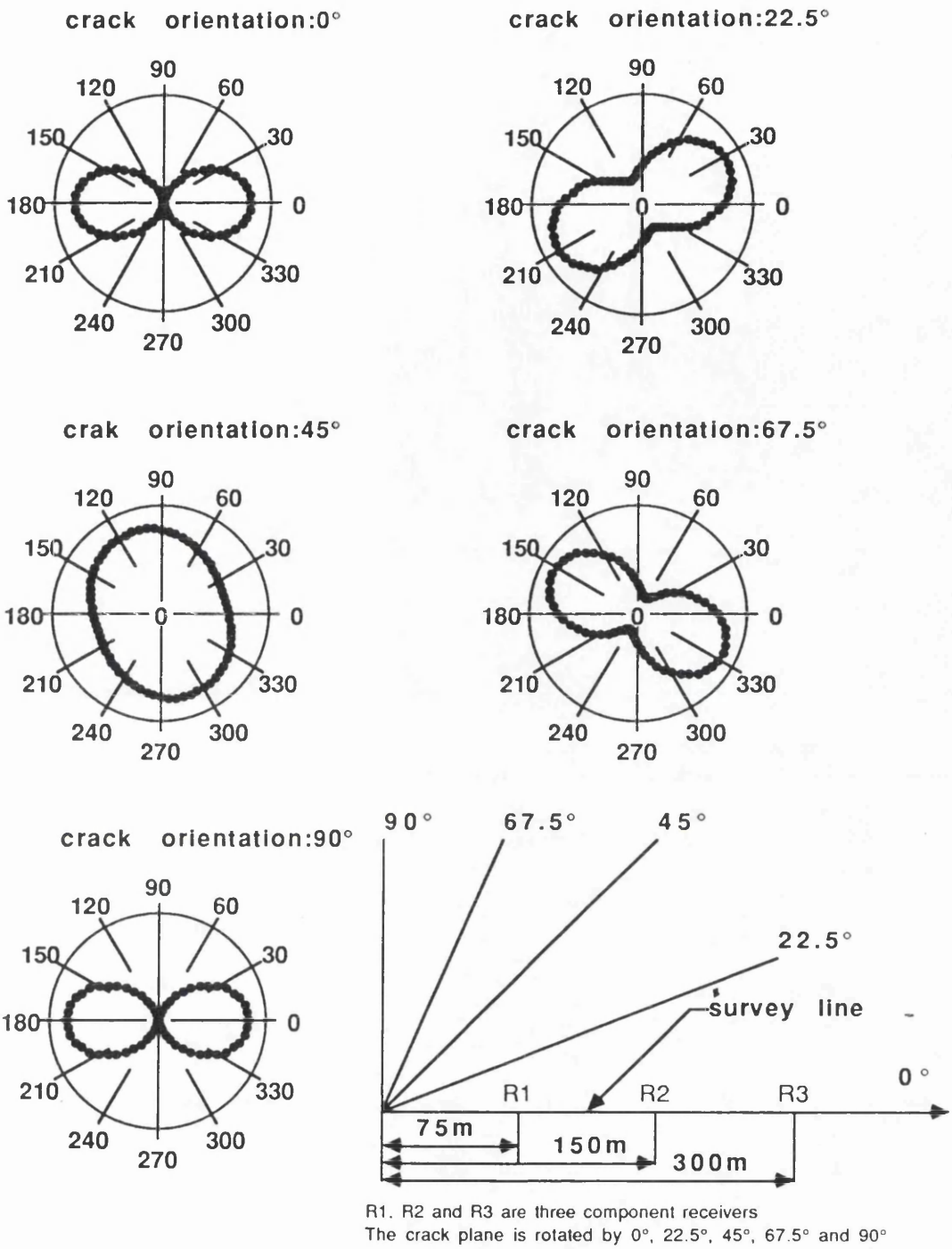

Figure 4.6. Rotated radial trace energy versus angle of rotation corresponding to 5 orientations of the crack plane: 0°, 22.5°, 45°, 67.5° and 90°, respectively. All plots are for an in-line source and a 75 m offset. The same results are obtained for offsets of 150 m and 300 m.

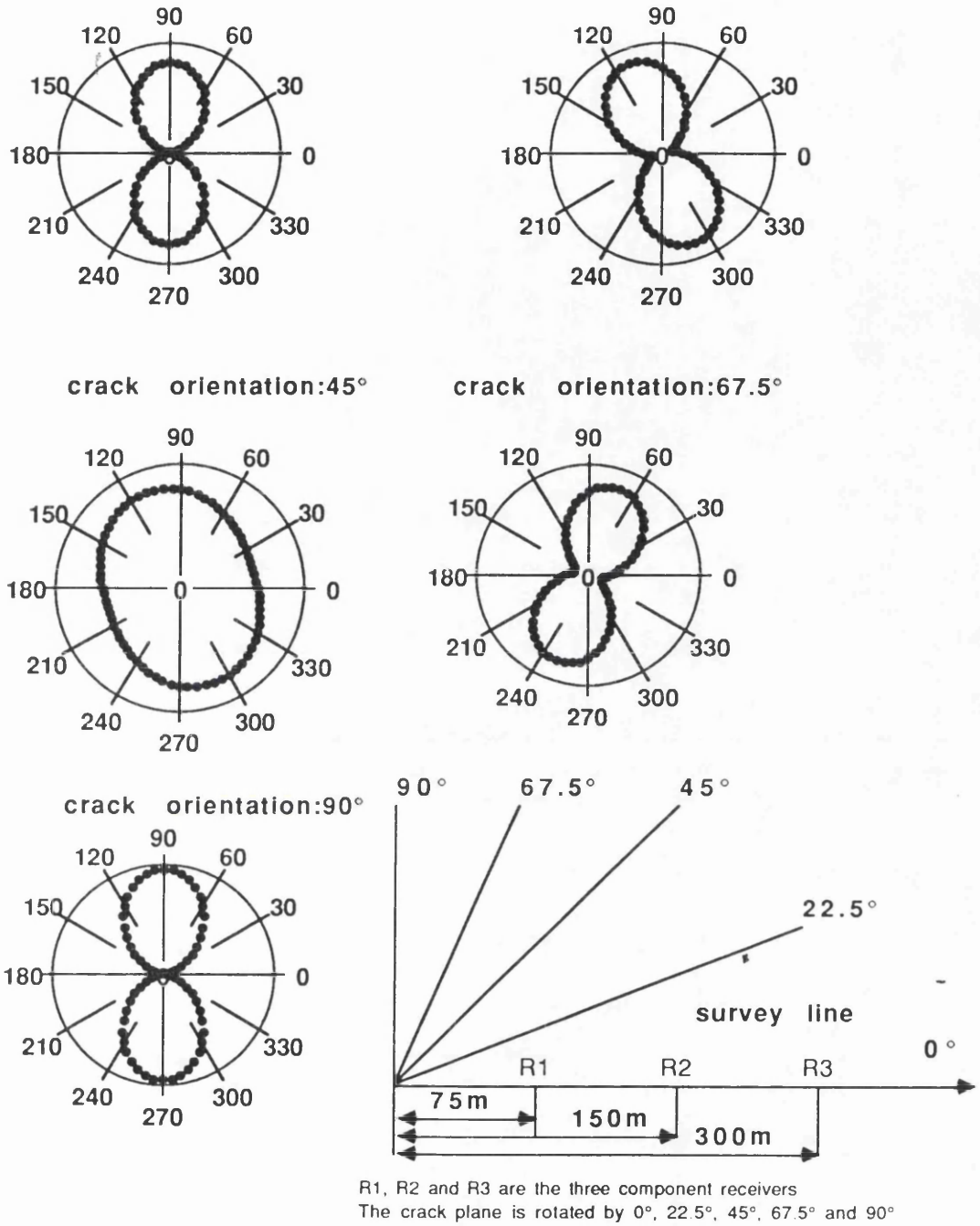

Figure 4.7. Similar to figure 4.6, except a cross-line source has been used.

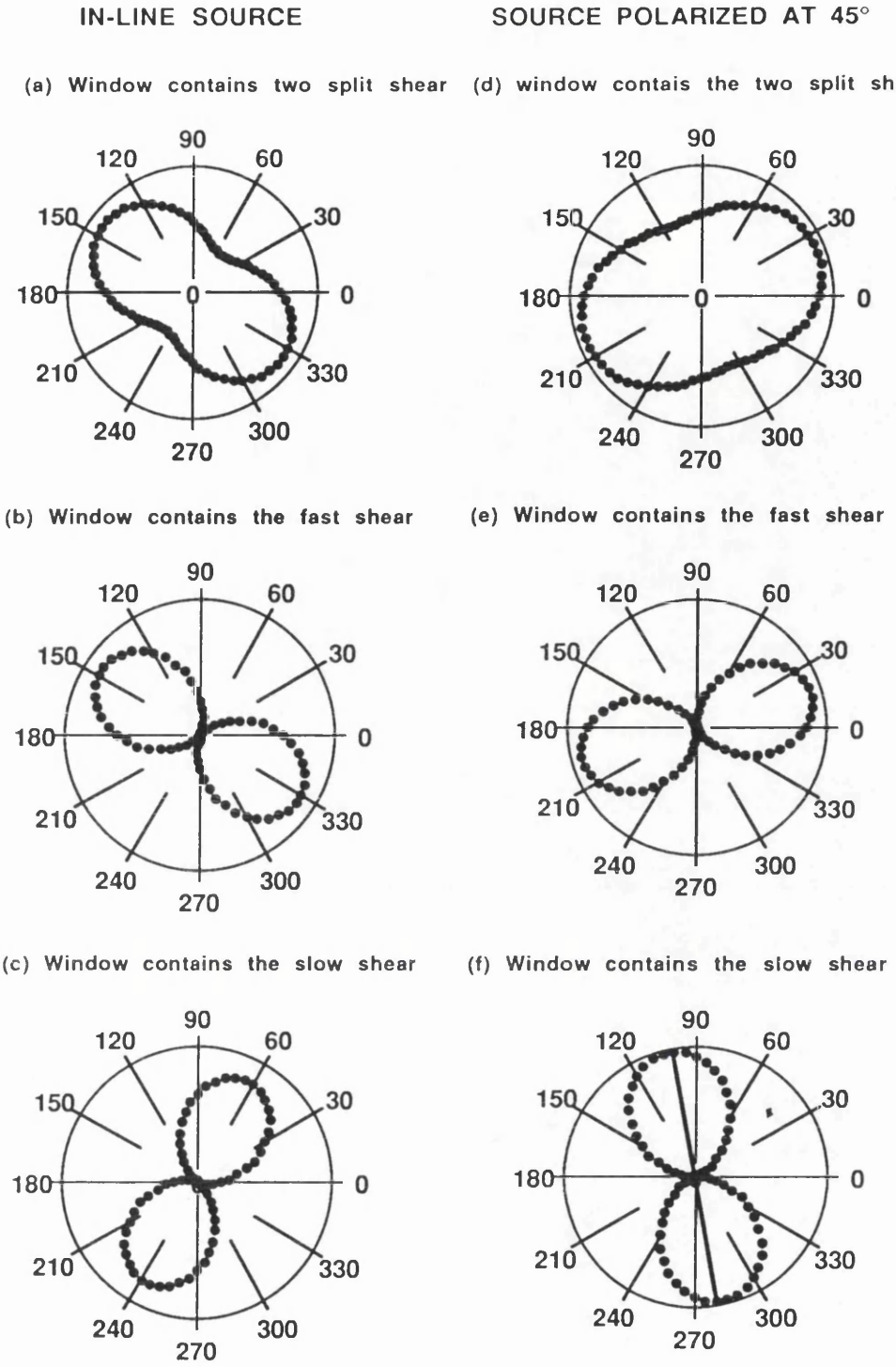

Figure 4.8. Polar plot, energy of the trace versus angle of rotation in case of an in-line source (a, b and c) with survey line 1 and a source polarized 45° to survey line 2 (d, e and f). The energy is computed within three windows, with data being rotated clockwise. A window containing both split shear, (a) and (d), and the two others contains the fast and the slower one, respectively. The polar plots of the separated split shear show a linear motion (percentage of minimum energy is 0.0%) along the crack strike and its normal. Polar plot (a) shows less elliptical motion than in polar plot (d), as evidenced by their energy percentages.

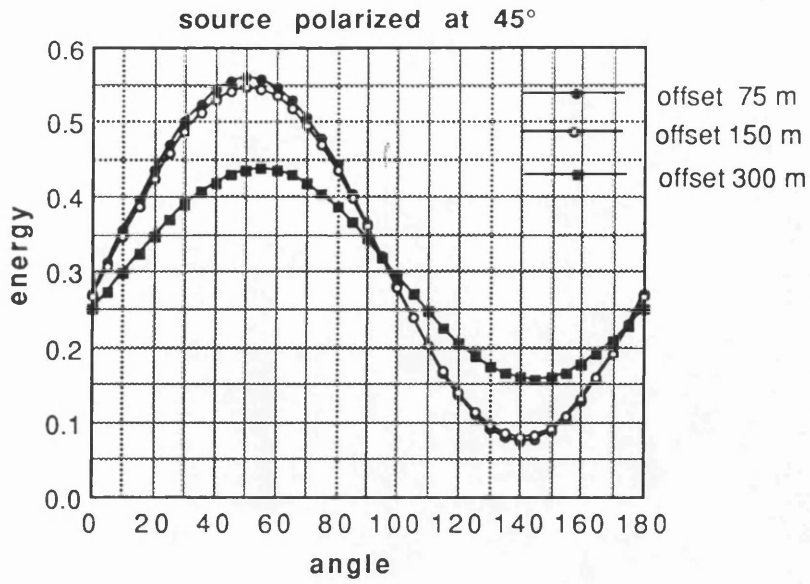

Figure 4.9. Energy versus angle of rotation for three offsets 75 m, 150 m and 300 m using a shear source making 45° with the survey line. The energy is computed over the whole record length (4 sec.). For this type of polarization the direction given by the maximum energy deviates from that of the shear source as offset increases.

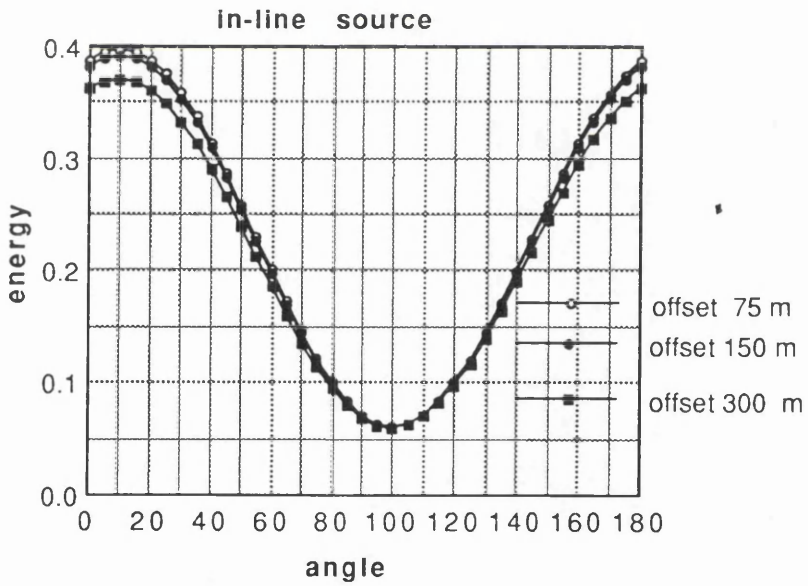

Figure 4.10. Similar as figure 4.9., but obtained when an in-line source is used. The direction given by the maximum energy deviates by 10° from the source orientation and is not offset dependent.

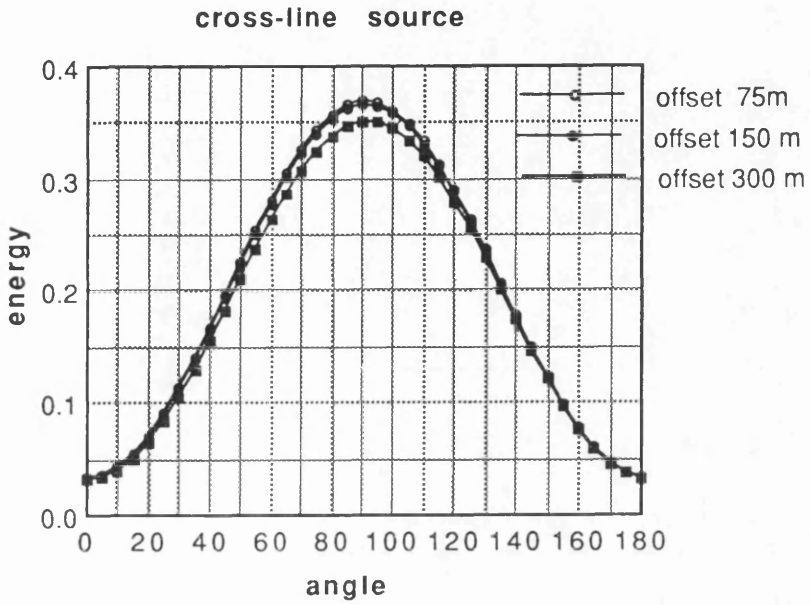

Figure 4.11. Similar to Figure 4.9, but a cross-line source is used. The direction given by the maximum energy is that of the shear source polarization for the considered three offsets.

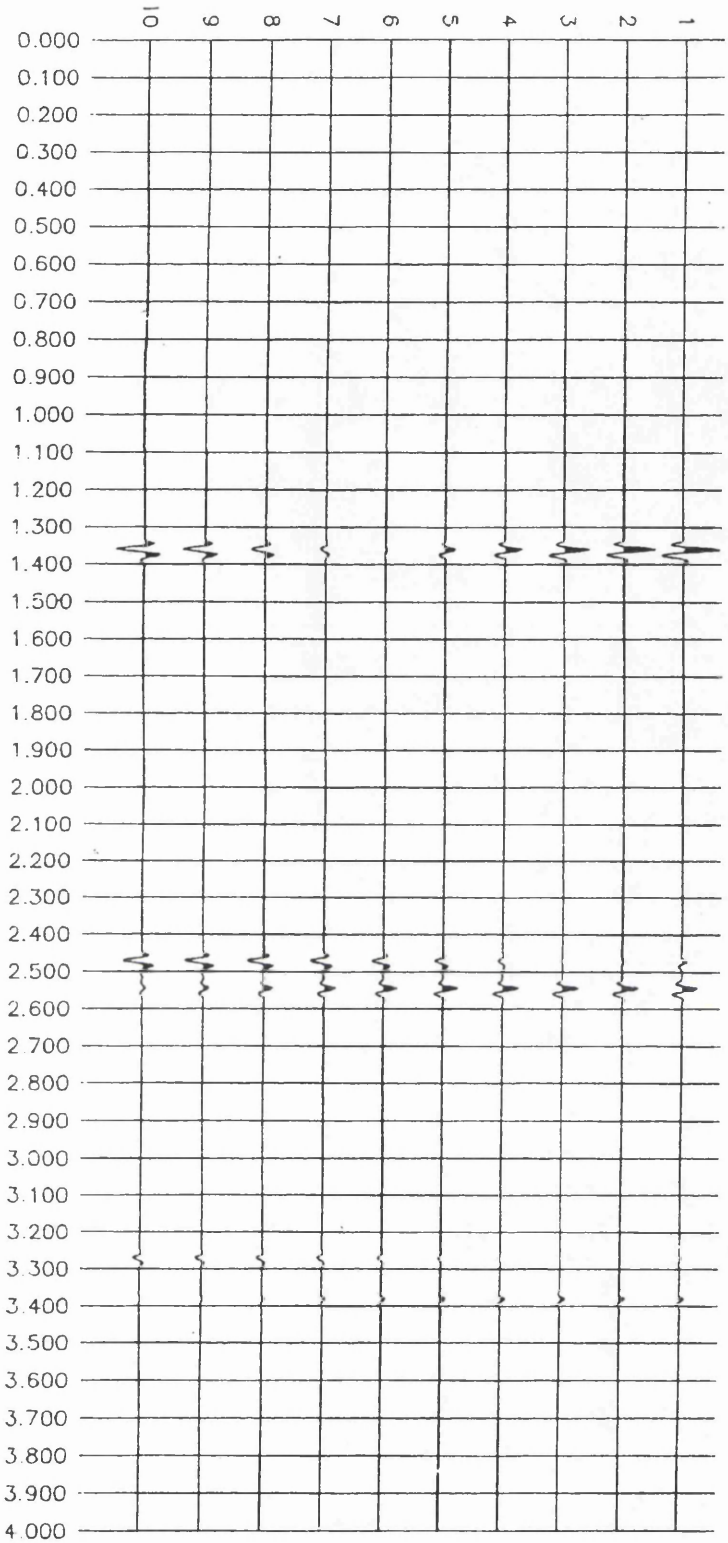

Figure 4.12. Same trace, trace 1 recorded by the transverse component, rotated 9 times (traces 2 to 10) by 10° increment. A shear source polarized 45° to the survey line and a 75 m offset have been used.

CHAPTER 5

Seismic Anisotropy Attributes and a Filter to automatically separate and enhance split shear waves.

SUMMARY

The horizontal traces are shifted (padded with zeroes) by the length of a moving window and the maximum and the minimum energy values are computed each time the window moves a step through the horizontal seismograms. This lead to new seismic attributes. Energy attributes and the instantaneous polarization angle are used to extract the time delay between the two split shear waves as well as the polarization direction of the leading shear wave.

A new polarization filter called the energy filter is implemented by

i) either rotating sample by sample the horizontal seismograms by the instantaneous polarization angle and weighting by the energy function to automatically separate the split shear waves and attenuate elliptically polarized waves. It is found that the split shear waves may well separate if the length of the moving window includes the two split wavelets and the amplitude of the fast shear wave is greater than that of the slower one.

ii) or rotating the horizontal seismograms toward the anisotropy axes by automatically computing the polarization direction of the fast one as the moving window passes through both split wavelets. This results in the complete separation of the split shear waves, irrespective of the length of the moving window and the amplitude of the fast shear wave.

The instantaneous largest and the second largest eigenvalues of the covariance matrix computed over the window are found to be equivalent to the instantaneous maximum and minimum energies,

respectively. Consequently, the energy filter may be computed using the covariance matrix by simply replacing the energy function by the rectilinearity function (Montalbetti & Kanasewhich,1970) and constraining the instantaneous polarization angle to vary between 0° and 180°, which is computed as the angle between the eigenvector corresponding to the largest eigenvalue and the radial axis. This increases the computation speed by more than 40 times compared to the conventional rotation technique when an increment of 5° is used for search of maximum energy.

5.1. INTRODUCTION

Azimuthal anisotropy and azimuthal isotropy (Crampin,1989) are common place and have been reported in exploration literature whenever horizontal components receivers have been used (Alford, 1986; Lynn &Thomsen, 1986; Becker & Perlberg, 1986; Obolentseva 1987; Thomsen 1988; Ahmed 1990; Queen & Rizer, 1990; Lynn, 1991; Winterstein & Meadow,1991a, b; Liu & Crampin,1991). In the last decade an extensive modeling have been done to understand the behavior of shear waves in anisotropic media (Keith & Crampin, 1977a, b, c; Crampin,1978,1981; Levin,1979; Berryman,1979; Liu & Crampin, 1990a, b, and others).

Several techniques have been implemented for extracting the polarization and the time delay. Macbeth (1989) developed an automated technique for extracting the polarization of the leading split shear wave as well as the time delay between them. His method involves a correlation of the observed three component data with the source orientation. Aster et al (1989) used two linearity functions as functions of the eigenvalues derived from the covariance matrix, each corresponding to the fast and the slower one. Those functions are computed over a window which slides down by a step along the horizontal seismograms. Macbeth & Crampin (1991) presented a detailed review of some of the techniques. Obolentseva et al (1987) presented an algorithm for

wave separation. It involves the rotation of the receivers to search for the angle which maximizes the lag between the two S-waves; Li & Crampin (1989) showed that stacking geophone components containing shear waves, which have not been rotated to separate the split shear waves, can seriously degrade the information in the wavetrain, and they proposed a procedure that finds the most appropriate rotation to apply at each arrival at each geophone.

Several polarization filters have been developed for enhancing polarized shear waves in the direction parallel to the plane of incidence or normal to it. Shimsoni & Smith (1964) used the time average product of, for example, the vertical and the radial components of ground motion, to be multiplied by the original signal producing a function of ground motion, in which rectilinearly polarized motions are enhanced. This filter had been applied to earthquake data. However, this filter has the drawback of distorting the signal. Montalbetti & Kanasewich (1970) developed a new polarization filter using the covariance matrix. This filter enhances shear waves polarized in the radial and the transverse directions; Benhama et al (1988) computed a polarization filter called the spatial directional filter to select particle motions whose polarization axes (major axes of the pseudoellipses) are nearly parallel to a given direction.

In the present technique the horizontal seismograms from a single shear source are rotated toward the anisotropy axes by the instantaneous rotation angle (**computed from horizontal traces shifted by the length of the moving window**) which is kept constant as the moving window goes through the two split shear waves to automatically separate the two split shear waves, irrespective of the length of the moving window and the amplitude of the fast shear wave. It is emphasized that the shifting of the horizontal traces by the length of the moving window is the key of this technique. This leads to the automatic computation of two time series, the fast shear and the the slower one. After the separation process is performed, the separated seismograms are

then multiplied by the energy function to attenuate elliptically polarized waves. This process is called energy filtering. The energy filter is more appropriate than other polarization filters, as in the presence of anisotropy the polarization direction of a seismic signal is neither oriented in the radial nor in the transverse direction, but fixed with the direction of crack strike or the normal to it.

Energy attributes are used to monitor the time delay between the two split shear waves, and the instantaneous polarization angle to extract the polarization direction of the leading split shear wave. Through this chapter, we mean by instantaneously rotated seismograms, that each sample vector of the horizontal seismograms is rotated toward the direction of its corresponding maximum energy.

The analogy made between the energy function and the rectilinearity function has made it possible to compute the energy filter by using the covariance matrix. This has the advantage of increasing the computation speed by more than 40 times compared to the conventional rotation technique when an increment of 5° is used for search of maximum energy.

5.2. INSTANTANEOUS ENERGY ATTRIBUTES AND THE SPLITTING

The method may be easily automated by computing the maximum and the minimum value of the energy of the rotated trace and their corresponding angles over a window which advances through the horizontal seismograms. The length of the window and the step size can be specified.

Let us define the instantaneous angle, which measures the angle between the direction of polarization given by the maximum energy each time the window slides down by a step and one of the horizontal axis, say, the radial one in this case, as the instantaneous polarization angle; the maximum and the minimum

values computed over the whole trace may also be called instantaneous maximum energy max(t), and instantaneous minimum energy min(t). The energy function may be defined as:

$$E(t) = 1 - \left(\frac{\min(t)}{\max(t)}\right)^{N} \tag{5.1}$$

and the instantaneous energy ratio is

$$\propto(t) = \frac{\max(t)}{\min(t)} \tag{5.2}$$

If the motion is linear within a time window, then E(t)=1; if the motion is circular, then E(t)=0. Consequently, the instantaneous values of the major and the minor axes may be known at any instant time, since they may be taken as proportional to the the roots of the instantaneous energy attributes as demonstrated in Chapter 4. Hence, five new attributes are defined which are related in the following to anisotropy.

The experimental work has been carried out on synthetic free noise reflection seismic data computed using model 2 (see Chapter 4) with a shear source polarized 45° to the survey line 1 and model 4 using a cross-line source. The latter model simulates a thin cracked layer, so that this technique is fully investigated even for small time delay. It consists of sandstone with a crack orientation of N75E overlying a sandstone with a different crack orientation N55E. Two thicknesses of 20 m and 10 m, have been modelled, respectively. Figure 5.1a, b, shows model 4 with 20 m thickness of the thin layer and its computed horizontal reflected seismograms at 6m offset. Seismograms 1 and 2 are unrotated horizontal radial and the transverse traces, respectively; seismograms 3 and 4 are their rotated version toward the anisotropic axes of the thin layer. Contrary to data from model 2, where the two split shear waves

are clearly seen; reflected split events from model 4 overlap, making a distorted wavelet and it is difficult to determine the small time delay (phase difference) or to see any splitting even using polarization diagrams, since the motion becomes highly elliptical and it is difficult to identify the polarization direction of the split shear waves with any reliability, because of this overlap.

In the following, the methodology of the automated technique is described using only data from models 2 and 4.

The instantaneous maximum energy, its corresponding instantaneous polarization angle and the instantaneous minimum energy are computed for a specified time window of length $N\Delta t$, where N is the number of samples and Δt is the sample rate. The time window slides down a step, which can be equal to or a multiple of the sampling rate, for the next computation. The process is repeated until the end of the trace. Before any computation the data of the horizontal components are shifted (padded with zeroes) by the length of the moving window, so that the onsets of the attributes are not delayed by the length of the moving window compared to the time arrival on the seismograms from which they are computed, i.e., the first sample of each attribute is set at the time origin to allow automatic separation of the split shear waves. The shift of the data is extremly important. The technique simply does not wotk without the shift.

As the window advances through the seismograms, the data within the window are rotated so that the maximum and the minimum energy are extracted. If a waveform is encountered and composed of a superposition of two split wavelets, windows 2.4-2.8 sec and 3.2-3.6 sec, the instantaneous polarization angle giving the instantaneous maximum and minimum energy will be equal to that of the direction of the strike, 15°, as seen in Figure 5.3b, c, as the moving window first encounters the fast shear, relative to the acquisition coordinate system. The instantaneous minimum energy will remain nearly equal to zero (or confounded with noise) in case

of real data, until the moving window reaches the onset of the slower shear wavelet ,i.e. within the time separating the split shear waves or the time delay. At that time it begins to enter the slow shear and advances through both of them. The instantaneous minimum energy will be no longer weak but increases rapidly to become proportional to the amplitude of the slower one.

When the sliding window gets through the fast shear, but remaining within the slower one, the instantaneous minimum energy falls to zero or to the noise level and the instantaneous maximum energy drops sharply to become proportional to the amplitude of the slower one, remains somewhat constant for the time delay and then falls to zero (noise level). This makes the shape of the graph instantaneous maximum energy versus time looks like a deformed rectangle within, for example, the window 2.4-2.8 sec. The instantaneous polarization angle, also, simultaneously varies from 15° to 105° to give the direction of the normal to the strike (Figure 5.3b, c), and remains constant, until the moving window is completely out of the slower shear. Out of this window the variation of this angle is random.

In case of no splitting, as in window 1.3-1.6 sec. (Figure 5.3a), all the energy is transferred to the rotated radial seismogram as the instantaneous polarization angle becomes equal to the source polarization angle defined as the angle between the radial axis and the polarization of the shear source, when the moving window moves into the wavelet, until it gets through it. Consequently, the instantaneous minimum energy remains very weak (nearly zero).

The working procedure of the moving window is well illustrated in Figure 5.2, showing two delayed wavelets. 3 positions of the moving window are considered: when it reaches the onset of the fast shear (position 1), then the onset of the slower shear (position 2) and at the time when it leaves the fast one (position 3).

Several windows and step sizes have been tested. From the analysis of synthetic data, it seems that windows less than 100 msec. in length may be appropriate with a step size less than or

equal to 16 msec present better figures for analyzing the splitting phenomenon. A step size equal to the sample interval could be the most appropriate.

Figure 5.3a, b, c, shows the results obtained from the horizontal components recorded at 75 m offset using a sliding window 160 msec long and a step size of 4 msec, equal to the sample rate. The plots with increasing dashed lines are for the instantaneous maximum and the minimum energy, the solid line is for the instantaneous polarization angle; all three plots are computed each time the window slides down by a step of 4 msec., to the end of the trace. Observe that within the window 2.4-2.8 sec (Figure 5.3b) containing the two split wavelets, the plot of the minimum energy is delayed from that of the maximum and has parallel edges. The instantaneous polarization angle is constant and changes sharply from 15° to 105° at the time when both energies decreases sharply, remains constant (105°) again for a while and changes sharply and randomly. Those characteristics are seen in all Figures computed using moving windows larger than 60 msec and step size less than 32 msec.

The time delay separating the two edges or the two onsets, is exactly the same as that of the time delay between the two split shear wavelets. The values 15° and 105° are exactly the direction of the strike and the normal to it relative to the radial axis or survey line. Figure 5.3c corresponds to window 3.2-3.6 sec. The attributes are similar to those of Figure 5.6b, except for the time delay is increased. When there is no splitting, .i.e., at window 1.3-1.6 sec (Figure 5.3a) , the instantaneous minimum energy is nearly equal to zero and the maximum energy has drastically increased. The instantaneous polarization angle becomes constant, equal to 50° giving approximately the polarization direction of the shear source, as the moving window gets through the reflected event contained within this window.

The effects of the step size and the length of the moving window on the instantaneous attributes are shown in Figures 5.4 and 5.5,

respectively, calculated over the window 2.4-2.8 sec. Figure 5.4a, b and c are computed with a 100 msec. moving window and three steps, 8 msec., 32 msec. and 64 msec., respectively. For Figure 5.5a, b, and c the step is kept constant, equal to the sample rate and three moving windows of 100 msec. , 80 msec. and 60 mesc., respectively.

Figure 5.6a, b ,c shows results from model 4 with 20 m thickness of the thin layer, obtained using the same step, 4 msec, and three windows of 100 msec, 50 msec. and 20 msec, respectively. The time delay, 8 msec, and the crack strike direction are easily extracted. As the moving window first reaches the leading shear the instantaneous polarization angle becomes equal to 170° giving the direction of the strike (counted clockwise from the original radial axis), then drops abruptly to 80° which is approximately equal to the normal of it. Figure 5.7a, b, c shows results from 10 m thickness. The time delay, equal to the sampling rate (4 msec.), is difficult to extract as this time is either not enough to allow the two split shear waves to separate or the sample rate is too large to allow small time delays to be picked. The constant value of the polarization angle within the plots of the energy attributes is that of the shear source direction, because this time is not enough to allow the two split shear waves to separate.

The width of the deformed rectangular shape of the plot instantaneous maximum energy versus time within the considered windows is dependent on the length of the moving window, the time delay (if there is any splitting) and on the wavelength of the processed wavelet. It is clearly seen from the Figures that the onsets of either the fast or the slower one when picked from the energy attributes (or the energy ratio) are equal to arrival time of the fast and the slower one, when picked from the rotated seismograms toward the principal axes of anisotropy.

Figures 5.8a and 5.9a, shows plots of energy function and instantaneous energy ratio with plots of the energy attributes,

respectively. The instantaneous energy ratio increases drastically as the moving window reaches the fast one and decreases abruptly when it begins to move through both split shear waves, i.e. identifying the arrival (or the onset) of the slower one. It remains very small (because of high ellipticity due to the presence of both shear waves) then increases sharply, as the moving window is out of the fast one, until a maximum is reached. Consequently, when two shear waves are identified by the energy attributes, their ratio may be used to pick the onset of either the fast or the slower one and may help in choosing appropriate windows where polarization diagrams are to be drawn for their identification to be confirmed.

5.3. COMPUTATION OF THE ENERGY FILTER

The computed values (from shifted horizontal traces by the length of the moving window) of the instantaneous polarization angle are now used to allow the separation of the two split wavelets. Each sample vector of the horizontal (unshifted) components is rotated by its corresponding value of the instantaneous polarization angle to allow the split wavelets to be automatically separated.
The separation process may be mathematically expressed by an instantaneous clockwise rotation of each sample of the horizontal components

$$\begin{bmatrix} RX_i \\ RY_i \end{bmatrix} = \begin{bmatrix} \cos\theta_i & \sin\theta_i \\ -\sin\theta_i & \cos\theta_i \end{bmatrix} \begin{bmatrix} X_i \\ Y_i \end{bmatrix}; \qquad i=1, 2, \ldots\ldots N \qquad (5.3)$$

where N is the number of samples; X_i and Y_i are two sample vectors of the recorded radial and the transverse components, respectively. RX_i and RY_i are their rotated versions toward the direction of maximum energy; and θ_i is the value of the instantaneous polarization angle giving the direction of maximum energy.

It has been demonstrated that the energy function is equal to 1,

if the reflected wavelet is linearly polarized or equal to 0.0, if it is circularly polarized. Hence, by multiplying each sample by its corresponding energy function this technique will enhance linearly polarized shear waves and attenuate elliptically polarized waves. The final processed seismograms may be expressed as

$$x_f(t) = RX(t) \cdot E(t)$$
$$y_f(t) = RY(t) \cdot E(t) \qquad (5.4)$$

Where RX(t) and RY(t)are the instantaneous rotated seismograms, and E(t) is the energy function.

It is shown from Figures 5.10 and 5.11 that the success of this separation is dependent on the length of the moving window. Figure 5.10 shows 10 seismograms grouped into five pairs, from right to left, (1,2); (3,4); (5,6); (7;8); (9,10). The first trace and the second one making a pair are the instantaneously rotated radial and the instantaneously rotated transverse (their original versions are traces 1 and 2 in Figure 2.3), respectively. The lengths of the sliding windows utilized to calculate the instantaneous polarization angles for rotating the original data to get those pairs vary from 40 msec. to 120 msec., with an increment of 20 msec.

Consider the waveform contained within the window 2.4-2.8 sec. As the length of the moving window increases the amplitude of the slower shear decreases in the rotated radial component and appears partially on the rotated transverse. When the length of the moving window becomes equal to 100 msec., pair (7,8), the slower shear appears in its total form on the rotated transverse and vanishes completely from the rotated radial. This is not the case for the split wavelets contained within the window 3.2-3.6 sec., since the length of the sliding window is still smaller than the length of the composite wavelet. However, both split wavelets separate for a giving window length greater than or equal to 140 msec., as seen from pair (1,2) in Figure 5.11, which is the same as Figure 5.10,

except that the length of the sliding window increases from 140 msec to 220 msec by an increment of 20 msec.

The amplitude of the reflected wavelet within 1.3-1.6 sec increases drastically when the axis of the radial component is rotated toward the direction of maximum energy. This shows that rotating by the instantaneous polarization angle enhances shear waves linearly polarized, thus, improving the quality of the seismic signal. This could be an important achievement in using this technique for improving data quality of shear waves on shot records for imaging.

It is found that, when the amplitude of the leading shear wave is less than that of the slower one, the separation is not complete. However, by using the coordinates of the first eigenvector given by the covariance matrix, the two split shear waves may well separate irrespective of the length of the moving window and the amplitude of the fast shear, as will be demonstrated later in this chapter.

5.4. ENERGY FILTER COMPUTED BY THE COVARIANCE MATRIX

5.4.1 Introduction

The energy filter is computed using the covariance matrix. The instantaneous polarization angle is computed as the angle between the radial axis and the eigenvector corresponding to the largest eigenvalue and restricted to vary between 0° and 180°. The energy function is taken as the rectilinearity function. The horizontal seismograms are rotated by the instantaneous polarization angle then weighted by the rectilinearity function. When the instantaneous polarization angle is kept constant within the composite split wavelet for rotating it toward the anisotropy axes, the two split shear waves separate irrespective of the length of the moving window and the amplitude of the fast shear wave. However when rotating sample by sample, for the two split shear waves to separate the length of the moving window should be equal

or exceed the length of the composite split wavelet.

By applying the energy filter on a set of traces recorded from explosive sources it is shown that, the quality of the signal is improved compared to that of obtained using the polarization filter, where the signal is distorted.

5.4.2. A review of the Polarization Filter

The design of the polarization filter is based on measuring both the rectilinearity and directionality of particle motion by computing the covariance matrix for a set of N samples taken over each of the three orthogonal components of ground motion, the radial (X), the transverse (Y) and the vertical (Z).

Let us consider a time window $N\Delta t$, where N is the number of samples and Δt,the sample rate. The mean value for each component, for example the radial one, can be defined over the time window as

$$\bar{x} = \frac{1}{N}\sum_{i=1}^{N} x_i \quad i=1,2,.....,N \tag{5.5}$$

The covariance between N samples of two variables x_1 and x_2 is given by

$$cov(x_1, x_2) = \frac{1}{N}\sum_{i=1}^{N}(x_1 - \bar{x}_1)(x_2 - \bar{x}_2) \tag{5.6}$$

The quantity $cov(x, x)$ is defined as the autocovariance or the variance of the variable x. Hence the covariance matrix can be written as

$$V = \begin{bmatrix} cov(x, x) & cov(x, y) & cov(x, z) \\ cov(y, x) & cov(y, y) & cov(y, z) \\ cov(z, x) & cov(z, y) & cov(z, z) \end{bmatrix} \tag{5.7}$$

The covariance matrix is computed over a specified time window of length $N\Delta t$, centered about t_0; the measure of rectilinearity for the time t_0 is given by

$$RL(t_0) = \left[f(\lambda_1, \lambda_2) \right]^J, \quad \text{with} \quad F(\lambda_1, \lambda_2) = 1 - \left(\frac{\lambda_2}{\lambda_1} \right)^N \tag{5.8}$$

where λ_1 and λ_2 are the largest and the next largest eigenvalues of the covariance matrix, respectively. The direction of polarization is given by the eigenvector corresponding to the largest eigenvalue, which is the direction of the major axis of the ellipse describing the particle motion within the considered window.

Considering only the two horizontal components, the lengths a and b of the semi-major and the semi-minor axis of the ellipse are $a = m\sqrt{\lambda_1}$ and $b = m\sqrt{\lambda_2}$ with m close to $\sqrt{3}$ (Benhama et al, 1988).

Let (v_x, v_y) be the coordinates of the eigenvector corresponding to the largest eigenvalue, giving the polarization direction within the horizontal plane. The direction functions at times t_0 are given by

$$D_i(t_0) = (v_i)^K \quad \ldots\ldots\ldots\ldots \quad i = x, y \tag{5.9}$$

$0 \leq D_i \leq 1$, since the eigenvector is normalized.

The two weighting functions (5.8) and (5.9) were used by Montalbetti & Kanasewich, 1970, as a point by point gain control to modulate the seismograms, so that at any time the filtered seismograms are given by

$$\begin{aligned} x_f(t) &= x(t) \,.\, RL(t) \,.\, D_x(t) \\ y_f(t) &= y(t) \,.\, RL(t) \,.\, D_y(t) \end{aligned} \tag{5.10}$$

5.4.3. Computation of the energy filter

5.4.3.1. Rotating sample by sample

The covariance matrix of the shifted horizontal seismograms may be written as:

$$V = \frac{1}{N}\begin{bmatrix} \sum x(t - N\Delta t)x(t - N\Delta t) & \sum x(t - N\Delta t)y(t - N\Delta t) \\ \sum y(t - N\Delta t)x(t - N\Delta t) & \sum y(t - N\Delta t)y(t - N\Delta t) \end{bmatrix} \qquad (5.11)$$

from which the largest, the second largest eigenvalues and the instantaneous polarization angle (using equation 5.13) are computed and set at the end (not at the centre) of the moving window each time it slides down by a step. Figure 5.8b shows plots of the first largest eigenvalue, the second largest eigenvalue and the rectilinearity function with increased dashed lines and solid line, respectively. The similarity of the energy function (Figure 5.8a, solid line) with the rectilinearity function is straightforward. Figure 12a, b, shows plots of the maximum energy versus first largest eigenvalue and minimum energy versus second largest eigenvalue, respectively, computed over the window 2.4-2.6 sec using a sliding window of 120 msec. Each plot is a straight line passing through the origin with a slope equal to 1. Hence, the first largest and second largest eigenvalues as computed are equivalent to the maximum and the minimum value of the energy of the trace, respectively. They may be used as new seismic attributes for investigating azimuthal anisotropy. The energy function may also be replaced by the new rectilinearity function in designing the energy filter.

Equation (5.4), giving the filtered seismograms may be rewritten as

$$\begin{bmatrix} x_r(t) \\ y_r(t) \end{bmatrix} = E(t) \cdot \begin{bmatrix} \cos\theta(t) & \sin\theta(t) \\ -\sin\theta(t) & \cos\theta(t) \end{bmatrix} \begin{bmatrix} x(t) \\ y)t) \end{bmatrix} \tag{5.12}$$

Utilizing the covariance matrix, the energy function may be replaced by the rectilinearity function; the instantaneous polarization angle is the angle between the eigenvector corresponding to the largest eigenvalue and may be computed as follows:

$$\theta(t) = \left| \tan^{-1}\left(\frac{v_y(t)}{v_x(t)}\right) \right|$$
$$if,\ v_y(t) < 0,\ or,\ v_x(t) < 0$$
$$or \tag{5.13}$$
$$\theta(t) = \pi - \tan^{-1}\left(\frac{v_y(t)}{v_x(t)}\right)$$
$$if,\ v_y(t) < 0 and v_x(t) < 0,\ or,\ v_y(t) > 0 and v_x(t) > 0$$

This is simply to restrict the instantaneous polarization angle to vary between 0° and 180°, from the radial axis in a clockwise direction, so as to conform with the design of the energy filter.

Figure 5.13a, b, c, shows the instantaneous largest and second largest eigenvalues with increasing dashed lines, and the instantaneous polarization angle (computed from equation 5.13) with solid lines, calculated over the three windows: 1.3-1.6 sec, 2.4-2.8 sec, 3.2-3.6 sec, respectively, using the same input data as for obtaining Figure 5.3a, b, c. The comparison of the two Figures shows a straightforward similarity between the energy and the eigenvalue attributes. Plots of the polarization angles of both Figures are identical (except for the scale).

The application of the computed energy filter by the covariance matrix on the radial and the transverse components of Figure 2.3 (traces 1 and 2) is shown in Figure 5.14. The length of the moving window has been varied from 60 msec. to 180 msec. with an

increment of 20 msec., and applied to the original data. This results in 7 pairs of filtered seismograms, (1,2), (3,4),....., (13,14), from right to left. The split wavelets at 2.4-2.8 sec. and at 3.2-3.6sec., separate well for a window length greater than or equal to 140 msec. This figure is similar to Figures 5.10 and 5.11, as expected.

The application of the polarization filter does not separate the split wavelet, by attenuating either the fast or the slow shear wave, since neither of them is polarized along the radial or the transverse axis, as it is shown in Figure 5.15. This shows the extreme importance of shifting the horizontal traces to compute the instantaneous rotation angle to be used for rotation.

5.4.3.2. Automatic rotation of the acquisition coordinate frame toward the anisotropy axes.

Let us divide the plane of the acquisition coordinate frame (ox, oy), where ox and oy are the in-line and the cross-line directions, into 4 (four) quadrants or regions, as shown in Figure 5.16. The coordinates (V_x, V_y) of the eigenvector corresponding to the largest eigenvalue are used to identify each quadrant

The polarization direction of the fast and the slow shear waves are supposed to be orthogonal. Consequently, if the direction of polarization of one is within quadrant 1 and quadrant 3, the other direction is within quadrant 2 and quadrant 4. For example , suppose the direction of polarization of the fast wave is within the quadrants 1 and 3 at angle θ from the inline direction. Consequently, the direction of polarization of the slow one is within the quadrants 2 and 4 at an angle φ from the inline direction, the complement of angle θ, from the inline direction (see Figure 5.16). As the moving window remains within the fast shear, the data is instantaneously rotated by $\pi - \theta$; as it begins to enter the slower shear and advances through both of them, the polarization angle is either equal to θ or φ , depending on whether the amplitude of the fast is greater or smaller than the slower one

(see chapter 4), and the angle Ψ of rotation (clockwise) is kept constant and may expressed as:

$$\Psi = \pi - \theta = \frac{\pi}{2} + \varphi \tag{5.14}$$

When the sliding window gets through the fast shear but remaining within the slow one, the polarization angle given by the eigenvector corresponding to the largest eigenvalue is equal to φ and the rotation angle is $\pi/2 + \varphi$. Hence, the angle of rotation is kept constant within the composite split shear wavelet and the aquisition coordinate frame are rotated automatically towards the anisotropic axes, with the inline direction always rotated toward the axis of anisotropy found within the quadrant1 and the quadrant 3, which could be either that of the crack strike or the normal to it, depending on whether the fast one is polarized within quadrants 1 and 3 or within quadrants 2 and 4. This leads to an automatic separation of the split shear waves; and as the moving window slides down the horizontal components, each split wavelet is processed separately. This technique could deal with multiple splitting, and is appropriate for reflection data as polarizations of reflected events change with offset.

The instantaneous polarization angle used to rotate the data may be computed as follows:

$$\begin{aligned}
&\Psi = \pi - \tan^{-1}\left(\frac{v_y(t)}{v_x(t)}\right) \\
&if,\ v_y(t) < 0\ and v_x(t) < 0,\ or,\ v_y(t) > 0\ and v_x(t) > 0 \\
&OR \\
&\Psi = \frac{\pi}{2} + \left|\tan^{-1}\left(\frac{v_y(t)}{v_x(t)}\right)\right| \\
&if,\ v_y(t) < 0,\ or,\ v_x(t) < 0
\end{aligned} \tag{5.15}$$

in case of a counter-clockwise rotation, the instantaneous

polarization angle is:

$$\Psi = \tan^{-1}\left(\frac{v_y(t)}{v_x(t)}\right)$$
$$if,\ v_y(t) < 0\ and v_x(t) < 0,\ or,\ v_y(t) > 0\ and v_x(t) > 0$$
$$OR$$
$$\Psi = \left|\tan^{-1}\left(\frac{v_x(t)}{v_y(t)}\right)\right| \qquad (5.16)$$
$$if,\ v_y(t) < 0,\ or,\ v_x(t) < 0$$

Figure 5.17 shows the results of the application of the energy filter using equation 5.16, over the horizontal seismograms recorded along survey line 3 at 75 m offset (Figure 4.1) by using an inline shear source. In this case the amplitude of the fast shear is smaller than that of the slower one. This Figure shows 14 seismograms which are grouped into 7 pairs, from right to left; (1, 2); (3, 4);.....; (13, 14). Each pair represents the rotated radial and the rotated transverse, respectively. The length of the moving window used to compute the instantaneous polarization angle for rotating the original data varies from 40 msec to 160 msec., respectively. It is seen that the separation of the split wavelets is neither dependent on the length of the moving window nor on the amplitude of the fast shear. However, it is suggested that the length of the moving window should be greater than or equal to 40 msec., for a better average of the instantaneous polarization angle.

5.5. DISCUSSION

The instantaneous polarization angle remains constant and equal to the angle of the direction of the strike, as the time window moves along the fast shear wavelet, until it gets through it giving the polarization direction of the fast shear (the leading shear).

When the tail of the moving window reaches the end of the fast shear wavelet, the instantaneous polarization angle varies abruptly

from the direction of the strike to the normal of it giving the polarization of the slow shear. This is well illustrated in Figures 5.3 to 5.7. Consequently, those three attributes when combined together could be a strong tool in monitoring anisotropy, particularly EDA-type anisotropy in case of vertically travelling shear waves, such as VSP data, near-zero offset reflection seismic data and even earthquake data, since the three fundamental characteristics of anisotropy may be seen on the combined graphs of: A differential amplitude given by the instantaneous maximum and minimum energy, the time delay and the polarization of the leading shear wave.

In case of reflection shear data polarization could be modified by interaction with the free surface topography. Also effects of internal interfaces have been discussed by Liu & Crampin, 1990. The effect of a low velocity layer could only distort the signal if the medium is azimuthally anisotropic (Yardley & Crampin, 1991). This demonstrates the complexity of trying to extract the anisotropy axes from the seismic reflection data. However, the energy attributes may be used to monitor subsurface anisotopy.

The technique has demonstrated the ability to separate automatically the split shear waves and may attenuate elliptically polarized shear waves. So, after applying this technique, a conventional processing flow may follow the energy filtering process to get two shear seismic sections.

Also, the energy filter is easily computed by using the covariance matrix; the eigenvalue attributes can be used to extract the time delay between the split shear waves. This increases the computation speed by more than 40 times compared to the conventional rotation technique when an increment of 5° is used for search of maximum energy.

The ability of the technique in dealing with multiple splitting can be investigated on simple synthetic seismograms recorded using a crossline shear source propagating, for example, within two cracked media with different crack orientations.

With this technique, it is now possible to conduct a three component seismic survey using simple source multireceiver acquisition technique. The source should be a crossline shear source, since with this source orientation practically no mode conversions are recorded on the inline components. This technique should be especially valuable for imaging with shear waves as wavelet quality is much improved. Indeed, as demonstrated in the next section, it can turn bad data into usuable data.

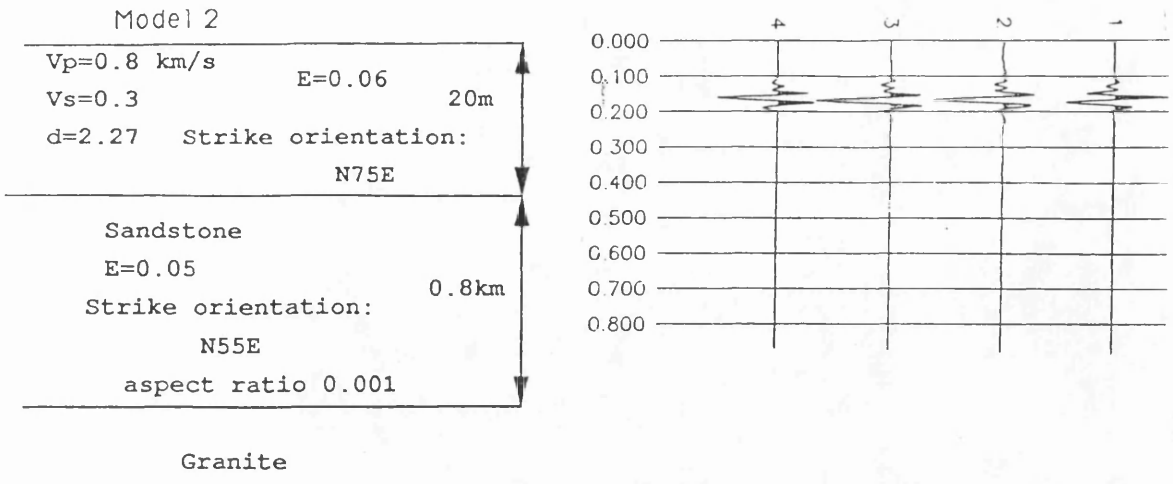

Figure 5.1. (a) Model 4 with the thickness of the thin layer being 20 m and (b) the computed horizontal seismograms at 6m offset. Seismograms 1 and 2 are the radial and the transverse, respectively; 3 and 4 are their rotated version toward the anisotropy axis.

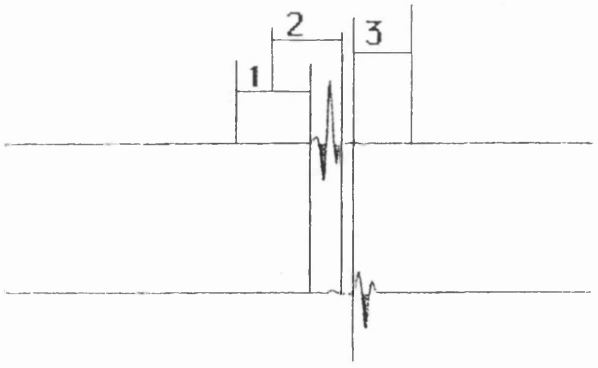

Figure 5.2. The moving window. At position 1, the window enters into the fast shear (the motion is highly linear); at position 2, the window reaches the onset of the slower one giving a high elliptical motion; at position 3 it gets through the fast but still remains within the slower one giving a linear motion. The sample vector positioned at the end of the moving window is instantaneously rotated by the angle giving the maximum energy.

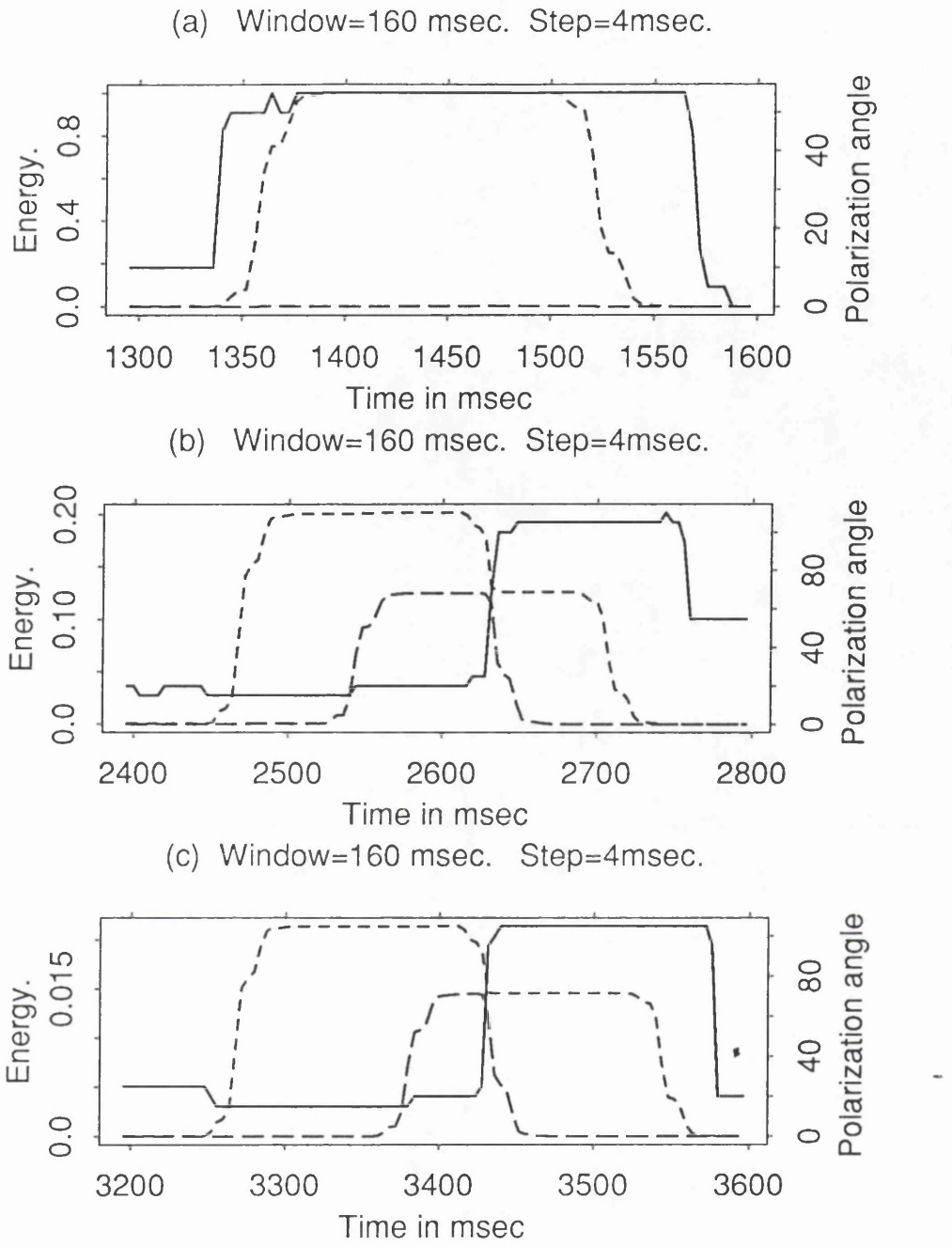

Figure 5.3. Plots of the three instantaneous attributes computed using a moving window of 160 msec. and a step size of 4 msec. (a), (b) and (c) are plots over windows 1.3-1.6 sec, 2.4-2.8 sec and 3.2-3.6 sec, respectively. The instantaneous maximum energy, the instantaneous minimum energy and the instantaneous polarization angle (y-axis on the right side), are with increasing dashed lines and solid line, respectively. The time delay is given by the onsets of the two energy attributes or their parallel edges. The instantaneous polarization angle remains somewhat constant giving the crack strike (15°) then jumps to 105° to give the normal of it.

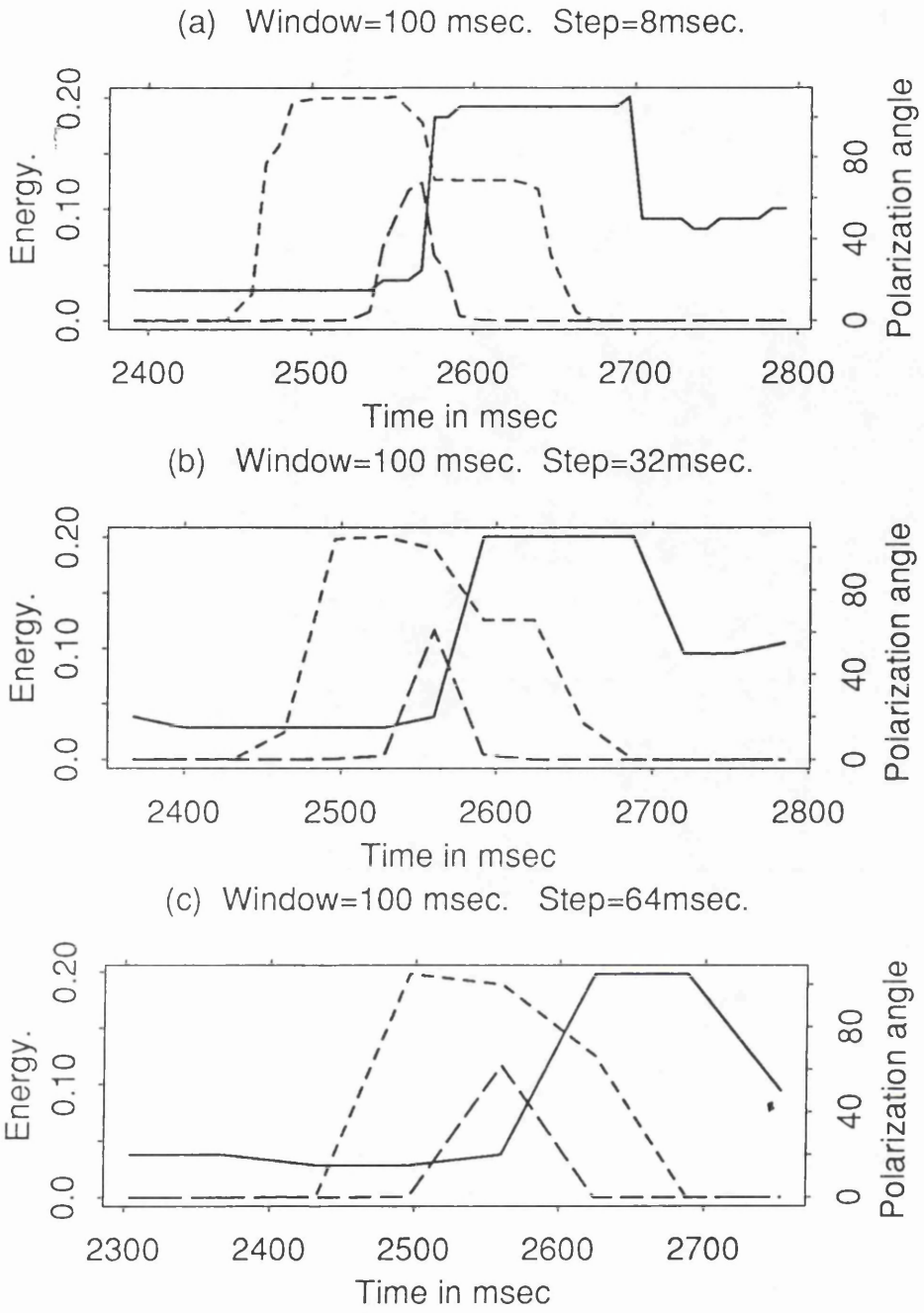

Figure 5.4. Plots of the three instantaneous attributes computed over the window 2.4-2.8 sec., using a moving window of 100 msec. and three different step sizes of 8 msec., 32 msec. and 64 msec. corresponding to plots (a), (b) and (c), respectively. The instantaneous maximum energy, the instantaneous minimum energy and the instantaneous polarization angle are with increasing dashed lines and solid line, respectively.

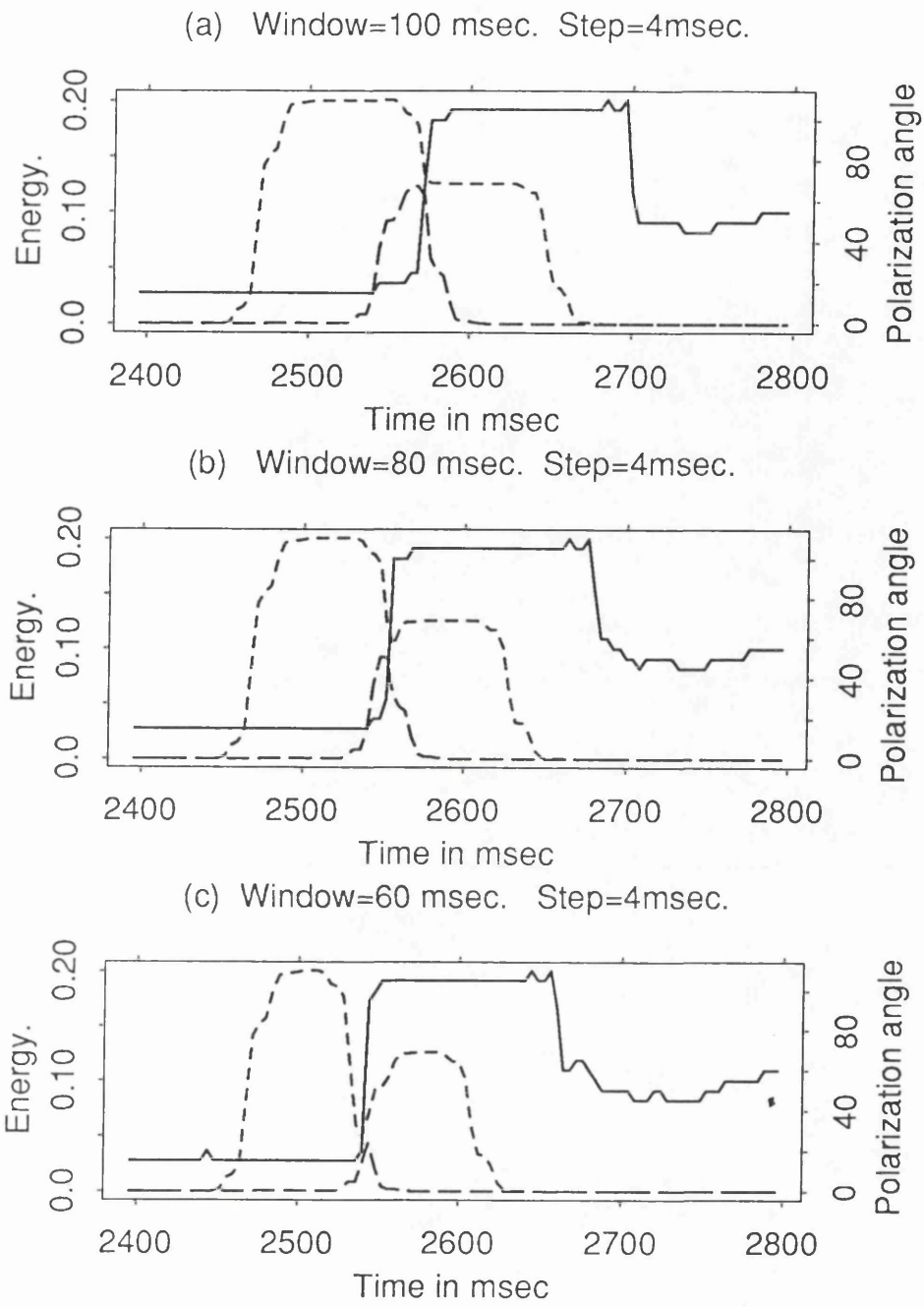

Figure 5.5. Plots of the three instantaneous attributes computed over the window 2.4-2.8 sec., using a step size of 4 msec. and three different windows of 100 msec., 80 msec. and 60 msec. corresponding to (a), (b) and (c), respectively. The instantaneous maximum energy, the instantaneous minimum energy and the instantaneous polarization angle are with increasing dashed lines and solid line, respectively.

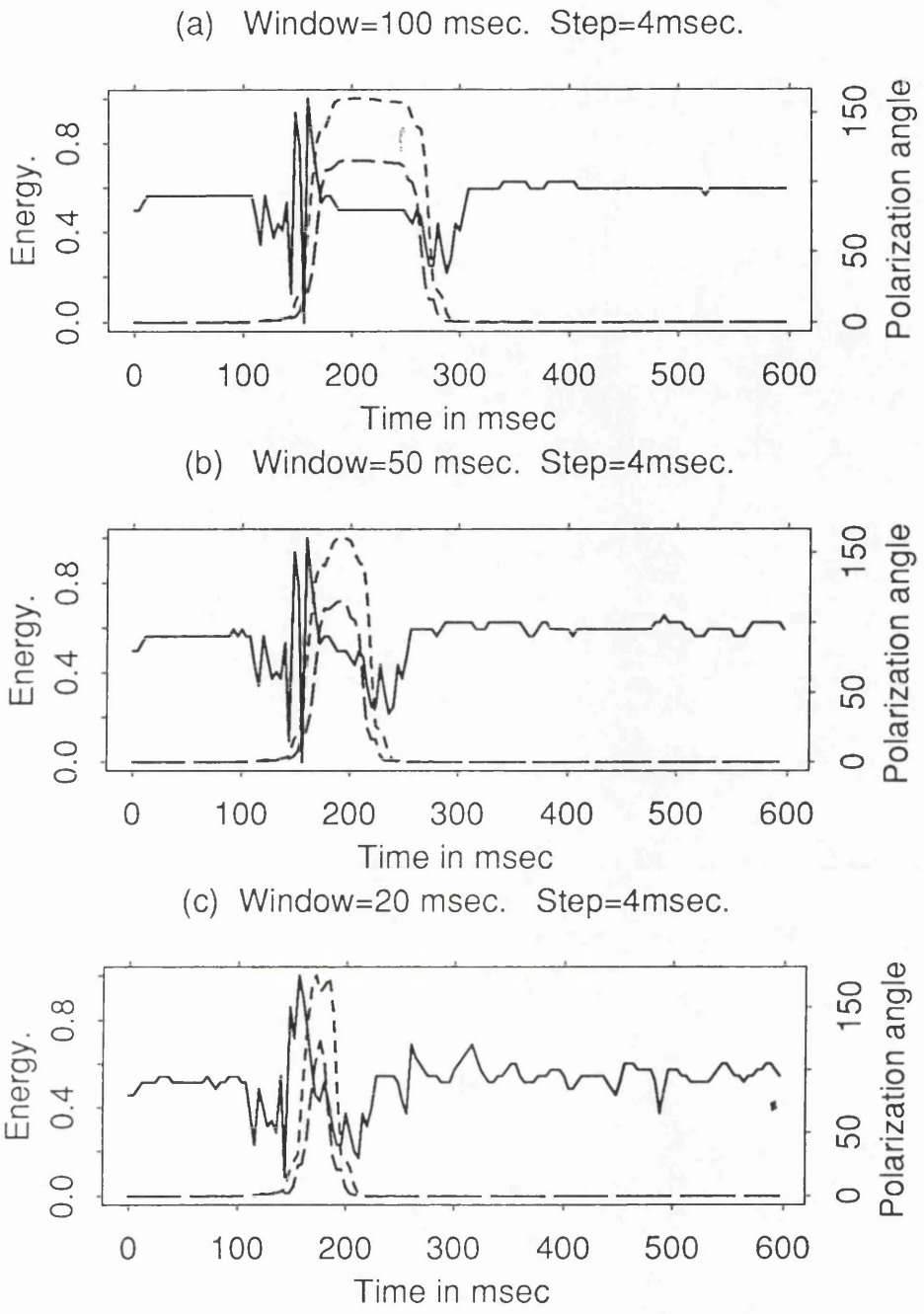

Figure 5.6. Instantaneous attributes computed from model 4 with the thickness of the thin layer being 20 m. (a), (b), and (c) are from moving window of 100 msec., 50 msec. and 20 msec., respectively, using a 4 msec. step. The time delay of 8 msec. is easily extracted from all Figures. The directions of anisotropy axes are given by the polarization angle. It drops from 170°, giving the direction of the strike counter-clockwise from the original radial axis or survey line, to 80° giving the normal of it.

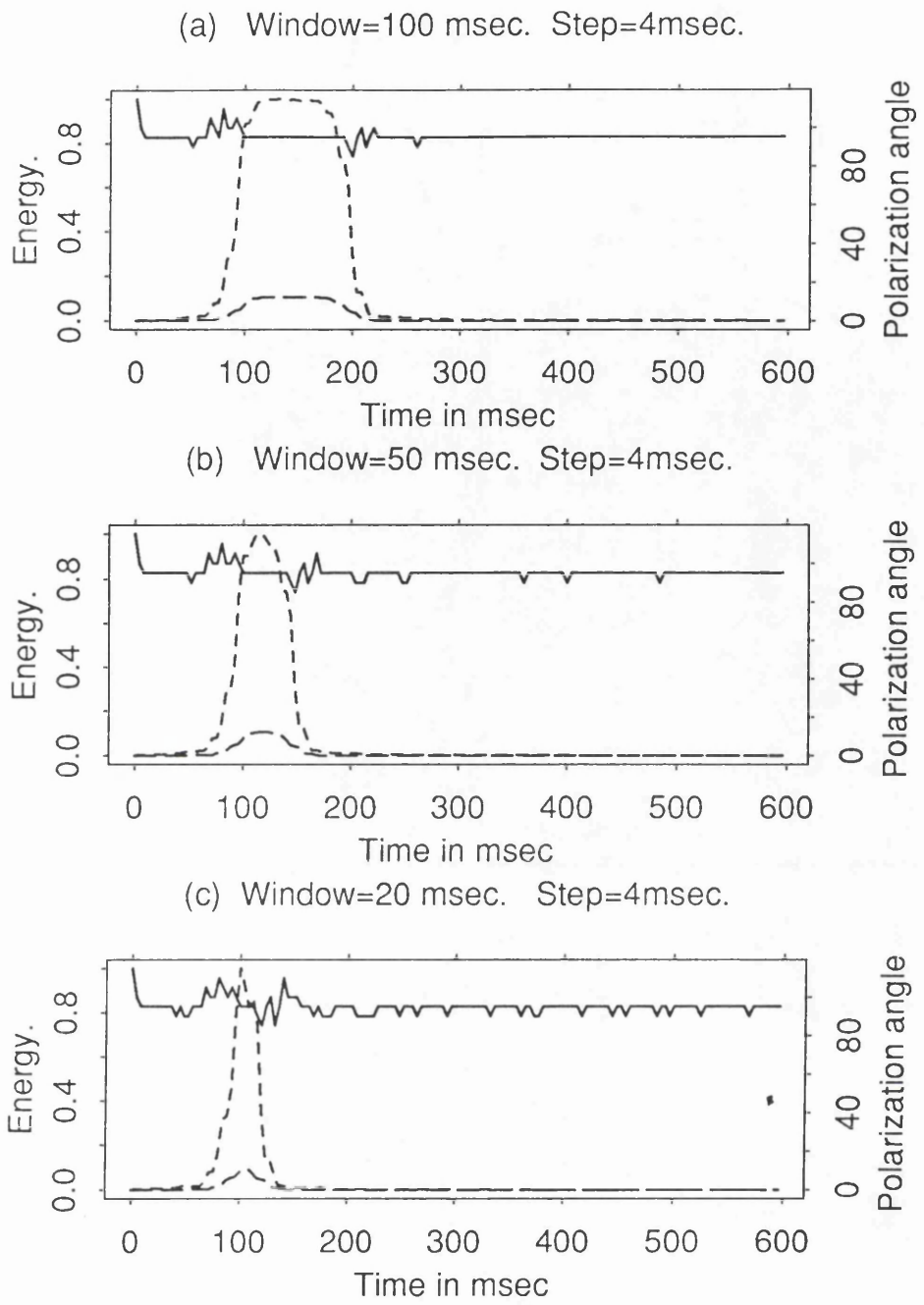

Figure 5.7. Similar to Figure 5.6, except for the thickness of the thin layer being 10 m. the time delay, equal to the sample rate, is difficult to be extracted and the constant value of the instantaneous polarization angle within the plots of the energy attributes (moving window= 100 msec.) is that of the shear source direction, as this time is not enough to allow the two split shear to separate.

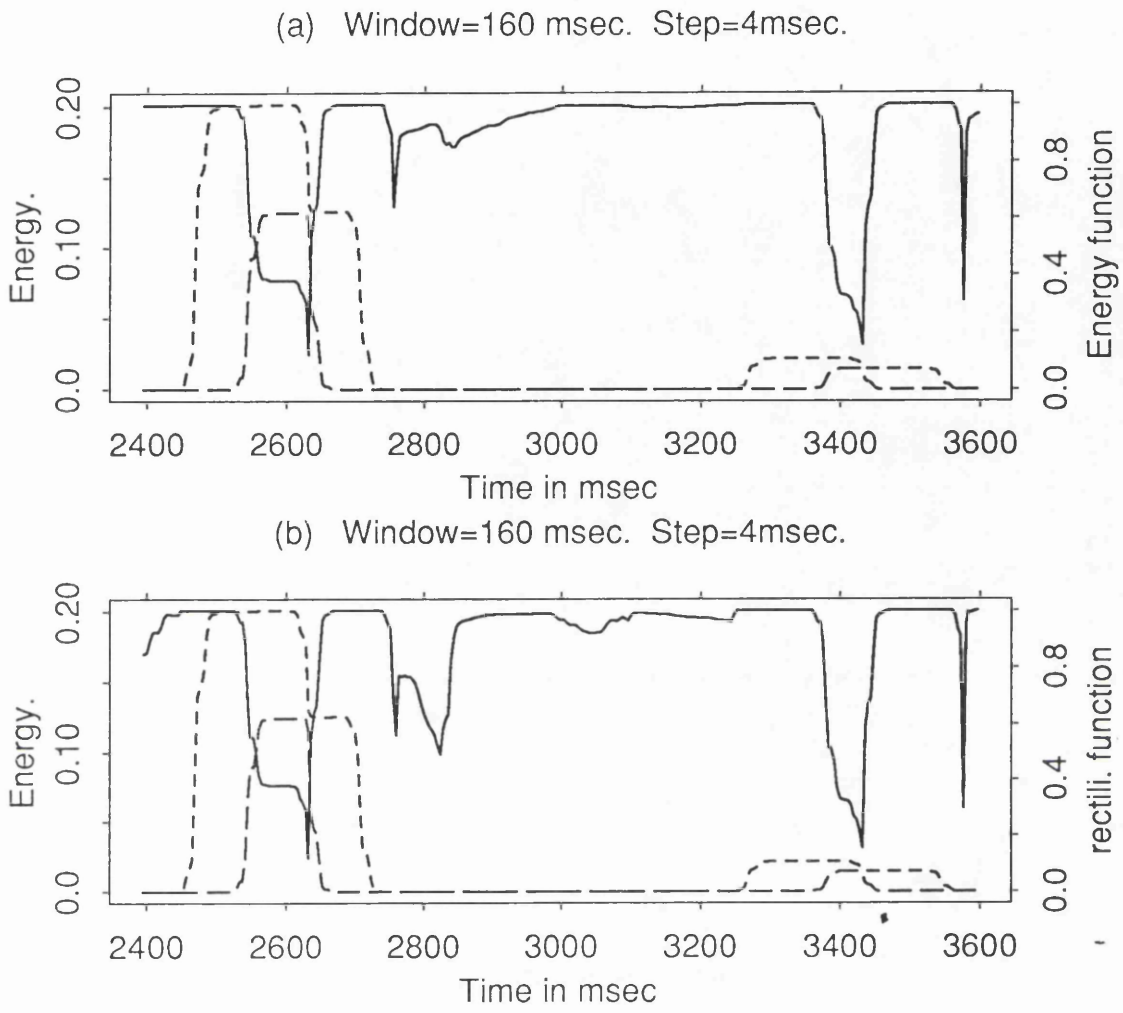

Figure 5.8. (a) Plot of the energy function(solid line) and (b) plot of the rectilinearity function (solid line) with the energy attributes. Note the straightforward similarity between the energy function and the rectilinearity function.

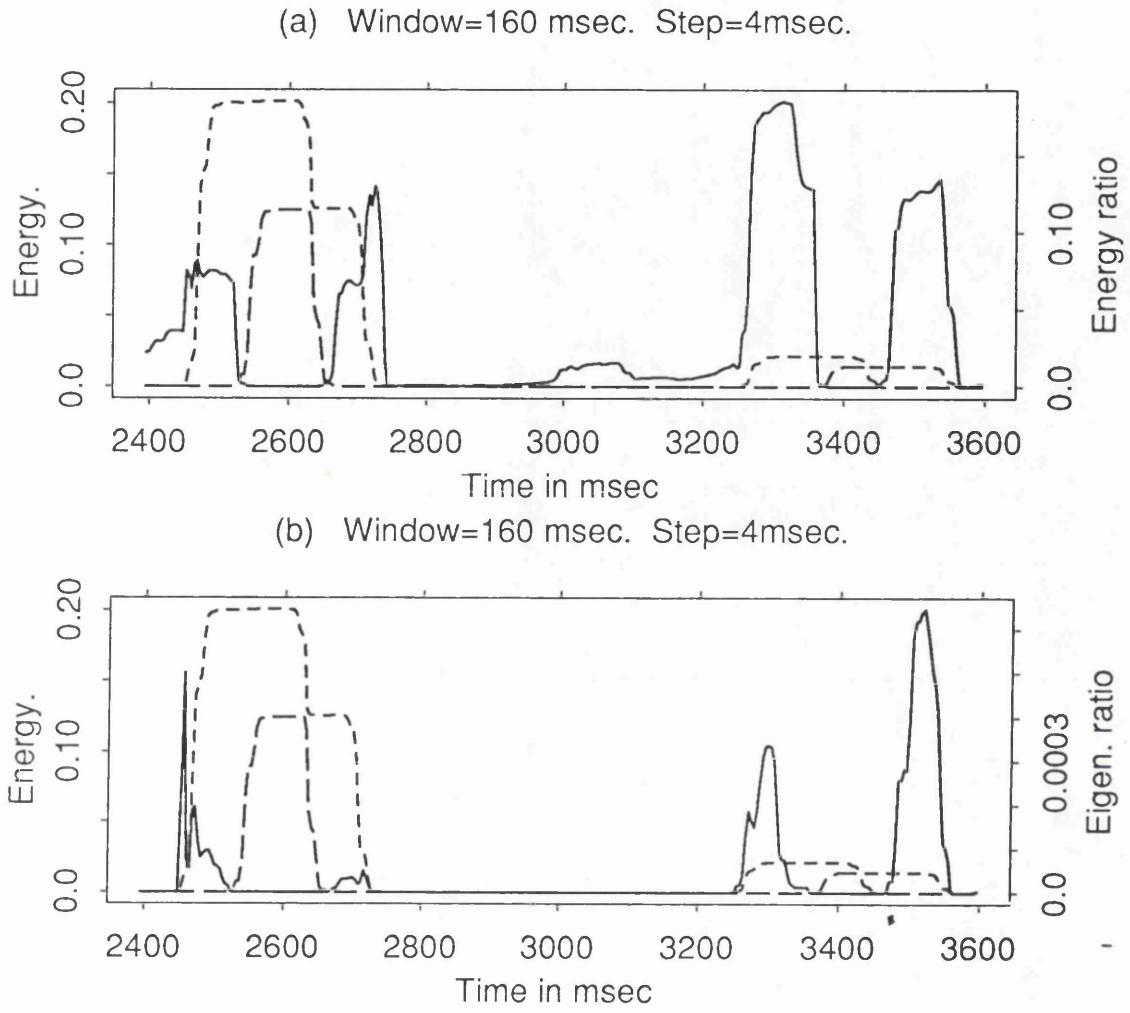

Figure 5.9. (a) Plot of the energy ratio (solid line), and (b) the eigenvalue ratio (solid line) with the energy and the eigenvalue attributes, respectively. Both ratios are equivalent and may be used to pick up the onsets of the split wavelets or to identify their presence. The largest and the second largest eigenvalues are with increasing dashed lines. Note the similarity between the energy and the eigenvalue attributes.

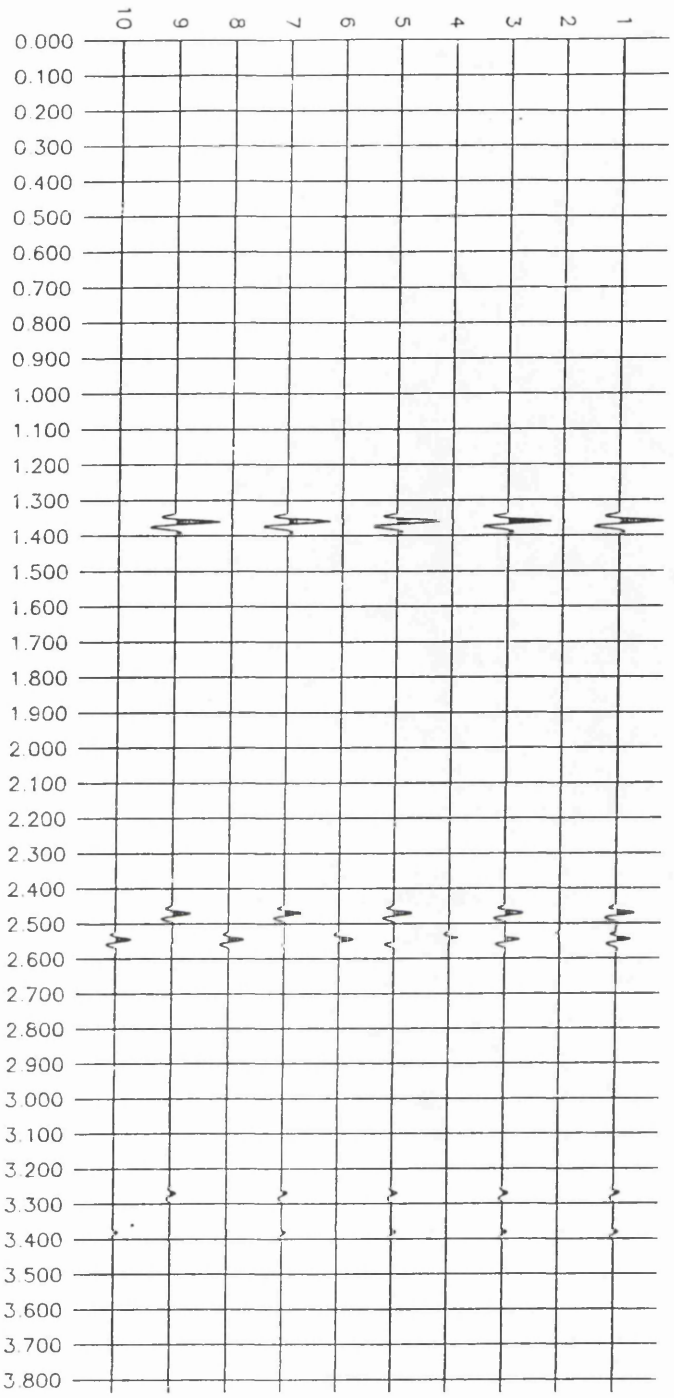

Figure 5.10. 5 pairs of seismograms, (1, 2); (3, 4); (5, 6); (7, 8); (9, 10), from right to left. The first trace and the second one of each pair are the filtered radial and transverse, respectively. The lengths of the sliding windows used for to compute the polarization angles for rotating the original data vary from 40 msec. to 120 msec. by an increment of 20 msec., respectively. The split wavelets within the window 2.4-2.6 sec. separate completely when the length of the sliding window is equal to 100 msec.

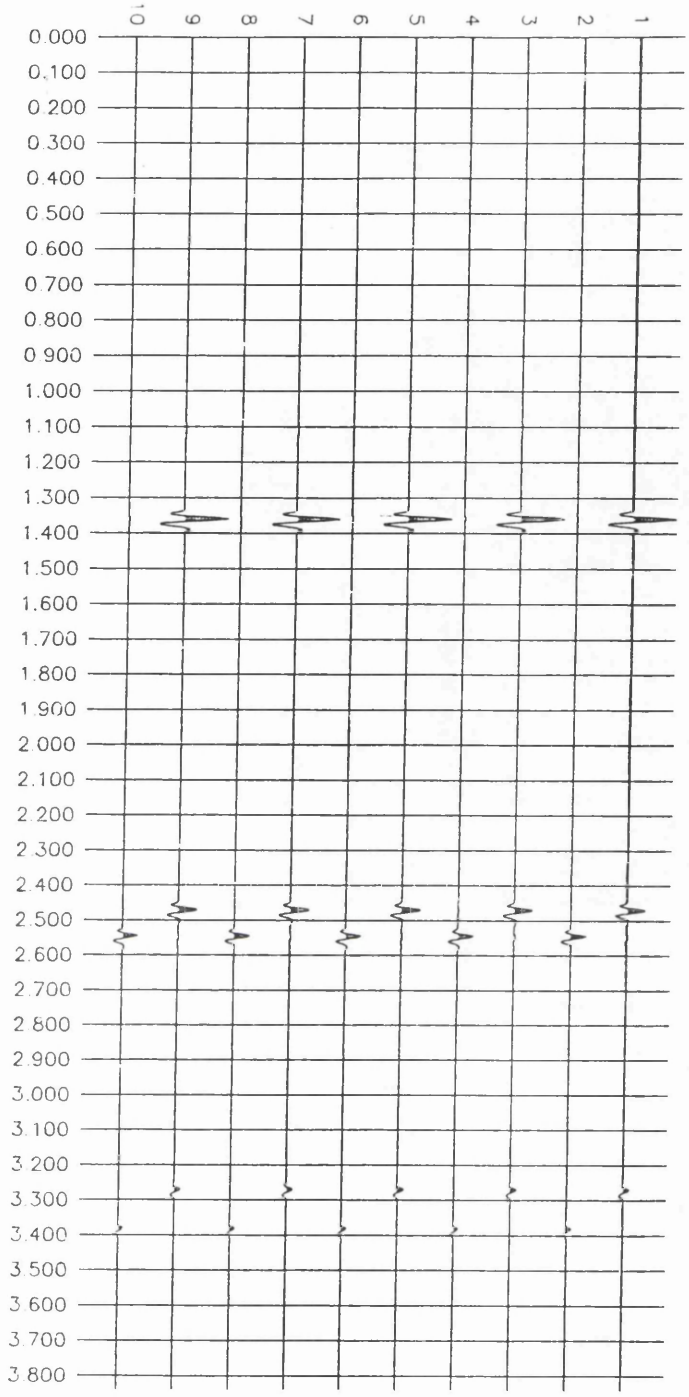

Figure 5.11. Similar to Figure 5.10. The lengths of the sliding windows used to compute the polarization angles for rotating each pair vary from 140 msec. to 220 msec. by an increment of 20 msec., respectively. the split wavelets within the two windows 2.4-2.6 sec. and 3.2-3.5 sec. are well separated, as the length of the moving window is greater than or equal to the length of the two split wavelets.

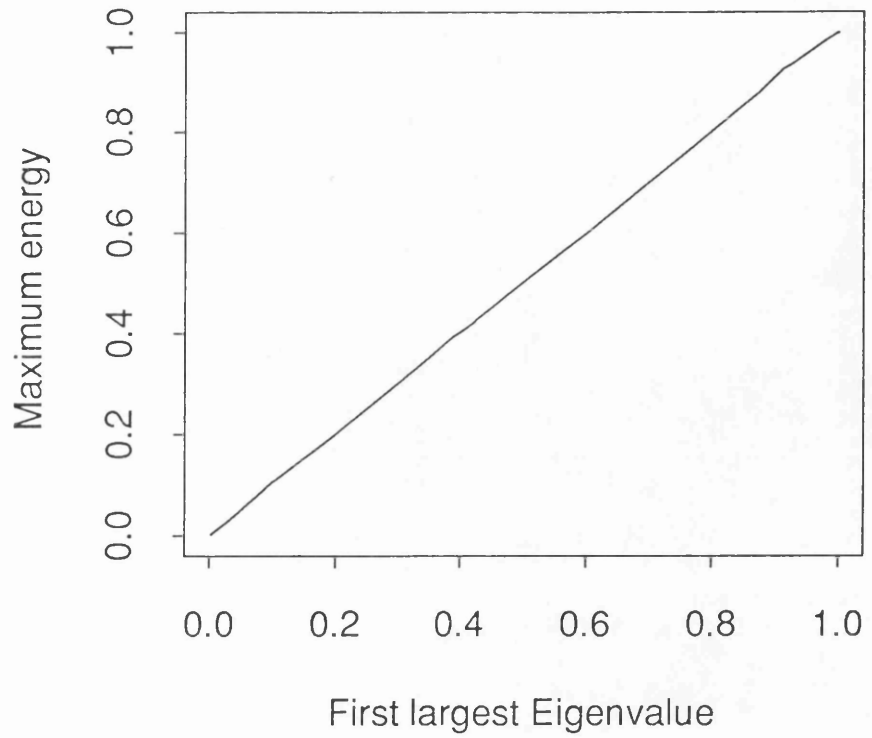

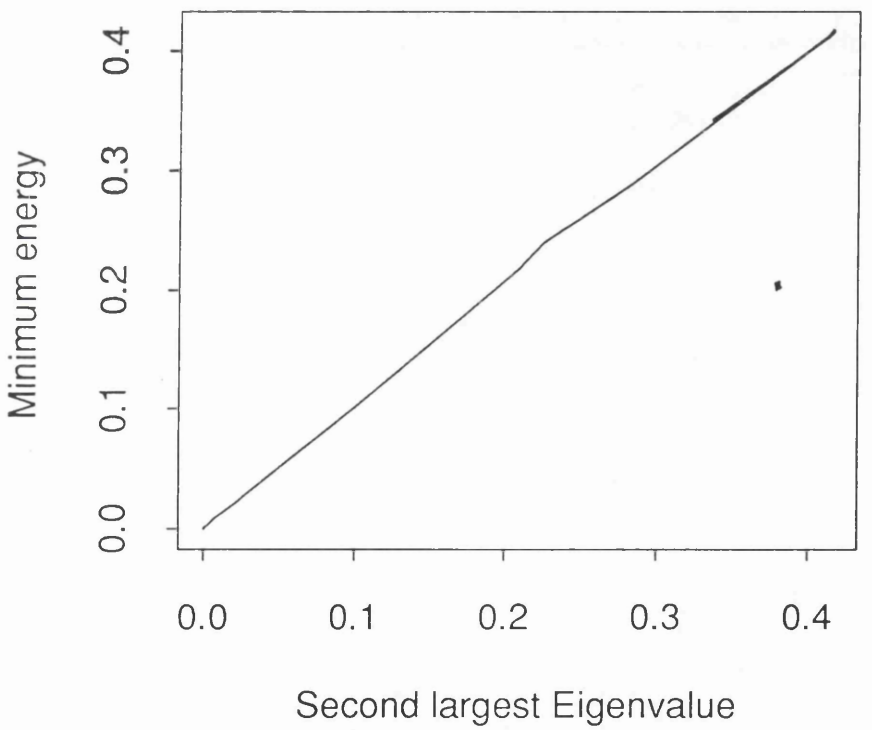

Figure 5.12. (a) Maximum energy versus first largest eigenvalue; (b) minimum energy versus second largest eigenvalue. All the attributes have been computed over the window 2.4-2.6 sec with a sliding window of 120 msec.

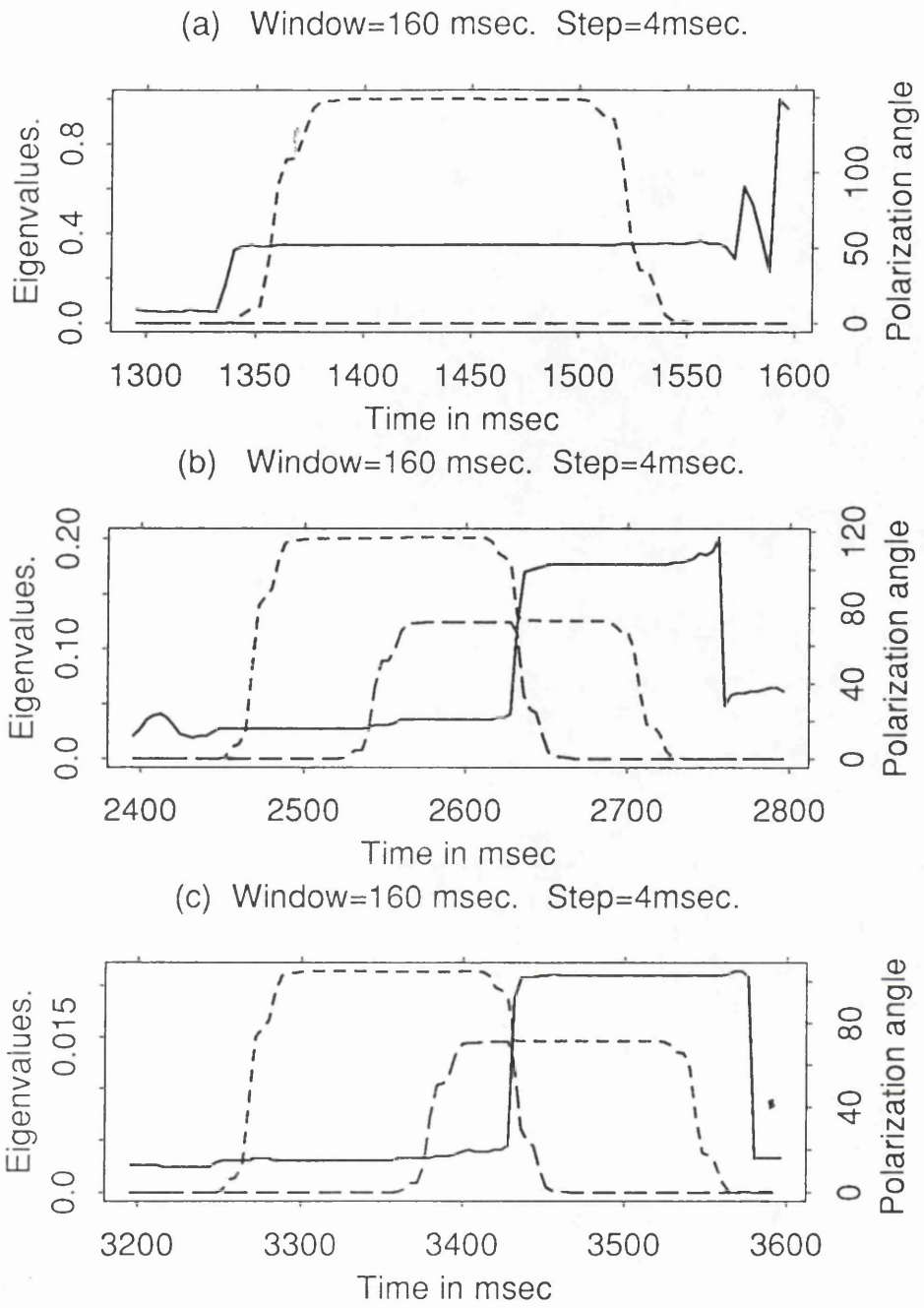

Figure 5.13. Instantaneous largest and second largest eigenvalues with increasing dashed lines and the instantaneous polarization angle (computed from equations 5.13) with solid line, calculated over the three windows: 1.3-1.6 sec, 2.4-2.8 sec, 3.2-3.6 sec, respectively, using the same input data as for obtaining Figure 5.3. The comparison of the two Figures shows a straightforward similarity between the attributes.

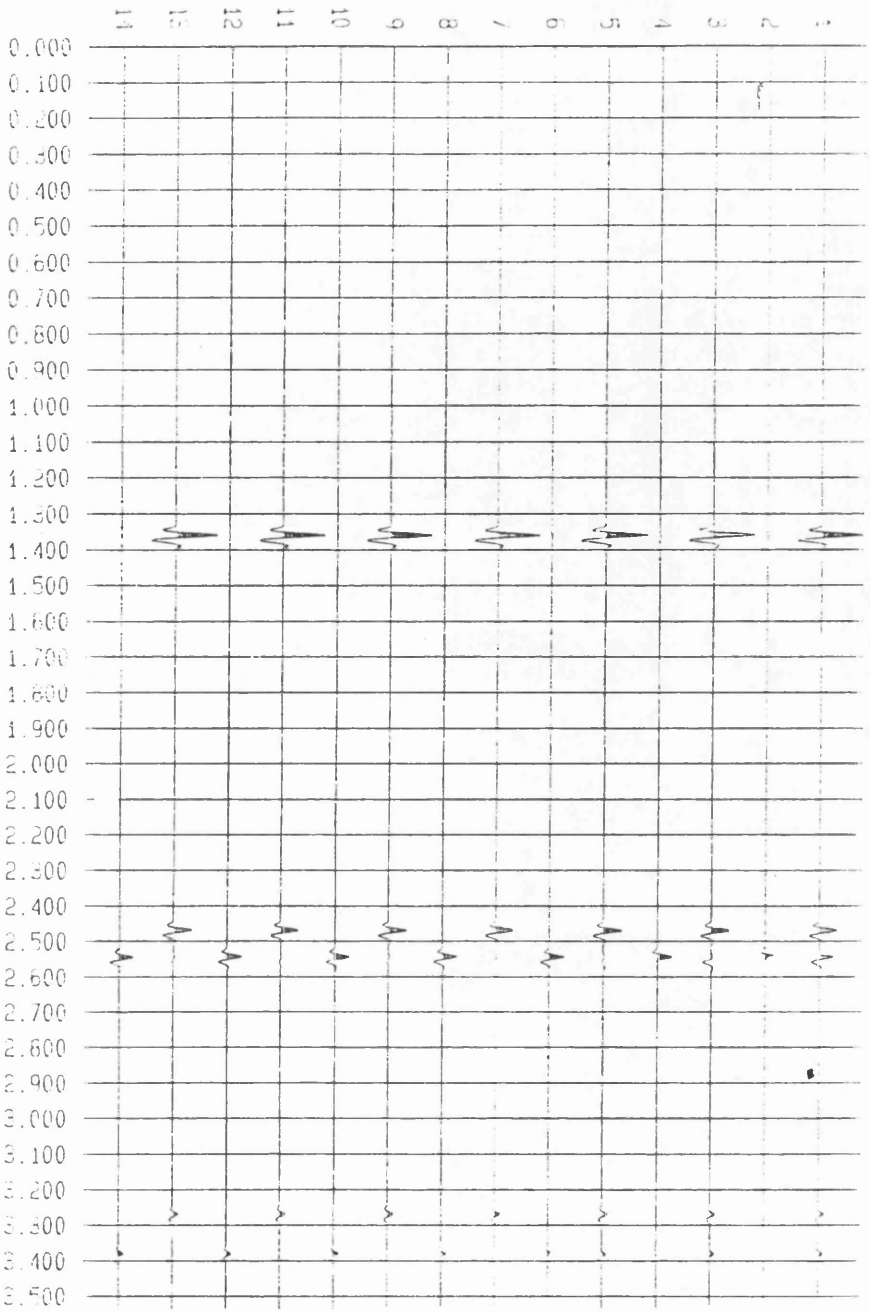

Figure 5.14. Filtered horizontal seismograms, traces 1 and 2 of Figure 2.3, by the energy filter computed using the covariance matrix. The length of the moving window varies from 60 msec. to 180 msec., by an increment of 20 msec., to get 7 pairs of filtered seismograms, (1,2), (3,4),....., (13,14).

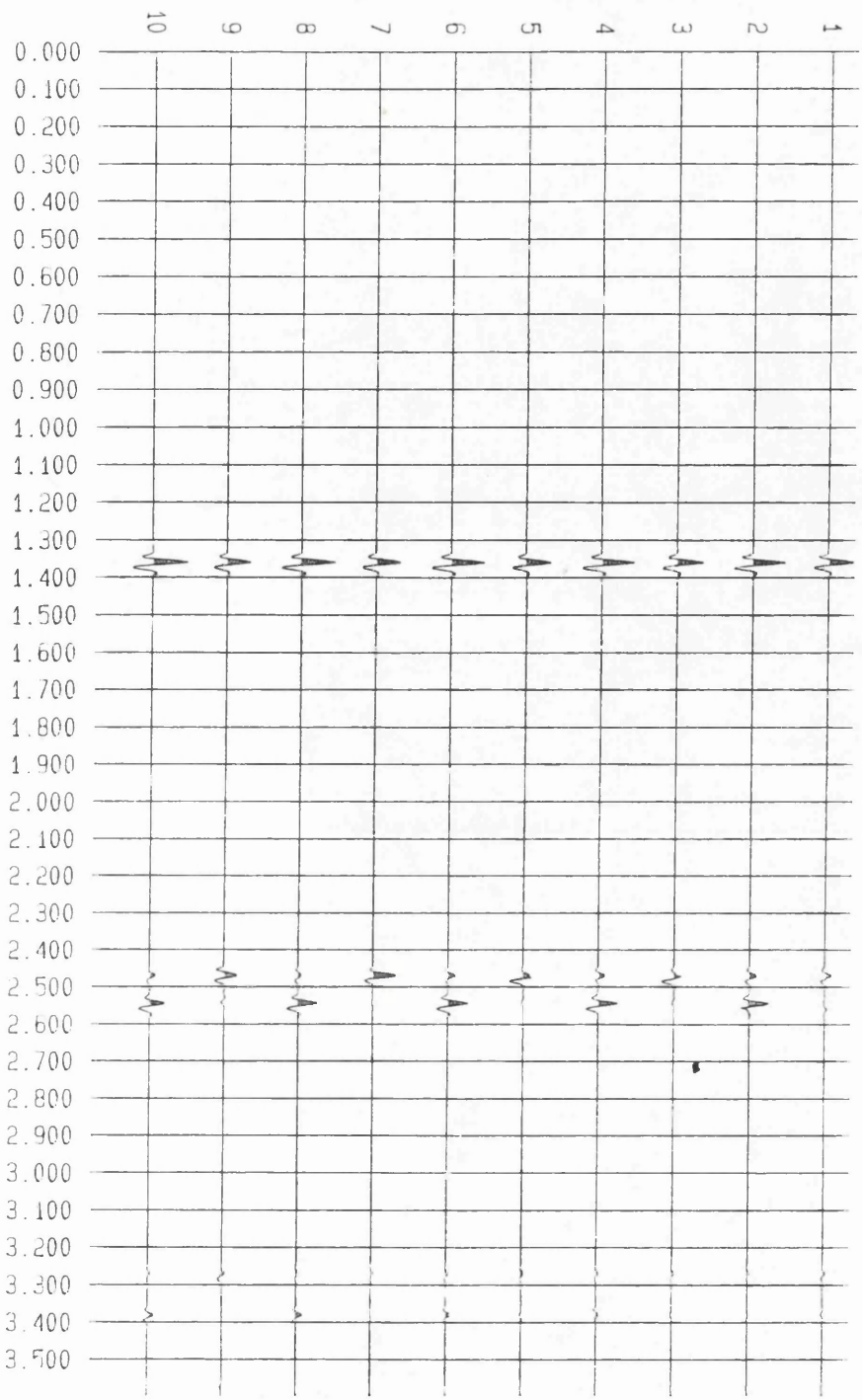

Figure 5.15. Filtered horizontal seismograms, traces 1 and 2 of Figure 2.3, by the polarization filter. The length of the moving window corresponding to each filtered pair of seismograms are 100 msec, 124 msec, 140 msec, 164 msec and 204 msec, respectively, from right to left. The polarization filter is not suitable for azimuthal anisotropic media

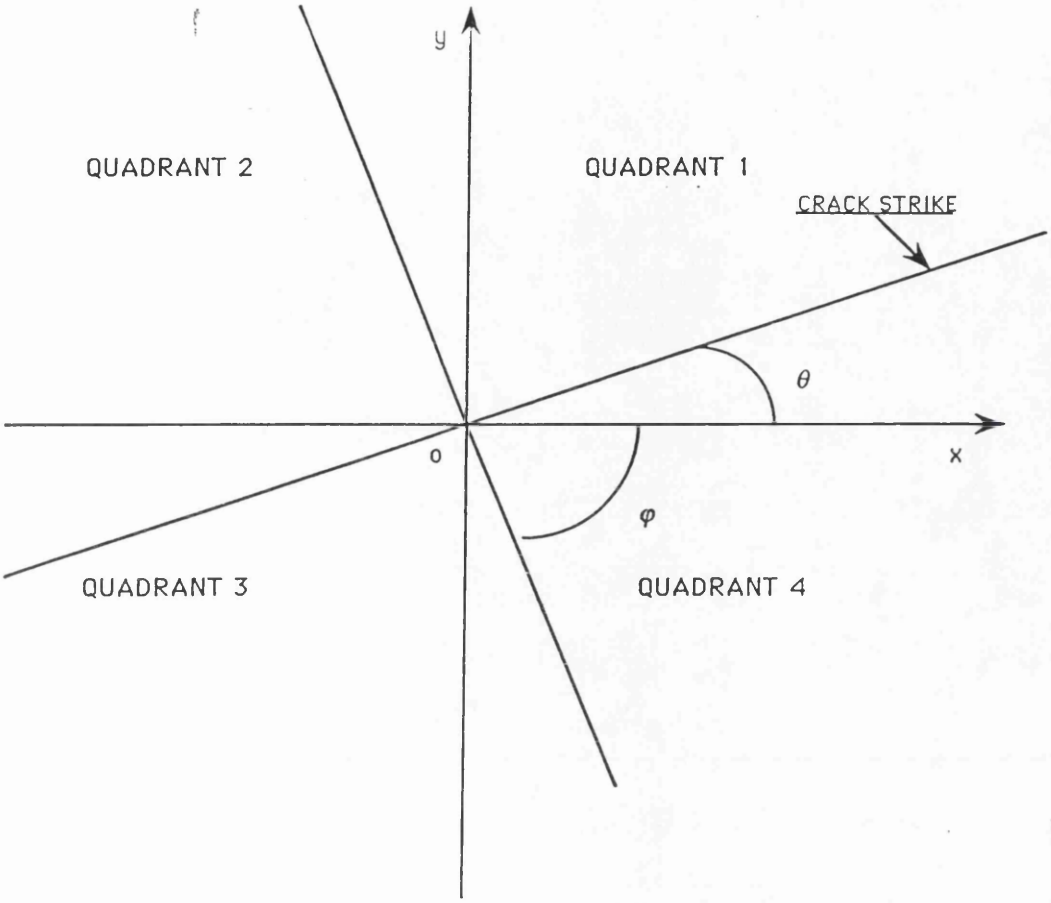

Figure 5.16. The plane of the acquisition coordinate frame (ox,oy) is divided into 4 quadrants.In this example, the crack strike is within the quadrants 1 and 3 at angle θ from the survey line; the normal to it is within the quadrants 3 and 4 at angle φ from th survey line. the angle of rotation is $\pi - \theta = \varphi + \pi / 2$.

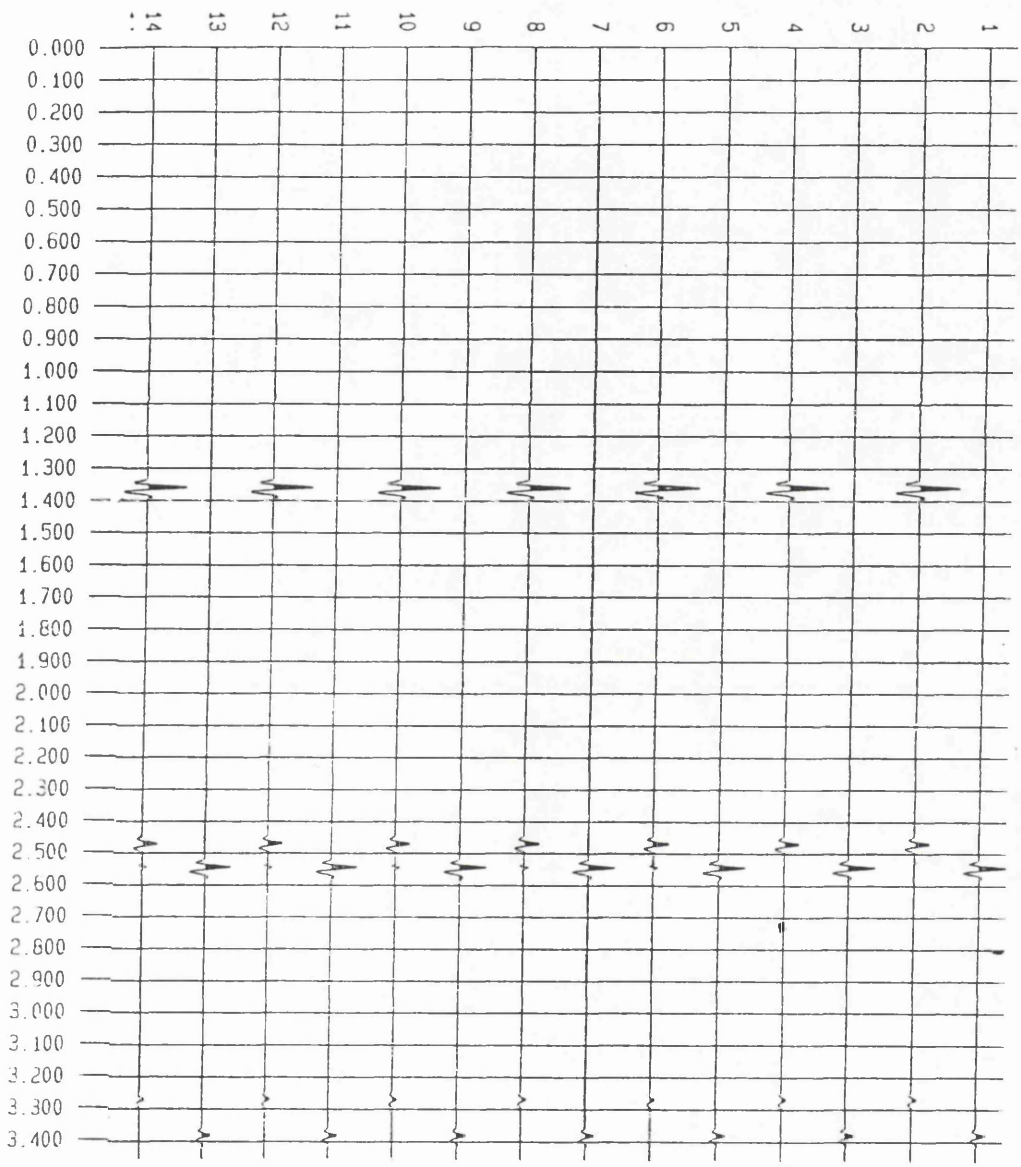

Figure 5.17. Application of the energy filter using equation 5.16, over the horizontal seismograms recorded along the survey line 3 at 75 m offset (Figure 4.1) by using an in-line shear source. In this case the amplitude of the fast shear is smaller than that of the slower one. This Figure shows 14 seismograms which are grouped into 7 pairs, from right to left; (1, 2); (3, 4) through (13, 14). Each pair represents the rotated radial and the rotated transverse, respectively. The length of the moving window used to compute the instantaneous polarization angle for rotating the original data varies from 40 msec to 160 msec., respectively. It is seen that the separation of the split wavelets is neither dependent on the length of the moving window nor on the amplitude of the fast shear.

CHAPTER 6

Application of energy attributes and Energy Filter to BIRPS data

6.1 INTRODUCTION

A three component deep seismic survey was carried out near Consett in England by CGG (Compagnie Generale de Geophysique) company in September 1988 for BIRPS (British Institution Reflection Profile Syndicate). The three hole technique for generating shear waves was attempted. Unfortunately, the sidehole shots did not generate shear waves with opposite polarization directions and normal to the survey line.

Using the energy of the rotated trace it is shown that

i) The sidehole shots are identical and produce the same amount of shear energy.

ii) Individual shots at the same shotpoint did produce shear energy and polarization varies randomly with offset. This may be due to an explosive source producing random shear polarization, because of the complexity of an explosion, and to the complex interaction of the earth with seismic shear waves and the free surface.

iii) The polarization filter and the energy filter are applied to shot records for comparison. Energy attributes computed from zero-offset data confirmed the theoretical promises in using those attributes to assess anisotropy.

6.2 DATA ACQUISITION

The three hole technique for generating shear waves were attempted on the South-North line 1 (Figure 6.1). The three holes had been aligned along East-West direction, i.e., perpendicular to

the survey line.

For most shotpoints three holes with 20kg of dynamite were detonated. Some shot points used 5 holes oriented West-East-North-South with respect to the centre. The charge of the central hole was varied from 10kg to 20kg. The use of 5 holes in some shotpoints was an attempt to recover the direction of the anisotropy axes using Alford's 1986 or Thomsen's algorithm. In some shot points when the central shot was fired the charge in the side holes blew simultaneously with it. Shot point numbers increase from North to South. Three separate colored parallel electrical cables recorded each component of the triphone receivers, and connected to the SN 368 LXU recording unit.

Each receiver station comprises 6 triphones connected in series and put in-line with a geophone interval of 4 m. Figures 6.1 and 6.2. show the position of each station and that of each shotpoint for the three survey lines, respectively.The survey lines were not quite straight lines, however, the orientations of the horizontal receivers were fixed with respect to the geographical orientations.

The recording unit may record up to 360 traces per shot, i.e. 360 active channels. Channels 1 to 120 are for cross-line components (East-West); channels 121 to 240 for vertical components and channels 241 to 360 for in-line components (North-South).

The spread length comprised 120 groups (each group made of 6 triphones) or 120 stations; the group interval was 50 m; the recording sampling rate was 4 ms and the recording length was 32 sec.

6.3. PROCESSING STEPS

The generation of shear waves with two opposite polarization direction from the East and West shot at each shot point proved to be unsuccessful. This can simply be demonstrated by subtracting two traces, either the transverse or the radial ones, recorded by

the same receiver from the two opposite shots. If the two shots generate shear wave with opposite polarization directions, it is expected that shear events will be enhanced because of their opposite polarity; otherwise the two subtracted traces give a nearly dead trace.

Another alternative in looking at this problem is by either adding or subtracting those traces and computing the variation of the energy of the trace versus angle of rotation of the resulting horizontal traces. This gives an insight on how much shear energy is released and its probable direction of polarization. If the two generated shear waves are of opposite polarization direction the maximum value of the energy of the trace will be extremely large. The angle of rotation for which this value is computed may be considered as the direction of polarization of the two shear sources as it will be demonstrated in the following.

A composite trace is computed by either adding or subtracting the traces recorded from the two opposite shots at the same station by the same receiver. Figure 6.3 shows the energy of the trace versus angle of rotation of the rotated composite radial trace, computed from the two radial traces recorded at offset 250 m. When the two traces are added the energy of the composite trace increases with the angle of rotation until a maximum is attained, at 50°. However, when they are subtracted the energy of the rotated composite trace is nearly zero for all angles of rotation.

As the two side holes did not generate expected shear waves and are similar to the centre shot (as demonstrated below), vertical stack of the three shots has been done and the data have been sorted in CDP gathers with a CDP interval equal to 25 m. The processing sequence carried out by CCG consisted mainly of amplitude recovery (spherical divergence), predictive deconvolution with operator length 180 ms and a gap of 42 ms, band pass-filtering. However, the processed shear data does not match the quality of P-wave data.

In contrast to the P-wave data, S-waves are randomly polarized

(Figure 6.5 & 6.6) within a CDP gather and may not stack properly. Besides, shear energy released from an explosive source is far less than P-wave energy. The former one may be minimized by applying the energy filter (paragraph 6.5) to the data at the first stage of the processing, and the latter one may be resolved by using proper shear source generators.

6.4. BIRPS DATA ANALYSIS.

Figure 6.4 shows three graphs energy of the rotated radial trace versus angle of rotation computed using the horizontal traces recorded at 250 m offset, of the three shot holes West, East and Centre of shotpoint 11. It is seen that the West and the East are identical as it is confirmed by similar plots from other traces and produce more shear energy than the central shot, since their charge (20kg in each hole) is twice that of the centre. The similarity of the three shots is clearly evidenced by observing that the angle of rotation giving the maximum value of the energy of the rotated trace from all the three shots is 50°.

The variation of the energy percentage with offset for the radial, the transverse and the vertical components is seen on Tables 5.1 & 5.2 of West shots of shot points 11 and 14. There is a clear evidence that the energy percentage of the transverse component decreases with increasing offset until a certain limit where it seems to begin to increase again.

Figure 6.5a, b shows the variation of the polarization direction with offset computed taking the data length as the window, i.e. 23.8 sec. These are polar plots of the energy of the rotated radial trace versus angle of rotation or azimuth. Polar plots of Figure 6.5a are from unfiltered data and that of Figure 6.5b is the result after application of a band pass filter, with the following frequency limits: 12-40 Hz for data from 0.0 to 500 ms, and 8-40 Hz for data from 1.0 to 24 s. The filtering has greatly reduced the effect of ground roll, which have in general frequencies less than 12 Hz.

TABLE 6.1

OFFSET / TRACE	100/21	250/24	400/27	550/30	750/34	1000/39	1750/54	2500/69	3250/84	4000/99	4750/114	5000/120
RADIAL	35.05	35.05	27.59	22.35	16.99	10.80	10.23	27.75	38.87	54.54	27.54	16.24
TRANSVERSE	26.39	39.22	20.70	21.65	17.67	09.91	11.58	08.29	04.96	06.40	13.28	16.52
VERTICAL	38.59	25.76	51.71	56.06	65.36	79.29	78.20	63.96	56.25	39.25	59.67	67.42

TABLE 6.2

OFFSET / TRACE	150/54	300/57	450/60	600/63	800/67	1550/82	2300/97	3000/112	3400/120
RADIAL	32.97	36.59	45.76	47.69	44.96	23.10	42.30	59.85	42.25
TRANSVERSE	34.29	29.77	28.97	17.68	09.73	08.17	07.18	17.13	10.71
VERTICAL	32.75	33.67	25.27	34.68	45.42	68.75	50.52	23.36	47.19

From those two figures, it is seen that the effect of noise on the polarization direction is not significant, particularly for strongly polarized events as it is demonstrated by the polar plots of traces 24 through 120.

The variation of the polarization direction with offset has been discussed by Liu & Crampin (1990). However, for near zero offset as modelling results in Chapter 4 have demonstrated, if an explosive source could create a stable shear source and the resulting reflection data could be recorded with high Signal to Noise ratio, it is expected that its polarization remains nearly the same or its deviation will not be significant at near zero-offset traces. This is not the case since polar plots from stations 21, 24 and 27 show three polarization directions completely different, deviating considerably from one another, both for unfiltered and filtered data. This demonstrates the real difficulty in trying to extract or interpret the polarization direction of the shear energy released from an explosive source, since it seems from those graphs to be random.

Strong reflected shear events have been identified within the windows 13.4-13.6 s. and 15-16 s. Their polar plots may be seen in Figure 6.6a, b, respectively. Some of them are well polarized but the polarization direction deviates considerably from either the axis of the transverse or the radial component (traces 60; 70; 100 of Figure 6.6a and traces 30; 69; 99 of Figure 6.6b). The others are less polarized. The high ellipticity may be due to interference of many signals, such as overlap of shear waves resulting from the splitting, noise, multiples and scattering.

The degree of ellipticity of the particle motion, may be, as it is seen from those examples, exactly described by the energy percentage of the maximum and the minimum value of the energy of the trace. They may be considered as directly proportional to the square root of the major and the minor axes of the ellipse, respectively.

6.5. ENERGY ATTRIBUTES FROM ZERO-OFFSET BIRPS DATA

Figure 6.7a, b, represents plots of instantaneous energy attributes and the instantaneous energy ratio computed from data recorded at 250 m and 350 m offsets, respectively, within the window 14-16 s., to ensure the data used has a vertical raypath and consequently, no P-wave energy on the horizontal components. The length of the moving window was 140 ms. Although shear energy was produced by an explosive source and the earth (Kisslinger et al, 1961; Wright & Carpenter, 1962; Geyer & Martner, 1969) some theoretical predictions (although based on a horizontally polarized shear source) can be seen from the graphs. Those attributes have been computed from VSP shear data (Chapter 8) to investigate the variation of the time delay between split shear waves.

Figure 6.7a illustrates a higher peak of minimum energy attribute within the window 14468-14632 ms, where the energy ratio is minimum. The hodogram within this window is shown on top left of Figure 6.8, evidencing the existence of two split shear wavelets with distinct polarization directions, roughly orthogonal. The three remaining hodograms drawn from windows 14000-14180 ms, 14684-14804 ms and 15000-15224 ms, respectively, chosen from Figure 6.7b (receiver offset is 350 m) , where three peaks of minimum energy are seen. The last hodogram (bottom right) is more complicated, but this is to be expected, as the minimum energy attribute within this window is small approximating noise level. The others clearly, identify two split shear waves with directions of motion roughly orthogonal.

6.6. APPLICATION OF THE ENERGY FILTER TO BIRPS DATA.

It has been shown from synthetic data in Chapter 5 that the energy filter may be efficiently used in case of anisotropy due to aligned cracks to separate and enhance the two shear waves resulting from

the splitting. This filter performs well, irrespective of the amplitude of the reflected waveform of one of the two shear waves when using the instantaneous polarization given by equation 5.15 to rotate the horizontal components.

It is commonly thought that crack formation and assymmetric camouflets (cavity created in the rock by the expolsion)due to an explosion are an important source of shear energy. From Figures 6.5 and 6.6 it shown that the directions of polarization of well polarized shear waves are neither parallel to the radial nor to the transverse axis, even for near-zero offset data. This randomness might be due to the complex nature of an explosion, to the interaction with the free surface or to the presence of anisotropy. In any case, it is thought that rotating the data toward the direction of maximum energy, which is a linear process, might enhance the Signal to Noise ratio and improve the quality of the signal; moreover if there is any splitting, the two split shear waves could separate well, as it has been demonstrated on synthetic data. Consequently, shear data might be well improved, if the energy filter is applied.

The energy filter is first applied to a set of data made of 8 traces (Figure 6.9) from West shot of shotpoint 11, traces 21 to 28, recorded at offsets 100 m to 350 m, respectively; the display has been confined to the window 14.6- 15.2 s, corresponding to 0.0-0.6 s in the figure, where some strong shear events have been observed. Figure 6.9a, b shows the unrotated radial and transverse components, respectively; Figure 6.9c, d their rotated versions, the instantaneous rotated radial and the instantaneous rotated transverse, respectively, using a sliding window of 160 ms length. The rotated radial and transverse components have been weighted by the energy function and the results are displayed on Figure 6.10a, b, respectively.

The same set of data is filtered with the polarization filter (Montalbetti & Kanasewich 1970) to compare its performance with the energy filter. The filtered set of data of the radial and the

transverse components are shown in figure 6.10c, d, respectively. The filtered signals present highly marked distortions. The polarization filter is only made to enhance shear waves polarized either parallel or normal to the in-line direction. Consequently, this filter might be appropriate only in the case of isotropic media for near vertical incidence, as polarization direction of shear waves changes with offset.

Figure 6.11 shows a portion of a shot gather produced by summing three records generated at one shotpoint (shotpoint 11) by the multiple hole technique. The in-line traces are shown in Figure 6.11a and the cross-line traces in Figure 6.11b. Bandpass filtering (5-20 Hz) and automatic gain control (AGC) were applied. Attempts to improve the quality of these sections by application of rotations to the entire trace length, were unsuccessful and actually degraded the data.

The instantaneous rotated radial and the instantaneous rotated transverse traces (both weighted by the energy function), rotated using the instantaneous polarization angle given by equation 5.15, are shown in Figure 6.12a, b, respectively. They were computed by implementing the energy filter (using the covariance matrix method) as a new processor written for Sierra-Seis (Sierra-Seis is a trademark of Sierra Geophysics). The processing parameters are otherwise identical to those used to produce the sections in Figure 6.11. The window length were 160 ms. The section in Figure 6.12b has events which can be traced nearly across the entire gather, in contrast to the pure in-line or the pure cross-line. The events in the in-line and the cross-line sections have a curved, discontinuous aspect. the events show a little move out as they are from deep within the crust, and no attempt has been made to correct for statics. Application of the algorithm does result in an improvement of the coherency of events on the sections where S-waves are recorded.

Application of FK filter before and after application of the energy filter is investigated. FK filtering is based on transforming

data from (x,t) domain into (f,k) domain by a double Fourier Transform where f is the frequency and k the wave number. several types of filters may be designed by considering the amplitude spectrum of the transformed data, such as low-pass FK filter, high-pass FK filter, dip reject filter, etc... The action of an FK filter is simply to retain the desired FK components and reject the unwanted ones. Such filters are known to possibly enhance considerably data quality.

Figure 6.13a shows the amplitude spectrum of the rotated radial transverse computed within the window 12.-14.0 sec. A high-pass FK filter with the starting and ending k values set to -0.025 and 0.025, respectively were used to filter the instantaneous rotated seismograms. The amplitude spectrum of the FK filtered rotated transverse seismograms is shown in Figure 6.13b, where the white zone symmetric about the f-axis is rejected. Figure 6.14a, b are the instantaneous rotated radial and transverse components, respectively, after application of FK filter. Reflections on the FK filtered rotated transverse seismograms stands out much more and can be followed to longer offset distances, particularly, events at approximately 12.5 sec and 12.9 sec, where clear hyperbolic move out can be seen. Consequently, a better stacking velocity may be determined.

The same high-pass FK filter were applied to:

i) the original data. The resultant sections showed no improvement.

ii) the original data before application of the energy filter. the results showed a slight improvement compared to Figure 6.12, but the sections showed enhanced broken events with no clear moveout as in Figure 6.14b.

6.7. DISCUSSION AND CONCLUSION

i) Polarization direction of reflected shear waves generated from an explosive source changes randomly with time and offset.

ii) Although computed from data generated by an explosive source, energy attributes confirmed theoretical promises of synthetic data and could be of great importance in applying them to data generated by horizontal vibrators.

iii) It was found in this case that rotation of entire trace sets did not improve the coherency of the data, but rather degraded it. However, the application of the energy filter does improve the coherency of a shot record. Unfortunately, we have not been supplied by static correction values and the velocity functions to try to apply it to CDP gathers and consequently derive a seismic section to be compared to the one obtained by the application of the conventional processing algorithms.

iv) Application of an FK filter on the instantaneously rotated seismograms does result in enhancing considerably shear data quality. S-waves generated from an explosive source and converted PS waves are split when entering an anisotropic medium. Both S-waves have different moveout (a non hypebolic moveout for the PS waves) and may be recorded by the same receiver. It is thought that split shear waves from both S-waves are separated after application of the energy filter and some of the separated split shear waves of mode converted PS waves may map near the f-axis of the FK amplitude spectrum.

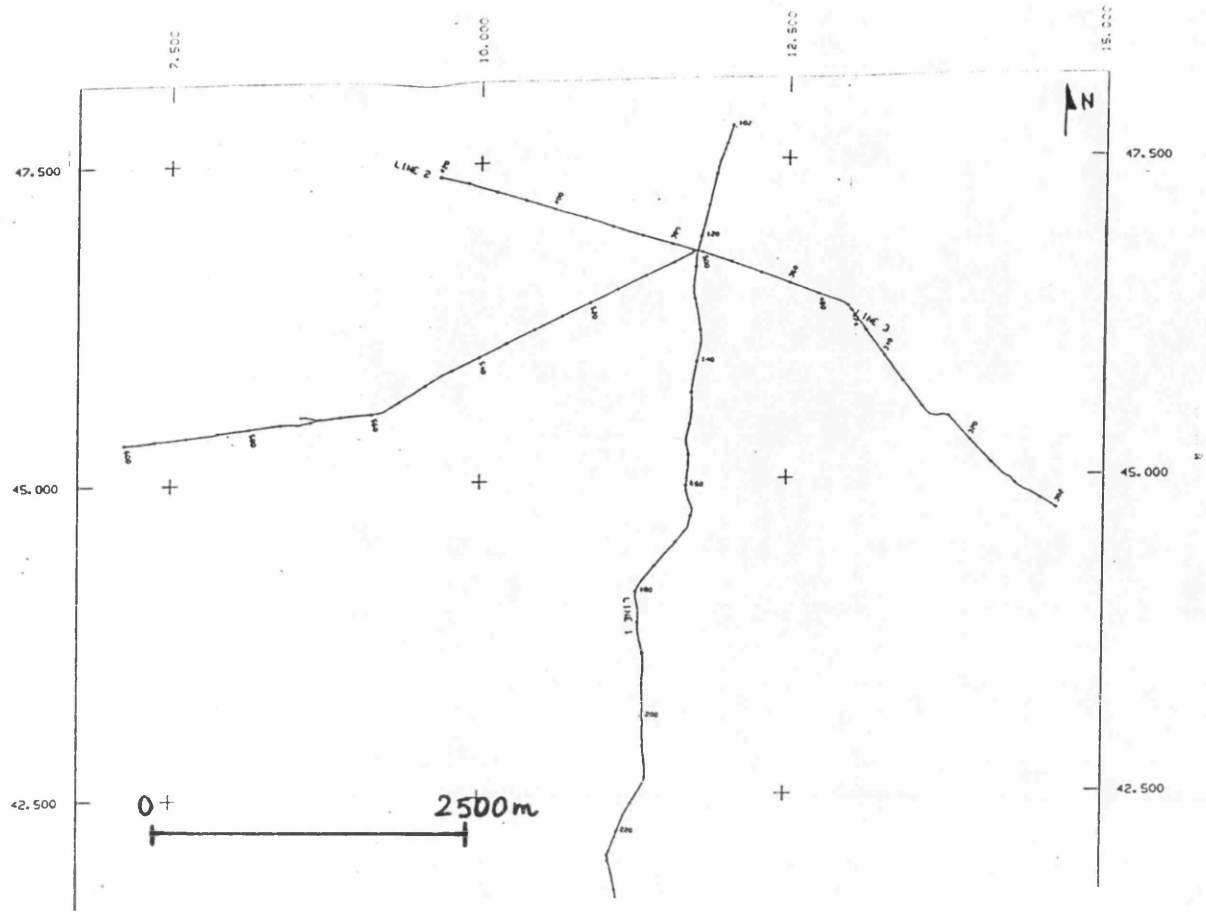

Figure 6.1. Three survey lines. Line 1 is oriented North-South; first receiver station is numbered 102 at the top of the line.

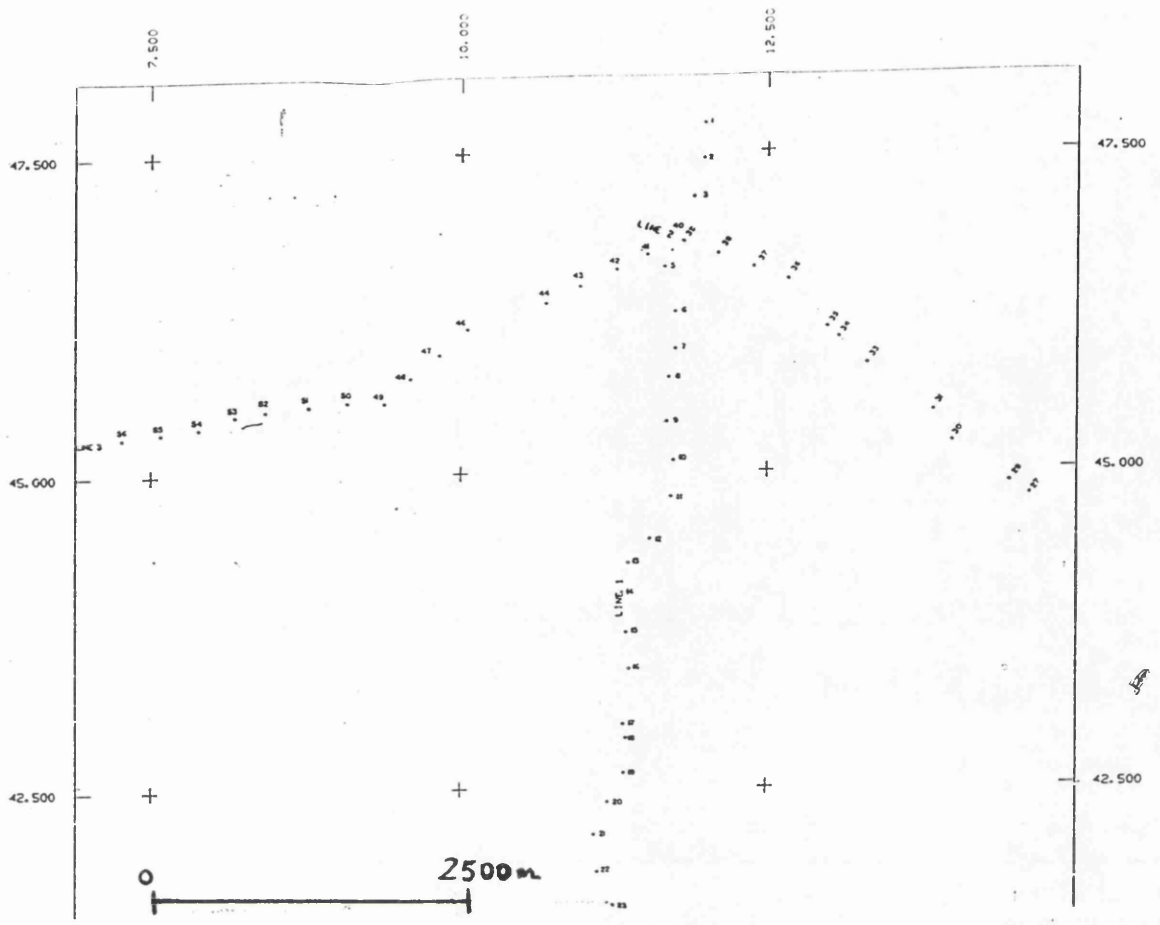

Figure 6.2. Shotpoint positions . Shot point number 1 is positioned at the top of the survey line 1. the direction of progress for line 1 is from North to South.

Figure 6.3

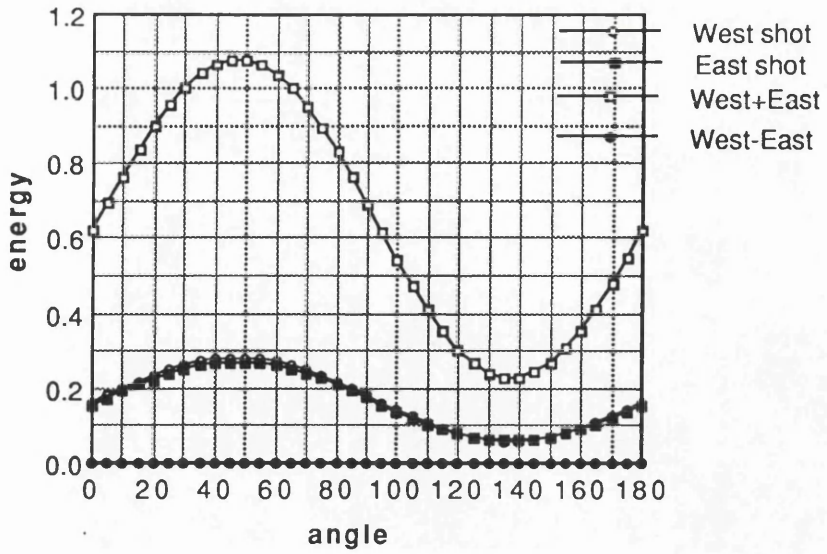

Figure 6.3. Energy of the trace of the rotated radial component recorded at offset 250 m versus angle of rotation. The lines joining the empty circles and the filled rectangles are from the horizontal components of the two side shots of shot point 11. the lines joining the empty rectangles and the filled circles are from the composite traces, obtained by adding and subtracting the horizontal components from the two opposite shots, respectively.

Figure 6.4

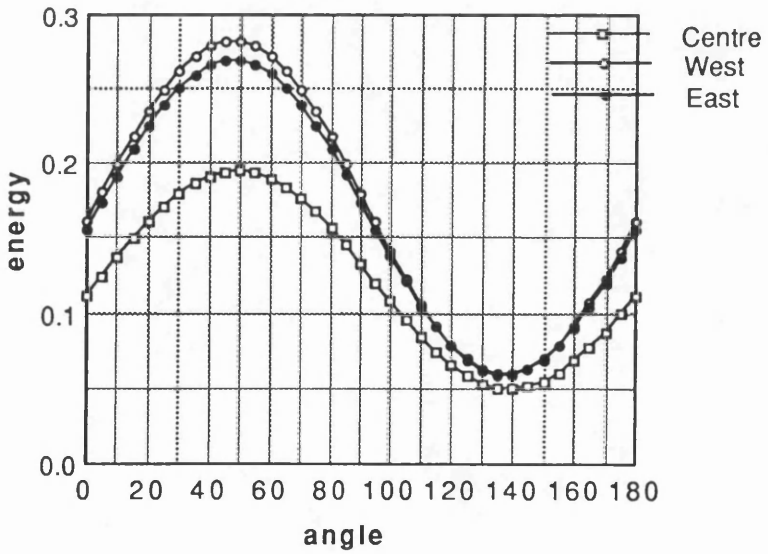

Figure 6.4. Energy of the trace of the rotated radial component recorded at offset 250 m versus angle of rotation of the three shots, West, Center and East of shot point 11. Lines joining the empty circles, filled circles and empty rectangle are that of the West, East and the center shots, respectively.

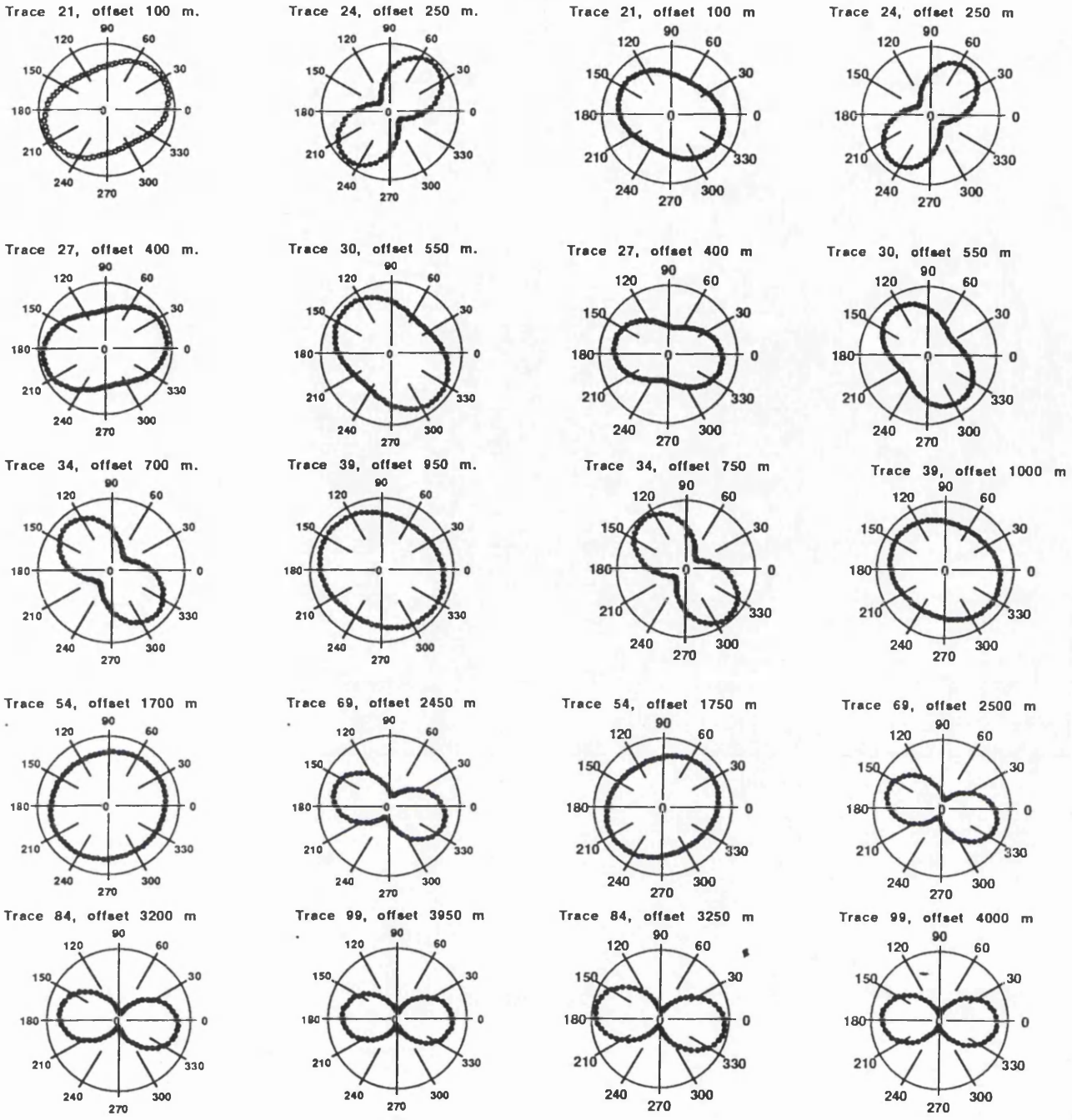

(a) (b)

Figure 6.5. Polar plots Energy of the trace of the rotated radial component computed over the whole data length versus angle of rotation at different offsets. 6.5a is from unfiltered data; 6.5b that of from filtered data by a bandpass filter (see text).

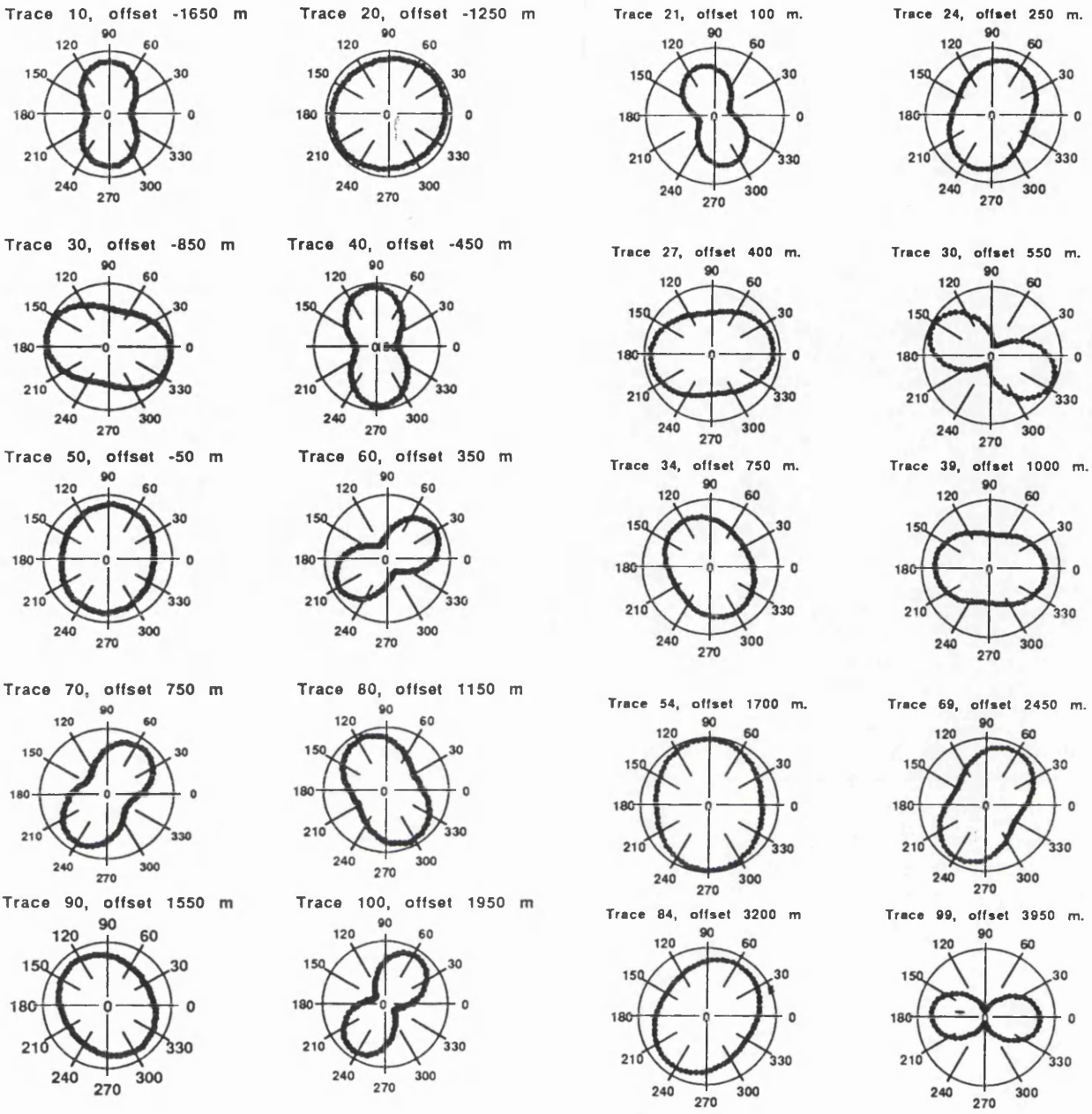

Figure 6.6. Same as Figure 6.5. (a) are polar plots computed over the window 13.4-13.6 sec; (b) computed over the window 15.0-16.0 sec., respectively.

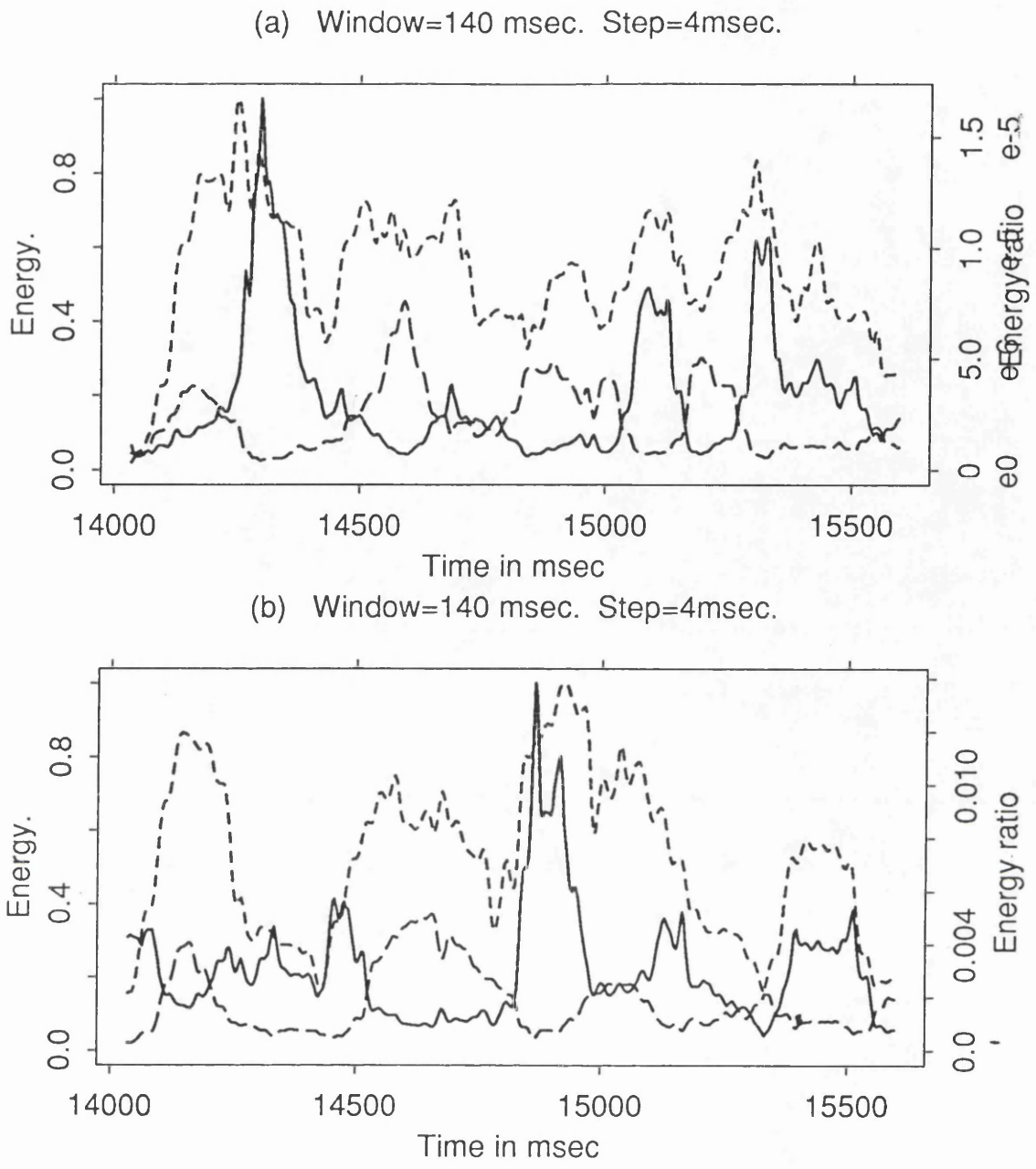

Figure 6.7. Plots of the instantaneous energy attributes and the energy ratio computed from BIRPS data recorded at 250 m (a) and 350 m (b) offsets, respectively, using a 140 msec sliding window. The instantaneous maximum energy, the instantaneous minimum energy and the energy ratio are with increasing dashed lines and solide line, respectively.

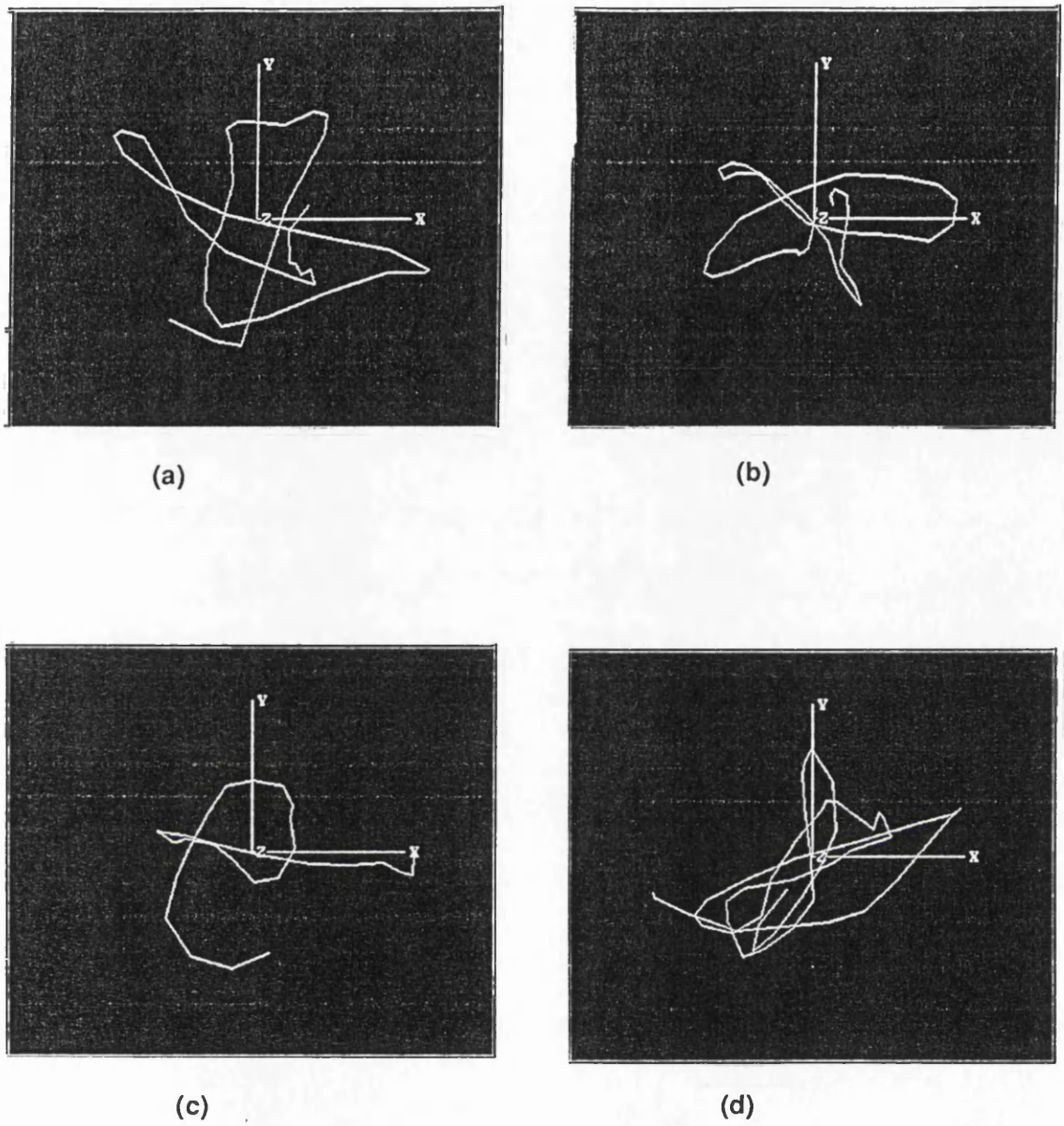

Figure 6.8. First hodogram (a) from window 14464-14644 ms chosen from Figure 6.7a. The three other are hodograms (b), (c) and (d) from windows 14000-14180 ms, 14684-14804 ms and 15000-15224 ms, respectively, chosen from Figure 6.7b where the energy ratio is small and an appreciable minimum energy.

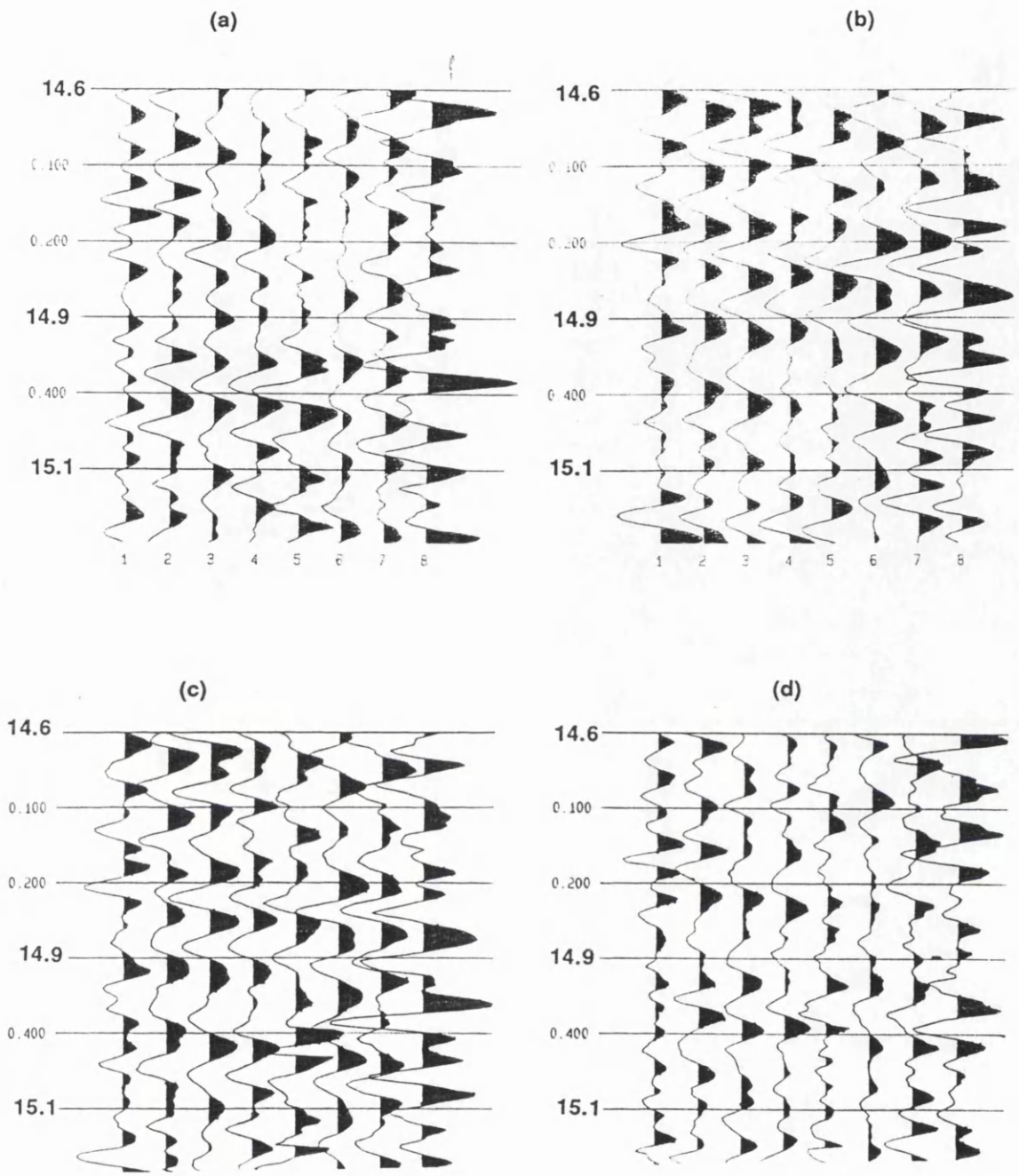

Figure 6.9. Traces 1 to 8 correspond to traces 21 to 28 (see text), respectively. (a) and (b) are the original data (unrotated) of the radial and the transverse components, respectively; (c) and (d) are their rotated versions, the rotated radial and rotated transverse seismograms, respectively.

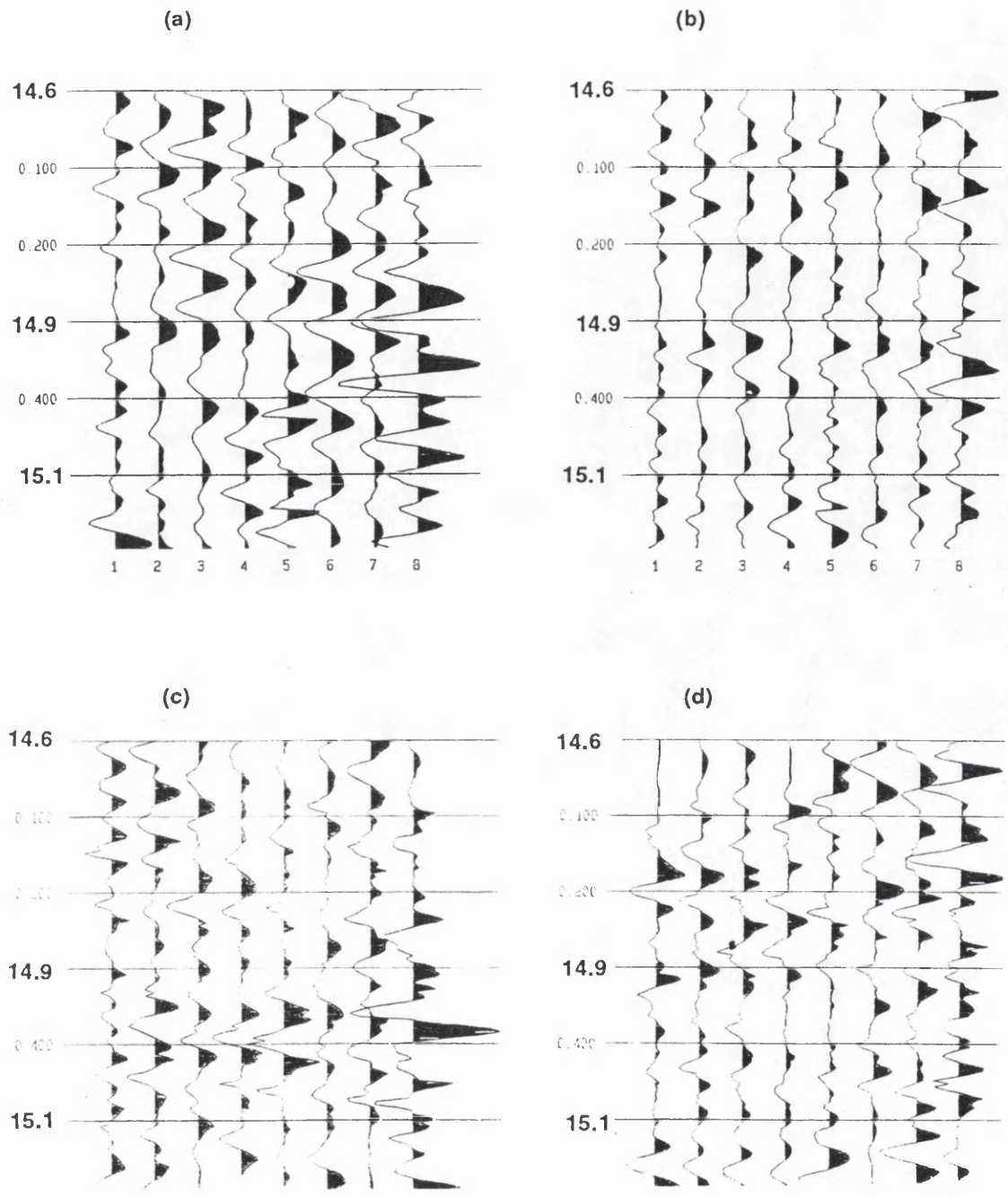

Figure 6.10. Traces 1 to 8 correspond to traces 21 to 28 (see text), respectively. (a) and (b) are the filtered versions of the original data of Figure 6.9a, b by the energy filter, i.e. rotated radial and rotated transverse seismograms, respectively, then weighted by the energy function. (c) and (d) are their filtered counterparts by the polarization filter, where the signal is seen to be distorted.

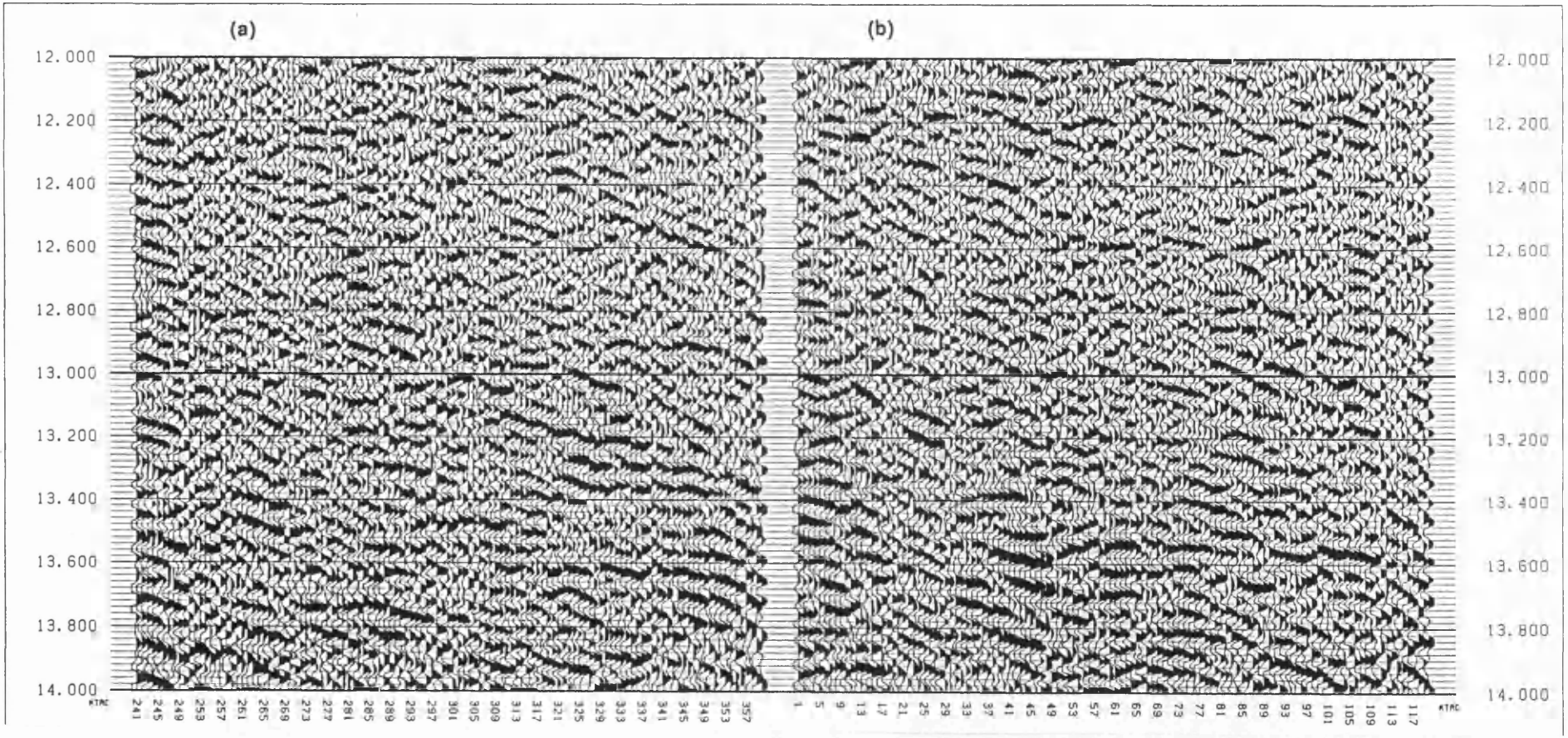

Figure 6.11. In-line (a) and cross-line (b) seismic shot records from BIRPS experiment. The sections are stacked from the three shots at shot point 11. Bandpass filtering (5-20 Hz) and AGC with 450 ms have been applied.

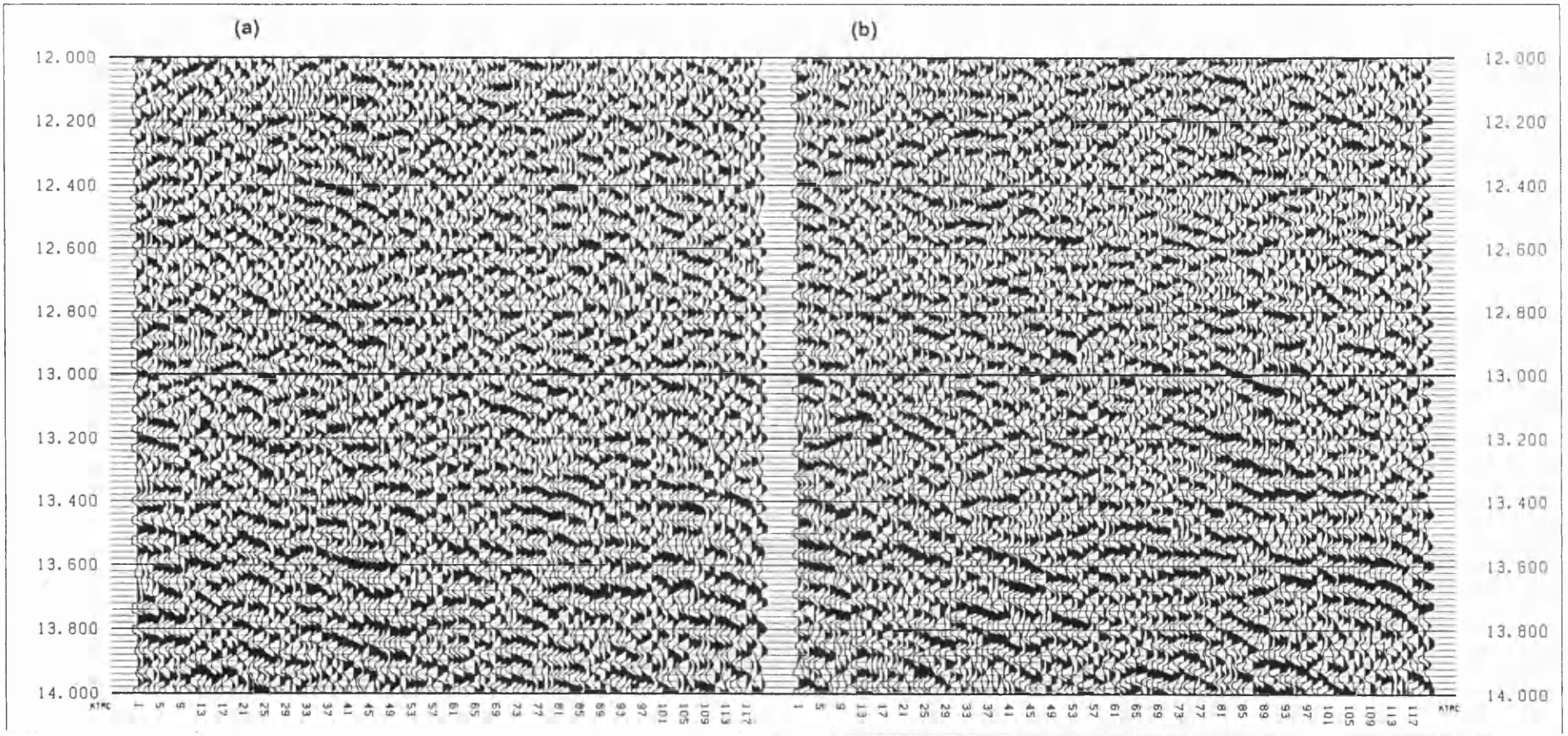

Figure 6.12. Instantaneous rotated radial (a) and instantaneous rotated transverse (b) obtained using the instantaneous polarization angle given by equation 5.15. These are computed from data shown in Figure 6.11 using a window length of 160 ms. Bandpass filtering (5-20 Hz) and AGC with 450 ms applied. Compare the events between 13 s and 14 s to those in Figure 6.11.

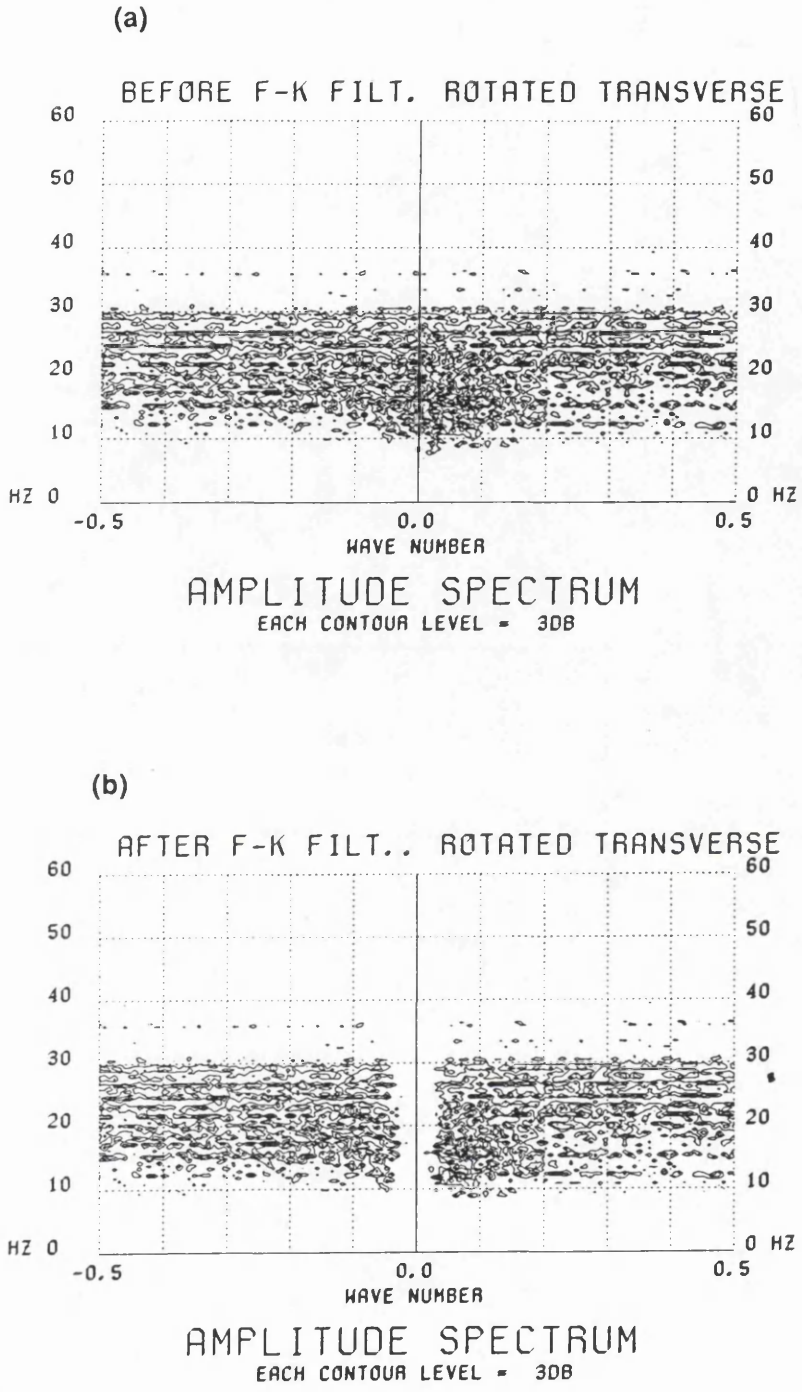

Figure 6.13. Amplitude spectrum of the instantaneous rotated transverse before (a) and after (b) a high-pass FK filter with the starting and ending k values -0.025 and 0.025, respectively.

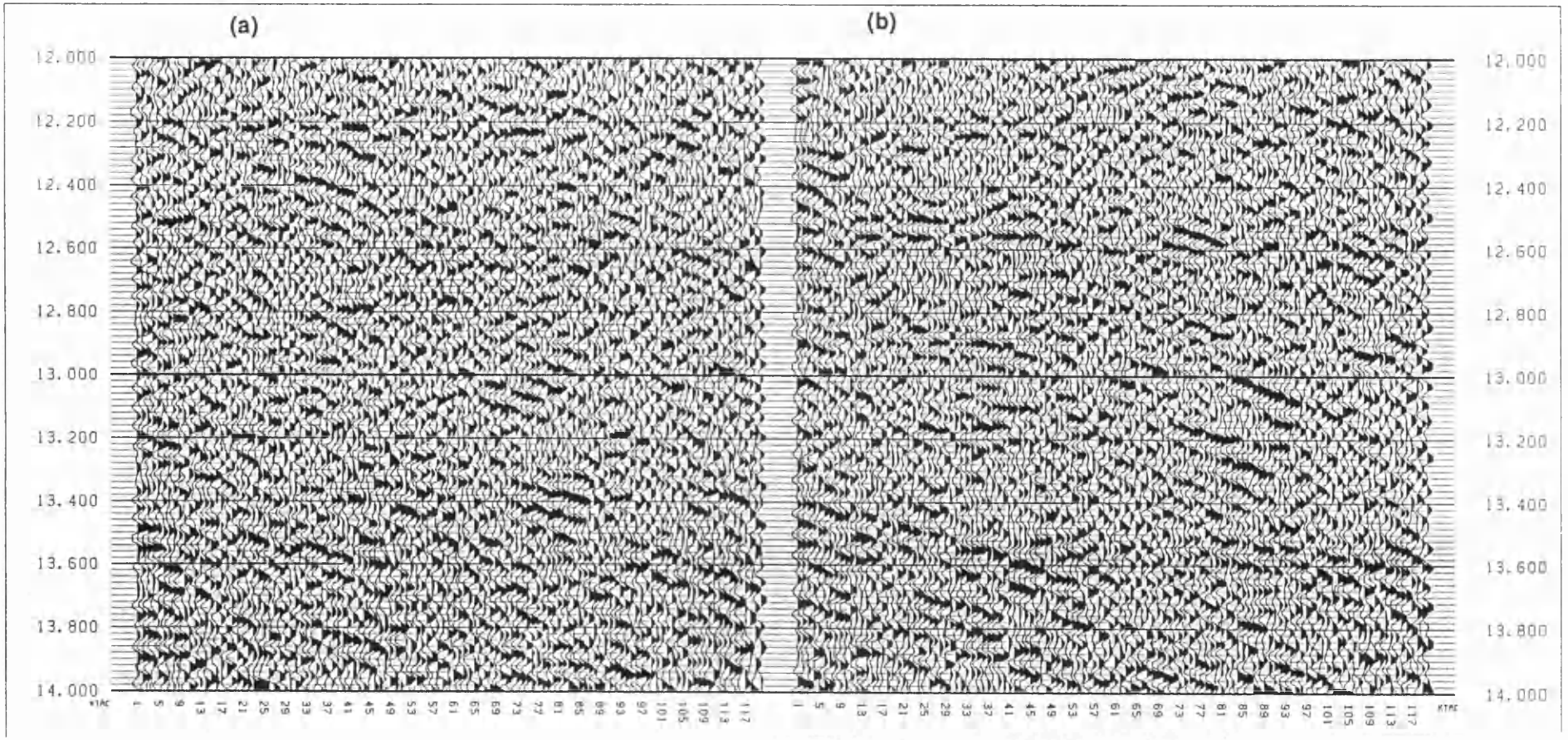

Figure 6.14. FK filtered instantaneous rotated radial (a) and FK filtered instantaneous rotated transverse (b) using a high-pass FK filter with the starting and ending k values -0.025 and 0.025, respectively. Compare to Figure 6.12.

CHAPTER 7

Testing the energy filter on vibroseis data

7.1. INTRODUCTION

A three-component seismic reflection profile with offsets of up to 10 km was shot during April-May 1992 through the Russian Kola superdeep well by the Department of Geology & Applied Geology of University of Glasgow, working with the Universities of Wyoming, USA, Bergen, Norway and several other Russian organizations. The problem addressed is the origin of seismic reflector layering in the crystalline crust seen almost wherever crustal CDP reflection lines are obtained. However, this chapter deals with the application of the Energy Filter on some shot files to assess its possible contribution in enhancing the quality of shear wave data generated from vibroseis source. The data processed shows that the filter improves the coherency of a shear shot record and can be used to separate split shear waves. The particle motions in the horizontal plane of some reflected events, which have been improved after application of the energy filter showed that some of the hodograms look elliptical and others have a more or less crucifix form, due probably to the interference of two shear events.

7.1. LOCATION OF THE AREA

The Kola region is located in the North-West of Russia, above the Arctic Circle, as shown in Figure 7.1, bounded in the West and in South by Norway and Finland, respectively. The star indicates the site of the borehole, the superdeep well SG-3, where crustal seismic reflection and new VSP data were acquired. The well has been drilled to over 12 km and is intended to go to 14 km, after which the hole will be converted into a geological observatory.

7.3. ACQUISITION OF SEISMIC DATA

The location of the main seismic line is shown in Figure 7.2, trending NN-SS. The final spread position was the superdeep well, as indicated by a star in the Figure. Thin lines in Figure 7.2 are geological boundaries and existing seismic and electrical profiles.

The geophones were oriented Up-North-East. The vertical component was recorded on strings of 12 geophones spread about 40 m. The horizontal components were recorded on single three-component geophones with the vertical disconnected, buried generally 1 m under the snow layer. The group interval was 50 m.

Vibrator points were at 100 m intervals, i.e., every second geophone station. Generally 8 vibroseis sweeps were used per vibrator (the vibrator vibrates vertically, thus generating only P-waves) position with a move up of 5 m per sweep, each sweep being 20 seconds long extending from 10 to 60 Hz. The recording time for each sweep was 40 s. Three vibrators with 20 m between each one formed a vibrator array; for the first sweep, the front was at the flag. The number of stations increased from South to North.

Three MDS-10's were used to record data at the sample rate of 4 ms.. Generally two auxiliary traces were used: one for time_break and the other for the sweep vibrator. Data were recorded on channels 1 to 90 in the following order: Vertical, In-line, Cross-line.

7.4. APPLICATION OF THE ENERGY FILTER.

The data are derived from exabyte tapes created in the field for quality control. This should be regarded as a preliminary test for complete shear wave processing after the complete data set has been demultiplexed.

The data have been correlated using the sweep trace and, the files corresponding to each vibrator position are summed to obtain

a single shot file. Figure 7.3 is a display of the first 5 shot files corresponding to vibrator positions 635, 637, 639, 641 and 643, respectively, within the window 4.0-6.0 s, representing the seismograms recorded by the transverse component (the data has been band-pass filtered by 10-35 Hz before and after application of AGC with a 350 ms window). As it is inferred from this Figure, nearly no continuous events are exhibited in files 1, 2 and 3. However, some good events are evident within shot files 4 and 5. The presence of random continuous events on the transverse component for successive shot files has been observed in almost all shot files, on which the search for shear events has been carried out. Figure 7.4 testify to this, where the transverse seismograms of shot files 12 to 17 corresponding to vibrator positions 663, 665, 667, 669, 671 and 673, respectively, resequenced as 1 to 6, are displayed within the window 4.0-6.0 s.

Among the 20 files studied, continuous events on the transverse component are almost absent above 7.0 s of recording time, except for file 5, shown in Figures 7.5 and 7.6 (first plot in each figure are the recorded radial and the recorded transverse seismograms, respectively), where some possible shear events may be seen. The records indicate poor to moderate quality data to 5 s, declining rapidly below this.

Figures 7.5 and 7.6 are the result of the application of the energy filter on shot file 5 (vibrator position 643) with different window lengths. These are the rotated radial and rotated transverse seismograms, respectively. The first plot in each figure are the original data, i.e., the radial and the transverse seismograms of shot file 5 over which the energy filter has been tested using window lengths of 40, 80, 120, 160, 200 and 400 ms, respectively. It is inferred from both figures that a window length comprised between 160 ms and 260 ms might be appropriate to improve the coherency of some shear events. For example, reflected events in Figure 7.6 within windows 11.0-11.2 s, 11.2-11.4 s and window 12.3-12.5 s, have become more apparent. Improved events

in Figure 7.5 may be seen within windows 11.3-11.4 s and 11.7-11.9 s; others have vanished such as events within windows 11.0-11.2 s and 12.3-12.5 s. However, those events become apparent in Figure 7.6 with improved coherency.

Events which have become less coherent after application of the energy filter, and can still be seen on the rotated radial and the rotated transverse seismograms, might have either weaker amplitudes (data quality problem) or random polarization directions, i.e., the polarization direction of reflected events by the same reflector recorded along the seismic line changes randomly in space within large limits. Noise interference might also contribute to that, and it is thought that shear wave interaction with the earth is complex.

The application of the energy filter with a 160 ms moving window on shot files 12 to 17, resequenced as 1 to 6, respectively is shown in Figures 7.7 and 7.8, representing the rotated radial and the rotated transverse seismograms, respectively. Note the particular improvement of the coherency for events in shot files 2 and 3 in Figure 7.8 within the window 4-4.2 s. Those events are also apparent in Figure 7.7 but weaker and less coherent. By looking at the arrival time of those two events in both Figures, it is clearly seen that the events in Figure 7.8 are ahead by approximately 40 ms from those two events in in Figure 7.7. To determine if there is any time delay between other events in the rotated radial and the rotated transverse seismograms is difficult because of the weakness or absence of coherency in the rotated seismograms.

Further investigations have been carried out by looking at the particle motions in the horizontal and the vertical plane within some selected windows. Figure 7.9 shows the particle motion in the horizontal and the vertical plane within window 4.54-4.64 s of seismograms 37, 40, 46 and 55, respectively of shot file 2 in Figure 7.4. The program for plotting hodograms was written for BIRPS data which are recorded in a different order compared to Kola data. Consequently, the axes (Y, Z, X) in BIRPS case become (Z,

X, Y) for Kola data. The hodograms within the horizontal plane in this Figure are more or less elliptical but show the presence of shear motion, particularly the last two ones.

The hodograms in the horizontal plane within the window 4.04-4.16 s of shot file 14 (file 3 in Figure 7.4), where two split shear waves have identified after application of the energy filter with the coherency improved on the rotated transverse are shown in Figure 7.10. They are plotted from three-component seismograms 37, 46, 49, 52, 55 and 64, respectively. Clearly, two distinct motions may be seen from each hodogram, but their orthogonality is not evident. Figure 7.11 are particle motions plotted over the window 4.44-4.6 s of the three component seismogrammes 34, 40, 49 and 61, respectively of shot file 4 Figure 7.4. Within this window the seismic event is apparent, but weak and less coherent on the rotated transverse seismograms (Figures 7.8) and vanishes on the rotated radial seismograms (Figure 7.7). The hodograms look rather elliptical. Hodograms are always difficult to interpret, because of the effect of interfering waves.

7.5. DISCUSSION AND CONCLUSION

This simple experiment has demonstrated the robustness of the energy filter in improving the coherency of shear wave data, and in dealing with anisotropy, particularly the possibility of obtaining two shear seismic sections. However, for shallow data recorded with non zero offset, the filter should be used with care, as it was designed for separating split shear waves and enhancing vertically reflected shear waves.

It is well known that in an isotropic medium the polarization of shear source, which is neither pure SV nor pure SH rotates as offset increases (Liu & Crampin, 1990), thus creating SV and SH waves travelling with the same velocity. In this case the application of the energy filter by rotating the horizontal seismograms sample by sample, using the instantaneous

polarization angle given either by equation 5.13 or equation 5.14 is very useful and may lead to an enhanced shear record, as the polarization direction of shear waves resulting from an explosive or vertical vibroseis source is random in time and space, as demonstrated in chapter 5.

By applying the energy filter, split shear waves have been separated and identified on shot records, some with improved coherency such as events in shot files 13 and 14 (resequenced as 2 and 3, respectively) within window 4.00-4.200 s. However, identification is not obvious in other shot records, as some events become less coherent or vanish from one of the rotated seismograms or from both. Bad data quality can contribute to poor performance of the technique. Also the method will be affected by waves with horizontal component of motion such as ground roll, elliptically polarized waves or P-waves with non vertical incidence and converted PS waves. It is suggested to use the P-Wave Filter (PWF) stated by equation (3.6) in chapter 3 prior to the energy filter. Also F-K filter can be used to attenuate ground roll. Editing and static correction followed by a broad bandpass filtering should be addressed at the early stage of the processing.

The instantaneous rotation angle computed using equation 5.15 is kept constant until the moving window goes through the composite split wavelet. Hence, the composite wavelet is rotated by this angle. Consequently, if the time delay between two splitting wavelets is long enough, say, longer than the length of a wavelet, which might be the case for deep reflection data, this technique can deal easily and automatically with multiple splitting, a case in which techniques published so far fail to do.

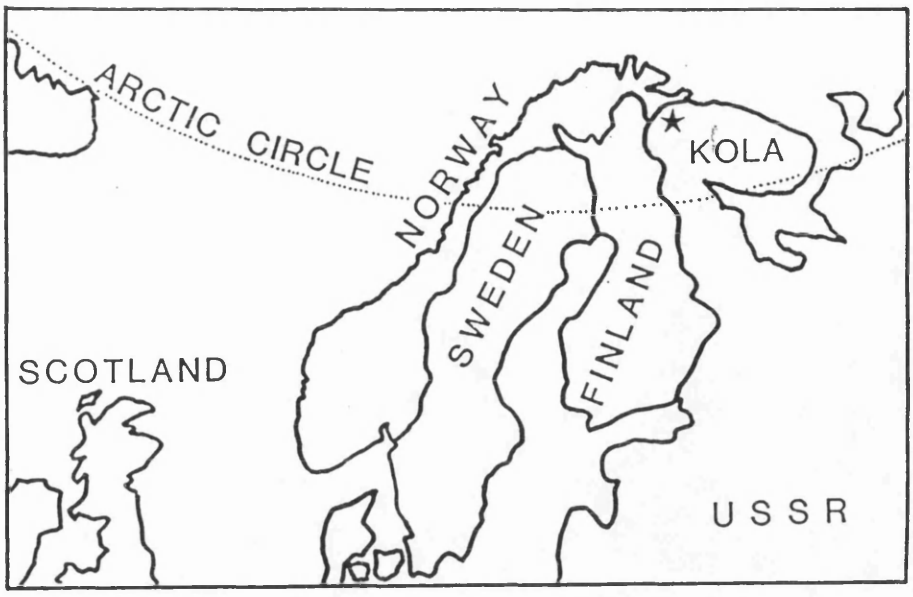

Figure 7.1. Location of the Kola region. The star indicates the site surveyed.

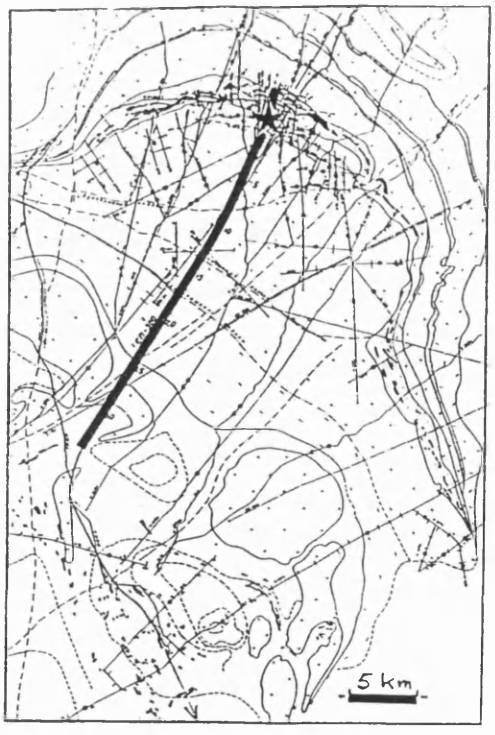

Figure 7.2. Location of main seismic reflection line through Kola superdeep well (star). Thin lines are geological boundaries and existing seismic and electrical profiles.

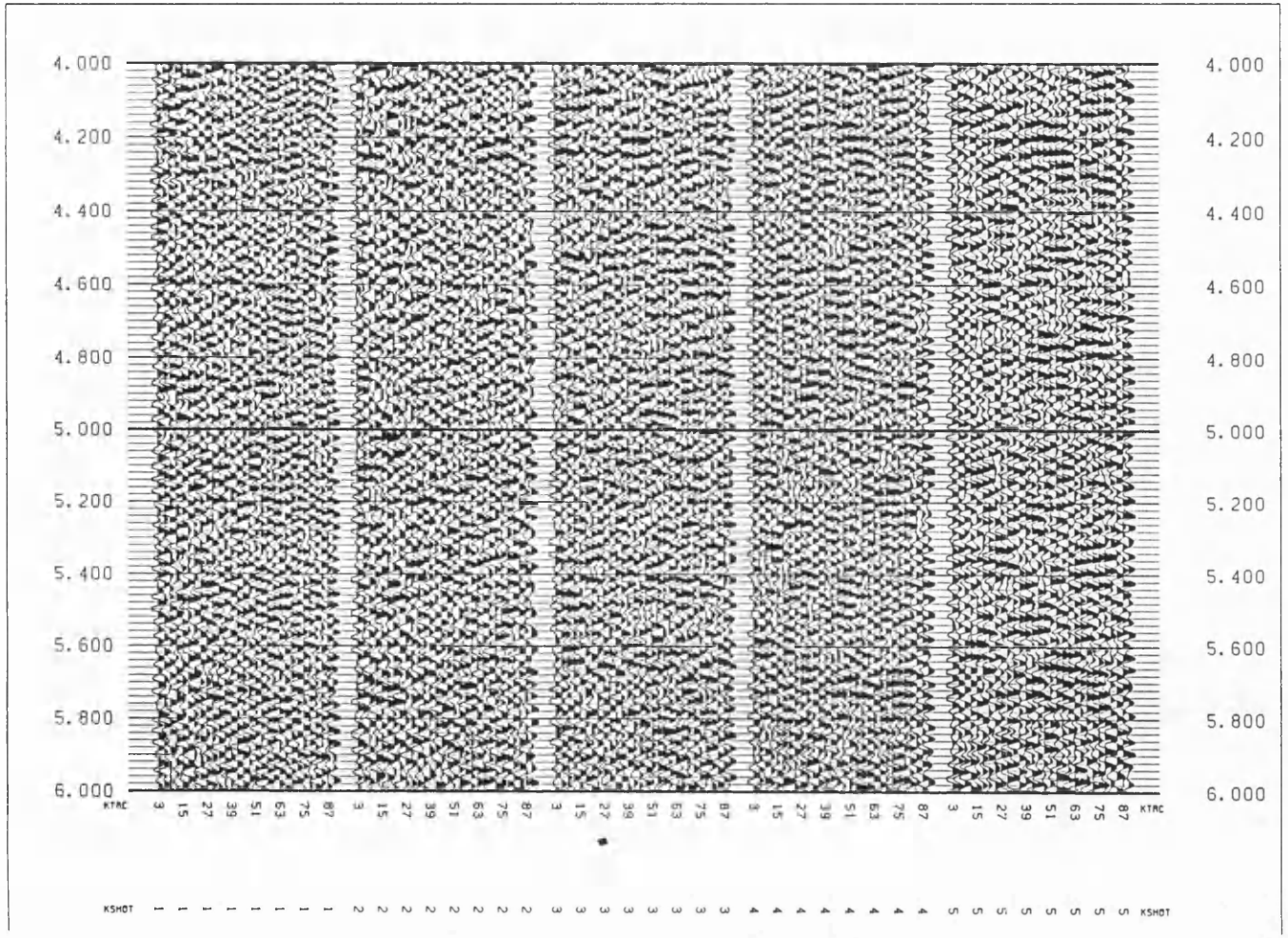

Figure 7.3. Display of seismograms recorded by the transverse geophones, of the first 5 shot files, within window 4.0-6.0 s. Band-pass filtered (10-35 Hz), AGC applied.

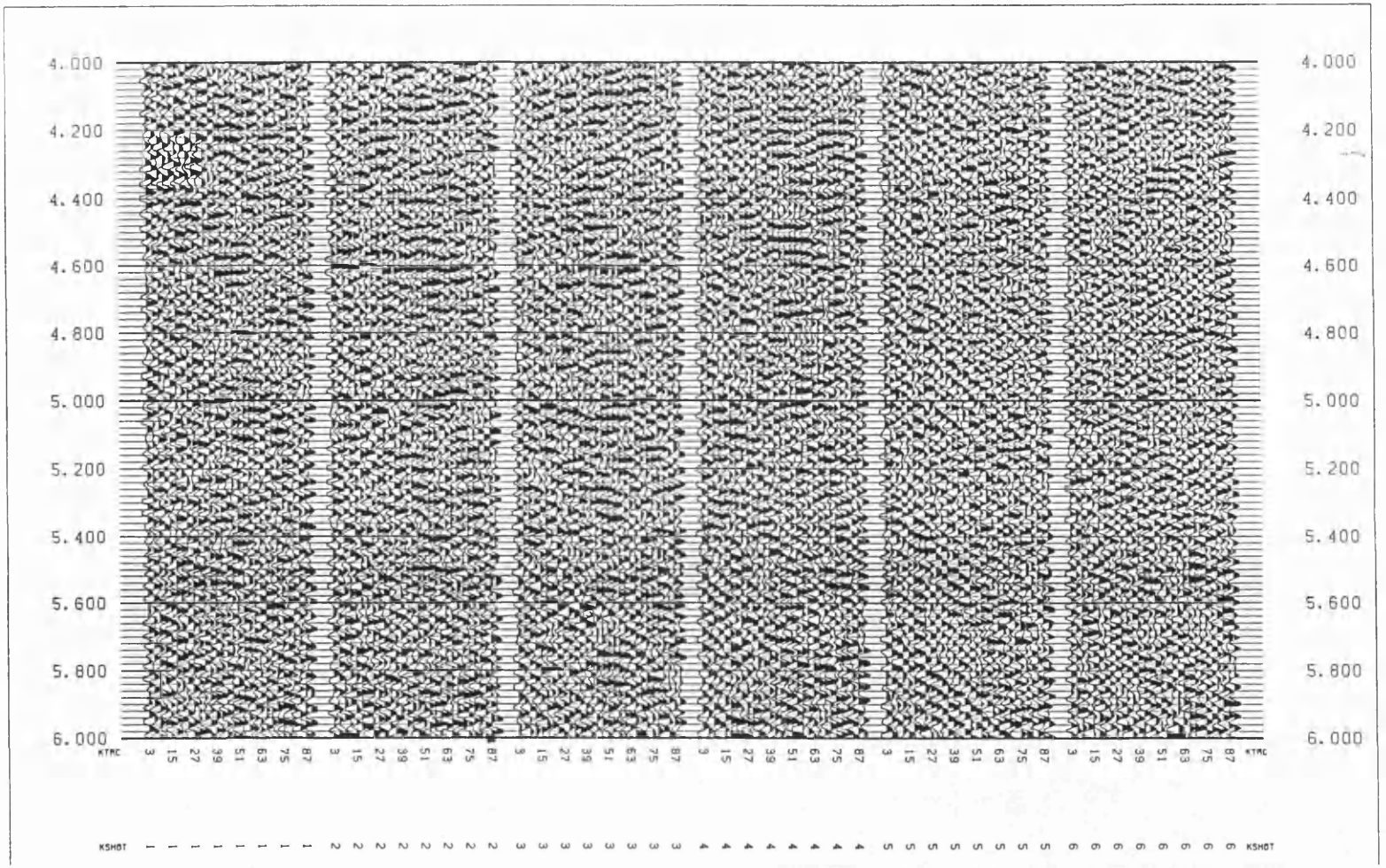

Figure 7.4. Display of seismograms recorded by the transverse geophones, of shot files 12 to 17, resequenced as 1 to 6, respectively, within the window 4.0-6.0 s. Band-pass filtered (10-35 Hz), AGC applied.

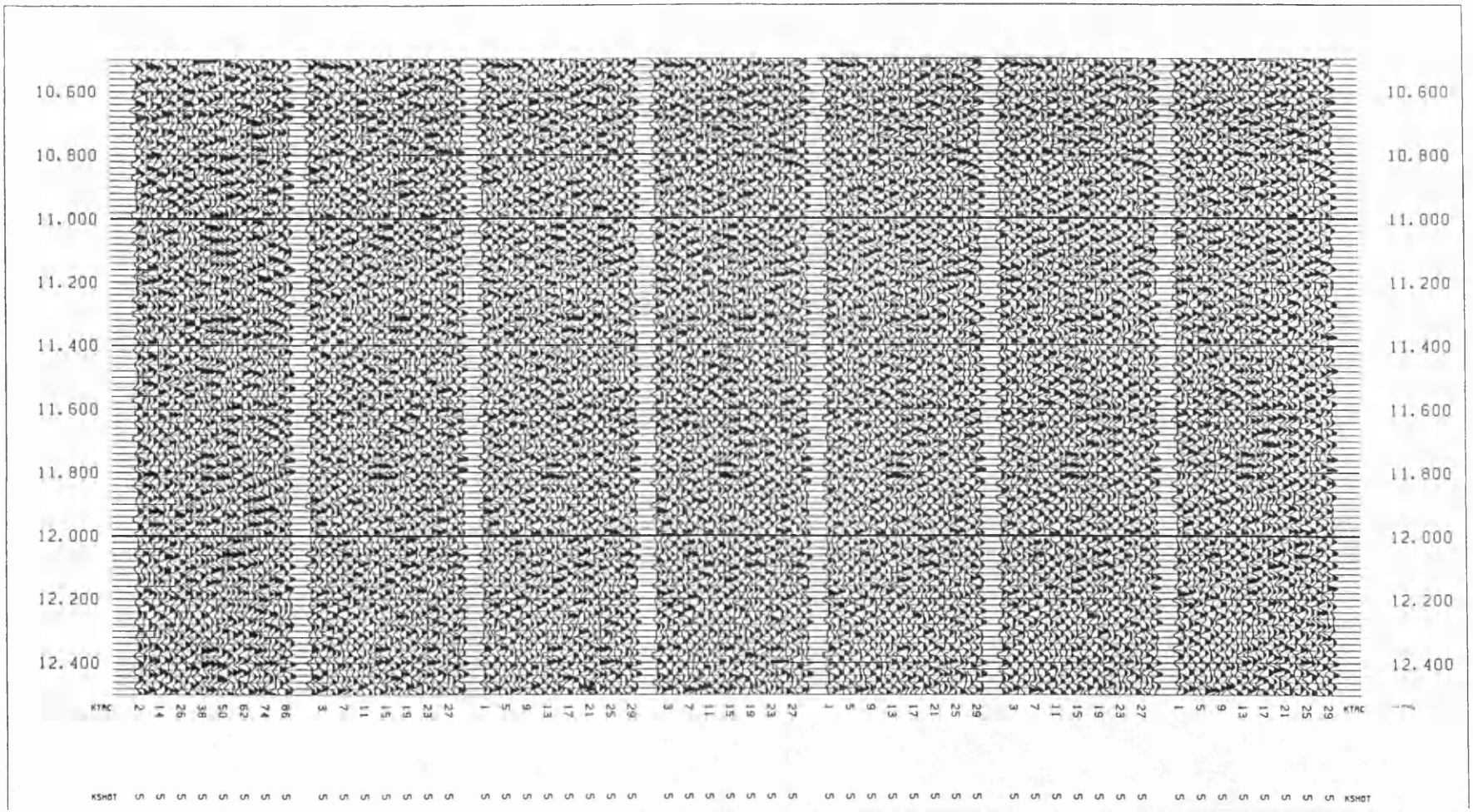

Figure 7.5. Test of the energy filter over horizontal components of shot file 5 (Figure 7.3). First plot are the unrotated radial seismograms, over which the energy filter with moving window lengths of 40, 80, 120,160, 200 and 400 ms, has been applied, respectively, to obtain rotated radial seismograms.

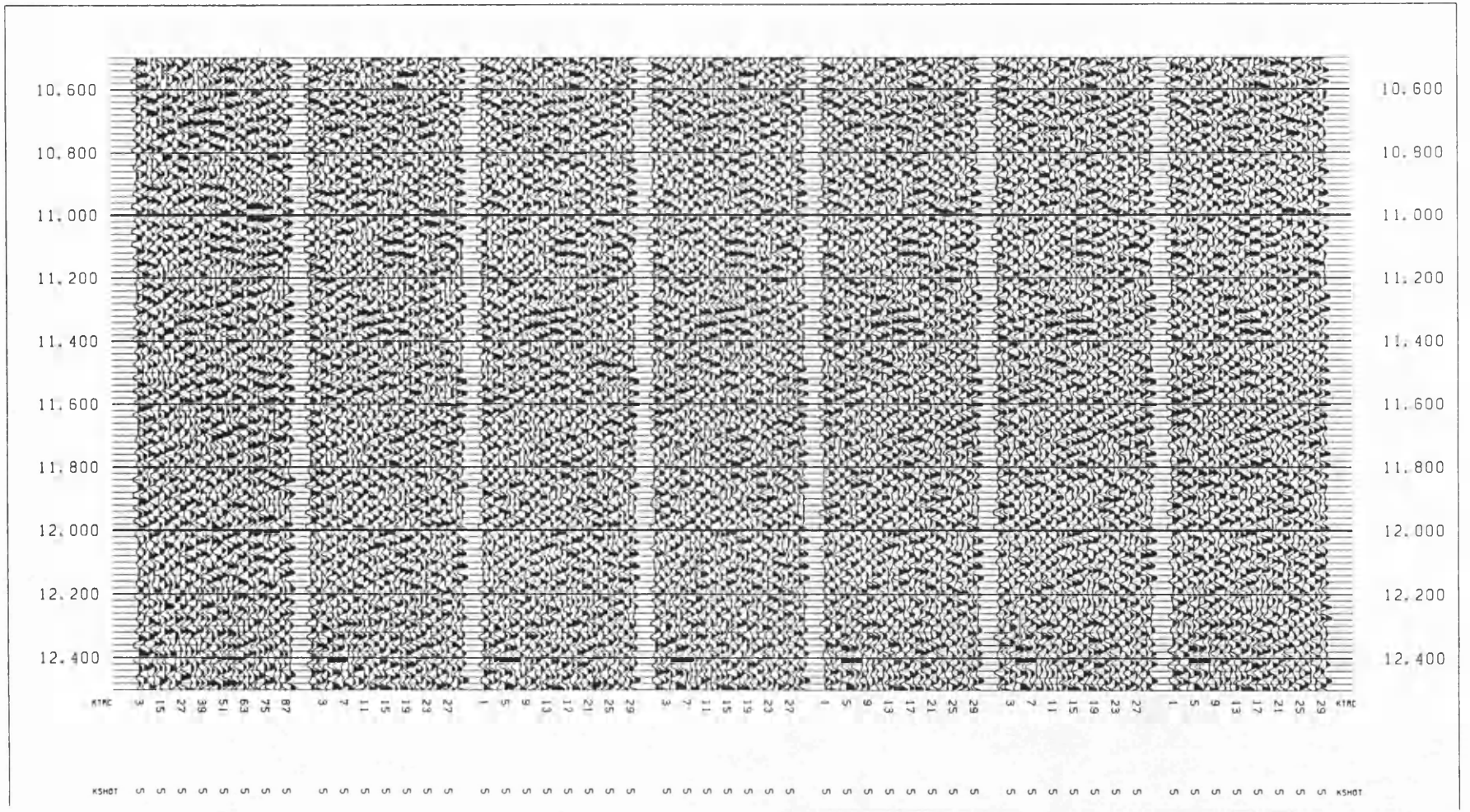

Figure 7.6. Test of the energy filter over horizontal components of shot file 5 (Figure 7.3). First plot are unrotated transverse seismograms, over which the energy filter with moving window lengths of 40, 80, 120,160, 200 and 400 ms, has been applied, respectively, to obtain rotated transverse seismograms.

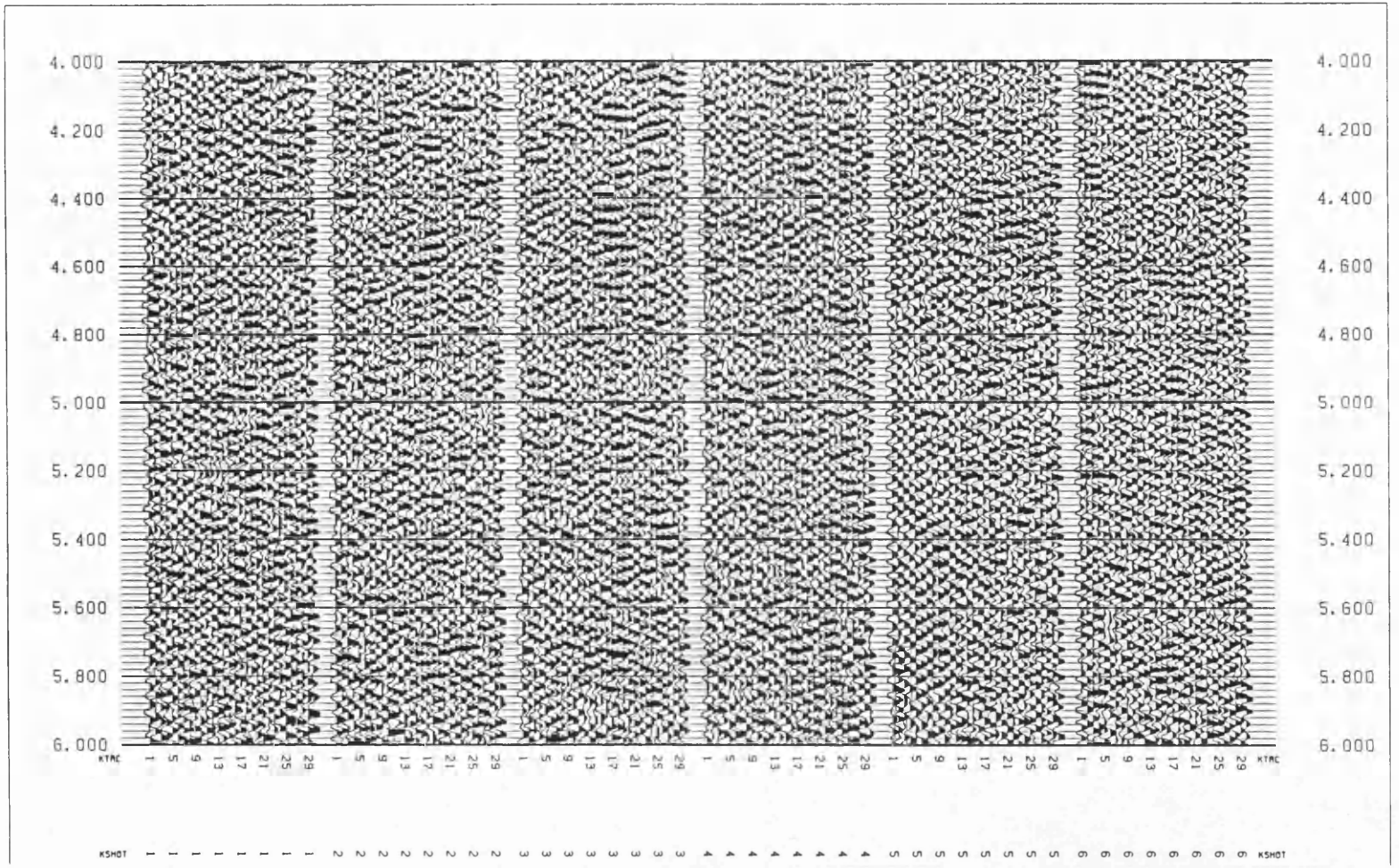

Figure 7.7. Rotated radial seismograms obtained from shot files 12 to 17, resequenced as 1 to 6 (Figure 7.4), respectively, using a moving window of 160 ms.

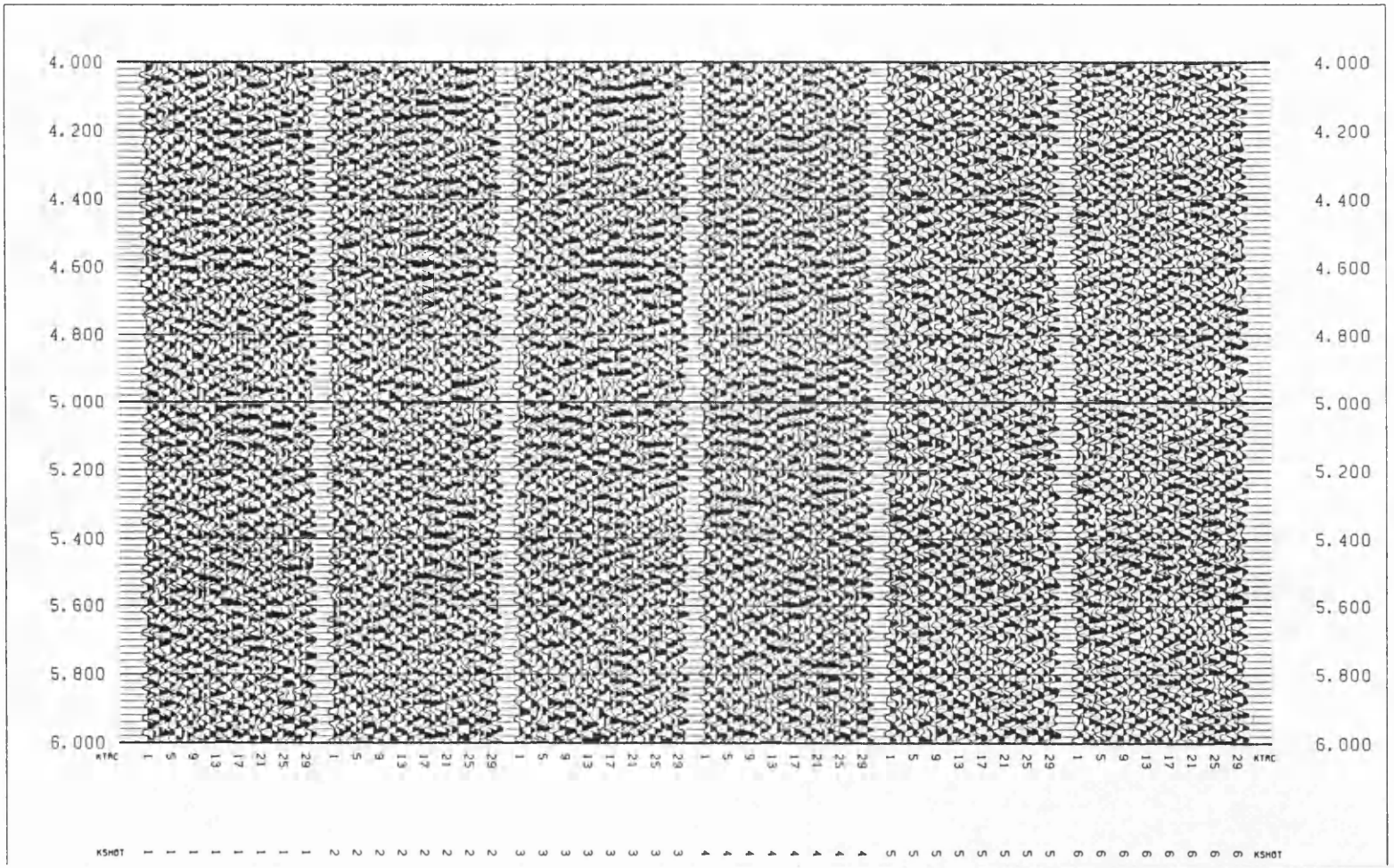

Figure 7.8. Rotated transverse seismograms obtained from shot files 12 to 17, resequenced as 1 to 6 (Figure 7.4), respectively, using a moving window of 160 ms.

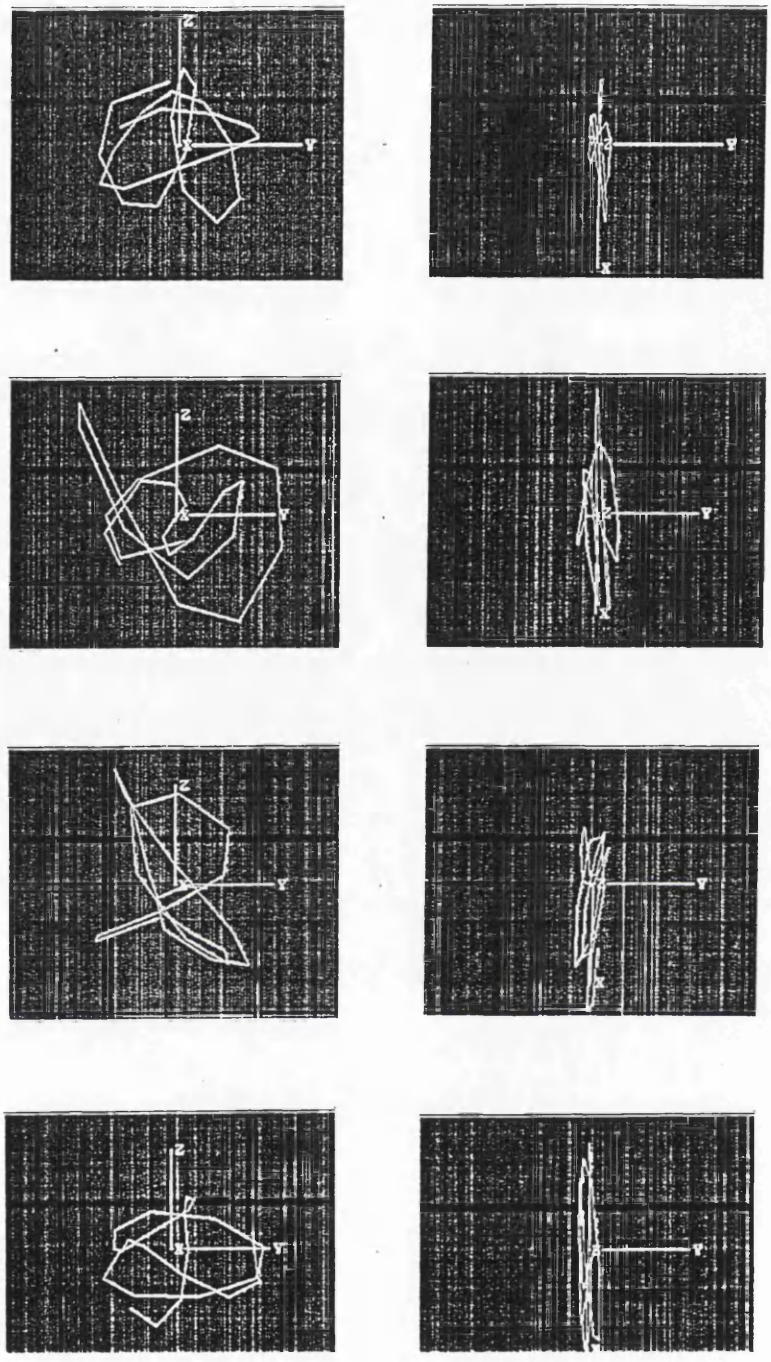

Figure 7.9 Particle motions in the horizontal and vertical planes plotted over the window 4.54-4.64 s of the three-component seismograms, 37, 40, 46 and 55, respectively, of shot file 13 (file 2 in Figure 7.4). the axes named Y, Z and X are X, Y and Z for Kola data, respectively (see text).

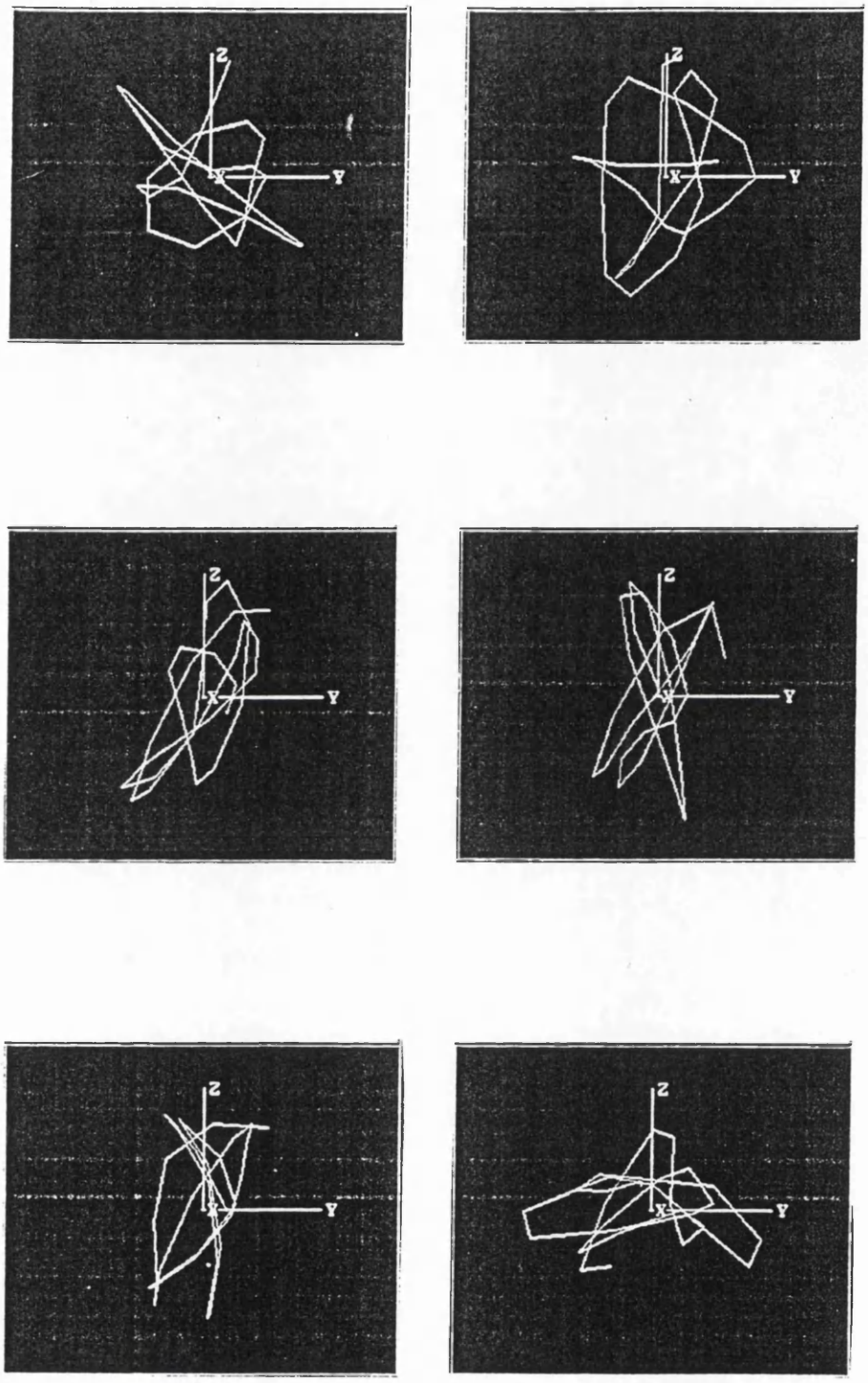

Figure 7.10. Particle motions in the horizontal plane plotted over the window 4.04-4.160 s of the three-component seismograms 37, 46, 52, 55, 64 and 70, respectively, of shot file 14 (file 3 in Figure 7.4).

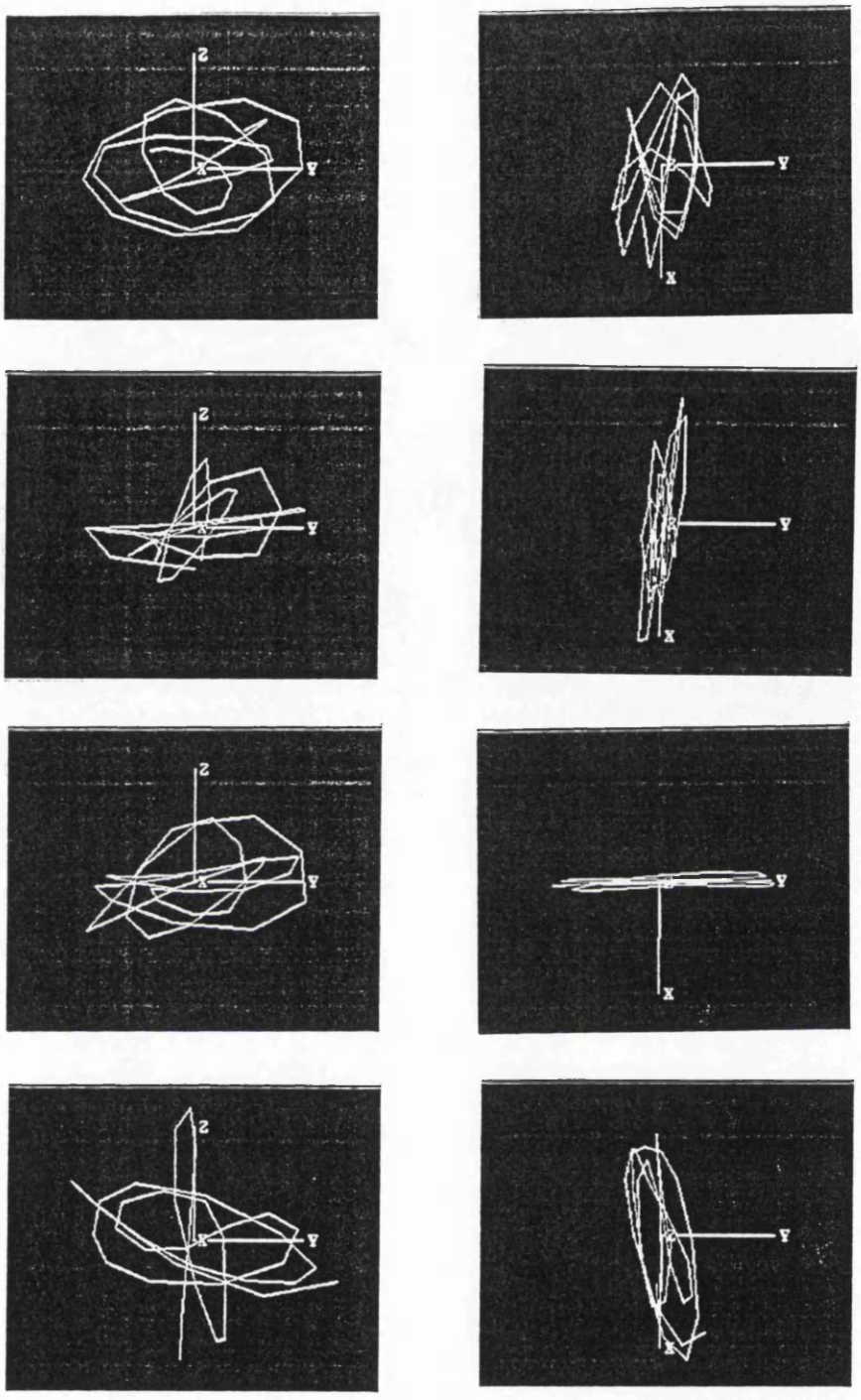

Figure 7.11. Particle motions in the Horizontal and the vertical planes plotted over the window 4.44-4.6 s of the three-component seismograms 34, 40, 49 and 61, respectively, of shot file 4 in Figure 7.4.

CHAPTER 8

Processing VSP shear wave data with the energy filter and computing seismic anisotropy attributes.

8.1. INTRODUCTION

The energy filter was tested on shear wave VSP data acquired by British Petroleum at their test site at Devine, Texas, using the multisource multireceiver acquisition technique.

It has been shown in chapter 5 that the polarization angle of the fast shear wave may be computed as the moving window slides down the two horizontal seismograms. Consequently, the radial component may be rotated to coincide with either the direction of polarization of the fast shear wave or the direction of polarization of the slow shear wave, depending on whether the fast shear is polarized within REGION 1 and REGION 3 (angle of rotation $\varphi = \pi - \theta$, where θ is the polarization angle of the fast shear wave relative to in-line direction), or within REGION 2 and REGION 4 (angle of rotation $\varphi = \pi/2 + \theta$), of the coordinate frame. This leads to the separation of the two split shear waves irrespective of their amplitudes and the constraint on the length of the moving window to contain both split shear wavelets is also removed, as the length of the moving window can be as small as 20 ms as demonstrated on synthetic data. The two split shear waves were assumed to be orthogonally polarized.

The data recorded from each shear source were rotated toward the anisotropy axes. The result is a two-by-two (2x2) rotated data matrix. The two elements of the first column of the rotated data matrix were summed to produce the resultant rotated seismograms. The two elements of the second column were subtracted to give the resultant rotated transverse seismograms. Both Downgoing and

Upgoing waves from zero- and offset- VSP S-wave data have been processed. In both cases the coherency and the resolution were improved on the final processed data, and a mis-tie can be seen between the resultant rotated radial and transverse seismograms. The energy attributes (or the eigenvalue attributes) and the instantaneous polarization angle have been computed to investigate the time delay and the direction of anisotropy axes.

8.2. DATA ACQUISITION

8.2.1. Source positions

VSP data were acquired by BP at the Divine Test Site in Texas between June 19th and 27th, 1989. The basic survey geometry is illustrated in Figure 8.1. An ARIS source, three LRS-1300 three component VSP sondes and three wireline trucks, two Mertz model 12 vibrators and a DFSV recording system were used.

Five source locations (S1 to S5 in Figure 8.1) were occupied by a vertical vibroseis source with an additional impulsive source being deployed at the zero offset positions S1, S2 and S4. The impulsive source was the ARCO ARIS, a powerful inclined weight drop source, which is capable of producing P, SV and SH energy. The ARIS source was oriented along the line joining the three wellheads such that an SV equivalent source could be produced by subtracting the signals generated by blows "backward" (i.e. to the South-East) from those recorded for "forward" blows (to the North-West). Similarly, subtracting signals for blows to the left from blows to the right should generate an SH equivalent source, while source generated shear energy is minimized by summing all 4 blows at a given level giving a P-wave equivalent source.

8.2.2. Receiver locations

The LRS-1300 three component sondes were deployed simultaneously in wells Wilson-4, Wilson-2 and Wilson-9. For each

source position VSP data were acquired from the bottom of the well (2950 ft in Wilson-9, 2850 ft in Wilson-2 and 2800 ft in Wilson-4), to a depth of 750 ft at 25 ft intervals, with additional check-shot levels acquired at 50 to 100 ft intervals between 750 ft and the surface.

The horizontal components of LRS-1300 three component sonde are oriented parallel and perpendicular to the clamping arm, respectively, for zero offset data. In each gather trace 1 is the vertical; trace 2 parallel to the clamping arm; trace 3 perpendicular to the clamping arm. For offset S-wave, data were rotated using incident P: trace 1 is the vertical; trace 2 the in-line horizontal and trace 3 the cross-line horizontal.

8.2.3. Basic acquisition parameters

For the ARIS, 4 pops were shot at each level, and the record length was 3 s. Care was taken to note the small time delays between blows in different directions at a single level, so that these can be corrected for, and optimal P/SV/SH stacks produced. The timing differences are generally small (less than 1 ms) but increase as the surface beneath the base plate becomes more compacted and the wheels of the ARIS start touching the ground. All data were recorded at a sample rate of 2 ms, anti-alias filter to 180 Hz and the low cut filter out.

8.2.4. Quality control in the field

ARIS timing and general record quality, which was carried out by the DFSV operator in the recording truck was carefully controlled. When problems were detected, the source was adjusted or the tool reclamped as appropriate, and the shot repeated immediately. The major problem encountered in quality was the presence of severe ringing on the H2 (horizontal perpendicular to the clamping arm) component for many levels. A number of attempts were made to

isolate and remove this resonance, but none met with consistent success.

8.3. DATA PROCESSING

The zero offset shear data processed was acquired at well Wilson-2 (Figure 8.1), with the ARIS source located at point S2, 61 feet from the well. The original data were filtered with a bandpass filter of 10/24-45/72 Hz. FK filtering have been used to separate downgoing waves from upgoing waves. Within (f,k) domain upgoing waves, which slope downwards from left to right in (x,t) domain map to the negative quadrant in (f,k) domain while the downgoing waves sloping upwards in the (x,t) domain map to the positive quadrant. by zeroing, say, the negative quadrant to design the amplitude spectrum of the filter then transforming back the filtered data into (x, t) domain, downgoing waves are obtained. The characteristics of shear wave splitting will not be affected after Velocity filtering (Campden, 1991), i.e. polarization diagrams are found to be similar after FK filtering. Figure 8.2 shows downgoing waves recorded from both shear sources. This Figure is a two-by-two (2x2) S-wave data matrix, i.e., XX (in-line source in-line receiver); XY (in-line source cross-line receiver); YX (cross-line source cross-line receiver); YY (cross-line source cross-line receiver). The in-line receiver direction is parallel to the clamping arm and the cross-line receiver is normal to it. No information is available on the position of the clamping arm.

Figure 8.3 shows two horizontal orthogonal shear sources, F1 and F2, normal and parallel to the in-line direction, respectively. Each one when propagating vertically in an azimuthally anisotropic medium splits along the anisotropic axes into a fast S-wave and a slow S-wave, with the fast one polarized along the direction of maximum horizontal compressive stress or crack strike direction. Data from each shear source are rotated automatically using equation 5.15 toward the direction of principal axes of anisotropy,

by computing the polarization angle of the fast shear wave (as the moving window slides down the horizontal seismograms searching for the direction of anisotropy axes relative to the in-line direction). The rotation angle is either equal to $\pi - \theta$ or $\pi / 2 + \theta$, depending on whether the fast shear wave is polarized within region 1 and region 3, or within region 2 and region 4 (see Figure 8.3), of the recording coordinate frame. The in-line component is always rotated toward the axis of anisotropy confined to region 1 and region 3, which can be either the direction of the crack strike or the normal to it. Figure 8.4. shows the rotated two-by-two (2x2) S-wave data matrix obtained using a moving window of 60 ms length, i.e., XRX (in-line source rotated radial); XRY (in-line source rotated transverse); YRX (cross-line source rotated radial) and YRY (cross-line source rotated transverse). consequently, no rotation is applied to the shear sources, only data from each shear source are instantaneously rotated toward the direction of anisotropy axes.

It is inferred from Figure 8.3 that summing the rotated radial seismograms represented by the vectors FS1 and FS2 or the first column of the rotated data matrix, resulting from the splitting of both orthogonal shear sources, will give the seismograms of the propagating fast shear wave within the anisotropic medium. Similarly, subtracting the rotated transverse seismograms represented by the vectors SS1 and SS2 or the second column of the rotated data matrix, will give the seismograms of the propagating slow shear wave. However, in practice the direction of the crack strikes are not known and the seismograms of the rotated radial components from both shear sources could be the seismograms of the propagating slow shear wave, if the fast shear wave is polarized within region 2 and region 4 of the recording coordinate frame. Figure 8.5a represents the resultant rotated seismograms resulting from the summation (after reversing the polarity of the rotated radial traces to confirm with Figure 8.3) of the rotated radial seismograms obtained from both orthogonal shear sources. similarly, Figure 8.5b is the resultant rotated transverse derived

from the subtraction of the rotated transverse seismograms obtained from both shear sources. Figure 8.5c is the juxtaposition of the resultant rotated radial and the resultant rotated transverse, respectively. A mis-tie can be clearly seen between the seismic horizons. Compared to the original data, both the resolution and the coherency have been improved, particularly of the first direct waves. The effect of ringing on the original transverse seismograms is no longer apparent on the final processed data. This noise disappeared after rotating the data from both shear sources toward the axes of anisotropy, as shown from the rotated data matrix in Figure 8.4.

Figure 8.6 shows the two-by-two (2x2) upgoing S-wave data matrix pass-band filtered by 10/24-45/72 Hz. Observe the considerable similarity between XY (in-line source crossline receiver and YX (cross-line source in-line receiver) elements of the data matrix; also, there is a severe ringing on the YY element extending down to 2 s. The noise on the upper part of the first arrivals has been muted.

The rotated two-by-two upgoing S-wave data matrix is shown on Figure 8.7. No ringing can be seen on any element of the rotated data matrix; and the coherency of the YRY element (rotated transverse-cross-line source) has been improved. Figure 8.8a and 8.8b are the resultant rotated radial and the resultant rotated transverse seismograms of upgoing waves, respectively, which are much more improved compared to the original ones. Figure 8.8c is the juxtaposition, showing a miss-tie between them. It would be interesting to construct a seismic image from the processed upgoing waves. However, the Department of Geology is not equipped with a VSP software.

The offset S-wave data to be processed was recorded in wells Wilson-2 and Wilson-9 wells with the shear source positioned at point S1, i.e. two offsets of 390 ft and 1020 ft, respectively. The unprocessed downgoing S-wave data matrix for each offset are shown in Figures 8.9 and 8.10, respectively. They are of better

quality compared to zero offset data.

The data were processed by the energy filter in the same way as zero offset data, using a 60 ms window length. The resultant rotated radial and transverse for each offset are shown in Figures 8.11 and 8.12, respectively. When looking at their juxtaposition, both Figures show a miss-tie , with the resultant rotated transverse (element to the right), representing the seismograms of the propagating fast shear wave; and that miss-tie is increasing with offset, as a result of increasing traveltime.

8.4. SEISMIC ATTRIBUTES

Seismic attributes were computed from data recorded in well Wilson-2, with a cross-line source located at point S2, 390 ft from the well. Figure 8.13 shows the eigenvalue attributes of the direct arrivals with the plots of the first eigenvalue on top of the second eigenvalue, computed using a 60 ms moving window. The attributes were calculated from traces recorded at the top of the well (750 ft) down to 975 ft with a 25 ft increment, corresponding to traces numbered 85 to 76, respectively. In to contrast with synthetic attributes those attributes were plotted with the same scale using the SierraSeis package. They show nearly the same features as in synthetic examples; particularly, there is a clear time delay between the first and the second eigenvalue attributes with the first eigenvalue ahead.

It is not evident from these graphs that the time delay increases linearly with depth. Statistical work using regression analysis to fit lines or curves to the data would be intersting. Through the whole data set, from top to bottom of the well the first eigenvalue is ahead. Also, the eigenvalue attributes computed from the resultant rotated radial and the resultant rotated transverse are similar to Figure 8.3. However, the computation of those attributes from an in-line source showed smaller time delays.

Figure 8.14 an 8.15 are the color display of the instantaneous

polarization angle with the color code on the right, computed from data generated by a cross-line and an in-line source, respectively, positioned at point S1, 1020 ft from the well Wilson 9. The color coded polarization quantifies the polarization direction by reference to the color key. The pictures were taken directly from the computer screen, as no versatec color plotter adapted to SierraSeis package was available, thus reducing the resolution in interpreting with precision those two pictures. Nevertheless, it can be seen from both figures that at the onset of the fast shear wave indicated by arrowheads, the same blue color appears on both figures and extending from the top to the bottom of the well, indicating a crack strike oriented 20° to 35° from the in-line direction, situated within the quadrants 2 and 4 (see Figure 8.3) of the coordinate acquisition frame, confirming that the resultant rotated seismograms represent the seismograms of the fast shear wave.

It is suggested that for an effective investigation of anisotropy the three attributes should be plotted together with, for example, the first and the second eigenvalues with dashed lines at the same scale, and the instantaneous polarization plotted in a color code.

8.5. CONCLUSION AND DISCUSSION

By processing multisource multireceiver S-wave VSP data using the energy filter to automatically separate the split shear waves resulting from each shear source, the data quality of the downgoing and the upgoing waves were improved and two new seismic records have been produced. These are the resultant rotated radial and the resultant rotated transverse, which in this case, represent the seismograms of the propagating slow and fast shear wave, respectively.

The technique is shown to be robust, even in the presence of noise severe ringing. It is computationally very quick, as it uses the covariance matrix to compute the direction of polarization of

the two split shear waves. Consequently, it can be used on single shot files of seismic reflection data before stack, as stacking degrades shear wave polarization (Li & Crampin, 1989)

The Alford technique, the most common rotation technique, is time consuming, particularly on reflection data, even on stacked data and does not take into consideration the fact that polarization of shear waves change with offset. From our experience on BIRPS and KOLA data, using the energy filter reduces the computation time by more than 40 times compared to the rotation techniques which maximize the energy to find the polarization directions of the shear waves.

With this method it would be interesting to record shear wave VSP data using single source multireceiver acquisition technique, with the single source being an SH source, i.e. rotating the horizontal components so that the axis of one geophone will be parallel to the shear source orientation. The use of two orthogonally polarized shear sources may not be adequate for any automated technique, as an In-line source results in generating mode converted waves with high energy.

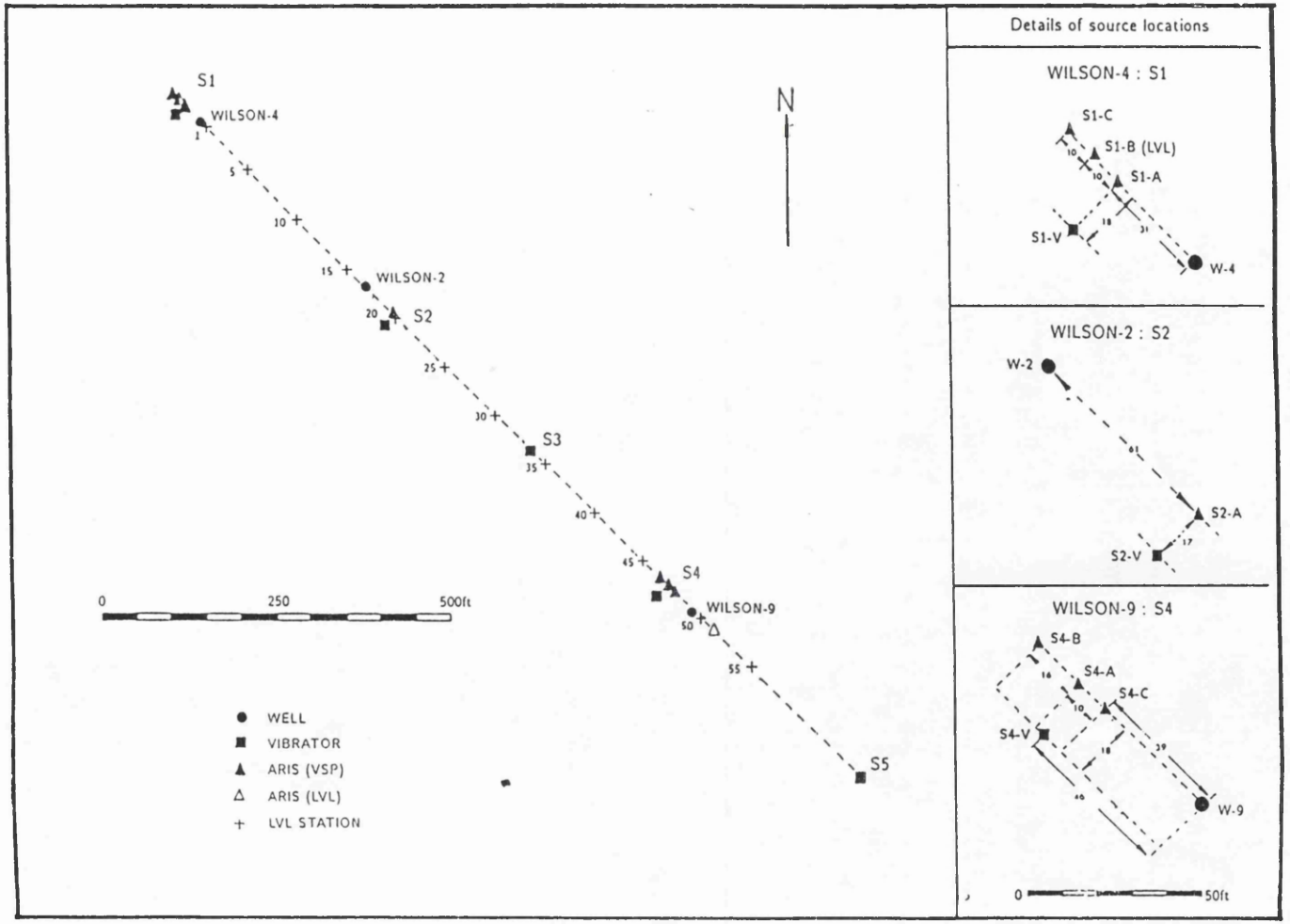

Figure 8.1. Survey geometry. S1 to S5 are the source locations. Details of source locations relative to wells with their offsets in feet are shown on the right.

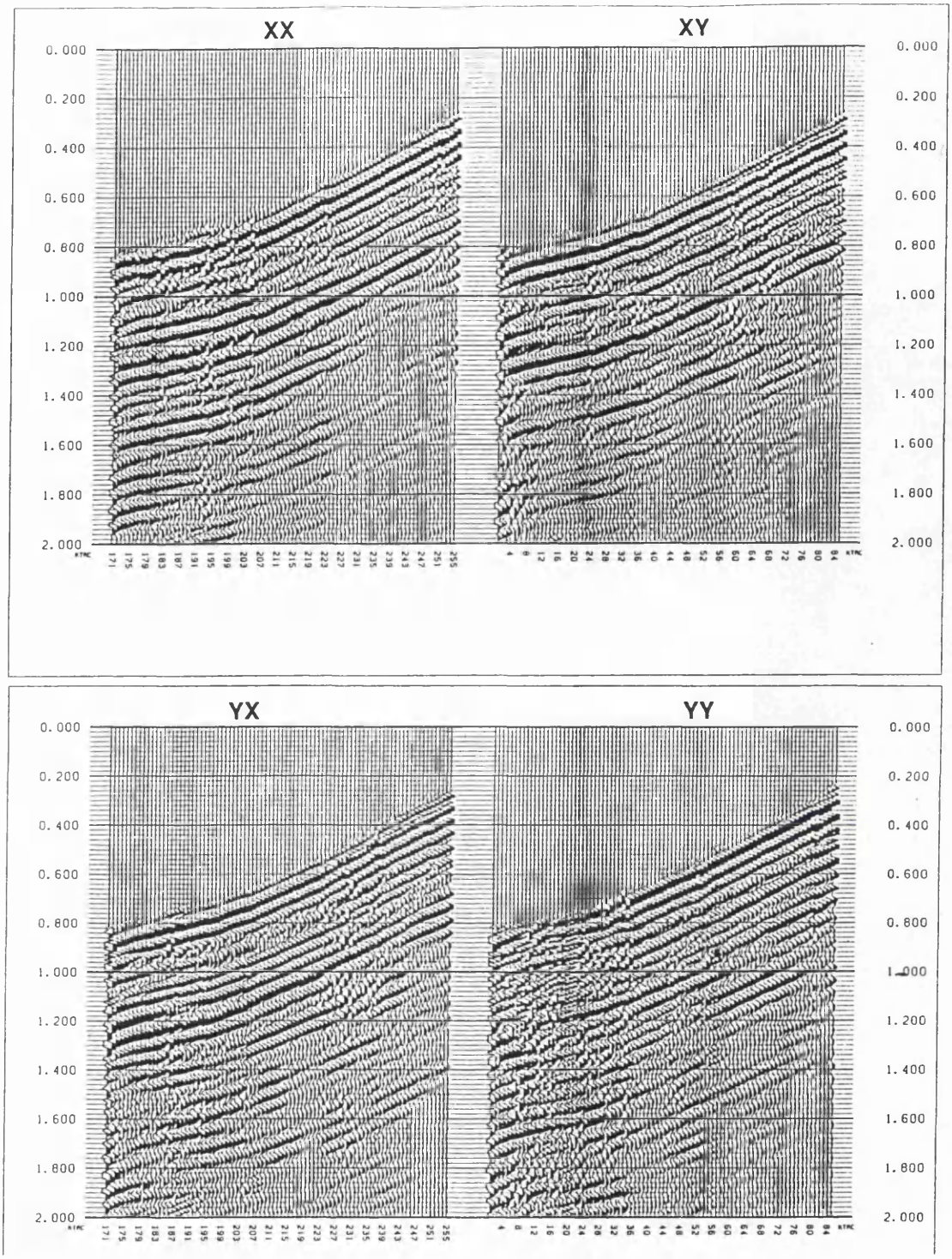

Figure 8.2. Unprocessed two-by-two (2x2) downgoing zero offset S-wave data matrix from well Wilson-2. Shear sources positioned at point S2, 61 ft from the well. Noise on the upper part of the first direct arrivals has been muted. XX (in-line source in-line receiver; XY (in-line source cross-line receiver); YX (cross-line source in-line receiver); YY (cross-line source cross-line receiver).

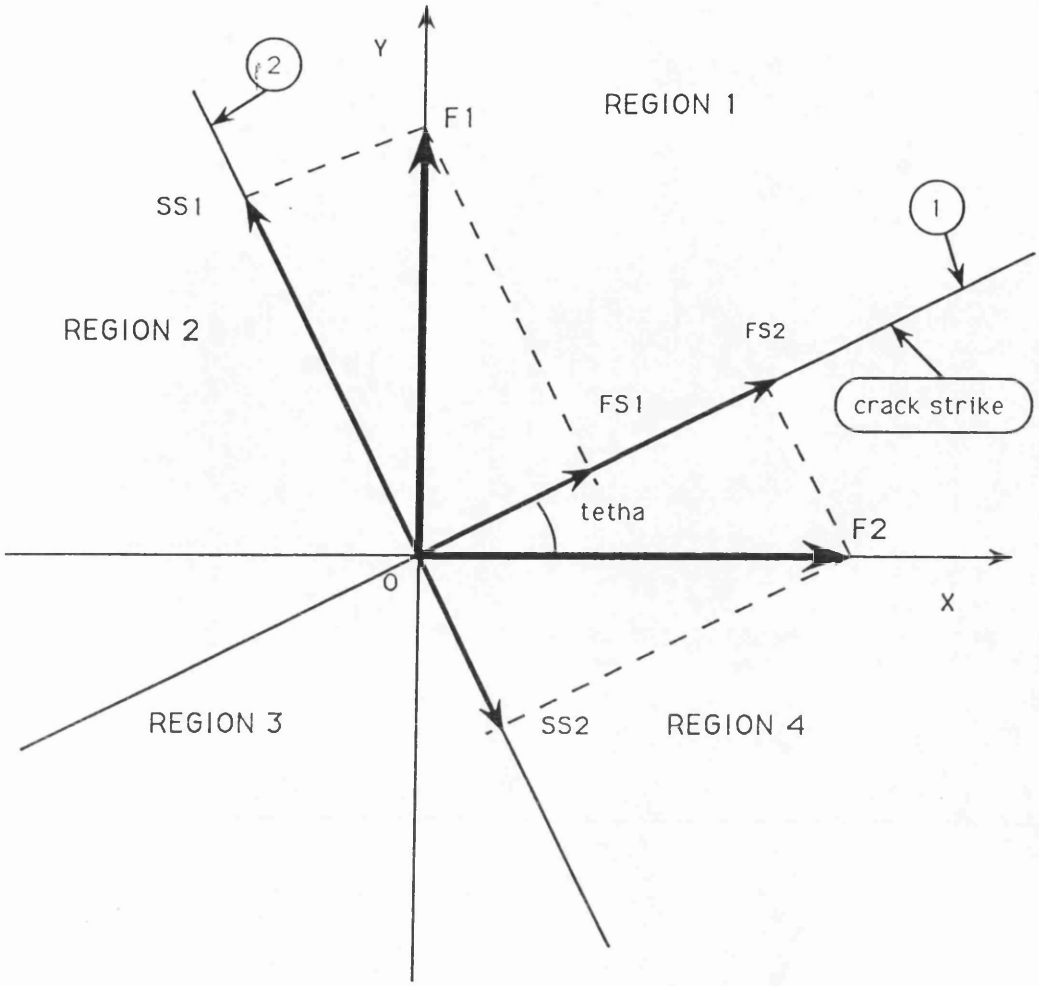

Figure 8.3. Splitting of two orthogonal shear sources along the anisotropy axes, with the plane of the coordinate frame (ox, oy) divided into four regions or four quadrants.

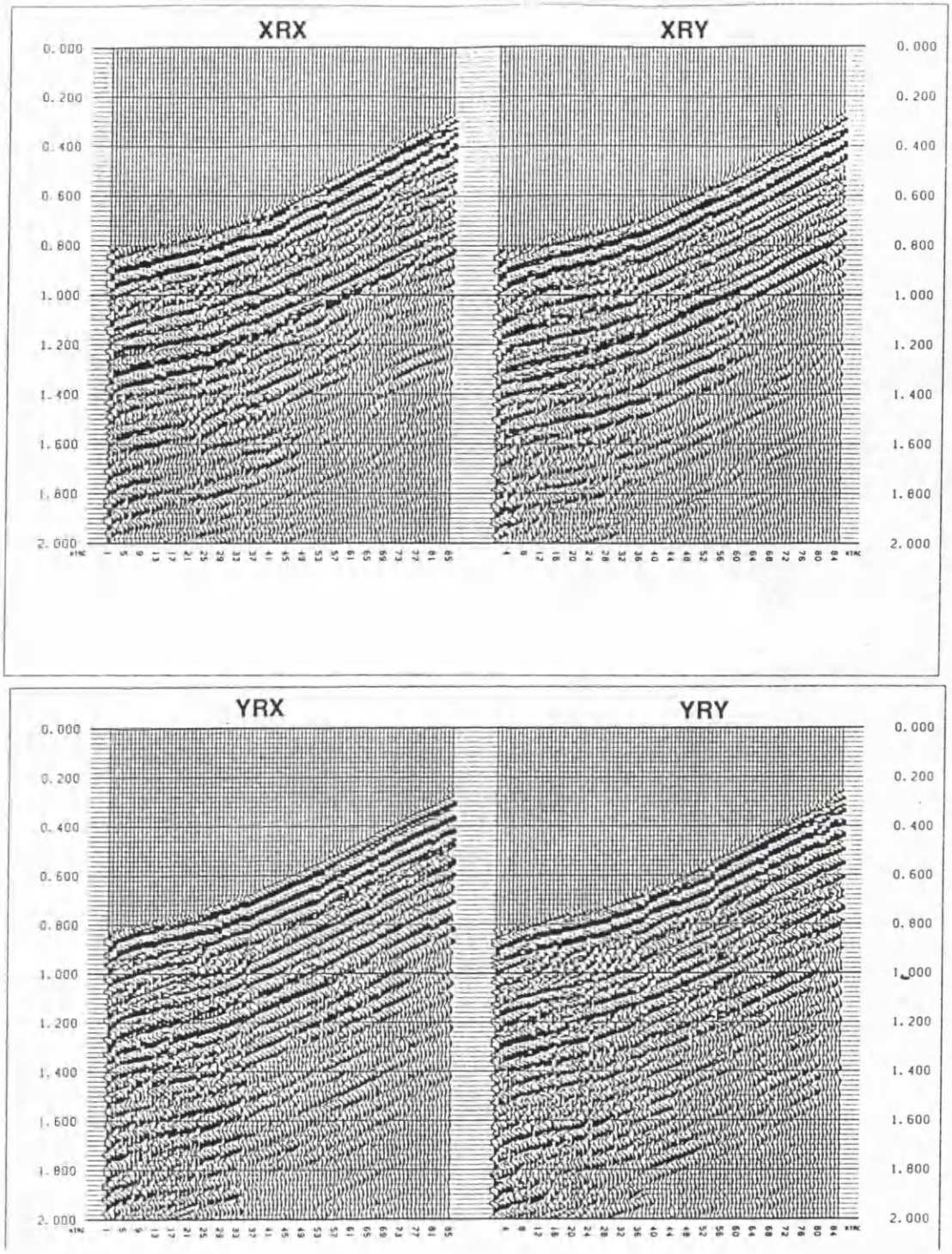

Figure 8.4. Rotated two-by-two (2x2) downgoing zero offset S-wave data matrix from well Wilson-2, with the energy filter applied using a moving window of 60 ms after muting the noise on the upper part. Applying the energy filter before or after muting the noise, makes no difference. XRX (in-line source rotated radial); XRY (in-line source rotated transverse); YRX (cross-line source rotated radial); YRY (cross-line source rotated transverse)

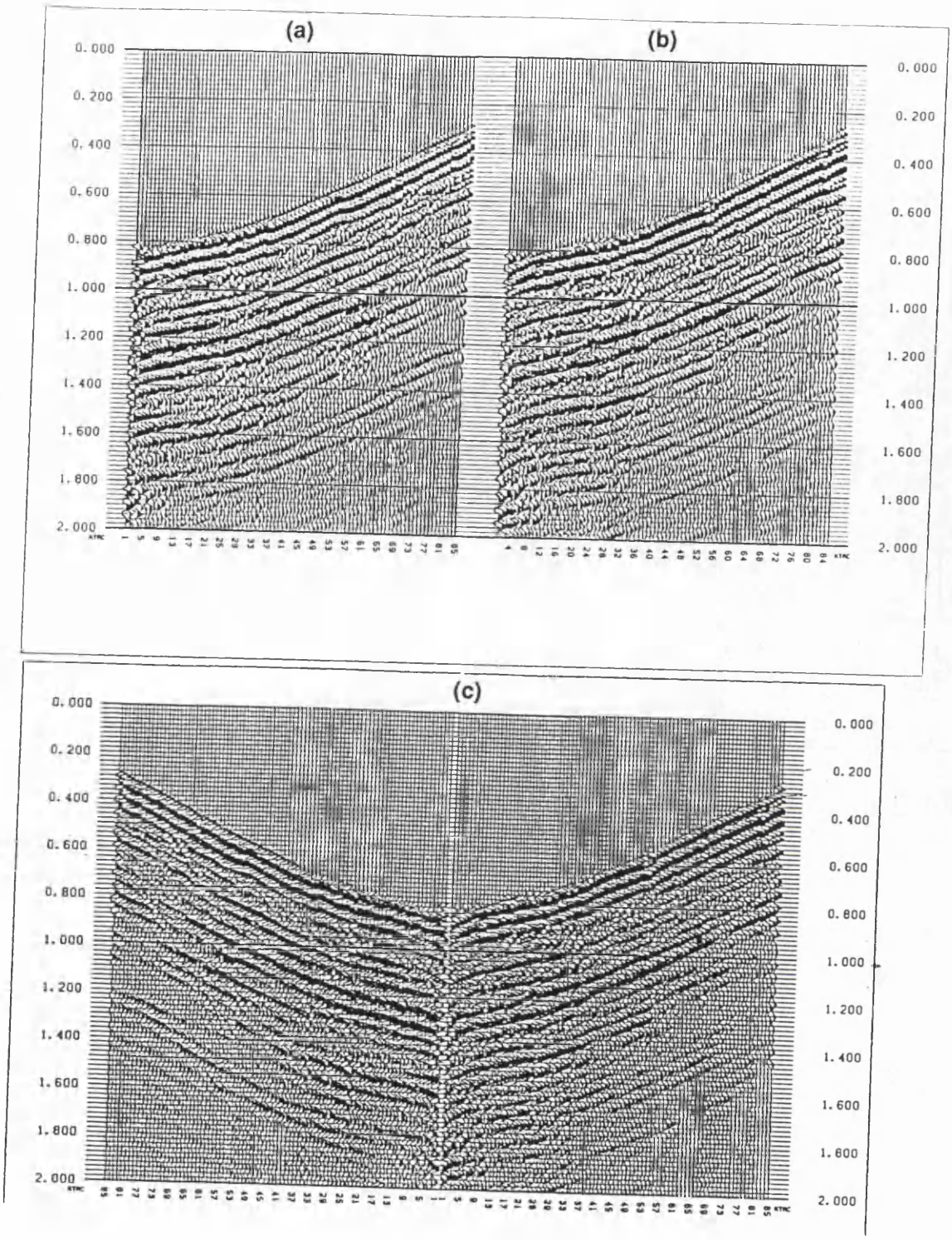

Figure 8.5. The resultant rotated radial (a) and the resultant rotated transverse (b) computed from the rotated two-by-two zero offset data matrix; (c) is the juxtaposition showing the miss-tie between them.

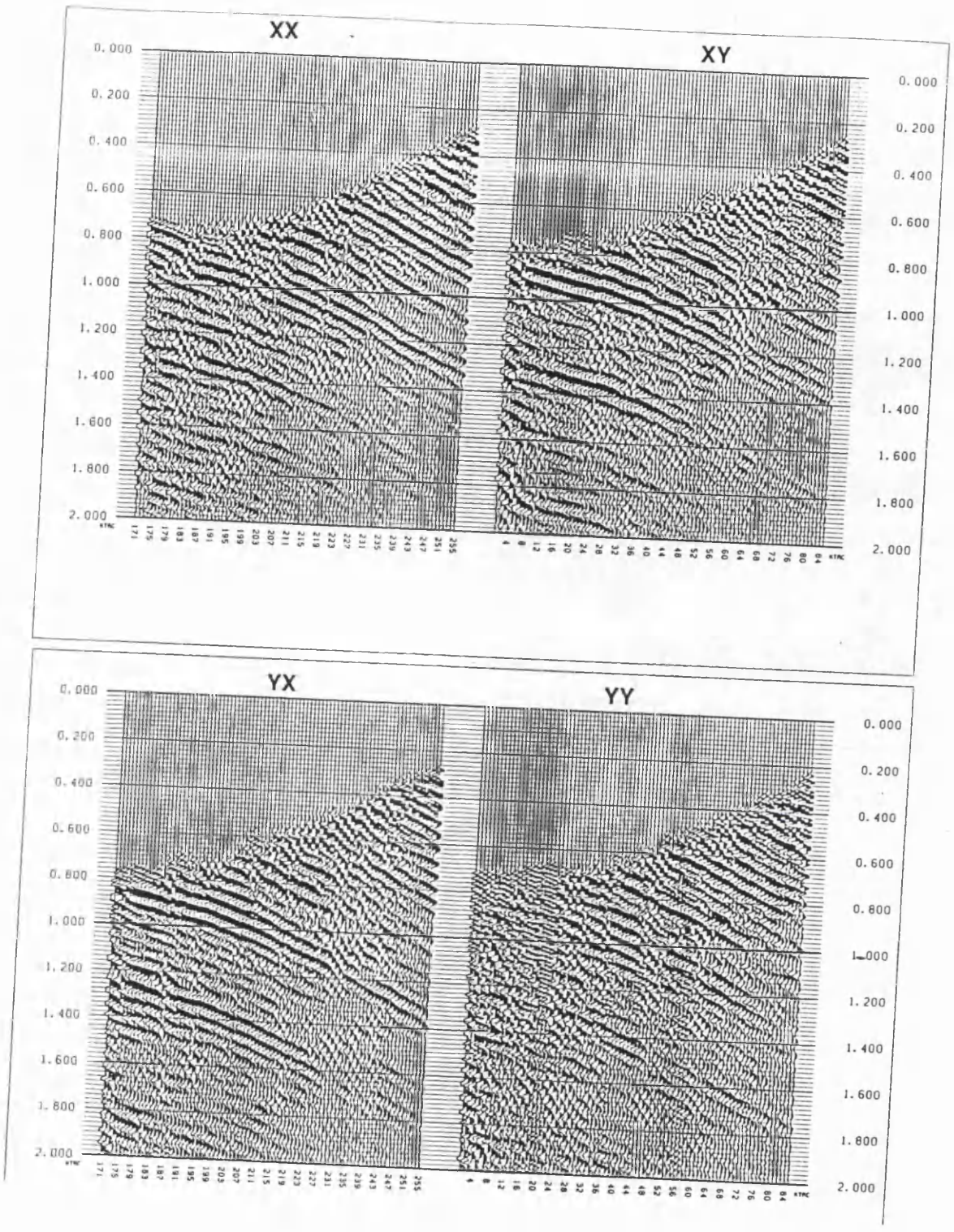

Figure 8.6. Unprocessed two-by-two (2x2) upgoing zero offset S-wave data matrix from well Wilson-2. Shear sources positioned at point S2, 61 ft from the well. Noise on the upper part of the first direct arrivals has been muted.

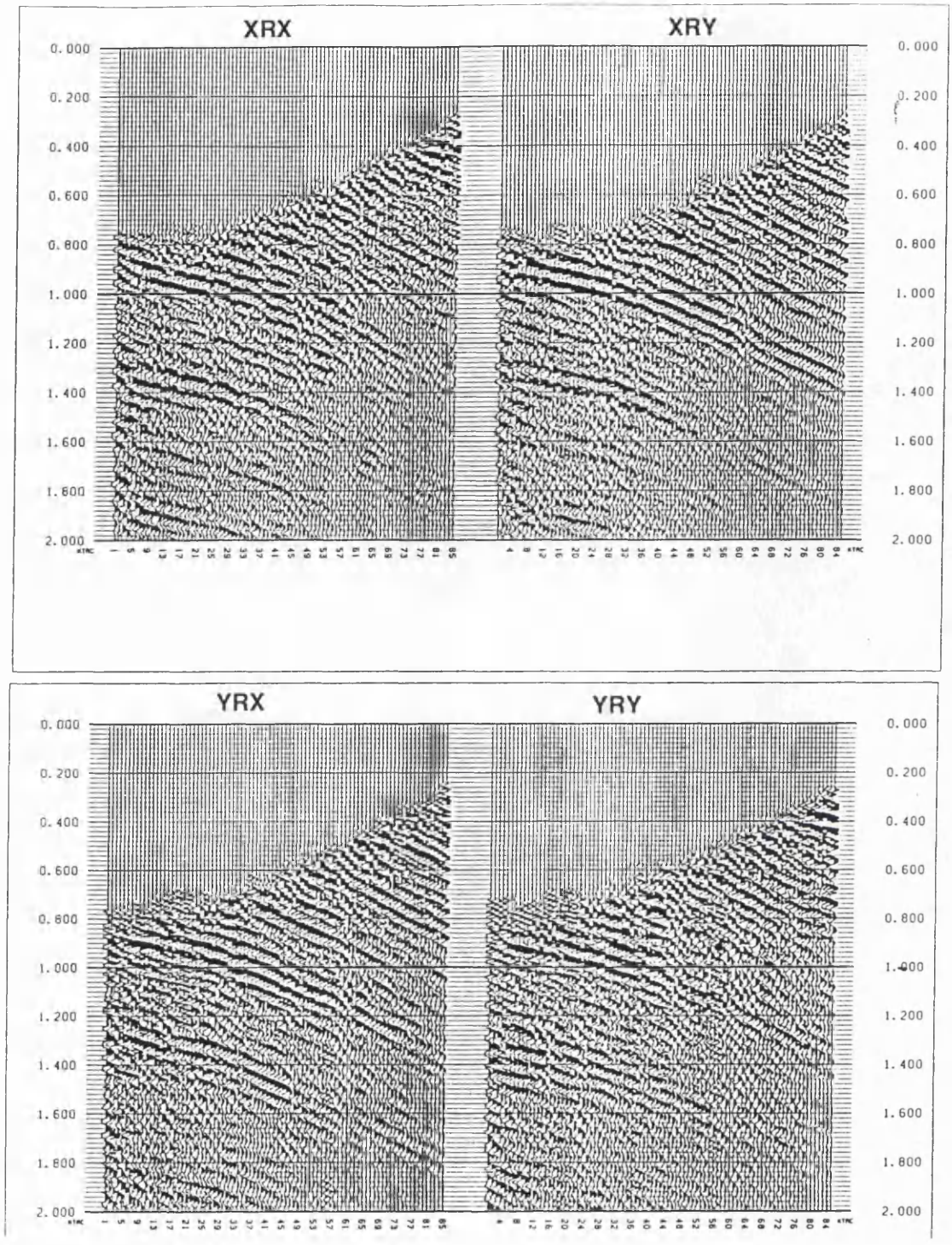

Figure 8.7. Rotated two-by-two (2x2) upgoing zero offset S-wave data matrix from well Wilson-2, with the energy filter applied using a moving window of 60 ms after muting the noise on the upper part. Applying the energy filter before or after muting the noise, makes no difference.

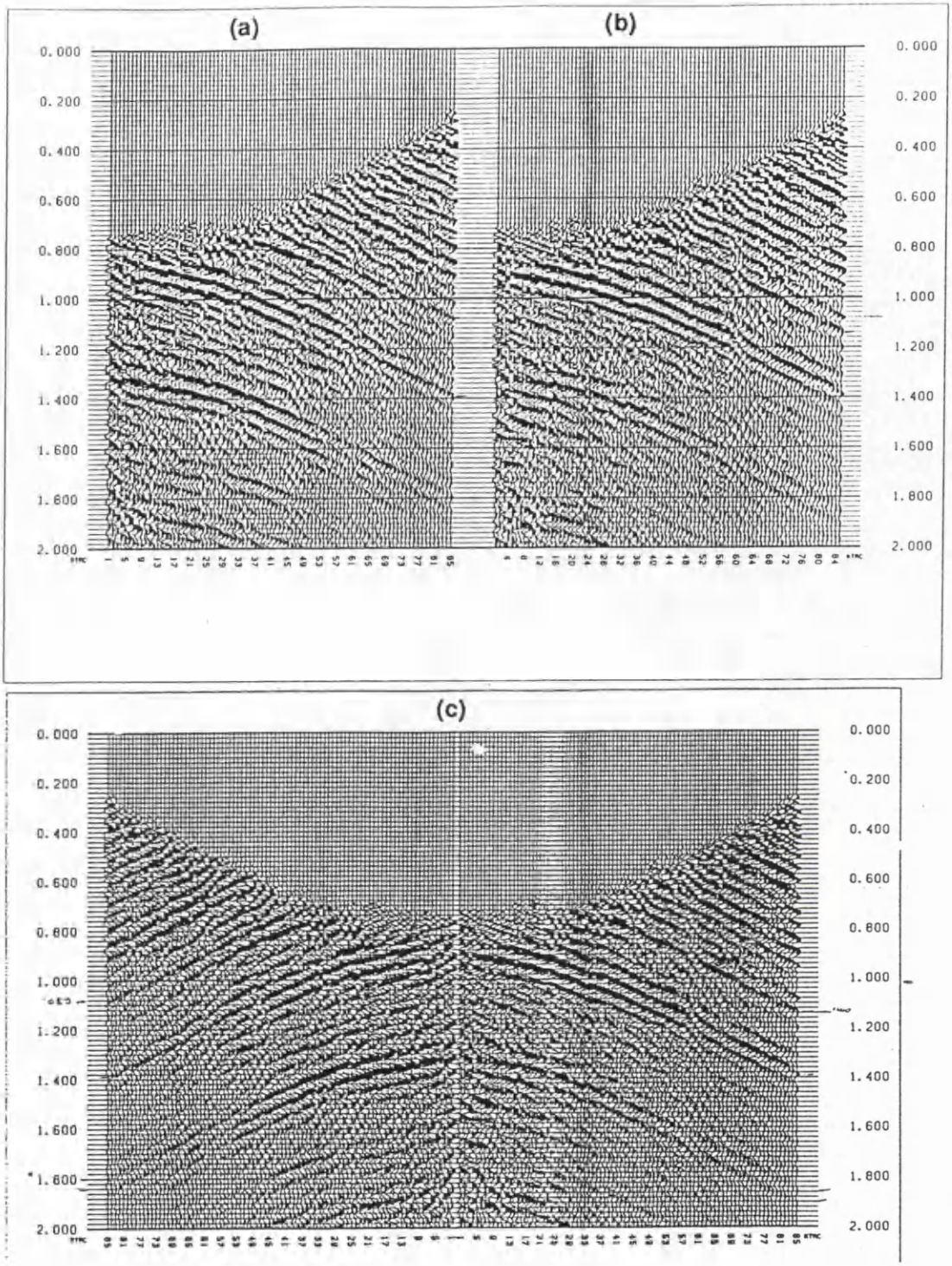

Figure 8.8. The resultant rotated radial (a) and the resultant rotated transverse (b) computed from the rotated two-by-two upgoing zero offset data matrix; (c) is the juxtaposition showing the miss-tie between them.

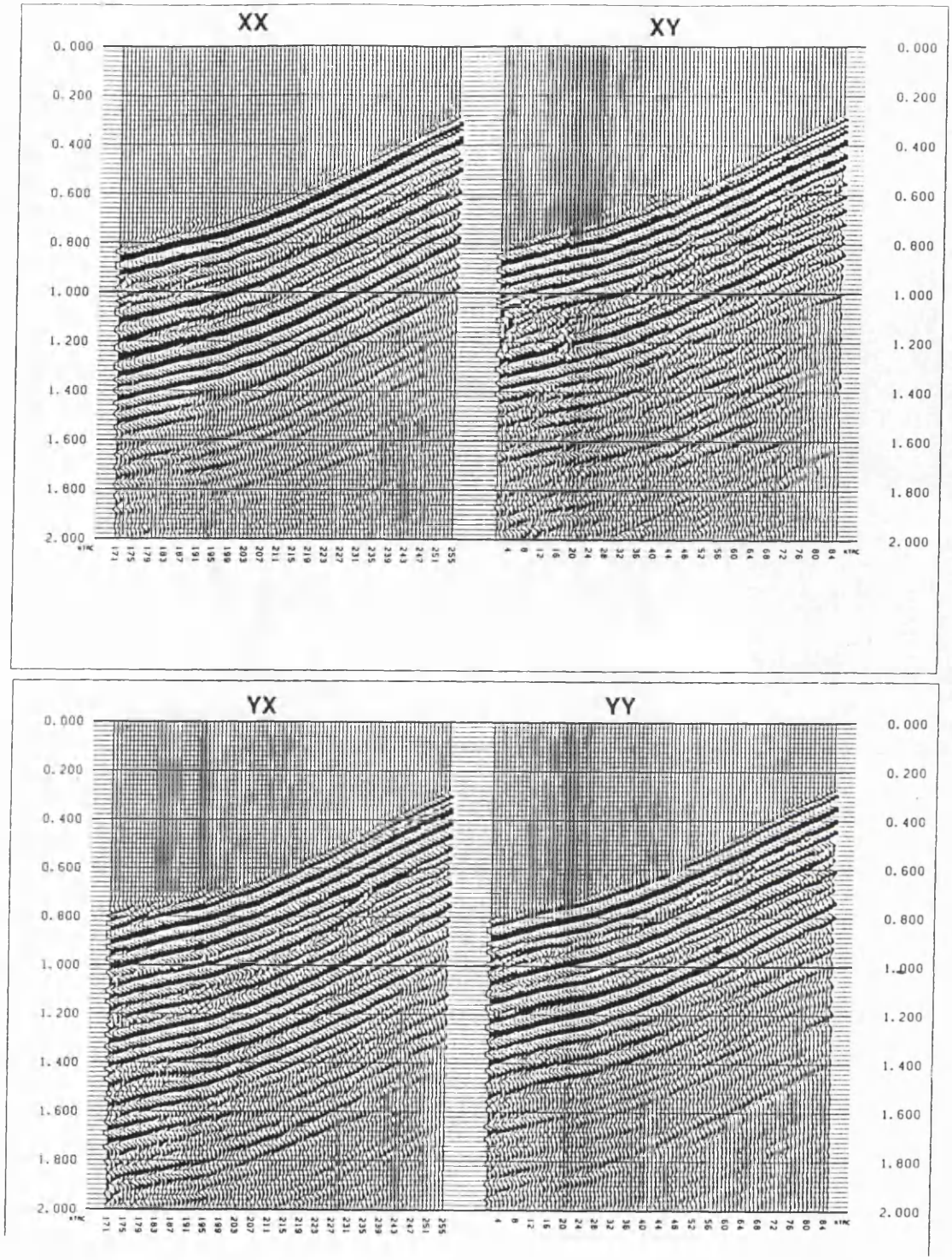

Figure 8.9. Unprocessed two-by-two (2x2) downgoing offset S-wave data matrix from well Wilson-2. Shear source positioned at point S2, 390 ft from the well.

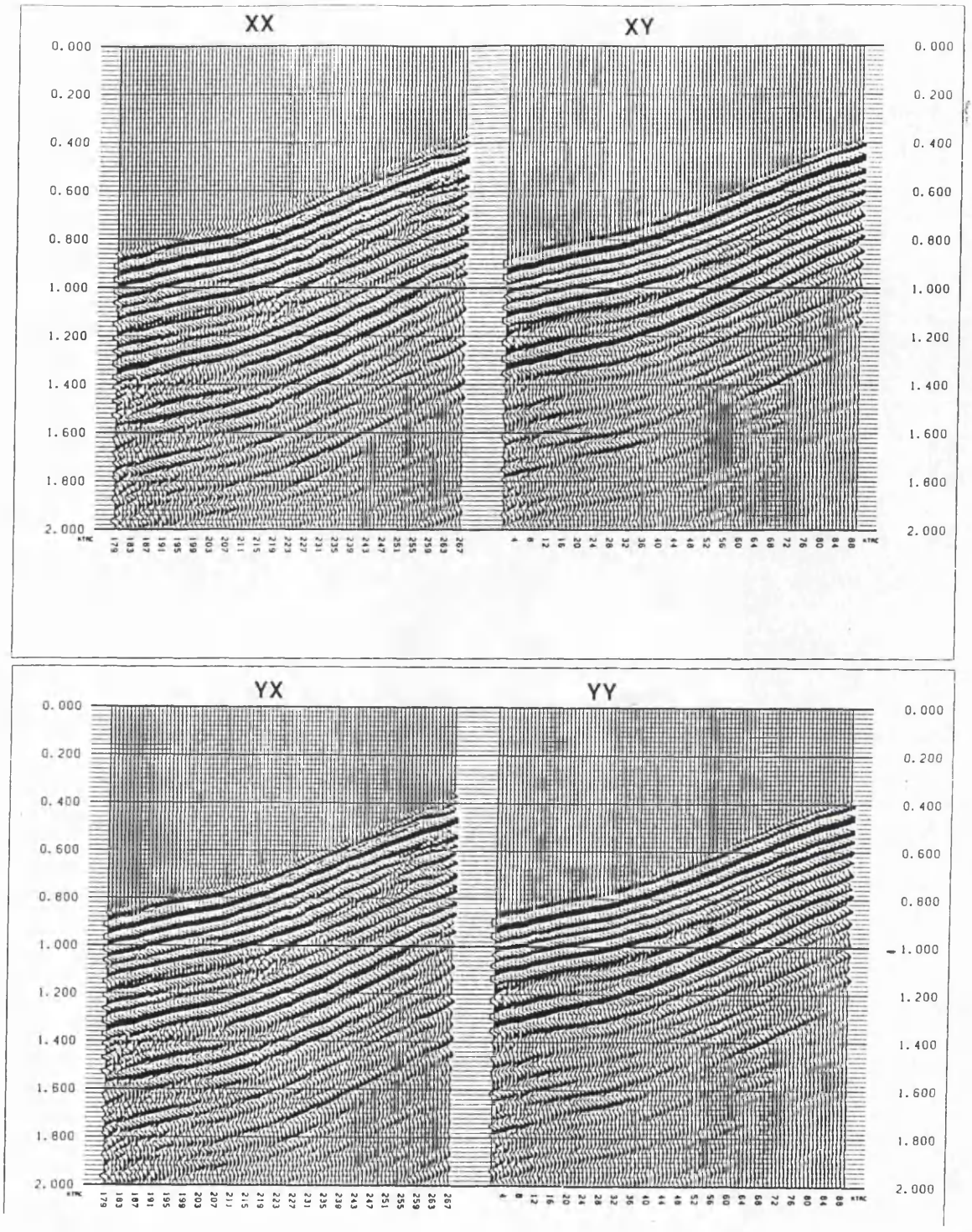

Figure 8.10. Unprocessed two-by-two (2x2) downgoing offset S-wave data matrix from well Wilson-9. Shear source positioned at point S2, 1020 ft from the well.

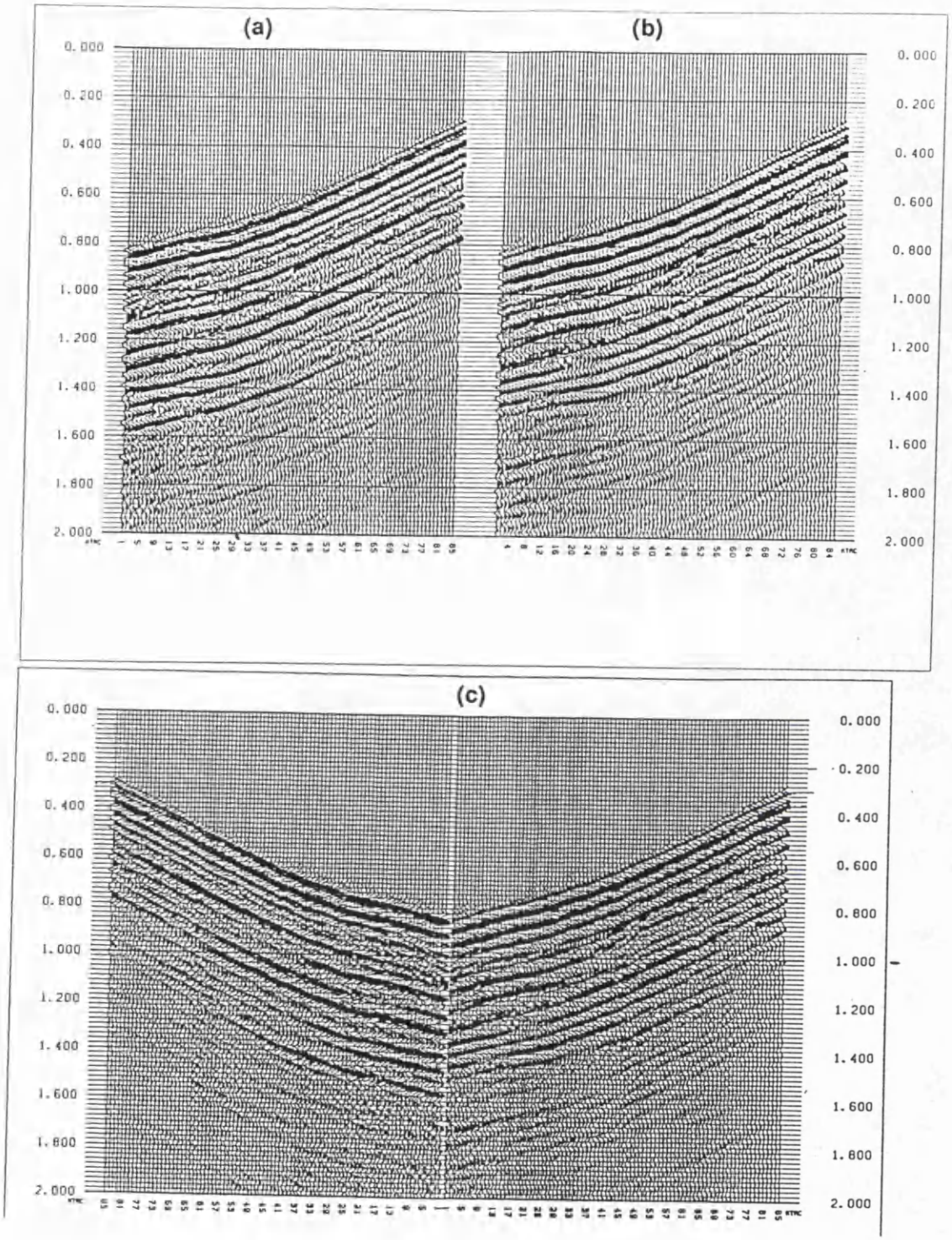

Figure 8.11. The resultant rotated radial (a) and the resultant rotated transverse (b) computed from the rotated two-by-two 390 ft offset data matrix; (c) is their juxtaposition to show the miss-tie between them.

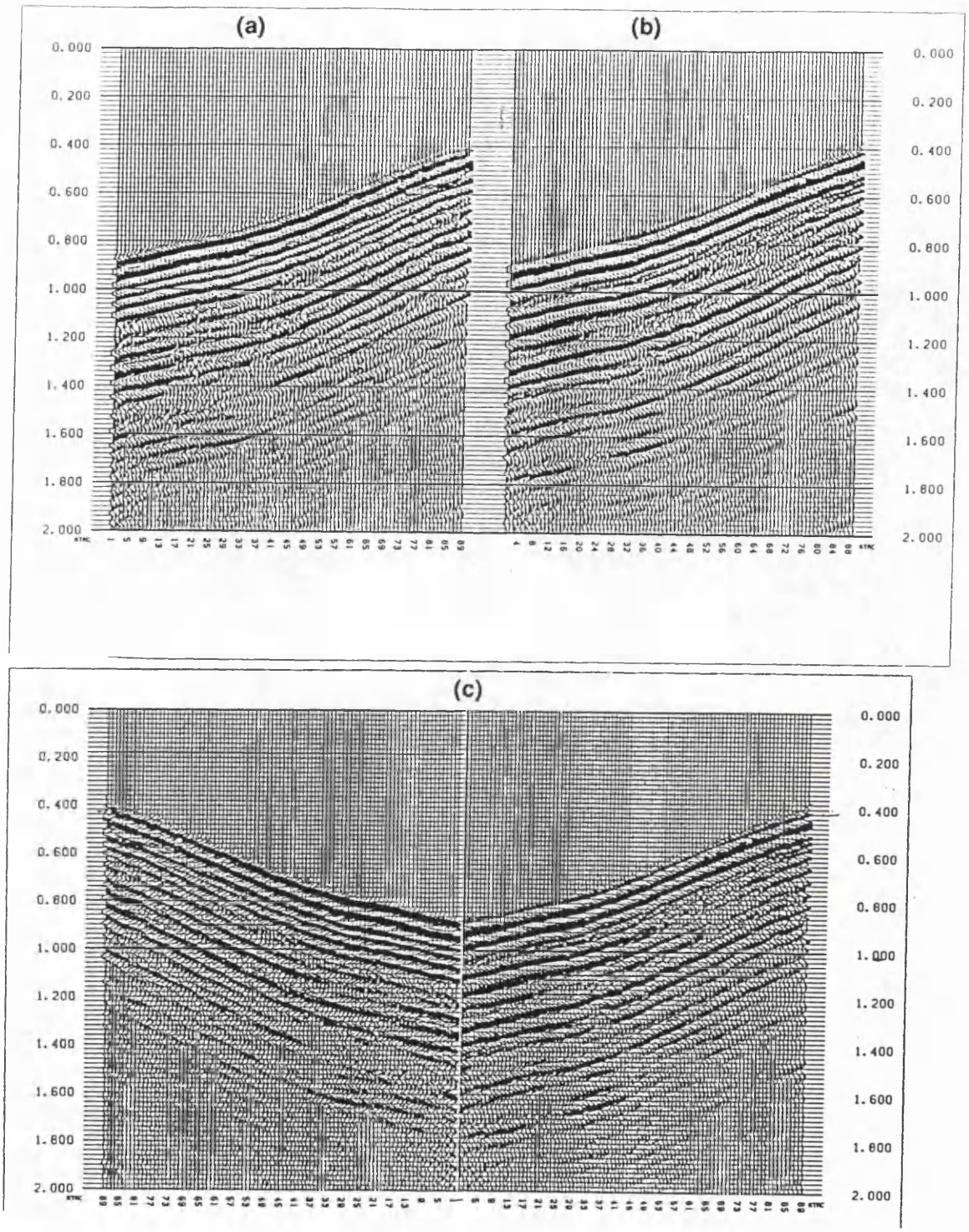

Figure 8.12. The resultant rotated radial (a) and the resultant rotated transverse (b) computed from the rotated two-by-two 1020 ft offset data matrix; (c) is the juxtaposition showing the miss-tie between them.

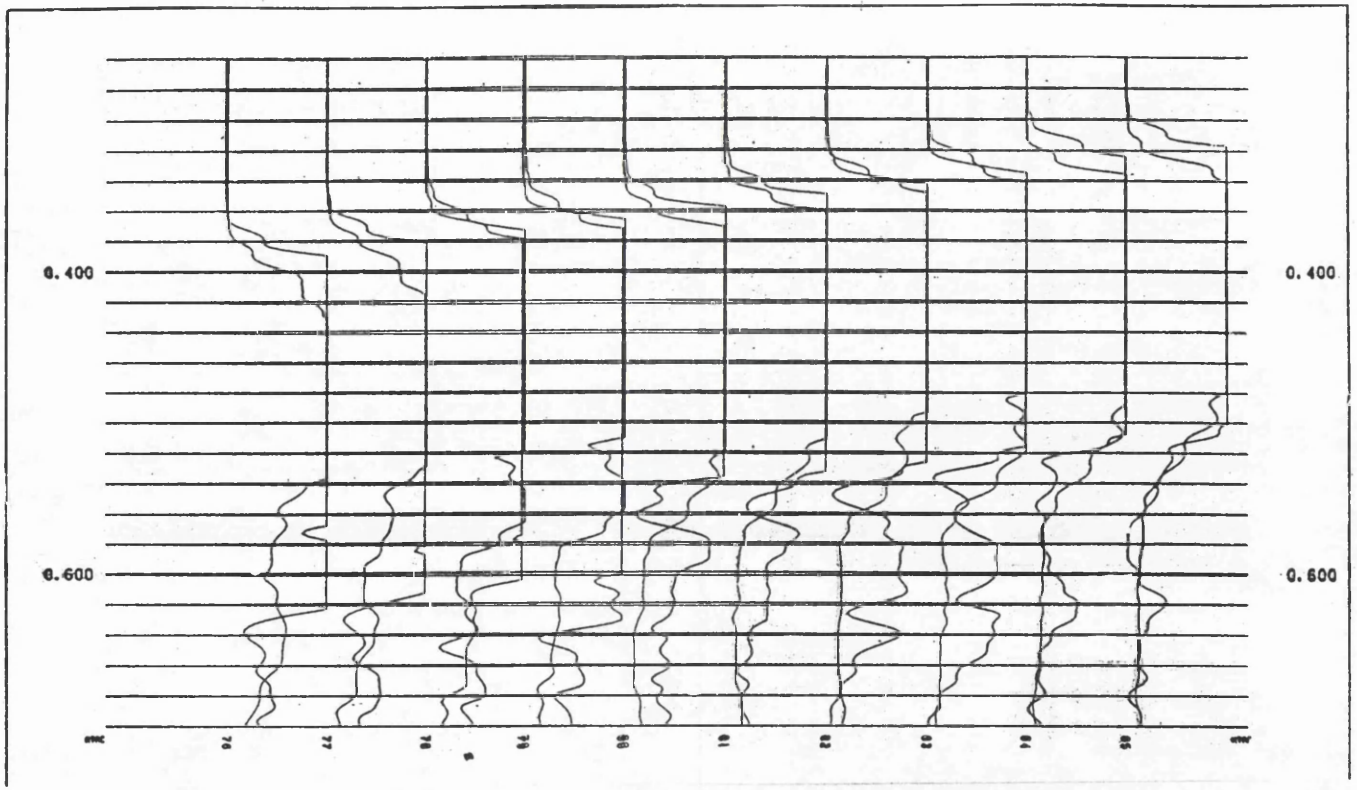

Figure 8.13. The first and the second eigenvalue attributes. The first is on top of the second and is ahead (in time) of it. These are computed from data generated by a cross-line source and recorded in well Wilson-2 with the shear source positioned at point S2, 390 ft from the well.The time delay is taken as the time difference between the two maximums, where both attributes become constant for a while.

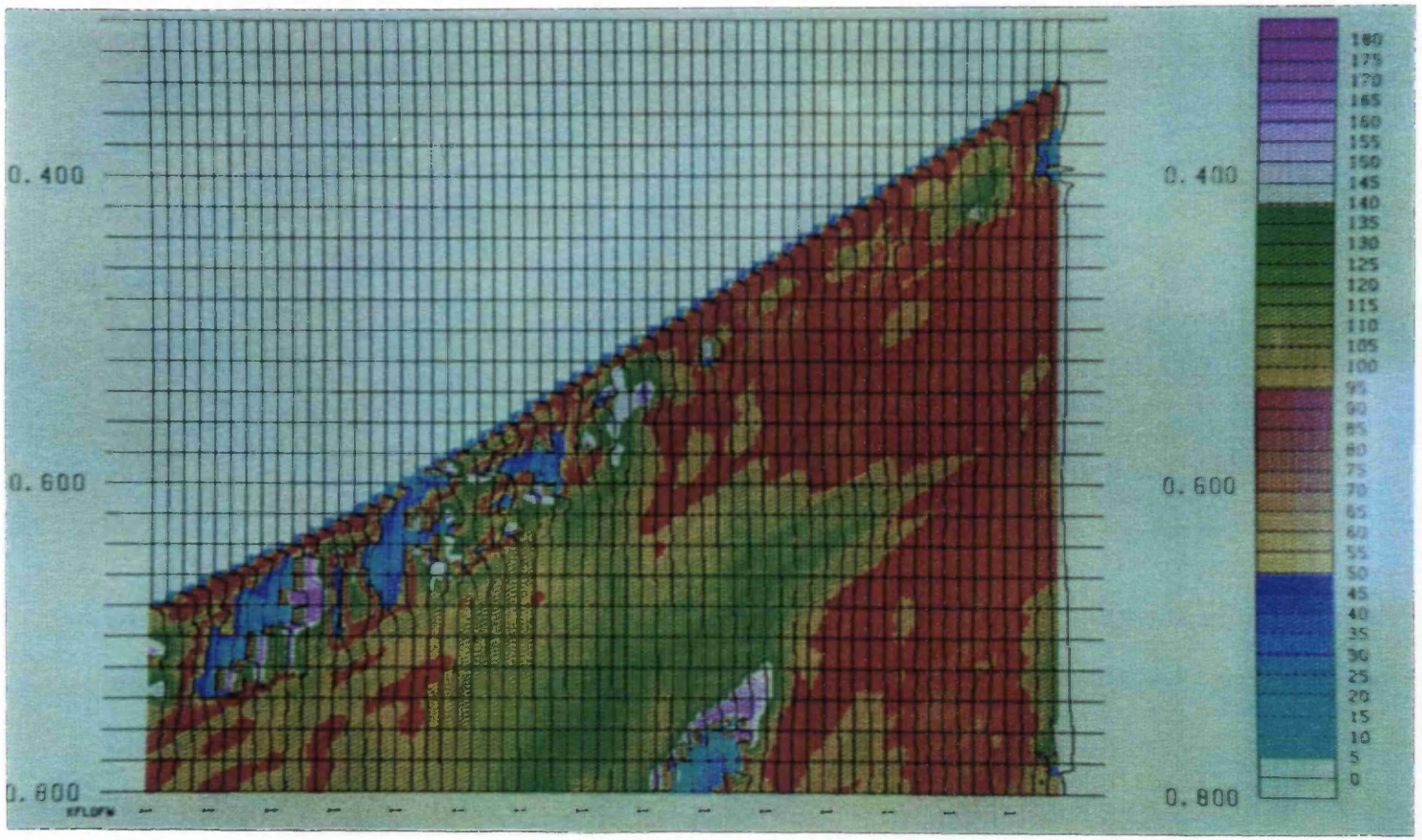

Figure 8.14. Color plot of the instantaneous polarization angle computed from data generated by a cross-line source and recorded in well Wilson 9 between 750 ft and 2250 ft . The shear source was positioned at point S1, 1020 ft from the well. The arrow indicates the onset of the fast shear wave with its polarization in blue (20° to 35°).

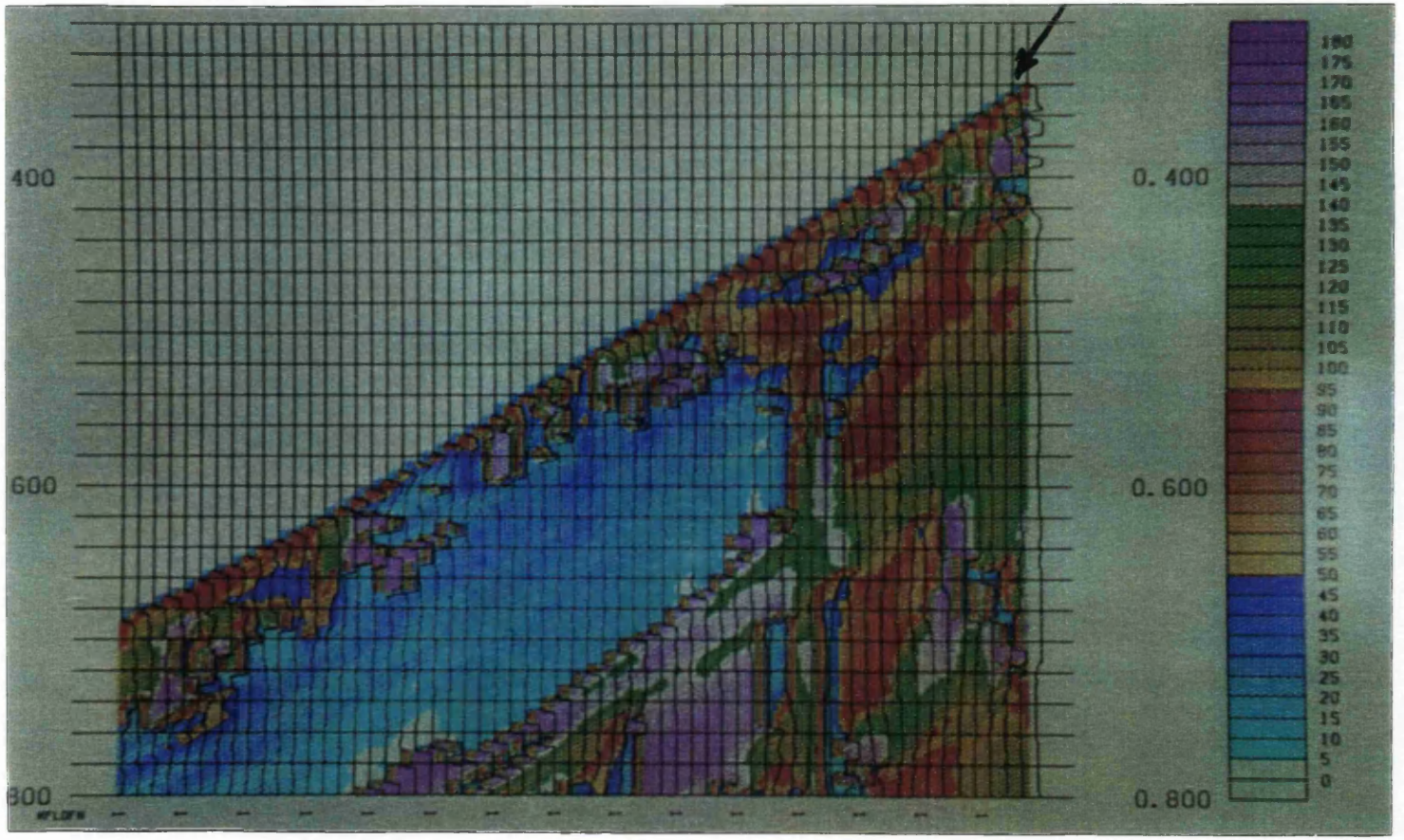

Figure 8.15. Color plot of the instantaneous polarization angle computed from data generated by an in-line source and recorded in well Wilson 9 between 750 ft and 2250 (bottom). The shear source was positioned at point S1, 1020 ft from the well. The arrow indicates the onset of the fast shear wave with its polarization in blue (20° to 35°).

CHAPTER 9

9.1. CONCLUSIONS

From synthetic data seismic attributes were computed and filters designed for processing three component seismic data.

The apparent azimuth angle may be used to determine crack orientation.

The eccentricity is useful for controlling the the polarization direction whether it is in the horizontal plane or not. Thus possibly using it to determine the tilt angle of a non vertical crack geometry.

Shear waves from either explosive or vibroseis sources are shown to be random within the horizontal plane of the acquisition coordinate frame. Consequently, a filter has been designed using the eccentricity to attenuate P-wave energy from the horizontal components.

The eigenvalue attributes and the instantaneous polarization angle have proven to be useful in assessing azimuthal anisotropy.

The comparison of the graphs from synthetic data of the apparent azimuth angle and the instantaneous polarization angle suggests that the eccentricity and the apparent azimuth be computed using the moving window technique, for smoothing the values

A filter for separating split S-waves and enhancing S-waves on shot records has been designed. It relies on the instantaneous rotation angle calculated from a moving window through the shifted horizontal traces (by the length of the moving window). It was found that the filter did improve the data quality of shear waves, although it were generated by single explosive sources with complex polarization.

With the design of the energy filter single source multireceiver technique is now possible for imaging the subsurface and studying anisotropy.

9.2. SUGGESTIONS FOR FURTHER WORK

The separation of split shear waves will be affected by waves with horizontal component of motions. These include ground roll, elliptically polarized P-waves, P-waves with non vertical incidence, mode converted waves SP and PS, which can interfere with SS-waves.

Attenuating P-waves or elliptically polarized waves in the horizontal components is possible through the use of the P-wave filter (PWF). The performance of this filter remains to be thoroughly demonstrated. This filter was applied on a small set of traces and showed good promises.

The energy filter acts as a time varying rotation process along the horizontal seismograms. Therefore it has the potential to deal with multiple splitting, particularly for reflection data where sufficient time delay may exist between the two split S-waves. This can be modelled by using two cracked layers with different crack orientations. By varying the thickness of the second layer, thereby simulating regional splitting, it is possible to investigate the performance and the limits of the method on multiple splitting. Also, the energy filter should be applied to shear data acquired using the multisource multireceiver technique and compared to other techniques; specifically Alford's technique.

When using explosive or vibroseis sources, mode conversion waves are recorded in addition to SS-wave data. With a multisource multireceiver acquisition technique the in-line source generates mode conversions. Consequently, the computation of the rotation angle might be erroneous. The single source multireceiver technique, however with the shear source normal to survey line, could be an ideal geometry for minimizing mode conversions.

In addition, single rotation may not improve data quality, as shown from BIRPS data, where polarization direction was observed to vary with offset.

REFERENCES

Adesanya, O., 1982. Seismic velocities of the upper crust of the Southern Uplands. Ph.D. dissertation, University of Glasgow.

Ahmed H., 1990. Investigation of azimuthal anisotropy from offset VSP data-a case study.

Alford, R. M., Multisource multireceiver method and system for geophysical exploration, European patent Nº 0169075.

Alford, R. M., Lynn, H. B. & Thomsen, L. A., 1985. Method of surveying the earth's subsurface formations, European patent Nº 0169076.

Alford, R. M., 1986. Shear data in the presence of azimuthal anisotropy: Dilley, Texas, SEG, 473-476.

Aster, R. C., Shearer, P. & Berger, J., 1989. Shear wave polarizations at the Anza array. EOS Transactions of the American Geophysical Union, 70 No. 43, 1211-1212.

Auld, B. A., 1973. Fields and waves in solids, volume 1 and 2.

Backus, E.G., 1962. Long-wave elastic anisotropy produced by horizontal layering, Geophysics, 7, 4427-4441.

Backus, E.G., 1965. Possible form of seismic anisotropy of the uppermost mantle under oceans, Geophysics, 14, 3429-3439.

Barry, K.M., Cavers, D. A. & Kneale, C. W., 1975. Recommended standards for digital tape formats, Geophysics, 40, 344-352.

Becker, D. F. & Perlelberg, A.I., Seismic detection of subsurface fractures, SEG 1986, 466-468.

Becker, D. F., et al. Implications of Seismic Anisotropy within Pembrook Unit, Midland, Texas, technical abstract. Presented at 1989 SEG Research Workshop on Recording and Processing Vector Wavefield data, Snowbird, Utah.

Beckham, W. E. & Glassman, H. B. Texaco processing of multicomponent seismic survey, Pembrook field, technical abstract. Presented at 1989 SEG Research Workshop on Recording and Processing Vector Wavefield data, Snowbird, Utah.

Benhama, A., Cliet, C. & Dubesset, M., 1988. Study and application of spatial directional filtering in three- component recording, Geophysical prospecting, 36, 591-613.

Benoliel S. D., Shneider W. A. & Shurtleff R. N., 1987. Frequency wavenumber approach of the tau-p transform: some applications in seismic data processing

Berryman, J. G., 1979. Long-wave elastic anisotropy in transversely isotropic media, Geophysics, 44 No. 5, 896-917.

Booth, C. & Crampin, C., 1983. The anisotropy reflectivity technique: Theory, Geophys. J. R. astr. Soc., 72, 755-766.

Booth, C. & Crampin, C., 1983. The anisotropy reflectivity technique: Anomalous reflected arrivals from an anisotropic upper mantle, Geophys. J. R. astr. Soc., 72, 768-782.

Boulfoul, M. & Watts, D. R., 1991. Determination of Principal Directions of Anisotropy From vertically incident shear waves, technical abstract. Presented at Fifteenth U.K. Geophysical Assembly, University of Leicester, Geophys. J. Int., 104 No. 1, 683.

Brace, W. F, Paulding, B. W. & Scholtz, C., 1966. Dilatancy in the fracture of crystalline rocks, Journal of Geophysical Research, 71, 3939-3953.

Brown, R. L., 1990. Improving (?) exploration by using vector waves, The Leading Edge, 18-25.

Campden, D. A. & Crampin, S., 1991. Observation of shear wave splitting from marine VSPs in the southern North Sea, Geophys. J. Int., 107, 465-473.

Chun, J. H. & Jacewitz, 1981. Fundamentals of frequency domain migration, Geophysics, 46 No. 5, 717-733.

Cliet, C. & Dubesset, M., 1987. three-component recording: interest for land seismic source study, Geophysics, vol 52 nº82, 1048-1059.

Cliet, C., et al., 1991. Anisotropy survey for reservoir definition, Geophys. J. Int., 107, 417-427.

Corrigan, D. & Justice, M. C. Estimate of shear wave anisotropy

using multicomponent seismic data, SEG 1986.

Crampin, S., A review of the effects of anisotropic layering on the propagation of seismic waves, Geophys. J.R. astro. Soc., 49, 9-27.

Crampin, S., McGonigle, R. & Bamford, D., 1980. Estimation of crack parameters from observation of P-wave velocity anisotropy, Geophysics, 45, 345-360.

Crampin, S.,1984. Effective anisotropic elastic constants for wave propagation through cracked solids, Geophys. J.R. astro. Soc.,76,135-145.

Crampin, S.,1984. An introduction to wave propagation in anisotropic media, Geophys. J. R. astr. Soc., 76, 17-28

Crampin, S., 1989. Suggestions for a consistant terminology for seismic anisotropy, Geophysical prospecting, 37, 753-770.

Crampin, S., 1984. Anisotropy in exploration seismic, First Break, March 1984, 19-21.

Crampin, S. & Radovich, B. J. Interpretation of synthetic common-depth-point Gathers for a single anisotropic layer, Geophysics, 47, 323-335.

Crampin, S., 1978, Seismic-wave propagation through a cracked-solid: polarization as a possible dilatancy diagnostic, Geophys. J.R. astro. Soc., 53, 467-496.

Crampin, S., 1981, A review of wave motion in anisotropic and cracked elastic-media, Wave motion, 3, 343-391.

Crampin, S., 1985, Evaluation of anisotropy by shear wave splitting, Geophysics, 50, 142-152.

Crampin, S.,1987, Geological and industrial implications of extensive dilatancy anisotropy, Nature, 328, 491-495.

Crampin, S. & Bush, I., Shear waves revealed: Extensive-dilatency confirmed, SEG 1986, 481-485.

Crampin, S., 1989. Appropriate crack-geometries for experiments in hot-dry-rock geothermal heat production, intended for publication in Scientific drilling.

Daley, P. F. & Hron, F. 1979. Reflection and transmission

coefficients for seismic waves in ellipsoidally anisotropic media, Geophysics, 44, 27-38.

Dankbaar, J. W. M., 1987. Vertical seismic profiling: separation of P-and S-waves, Geophysical Prospecting, 35, 803-814.

Diebold J. B. & Stoffa P. L., 1981. The travel time equation, tau-p mapping, and inversion of common midpoint data.

Domenico, S. N., 1984. Rock lithology and porosity determination from shear and compressional wave velocity,Geophysics, 49,1188-1195.

Dohr, G. & Janel, H., 1980. Improvement in the observation of shear waves, Geophysical Prospecting, 28, 208-220.

Dubesset, M. & Cliet, C., 1989. Different ways for the estimation of polarization parameters, technical abstract. Presented at 1989 SEG Research Workshop on Recording and Processing Vector Wavefield data, Snowbird, Utah.

Ebrom D. A. et al., 1990. Hyberbolic traveltime analysis of first arrivals in an azimuthally anisotropic medium: a physical modelling study, Geophysics, V55 No.2, 185-191.

Ensley, R. A., 1984. Comparison of P- and S-wave seismic data: a new method for detecting gas-reservoirs, Geophysics 49,1420-1431.

Ensley, R. A., 1985. Evaluation of Direct Hydrocarbon Indicators through comparison of compressional and shear wave seismic data: a case study of the Myrnam field, Alberta, Geophysics, 50, 37-48.

Erickson, E. L., Miller, D. E. & Waters, K. H., 1968. Shear wave recordingusing continueous signal methods. Part 1. Early development, Geophysics, 33, 229-239.

Erickson, E. L., Miller, D. E. & Waters, K. H., 1968. Shear wave recording using continueous signal methods. Part 2. Later experimentation, Geophysics,33, 240-254.

Esmersoy C., 1990. Inversion of P and S Waves from multicomponent offset Vertical Seismic Profiles, Geophysics, V55 No.1, 39-50.

Fertig, J. & Hentscheke, M. K., 1987. Data acquisition and processing of converted pS-waves, Geophysical Prospecting, 35, 148-166.

Gareth S. Y & Crampin S., 1991. Extensive-Dilatancy Anisotropy: relative information in VSPs and reflection surveys, Geophysical Prospecting, V39 No.3, 337-355.

Fuchs & Muller, 1971. Computation of Synthetic seismograms with the Reflectivity Method and Comparison with Observations, Geophys. J. R. astr. Soc., 23, 417-433.

Gazdag, J. & Sguazzero, 1984. Migration of seismic data by phase shift, Geophysics, 49 No. 2, 124-131.

Geyer, R. L. & Martner, S. T., 1969. SH-waves from explosive sources, Geophysics, vol 34 nº6, 893-905.

Greenhalgh, S. A. et al, 1990. Contolled direction reception filtering of P- and S-waves in tau-p space, Geophysical. J. Int.,100, 221-234.

Hale, D., 1984. Dip moveout by Fourier Transform, Geophysics, 46 No. 6, 741-757.

Haneveld C. J. & Herman G. C., 1990. A fast algorithm for the computation of radon transforms

Helbig, K. & Mesdag, C. S., 1982. The potential of shear wave observations, Geophysical Prospecting, 30, 413-431.

Hudson, J. A., 1981. Wave speeds and attenuation of elastic waves in material containing cracks, Geophys. J.R. astro. Soc.,

Igel H. & Crampin S., 1990. Extracting Shear Waves Polarizations from different source orientations: Synthetic Modeling, Journal of Geophysical Research, V95 NoB7, 11,283-11,292.

Johnston, D. H., VSP detection of fracture-induced velocity anisotropy, SEG 1986, 466-468.

Jolly, R. N., 1956. Investigation of shear waves, Geophysics, 4, 905-938.

Kanasewich, E. R., 1981, Time sequence analysis in Geophysics. The University Alberta Press, Edmond, Alberta, Canada.

Keith, C. M. & Crampin, S., 1977. Seismic body waves in anisotropic media: reflection and refraction at a plane interface, Geophys.

J.R. astro. Soc., 49, 181-208.

Keith, C. M. & Crampin, S., 1977. Seismic body waves in anisotropic media: propagation through a layer, Geophys. J.R. astro. Soc., 49, 209-223.

Keith, C. M. & Crampin, S., 1977. Seismic body waves in anisotropic media: synthetic seismograms, Geophys. J.R. astro. Soc., 49, 225-243.

Kisslinger, C., Mateker, E. J. & McEvilly, T. V., 1961. SH-motion from explosions in soil, Journal of Geophysical Research, vol 66 No.10, 3487-3497.

Krohn, C. E., 1984. Geophone Ground Coupling. Geophysics, 49 No. 6, 722-731.

Lash, C. C., 1985. Shear waves produced by explosive sources, Geophysics, 50, 1399-1408.

Lefeuvre, et al, 1992. Detection and measure of shear wave birefringence from vertical seismic data, Geophysics, vol.57 No.11, 1463-1481.

Levin,F. K., 1979. Seismic velocities in transversely isotropic media, Geophysics, 44, 918-936.

Li X. & Crampin S., 1989. Analysing Shear Wave Splitting in three component surface reflection surveys, technical abstract. Presented at 1989 SEG Research Workshop on Recording and Processing Vector Wavefield data, Snowbird, Utah.

Li X. & Crampin S., 1991.Complex component analysis of shear wave splitting: theory, Geophys. J. Int., 107, 605-613

Li X. & Crampin S., 1991. Complex component analysis of shear wave splitting: case studies, Geophys. J. Int., 107, 605-613.

Liu E. & Crampin S., 1990. Polarization of Reflected Shear Waves, Geophysical Research letters, V17 No8, 1137-1140.

Liu E. & Crampin S., 1990. Effects of Shear Wave Window: comparison with Anisotropy Induced Splitting, Journal of Geophysical Research, V95 NoB7, 11,275-11,281.

Liu E. & Crampin S., 1991. Fracture detection using crosshole

surveys and reverse seismic profiles at the Conoco Borehole Test Facility, Oklahoma, Geophys. J. Int., 107, 449-463.

Lynn, H. B., 1991. Field measurements of azimuthal anisotropy: Frst 60 meters, San Fransisco Bay area, CA, and estimation of horizontal stresses' ratio from , Geophysics, 56 No. 6, 822-832.

Lynn, H. B. & Thomsen, L.A., Reflection shear-wave data along the principal axes of azimuthal anisotropic media, SEG 1986, 473-476.

Ma, X. Q., 1990. New methods in Gravitational and Seismic reflection exploration. Ph.D. dissertation, University of Glasgow.

MacBeth, C. & Crampin S., 1991. comparison of signal processing techniques for estimating the effects of anisotropy, Geophysical Prospecting, V39 No.3, 357-385.

MacBeth, C. & Crampin, C., 1991. Processing of seismic data in the presence of anisotropy, Geophysics, 56 No. 9, 1320-1330.

MacBeth, C. & Yardley G. S., 1992. Optimal estimation of crack strike, Geophysical prospecting 40, 849-872.

MacCormack, M. D., Dunbar, J. R. & Sharp, W. W., 1984. A case study of stratigraphic interpretation using shear and compressional seismic data, Geophysics, 49 No. 6, 509-520.

Mari, J. L., 1984. Estimation of static corrections for shear wave profiling using the dispersion properties of Love waves, geophysics, 49, 1169-1179.

McMechan, G. A. & Ottolini, R., 1980. Direct observation of a p-tau curve in a slant stacked wave field, Bulletin of the Seismological Society of America, 70, 775-789.

McMechan G. A. & Yedlin M. J., 1981. Analysis of dispersive waves by wave field transformation

Mercado E. J., 1968. Linear phase filtering of multicomponent seismic data, Geophysics, V33 No6, 926-938.

Montalbetti, J. F. & Kanasewich, E. R., Enhancement of teleseismic body waves with a polarization filter, Geophys. J.R. astro. Soc.,

29, 119-129.

Mueller, M. C., 1992. Using shear waves to predict lateral variability in vertical fracture intensity, The Leading Edge, 11 No. 2, 29-35.

Murtha, P. F. Preliminary analysis of the ARCO multicomponent seismic group experiment, technical abstract. Presented at 1989 SEG Research Workshop on Recording and Processing Vector Wavefield data, Snowbird, Utah.

Naville, C. Detection of anisotropy using shear wave splitting in VSP suveys: requirement and applications, SEG 1986.

Nobel, M. D., Lambert, R. A., Ahmed, H. & Lyons, J., The application of three-component VSP data on the interpretation of the Volcano Gas Field and its impact on field development, First Break, 6, 131-149.

Obolentseva et al., 1987. Investigation of 3D Wavefields of Reflected Shear waves and converted waves: mathematical modeling and reflection data processing, Geophy. J. R. astro. Soc, 91, 543-554.

Pant, D. R .& Greenhalgh,1989. Multicomponent seismic reflection profiling over an ore-body-structure, a scale model investigation, Geophyssical research letters, 16, 1089-1092.

Polskov, M. K. et al, 1980. Utilisation combinee des ondes longitidunales et transversales en seismic reflection, Geophysical Prospecting, 28, 185- 207.

Queen J. H. & Rizer W. D., 1990. An investigated study of seismic Anisotropy and the natural fracture system at the Conoco Borehole Test Facility, Kay County, Oklahoma, Journal of Geophysical Research, V95 No B7, 11,255-11,273.

Rai, C. S. & Hanson, K.E., Shear wave birefringence: a laboratory study, SEG 1986, 471-473.

Rafavich, F.,Kendall, C. H. St. & Todd, T. P.,1984. The relationship between acoustic properties and the petrographic character of carbonate rocks, Geophysics, 49, 1622-1636.

Rene, R. M. et al, 1986. Multicomponent seismic studies using

complex trace analysis, Geophysics, 51, 1235-1251.

Robinson, E. A. & Durani, T. S, 1986. Geophysical Signal Processing. Prentice-Hall, Inc., Englewood Cliffs, New Jersey.

Schoenberg, M. & Douma, J., 1988. Elastic wave propagation in media with parallel fractures and aligned cracks, Geophysical Prospecting, 36, 571-590.

Shimsoni, M. & Smith, S.W. Seismic signal enhancement with three-component detectors, Geophysics, 29, 664-671.

Shuck, E. L., 1991. Azimuthal anisotropy analysis from shear VSPs., Geophys. J. Int., 107, 639-647.

Sondergeld, C. H. & Rai C. S., 1992. Laboratory observations of shear wave propagation in anisotropic media, The Leading Edge, 11 No. 2, 38-43.

Spiegel, M. R., 1980. Analyse de Fourier. MacGraw-Hill Inc., Paris.

Spencer, T. W. & Chi, H. C., 1991. Thin-layer fracture density, Geophysics, 56 No. 6, 833-843.

Stanley, R. D. The radon transform and some of its applications, book edited by John wiley and sons, 55-65.

Stoffa P. L. et al, 1981. Direct mapping of seismic data to the domain of intercept time and ray parameter. A plane-wave decomposition

Taner, M. T., Koehler, F. & Sheriff, R. E., 1979. Complex trace analysis, Geophysics, vol 44 nº6, 1041-1063.

Tatham, R. H. & Goolsbee, D. V., 1984. Separation of S-wave and P-wave reflections offshore western florida, Geophysics, 49,493-508.

Tatham, R. H. et al, 1983. Seismic shear-wave observations in a physical model experiment, Geophysics, V 48 No. 6, 688-701.

Thomsen, L. A., 1986. Weak elastic anisotropy, Geophysics, 51,1954-1966.

Thomsen, L. A., 1988. Reflection seismology over azimuthally anisotropic media, Geophysics, 53, 304-319.

White, J. E., 1983. Undergroud Sound Application of seismic waves, edited by elsvier.

Wilkens, R., Simmons, G. and Caruso, L.,1984. The ratio Vp/Vs as a discriminant of composition for siliceous limestones, Geophysics, 49, 1850-1860.

Willis, H. A., Rethford, G.L. & Bielanski, E. Azimuthal anisotropy: occurrence and effect on shear wave data quality, SEG 1986, 479-480.

Winterstein, D. F., 1986. Anisotropy in P-wave and SH-wave stacking velocities contain information on lithology, Geophysics, 51, 661-672.

Winterstein, D. F., Comparison of three methods for finding polarization direction of the fast shear waves, technical abstract. Presented at 1989 SEG Research Workshop on Recording and Processing Vector Wavefield data, Snowbird, Utah.

Winterstein, D. F. & Meadows, M. A., 1991a. Shear wave polarizations and subsurface stress directions at Lost Hills field, Geophysics, 56 No. 9, 1331-1348.

Winterstein, D. F. & Meadows, M. A.,1991b. Changes in shear-wave polarization azimuth with depth in Cymric and Railroad Gap oil fields, Geophysics, 56 No. 9, 1349-1364.

Wright, C. & Johnson, P., 1982. On the generation of P- and S-wave energy in crystalline rocks, Geophysical Prospecting, 30, 58-70.

Wright, J. K. & Carpenter, E. W., 1962. The generation of horizontally polarized shear waves by underground explosion, Journal of Geophysical research, 5, 1957-1963.

Yilmaz, O., 1987. Slant stack and applications, edited by Stephen, M. Doherty, 426-453.

APPENDIX

COMPUTER PROGRAMS

The FORTRAN routines written for this project are listed in the following order:

1. **COVENRG.**
2. **INIT. PHASE "ENGS20"** of two processors **COVRAD and. COVTRN.**
3. **EXEC. PHASE "ENGA20'** of the processor **COVRAD.**
4. **EXEC. PHASE 'ENGA21"**of the processor **COVTRN.**

```
 PROGRAM COVENRG
C - - - - - - - - - - - - - - - - - - - - - - - - - - - - - - - - - - - - - - - - - - - - - - - - - - - - - - - - - - - -
C THIS PROGRAM COMPUTES THE ENERGY ATTRIBUTES,THE INSTANTANEOUS
C POLARIZATION C  ANGLE EACH TIME THE MOVING WINDOW SLIDES DOWN BY A
CSTEP. ALSO, THE PROGRAM IS USED TO SEPARATE SPLIT SHEAR WAVES BY
C INSTANTANEOUSLY ROTATING THE  ORIGINAL DATA BY THE INSTANTANEOUS
C ROTATION ANGLE.  THE ROTATION IS CARRIED CLOCKWISE.
C - - - - - - - - - - - - - - - - - - - - - - - - - - - - - - - - - - - - - - - - - - - - - - - - - - - - - - - - - - - -
      REAL TIME(6000), B(6000)
        REAL  ROTX(6000),ROTY(6000),X(6000),Y(6000),Z(6000)
        REAL  X1(6000),Y1(6000),Z1(6000),  SX(6000),  SY(6000)
      REAL S1X(6000),  S1Y(6000),  ALPHA(6000)
        REAL  MAX(5000),  MIN(5000),  RATIO(5000),  BETA(5000),POLCO(5000)
      REAL COFF(5000),ENGR(5000),  MAXENG(5000),  MINENG(5000)
      REAL RAD(180),TRN(180),TOTENE(180),VER(180)
        REAL  D1(6000),  D2(6000),  FTN(6000),  VX(6000),  VY(6000)
C
      INTEGER P(6000),  S(6000),  GAMMA(6000)
C
      CHARACTER*8 OUTNAME1 ,OUTNAME2, OUTNAME3, OUTNAME4, OUTNAME5
      CHARACTER*8 ANS, ANGMAX, ANGMIN, ANSWER, RESP, COV, ENRG
C
      REAL SUM1, SUM2, SUM3, SUM4, PROD1, PROD2, PROD3
      REAL AMAX, AMIN, TETHA, NN
      REAL MX, MY, MXBAR, MYBAR
C
      INTEGER  ANGLE1, ANGLE2, M1, M2, M3, ENGW
      INTEGER  I, J, K, L, N1, N2, N3, LL
      INTEGER  M, BT, ET, DELT, STEP, LENGTH
      INTEGER  N, IA, IV, NMAX, IFAIL
C
       PARAMETER (N=2,IA=2,IV=2,IFAIL=0,NMAX=4,LENGTH=3720,DELT=4,
     + NN=0.5, STEP=4)
C
```

```
      DOUBLE PRECISION A(IA,N), E(NMAX), R(N), V(IV,N)
      DOUBLE PRECISION D(N)
C
      EXTERNAL F02ABF
C
      PI=3.1415927
C
C     STEP=DELT
C
      PRINT*,'What kind of data you want to process '
       PRINT*,'Type SYNTH if synthetic data or BIRPS if birps data'
C
      READ(5,'(A)') ANSWER
C
      IF(ANSWER.EQ.'SYNTH') THEN
C
        CALL SYNTH(X1, Y1, Z1, (LENGTH/DELT)+1)
C
       WRITE(6,*)  X1(601), Y1(601), Z1(601)
C
      ENDIF
C
      IF(ANSWER.EQ.'BIRPS') THEN
C
        CALL BIRPS(Y1, Z1, X1, (LENGTH/DELT)+1)
C
      ENDIF
C
       PRINT*, 'Enter the filename of the instantaneous rotated radial'  COV00640
       READ(5,'(A)')OUTNAME1
       OPEN(UNIT=1, FILE=OUTNAME1)
C
       PRINT*, 'Enter the filename of the instantaneous rotated transv.'
       READ(5,'(A)')OUTNAME2
```

```
      OPEN(UNIT=2, FILE=OUTNAME2)
C
      PRINT*, 'Enter the beginning and the ending times of the '
      PRINT*, 'window to be processed, BT and ET '
C
      READ(5, *) BT, ET
C
      PRINT*, 'Enter the length of the moving window'
C
      READ(5,*) ENGW
C
      WRITE(6,*)BT/DELT, ET/DELT
C - - - - - - - - - - - - - - - - - - - - - - - - - - - - - - - - - - - - - - - - - - - - - - - - - - - - - - - - - -
C SETTING THE WINDOW LIMITS  OVER WHICH  THE ATTRIBUTES ARE COMPUTED.
C          - - - - - - - - - - - - - - - - - - - - - - - - - - - - - - - - - - - - - - - - - - - - - - - - - - - - -
      M1=(BT/DELT)+1
C
      IF(ET.GT.(LENGTH-ENGW)) THEN
        M2=((ET-ENGW)/DELT)
      ELSE
        M2=(ET/DELT)
      ENDIF
C
      M3=STEP/DELT
C - - - - - - - - - - - - - - - - - - - - - - - - - - - - - - - - - - - - - - - - - - - - - - - - - - - - - - - - - -
C  SHIFTING THE DATA BY THE LENGTH OF THE MOVING WINDOW
C          - - - - - - - - - - - - - - - - - - - - - - - - - - - - - - - - - - - - - - - - - - - - - - - - - - - - -
      DO 10 I=1, (ENGW/DELT)-1
       X(I)=0.0
       Y(I)=0.0
 10   CONTINUE
C
      WRITE(6,*) X(10)
C
```

```
      DO 20 I=1,(LENGTH/DELT)+1
       X(I+ENGW/DELT)=X1(I)
       Y(I+ENGW/DELT)=Y1(I)
 20   CONTINUE
C
      WRITE(6,*)X(1+ENGW/DELT)
C
      PRINT*,'If you want to use the covariance matrix type COV '
      PRINT*,'If you want to use the energy of the trace type ENRG'
C
      READ(5,'(A)') RESP
       IF(RESP.EQ.'ENRG')THEN
        GO TO 777
       ENDIF
C
       IF(RESP.EQ.'COV')THEN
        GO TO 888
       ENDIF
C
 777   PRINT*,'Enter the Min, Max. angle values and the increment'
      PRINT*, 'for rotation'
      READ(5,*)N1, N2, N3
C
       PRINT*,'Enter the output filename for instantaneous attributes:'
       PRINT*,'Maximum, minimum energy and polarization angle'
C
      READ(5,'(A)')OUTNAME1
      OPEN(UNIT = 3, FILE = OUTNAME1)
C
       PRINT*,'Enter the output filename for energy attributes'
      PRINT*,'and their ratio'
      READ(5,'(A)')OUTNAME2
      OPEN(UNIT = 4, FILE = OUTNAME2)
C ------------------------------------------------------------
```

```
C COMPUTATION OF THE MAXIMUM VALUE OF THE ENERGY OF THE TRACE OVER A
C SPECIFIEDC WINDOW. THE WINDOW SLIDES DOWN BY A SAMPLE RATE EACH
C TIME THE ENERGY IS COMPUTED. THE COMPUTATION IS REPEATED FOR THE
 C WHOLE TRACE LENGTH.
C - - - - - - - - - - - - - - - - - - - - - - - - - - - - - - - - - - - - - - - - - - - - - - - - - - - - - - - - - -
C - - - - - - - - - - - - - - - - - - - - - - - - - - - - - - - - - - - - - - - - - - - - - - - - - - - - - - - - - -
C  ROTATING THE DATA WHITHIN THE MOVING  WINDOW TO FIND  THE
C MAXIMUM  ENERGY AND CORRESPONDING POLARIZATION ANGLE.
C - - - - - - - - - - - - - - - - - - - - - - - - - - - - - - - - - - - - - - - - - - - - - - - - - - - - - - - - - -
C - - - - - - - - - - - - - - - - - - - - - - - - - - - - - - - - - - - - - - - - - - - - - - - - - - - - - - - - - -
      DO 30 LL = M1, M2, M3
C
      DO 40 I = N1, N2, N3
C
       TETHA = I*PI/180.0
C
      DO 50 J = 1, (ENGW/DELT)+1
         ROTX(J)=COS(TETHA)*X(J+LL-1)+SIN(TETHA)*Y(J+LL-1)
         ROTY(J)=-SIN(TETHA)*X(J+LL-1)+COS(TETHA)*Y(J+LL-1)
 50    CONTINUE
C
     SUM1=0.0
     SUM2=0.0
     SUM3=0.0
     SUM4=0.0
C
     DO 60 K=1, (ENGW/DELT)+1
C
      PROD1=ROTX(K)*ROTX(K)
      SUM1=SUM1+PROD1
C
      PROD2=ROTY(K)*ROTY(K)
      SUM2=SUM2+PROD2
C
```

```
C       PROD3=Z(K+LL-1)*Z(K+LL-1)
C      SUM3=SUM3+PROD3
       SUM4=SUM4+PROD1+PROD2
C
 60   CONTINUE
C
          RAD((I/N3)+1) = SUM1
          TRN((I/N3)+1) = SUM2
C          VER((I/N3)+1) = SUM3
C        TOTENE((I/N3)+1) = SUM4
C
 40   CONTINUE
C
      CALL MAXPOS(RAD, ((N2-N1)/N3)+1, AMAX, ANGLE1)
C
      CALL MINPOS(RAD, ((N2-N1)/N3)+1, AMIN, ANGLE2)
C
     MAX(LL) = AMAX
     MIN(LL) = AMIN
     BETA(LL) = ANGLE1
     RATIO(LL) = AMAX/AMIN
     POLCO(LL)= 1 - (AMIN/AMAX)**NN
C
 30   CONTINUE
C - - - - - - - - - - - - - - - - - - - - - - - - - - - - - - - - - - - - - - - - - - - - - - - - - - - - - - - - -
C NORMALIZING THE ENERGY ATTRIBUTES. THE MAXMIMUM  VALUE OF THE
C MAXIMUM ENERGY  ATTRIBUTE IS SET TO FULL SCALE, WITH THE AMPLITUDES
C  OF THE MINIMUM  ENERGY  ATTRIBUTE PLOTTED RELATIVE TO THIS VALUE.
C - - - - - - - - - - - - - - - - - - - - - - - - - - - - - - - - - - - - - - - - - - - - - - - - - - - - - - - - -
     CALL MAXPOS2(MAX, M2, AMAX)
C
     DO 70 I=M1, M2, M3
      MAXENG(I)=MAX(I)/AMAX
 70   CONTINUE
```

```
C
      DO 80 I=M1, M2, M3
        MINENG(I)=MIN(I)/AMAX
 80   CONTINUE
C
      CALL MAXPOS2(RATIO, M2, AMAX)
C
      DO 90 I=M1, M2, M3
        ENGR(I)=RATIO(I)/AMAX
 90   CONTINUE
C
      DO 100 I=M1, M2, M3
         WRITE(3,*) (I-1)*DELT, MAXENG(I), MINENG(I), BETA(I)
 100  CONTINUE
C
      DO 110 I=M1, M2, M3
         WRITE(4,*) (I-1)*DELT, MAXENG(I), MINENG(I), ENGR(I)
 110  CONTINUE
C
C     DO 120 I=M1, M2, M3
C        WRITE(7,*) (I-1)*DELT, MAXENG(I), MINENG(I), POLCO(I)
C120  CONTINUE
C-----------------------------------------------------------------
C AUTOMATIC SEPARATION OF THE TWO SPLIT SHEAR  WAVES.
C-----------------------------------------------------------------
        DO 130 I= M1, M2, M3
          ALPHA(I)=(BETA(I)*PI)/180.0
 130     CONTINUE
C          ------------------------------------------------------------
C ROTATING THE ORIGINAL SEISMOGRAMS THEN  MULTIPLYING THE ROTATED
C SEISMOGRAMS BY THE ENERGY FUNCTION
C-----------------------------------------------------------------
        DO 140 I= M1, M2, M3
           S1X(I)= COS(ALPHA(I))*X1(I)+SIN(ALPHA(I))*Y1(I)
```

```
            S1Y(I)=-SIN(ALPHA(I))*X1(I)+COS(ALPHA(I))*Y1(I)
          SX(I)=S1X(I)*POLCO(I)
          SY(I)=S1Y(I)*POLCO(I)
 140      CONTINUE
C
         DO 150 I= M1, M2, M3
          WRITE(1,*) SX(I)
 150      CONTINUE
C
         DO 160 I= M1, M2, M3
          WRITE(2,*) SY(I)
 160      CONTINUE
C
     GO TO 999
C - - - - - - - - - - - - - - - - - - - - - - - - - - - - - - - - - - - - - - - - - - - - - - - - - - - - - - - - - -
C COMPUTATION OF THE ATTRIBUTES AND AUTOMATIC SEPARATION OF THE SPLIT
C SHEAR WAVES USING THE COVARIANCE MATRIX.
C - - - - - - - - - - - - - - - - - - - - - - - - - - - - - - - - - - - - - - - - - - - - - - - - - - - - - - - - - -
 888  PRINT*,'Enter the output filename for instantaneous attributes:'
      PRINT*,'Largest eigenvalue, 2sd eigenvalue and pl. angle'
C
     READ(5,'(A)')OUTNAME3
     OPEN(UNIT = 3, FILE = OUTNAME3)
C
      PRINT*,'Enter the output filename for the two eigenvalues and'

PRINT*,' their ratio'
     READ(5,'(A)')OUTNAME4
     OPEN(UNIT = 4, FILE = OUTNAME4)
C - - - - - - - - - - - - - - - - - - - - - - - - - - - - - - - - - - - - - - - - - - - - - - - - - - - - - - - - - -
C COMPUTATION OF THE COVARIANCE MATRIX, ITS EIGENV. AND EIGENVA. OVER A
C SPECIFIED WINDOW. THIS WINDOW SLIDES DOWN BY A SAMPLE RATE EACH TIME
C THE MATRIX IS COMPUTED. THE COMPUTATION IS REPEATED FOR THE WHOLE TRACE
C LENGTH.
```

```
C     ------------------------------------------------------------
C
      DO 170 I=M1, M2, M3
       A(1,1)=0.0
       A(1,2)=0.0
       A(2,1)=0.0
       A(2,2)=0.0
         MX=0.0
         MY=0.0
       DO 180 J=1, (ENGW/DELT) + 1
          MX=MX+X(I+J-1)
          MY=MY+Y(I+J-1)
 180   CONTINUE
C
          MXBAR = MX/((ENGW/DELT)+1)
          MYBAR = MY/((ENGW/DELT)+1)
C
       DO 190 K=1, (ENGW/DELT) + 1
            A(1,1)=A(1,1)+(X(I+K-1)-MXBAR)**2
              A(1,2)=A(1,2)+(X(I+K-1)-MXBAR)*(Y(I+K-1)-MYBAR)
          A(2,1)=A(1,2)
            A(2,2)=A(2,2)+(Y(I+K-1)-MYBAR)**2
 190   CONTINUE
      DO 200 L=1,2
        DO 210 M=1,2
          A(L,M)=A(L,M)/((ENGW/DELT) + 1)
 210    CONTINUE
 200   CONTINUE
C
     CALL F02ABF(A,IA,N,R,V,IV,E,IFAIL)
C
     R(1)= ABS(R(1))
     R(2)= ABS(R(2))
C    ------------------------------------------------------------
```

```
C FINDING THE LARGEST EIGENVALUE
C ------------------------------------------------------------------
     IF(R(1).GT.R(2)) THEN
       D1(I)=R(1)
       D2(I)=R(2)
     ELSE
       D1(I)=R(2)
       D2(I)=R(1)
     ENDIF
C ------------------------------------------------------------------
C COMPUTATION OF THE RECTILINEARITY FUNCTION AND THE POLARIZATION ANGLE.
C ------------------------------------------------------------------
C
     RATIO(I) = D1(I)/D2(I)
C
     FTN(I) = 1 - (D2(I)/D1(I))**NN
C
     VX(I) = (V(1,1))
     VY(I) = (V(2,1))
C
     IF(ANSWER.EQ.'SYNTH')THEN
C
          IF((VX(I).GT.0.0.AND.VY(I).GT.0.0).OR.(VX(I).LT.0.0.AND.VY(I)
    +     .LT.0.0)) THEN
           BETA(I) = PI - ATAN(VX(I)/VY(I))
       ELSE
           BETA(I) = PI/2 + (ATAN(VX(I)/VY(I)))
       ENDIF
     ENDIF
C
     IF(ANSWER.EQ.'BIRPS')THEN
C
          IF((VX(I).GT.0.0.AND.VY(I).GT.0.0).OR.(VX(I).LT.0.0.AND.VY(I)
    +     .LT.0.0)) THEN
```

```
          BETA(I) = PI - ATAN(VY(I)/VX(I))
        ELSE
          BETA(I) = PI/2 + ABS(ATAN(VY(I)/VX(I)))
        ENDIF
      ENDIF
C
 170  CONTINUE
C
      CALL MAXPOS2(D1, M2, AMAX)
C
      DO 220 I=M1, M2, M3
        D1(I)=D1(I)/AMAX
 220   CONTINUE
C
      DO 230 I=M1, M2, M3
        D2(I)=D2(I)/AMAX
 230   CONTINUE
C
      CALL MAXPOS2(RATIO, M2, AMAX)
C
      DO 240 I=M1, M2, M3
        RATIO(I)=RATIO(I)/AMAX
 240   CONTINUE
C
       WRITE(6,*)VX(250), VY(250), BETA(250)
      WRITE(6,*)D1(250), D2(250)
C-----------------------------------------------------------------
C AUTOMATIC SEPARATION OF THE SPLIT SHEAR WAVE.
C-----------------------------------------------------------------
        DO 250 I= M1, M2, M3
          GAMMA(I)=BETA(I)*180.0/PI
 250     CONTINUE
C-----------------------------------------------------------------
C ROTATING THE ORIGINAL SEISMOGRAMS, THEN MULTIPLYING THE ROTATED
```

```
SEISMOGRAMS BY THE RECTILINEARITY FUCTION
C - - - - - - - - - - - - - - - - - - - - - - - - - - - - - - - - - - - - - - - - - - - - - - - - - - - - - - - - - - - -
      DO 260 I= M1, M2, M3
         S1X(I)= COS(BETA(I))*X1(I)+SIN(BETA(I))*Y1(I)
         S1Y(I)= -SIN(BETA(I))*X1(I)+COS(BETA(I))*Y1(I)
       SX(I)=S1X(I)*FTN(I)
       SY(I)=S1Y(I)*FTN(I)
 260   CONTINUE
C
      DO 270 I= M1, M2, M3
       WRITE(1,*) SX(I)
 270   CONTINUE
C
      DO 280 I= M1, M2, M3
       WRITE(2,*) SY(I)
 280   CONTINUE
C
      DO 290 I= M1, M2, M3
         WRITE(3,*) (I-1)*DELT, D1(I), D2(I), GAMMA(I)
 290   CONTINUE
C
      DO 300 I= M1, M2, M3
         WRITE(4,*) (I-1)*DELT, D1(I), D2(I), FTN(I)
 300   CONTINUE
C
   GO TO 999
C
 999  STOP
   END
C
   SUBROUTINE SYNTH(B, C, D, M)
C - - - - - - - - - - - - - - - - - - - - - - - - - - - - - - - - - - - - - - - - - - - - - - - - - - - - - - - - - - - -
C THIS SUBPROGRAM READS ORIGINAL SYNTHETIC DATA AND PUT INTO ARRAYS TO
C BE USED FOR COMPUTATION.
```

```
C ------------------------------------------------------------
      DIMENSION TIME(626), A(626)
      DIMENSION B(M), C(M), D(M)
      INTEGER R(6000), S(6000)
      CHARACTER*8 FNAME
      INTEGER I, M, N
C
      PRINT*,'Enter the input file name'
      READ(5,'(A)')FNAME
      OPEN(UNIT = 1, FILE = FNAME, STATUS = 'OLD')
C
      PRINT*,'Enter the number of samples to be skipped'
      READ(5,*)N
C
      DO 10 I = 1, N
        READ(1,*)
 10   CONTINUE
C
      DO 20 I = 1, M
          READ(1,*) R(I), S(I), TIME(I), A(I), B(I), C(I), D(I)
 20   CONTINUE
C
      RETURN
      END
C
      SUBROUTINE BIRPS(A, B, C, N)
C ------------------------------------------------------------
C     THIS PROGRAM READ BIRPS DATA.
C ------------------------------------------------------------
      DIMENSION A(N), B(N), C(N)
      INTEGER M(5940)
      INTEGER I, N, L
      CHARACTER*8 FNAME, OUTNAME, RESP
C
```

```
      PRINT*,'Enter the input filename'
      READ(5,'(A)')FNAME
      OPEN(UNIT = 1, FILE = FNAME, STATUS = 'OLD')
C
      PRINT*,'Enter the number of samples to be skipped'
      READ(5,*)L
C
      DO 10 I = 1, L
       READ(1, *)
 10   CONTINUE
C
      DO 20 I = 1, N
        READ(1, 25) M(I), A(I), B(I), C(I)
 25     FORMAT(I5, 3(E12.4))
  20   CONTINUE
C
       WRITE(6,*) M(4), A(4), B(4), C(4)
C
      RETURN
      END
C
     SUBROUTINE MAXPOS(Z,N,AMAX,ANGLE1)
C - - - - - - - - - - - - - - - - - - - - - - - - - - - - - - - - - - - - - - - - - - - - - - - - - - - - - - - - -
C THIS PROGRAM RETURNS THE MAXIMUM VALUE OF AN ARRAY AND ITS POSITION
C - - - - - - - - - - - - - - - - - - - - - - - - - - - - - - - - - - - - - - - - - - - - - - - - - - - - - - - - -
      DIMENSION Z(N)
      INTEGER N, I, ANGLE1
      REAL AMAX
C
       AMAX = Z(1)
      ANGLE1 = 0
C
      DO 10 I = 2, N
       IF(Z(I).GT.AMAX)THEN
```

```
          AMAX = Z(I)
          ANGLE1 = (I-1)*5
        ENDIF
C
 10   CONTINUE
C
      RETURN
      END
C
      SUBROUTINE MAXPOS2(Z, N, AMAX)
C - - - - - - - - - - - - - - - - - - - - - - - - - - - - - - - - - - - - - - - - - - - - - - - - - - - - - - - - -
C THIS PROGRAM RETURNS THE MAXIMUM VALUE OF AN  ARRAY AND ITS POSITION.
C - - - - - - - - - - - - - - - - - - - - - - - - - - - - - - - - - - - - - - - - - - - - - - - - - - - - - - - - -
      DIMENSION Z(N)
      INTEGER N, I
      REAL AMAX
C
       AMAX = Z(1)
C
      DO 10 I = 2, N
       IF(Z(I).GT.AMAX)THEN
          AMAX = Z(I)
       ENDIF
C
 10   CONTINUE
C
      RETURN
      END
C
      SUBROUTINE MINPOS(Z, N, AMIN, ANGLE2)
C - - - - - - - - - - - - - - - - - - - - - - - - - - - - - - - - - - - - - - - - - - - - - - - - - - - - - - - - -
C THIS PROGRAM RETURNS THE MINIMUM VALUE OF AN ARRAY AND ITS POSITION
C - - - - - - - - - - - - - - - - - - - - - - - - - - - - - - - - - - - - - - - - - - - - - - - - - - - - - - - - -
      DIMENSION Z(N)
```

```
      INTEGER N, I, ANGLE2
      REAL AMIN
C
       AMIN = Z(1)
      ANGLE2 = 0
C
      DO 10 I = 2, N
       IF(Z(I).LT.AMIN)THEN
          AMIN = Z(I)
        ANGLE2 = (I-1)*5
       ENDIF
C
 10   CONTINUE
C
      RETURN
      END
```

```
      SUBROUTINE  ENGS20
C - - - - - - - - - - - - - - - - - - - - - - - - - - - - - - - - - - - - - - - - - - - - - - - - - - - - - - - - -
C ENGS20:  INIT PHASE FOR COVMAX PROCESSORS. THE INIT PHASE ENGA21 FOR
C THE COVMIN PROCESSOR IS IDENTICAL TO  THIS SUBROUTINE.
C - - - - - - - - - - - - - - - - - - - - - - - - - - - - - - - - - - - - - - - - - - - - - - - - - - - - - - - - -
C WINDOW ARGUMENTS:
C NAME       TYPE       DIM       IO        DESCRIPTION
C------          -----          -----        -----        -----------
C
C ROT         REAL        2                    ROTATION MATRIX
C
C RINC       REAL        1                    INCREMENT IN DEGREES OF ROTATION
C
C LEN         INT         1                    LENGTH OF OPERATOR WINDOW
C
C - - - - - - - - - - - - - - - - - - - - - - - - - - - - - - - - - - - - - - - - - - - - - - - - - - - - - - - - -
C
#include   "/usr/sierra/sseis14/inc/SSCOM.INC"
#include   "/usr/sierra/sseis14/inc/SSCUNI.INC"
C - - - - - - - - - - - - - - - - - - - - - - - - - - - - - - - - - - - - - - - - - - - - - - - - - - - - - - - - -
C LOCAL DECLARATIONS:
C - - - - - - - - - - - - - - - - - - - - - - - - - - - - - - - - - - - - - - - - - - - - - - - - - - - - - - - - -
      DIMENSION NWIN(2)
     CHARACTER*8 PRNAME
     CHARACTER*4 DEC
     INTEGER IRETC,NVALS,NHAVE,IPART,KSAM,NWIND,LEN
C - - - - - - - - - - - - - - - - - - - - - - - - - - - - - - - - - - - - - - - - - - - - - - - - - - - - - - - - -
C INITIALIZE VARIABLES
C - - - - - - - - - - - - - - - - - - - - - - - - - - - - - - - - - - - - - - - - - - - - - - - - - - - - - - - - -
           DEC = 'DEC '
      PRNAME  = 'COVMAX  '
       NHAVE   = 0
       NWIN(1) = 0
       NWIN(2) = 0
```

```
          LEN = 100
C - - - - - - - - - - - - - - - - - - - - - - - - - - - - - - - - - - - - - - - - - - - - - - - - - - - - - - - - - - - -
C PROCESS PARAMETER
C - - - - - - - - - - - - - - - - - - - - - - - - - - - - - - - - - - - - - - - - - - - - - - - - - - - - - - - - - - - -
     CALL DRTABL ('WINDOW  ', DEC,   NWIN, 1,  2,  .FALSE.)
     CALL DRTABL ('LENWIN   ', DEC,    LEN,   2,  1,  .FALSE.)
  10 CONTINUE
     CALL DRPRMS (IRETC, NVALS)
     IF (IRETC .EQ. -1) GO TO 20
C - - - - - - - - - - - - - - - - - - - - - - - - - - - - - - - - - - - - - - - - - - - - - - - - - - - - - - - - - - - -
C WINDOWS PARAMETER
C - - - - - - - - - - - - - - - - - - - - - - - - - - - - - - - - - - - - - - - - - - - - - - - - - - - - - - - - - - - -
      IF (NWIN(1) .EQ. 0 .AND. NWIN(2) .EQ. 0) THEN
     KSAM=KNSAMP
      NWIND=1
     ELSE
           KSAM=  INT((NWIN(2)-NWIN(1)+1)/(1000*SR))
          NWIND=INT((NWIN(1))/(1000*SR))
     ENDIF
     IF (NWIND .EQ. 0) THEN NWIND=1
C
    GO TO 10
  20 CONTINUE

      NLAB=KGLENI+KGLENR+(2*KGLEN8)+KGLEN4+1
     NW=KNSAMP+NLAB
      NV=KNSAMP+LEN-1
C - - - - - - - - - - - - - - - - - - - - - - - - - - - - - - - - - - - - - - - - - - - - - - - - - - - - - - - - - - - -
C  SET UP COMMUNICATION WITH EXEC PHASE
C - - - - - - - - - - - - - - - - - - - - - - - - - - - - - - - - - - - - - - - - - - - - - - - - - - - - - - - - - - - -
     CALL DRRSEG ('RAN  ', IPART, NW, KNTR/3)
     CALL DRRSRV (BUFF1, KNSAMP, 4)
     CALL DRRSRV (BUFF2, KNSAMP, 5)
     CALL DRRSRV (BUFF3,    NV ,  6)
```

```
      CALL DRRSRV (BUFF4,   NV ,  7)
      CALL DRRSRV (BUFF5,   LEN,  8)
      CALL DRRSRV (BUFF6,   LEN,  9)
      CALL DRRSRV (BUFF7,      2, 10)
      CALL DRRSRV (BUFF8,   LEN, 11)
      CALL DRRSRV (BUFF9,   LEN, 12)
      CALL DRRSRV (BUFF10,  LEN, 13)
      CALL DRRSRV (BUFF11, KNSAMP, 14)
      CALL DRRSRV (BUFF12, KNSAMP, 15)
      CALL DRRSRV (BUFF13, KNSAMP, 16)
      CALL DRRSRV (BUFF14, KNSAMP, 17)
      CALL DRRSRV (BUFF15, KNSAMP, 18)
      CALL DRRSRV (BUFF16, KNSAMP, 19)
      CALL DRRSRV (NHAVE ,      1, 20)
      CALL DRSAVE (A     ,      3, 21)
      CALL DRSAVE (NWIND ,      1, 22)
      CALL DRSAVE (KSAM  ,      1, 23)
      CALL DRSAVE (LEN   ,      1, 24)
      CALL DRGNCL (PRNAME,   NW, NW)
C-----------------------------------------------------------------
C END OF SUBROUTINE ENGS20.F:
C-----------------------------------------------------------------
9000 RETURN
      END
```

```
      SUBROUTINE ENGA20(JP,GLTRC,WORK,WORK1,WORK2,WORK3,WORK4,
     &WORK5,WORK6,WORK7,WORK8,WORK9,WORK10,WORK11,WORK12,WORK13,
     &WORK14, WORK15, WORK16,NHAVE,A,NWIND,KSAM,LEN)
C-----------------------------------------------------------------
C ENGA20: EXEC PHASE FOR COVMAX PROCESSOR
C-----------------------------------------------------------------
C THIS ROUTINE IS THE EXECUTION PHASE OF THE COVMAX PROCESSOR.  THIS
C PROCESSOR IS THE APPLICATION OF THE ENERGY FILTER. IT COMPUTES
C THE ROTATED RADIAL SEISMOGRAMS (CLOKWISE ROTATION)USING THE
C INSTANTANEOUS POLARIZATION ANGLE GIVEN BY EQUATION 5.15.  DATA ARE
C READ FROM A THREE COMPONENT RECORD ORDERED:
C CROSS-LINE, VERTICAL, IN-LINE (Y, Z, X).  FOR EVERY THREE TRACES INPUT,
C  ONE IS OUTPUT.
C-----------------------------------------------------------------
C
C WINDOW ARGUMENTS:
C NAME    TYPE       DIM    IO       DESCRIPTION
C  ----          ----                 ---      ---          ----------------------------------
C  JP       INT        SCA     I        DUMMY ARGUMENT NOT USED.
C
C GLTRC    REAL       ARY    IO       BUFFER CONTAINING TRACE SAMPLE VALUES.
C
C WORK    REAL       ARY     I        WORKSPACE ARRAY USED IN THIS ROUTINE.
C
C-----------------------------------------------------------------
C GLOBAL DECLARATIONS:
C-----------------------------------------------------------------
#include  "/usr/sierra/sseis14/inc/SSCOM.INC"
#include  "/usr/sierra/sseis14/inc/SSCUNI.INC"
 INTEGER JP,NHAVE,ISTAT,NWIND,KSAM,LEN
   REAL  GLTRC(1),WORK(1),WORK1(1),WORK2(1),WORK3(1),WORK4(1)
   REAL  WORK5(1)WORK6(1),WORK7(1),WORK8(1),WORK9(1),WORK10(1)
   REAL  WORK11(1)WORK12(1),WORK13(1),WORK14(1),WORK15(1)
  REAL  WORK16(1)A(1)
```

```
      COMMON  AR(2,2),V(2,2),NSIZE,NP,D(2),NROT
C - - - - - - - - - - - - - - - - - - - - - - - - - - - - - - - - - - - - - - - - - - - - - - - - - - - - - - - - -
C LOCAL DECLARATIONS:
C - - - - - - - - - - - - - - - - - - - - - - - - - - - - - - - - - - - - - - - - - - - - - - - - - - - - - - - - -
      INTEGER NGET,NSIZE,NP,NROT
            REAL  AR(2,2),V(2,2),D(2)
       NSIZE = 2
         NP = 2
         ROT = 1/SQRT(2.)
           PI = 3.1415927
C
C - - - - - - - - - - - - - - - - - - - - - - - - - - - - - - - - - - - - - - - - - - - - - - - - - - - - - - - - -
C START OF ENGA20
C - - - - - - - - - - - - - - - - - - - - - - - - - - - - - - - - - - - - - - - - - - - - - - - - - - - - - - - - -
C IF NO DATA PASSED THEN RETURN
C - - - - - - - - - - - - - - - - - - - - - - - - - - - - - - - - - - - - - - - - - - - - - - - - - - - - - - - - -
C
      IF (KSTATE .NE. 2) GO TO 9000
      IF (KTRC .EQ. 1) NHAVE=0
C
      NHAVE=NHAVE+1
C
      IF (NHAVE .LE. KNTR/3) THEN
      CALL RAOU(RAN,1,NHAVE,GLTRC,KNSAMP,ISTAT)
      KSTATE=1
      RETURN
      ENDIF
C - - - - - - - - - - - - - - - - - - - - - - - - - - - - - - - - - - - - - - - - - - - - - - - - - - - - - - - - -
C PASS THROUGH VERTICAL TRACES
C - - - - - - - - - - - - - - - - - - - - - - - - - - - - - - - - - - - - - - - - - - - - - - - - - - - - - - - - -
        IF (NHAVE.GE.((KNTR/3))+1.AND.NHAVE.LE.(KNTR*2)/3) THEN
      KSTATE=1
      RETURN
      ENDIF
```

```
C ------------------------------------------------------------
C CAPTURE INLINE TRACES
C ------------------------------------------------------------
      NGET=KTRC - (KNTR*2)/3
    CALL MPCVMV(GLTRC,WORK1,KNSAMP)
    CALL RAIN (RAN,1,NGET,WORK2,KNSAMP,ISTAT)
C ------------------------------------------------------------
C CALCULATE COVARIANCE MATRIX  OF SHIFTED DATA BY THE LENGTH OF
C MOVING WINDOW
C ------------------------------------------------------------
     KNLEN=KNSAMP+LEN-1
C
     CALL VPVCLR (WORK3,1,1,KNLEN)
     CALL VPVCLR (WORK4,1,1,KNLEN)
     CALL VPVMOV (WORK1,1,1,WORK3,LEN,1,KNSAMP)
     CALL VPVMOV (WORK2,1,1,WORK4,LEN,1,KNSAMP)
    CALL VPOUT (WORK3,1,WORK3,KNLEN)
    CALL VPOUT (WORK4,1,WORK4,KNLEN)
   CALL VPSTAT (STATUS,HARDST)
C ------------------------------------------------------------
C START CALCULATION
C ------------------------------------------------------------
    DO 20 K = 1, KNSAMP
C
     CALL VPVCLR (WORK5, 1, 1, LEN)
     CALL VPVCLR (WORK6, 1, 1, LEN)
     CALL VPVMOV (WORK3, K, 1, WORK5,1,1, LEN)
     CALL VPVMOV (WORK4, K, 1, WORK6,1,1, LEN)
     CALL VPSVE  (WORK5, 1, 1, WORK7(1), LEN)
     CALL VPSVE  (WORK6, 1, 1, WORK7(2), LEN)
    CALL VPOUT  (WORK7, 1, WORK7, 2)
   CALL VPSTAT (STATUS,HARDST)
C
      XBAR = -WORK7(1)/LEN
```

```
      YBAR = -WORK7(2)/LEN
C
      CALL VPSADD (WORK3,K,1,XBAR, WORK3,K,1,LEN)
      CALL VPSADD (WORK4,K,1,YBAR, WORK4,K,1,LEN)
       CALL VPVMUL (WORK3,K,1,WORK3,K,1,WORK8,1,1,LEN)
       CALL VPVMUL (WORK4,K,1,WORK4,K,1,WORK9,1,1,LEN)
       CALL VPVMUL (WORK3,K,1,WORK4,K,1,WORK10,1,1,LEN)
       CALL VPSVE (WORK8,1,1,A(1),LEN)
       CALL VPSVE (WORK9,1,1,A(2),LEN)
       CALL VPSVE (WORK10,1,1,A(3),LEN)
      CALL VPOUT (A,1,A,3)
     CALL VPSTAT (STATUS,HARDST)
C ------------------------------------------------------------
C DEFINE THE COVARIENCE MATRIX
C ------------------------------------------------------------
      AR(1,1) = (A(1)/LEN)
      AR(2,2) = (A(2)/LEN)
      AR(1,2) = (A(3)/LEN)
      AR(2,1) = (A(3)/LEN)
C
     CALL JACOBI(AR,NSIZE,NP,D,V,NROT)
     CALL EIGSRT(D,V,NSIZE,NP)
C         WORK11(K) = SQRT((D(1)-D(2))/D(1))
C
      IF ((V(1,1).GT.0.0 .AND. V(2,1).GT.0.0) .OR. (V(1,1).LT.0.0
     &   .AND. V(2,1).LT.0.0)) THEN
         WORK12(K) = PI - ATAN(V(2,1)/V(1,1))
     ELSE
         WORK12(K) = PI/2 + ABS(ATAN(V(2,1)/V(1,1)))
     ENDIF
C
  20 CONTINUE
C
     CALL VPVCOS (WORK12,1,1, WORK13,1,1, KNSAMP)
```

```
      CALL VPVSIN (WORK12,1,1, WORK14,1,1, KNSAMP)
C       CALL VPVMUL (WORK13,1,1, WORK11,1,1, WORK15,1,1, KNSAMP)
C       CALL VPVMUL (WORK14,1,1, WORK11,1,1, WORK16,1,1, KNSAMP)
      CALL VPVMUL (WORK1, 1,1, WORK13,1,1, WORK15,1,1, KNSAMP)
      CALL VPVMUL (WORK2, 1,1, WORK14,1,1, WORK16,1,1, KNSAMP)
C
      CALL VPVMOV (WORK15,1,1,WORK15,1,1,KNSAMP)
      CALL VPVMOV (WORK16,1,1,WORK16,1,1,KNSAMP)
     CALL VPOUT (WORK15,1, WORK15,KNSAMP)
     CALL VPOUT (WORK16,1, WORK16,KNSAMP)
    CALL VPSTAT (STATUS,HARDST)
C
      CALL VPVADD (WORK15,1,1, WORK16,1,1, WORK,1,1, KNSAMP)
    CALL VPOUT (WORK,1, GLTRC,KNSAMP)
    CALL VPSTAT (STATUS,HARDST)
    KNSHOT = 1
       KNTR = KNTR/3
       KTRC = NGET
     KTRECS = (NHAVE/3)
    KTRTYP = 1
     CALL MPMVCM (1,GLTRC(KNSAMP+1))
    KSTATE = 2
C
C - - - - - - - - - - - - - - - - - - - - - - - - - - - - - - - - - - - - - - - - - - - - - - - - - - - - - - - - - - - -
C END OF SUBPROGRAM ENGA20.F
C - - - - - - - - - - - - - - - - - - - - - - - - - - - - - - - - - - - - - - - - - - - - - - - - - - - - - - - - - - - -
C
 9000 RETURN
    END
```

```
      SUBROUTINE ENGA21(JP,GLTRC,WORK,WORK1,WORK2,WORK3,WORK4,
     &WORK5,WORK6,WORK7,WORK8,WORK9,WORK10,WORK11,WORK12,WORK13,
     &WORK14,WORK15,WORK16,NHAVE,A,NWIND,KSAM,LEN)
C-------------------------------------------------------------
C ENGA21: EXEC PHASE FOR COVMIN PROCESSOR
C-------------------------------------------------------------
C THIS ROUTINE IS THE EXECUTION PHASE OF THE COVMIN PROCESSOR.  THIS
C PROCESSOR IS THE APPLICATION OF THE ENERGY FILTER. IT COMPUTES THE
C  ROTATED TRANSVERSE SEISMOGRAMS (CLOCKWISE ROTATION)USING THE
C INSTANTANEOUS POLARIZATION ANGLE GIVEN BY EQUATION 5.15.  DATA ARE READ
C FROM A THREE COMPONENT RECORD ORDERED:  CROSS-LINE, VERTICAL, IN-LINE.
C FOR EVERY THREE TRACES INPUT, ONE IS OUTPUT.
C-------------------------------------------------------------
C
C WINDOW ARGUMENTS:
C NAME      TYPE     DIM    IO      DESCRIPTION
C ----        ----       ---      --        -----------
C  JP        INT      SCA     I      DUMMY ARGUMENT NOT USED.
C
C GLTRC    REAL     ARY     IO      BUFFER CONTAINING TRACE SAMPLE VALUES.
C
C WORK     REAL     ARY      I      WORKSPACE ARRAY USED IN THIS ROUTINE.
C
C
C-------------------------------------------------------------
C GLOBAL DECLARATIONS:
C-------------------------------------------------------------
#include  "/usr/sierra/sseis14/inc/SSCOM.INC"
#include  "/usr/sierra/sseis14/inc/SSCUNI.INC"
INTEGER JP,NHAVE,ISTAT,NWIND,KSAM,LEN
REAL  GLTRC(1),WORK(1),WORK1(1),WORK2(1),WORK3(1),WORK4(1)
REAL  WORK5(1)WORK6(1),WORK7(1),WORK8(1),WORK9(1),WORK10(1)
REAL  WORK11(1)WORK12(1),WORK13(1),WORK14(1),WORK15(1)
REAL  WORK16(1)A(1)
```

```
      COMMON  AR(2,2),V(2,2),NSIZE,NP,D(2),NROT
C - - - - - - - - - - - - - - - - - - - - - - - - - - - - - - - - - - - - - - - - - - - - - - - - - - - - - - - - - -
C LOCAL DECLARATIONS:
C - - - - - - - - - - - - - - - - - - - - - - - - - - - - - - - - - - - - - - - - - - - - - - - - - - - - - - - - - -
      INTEGER NGET,NSIZE,NP,NROT
         REAL  AR(2,2),V(2,2),D(2)
       NSIZE = 2
          NP = 2
         ROT = 1/SQRT(2.)
          PI = 3.1415927
C - - - - - - - - - - - - - - - - - - - - - - - - - - - - - - - - - - - - - - - - - - - - - - - - - - - - - - - - - -
C START OF ENGA21
C - - - - - - - - - - - - - - - - - - - - - - - - - - - - - - - - - - - - - - - - - - - - - - - - - - - - - - - - - -
C IF NO DATA PASSED THEN RETURN
C - - - - - - - - - - - - - - - - - - - - - - - - - - - - - - - - - - - - - - - - - - - - - - - - - - - - - - - - - -
      IF (KSTATE .NE. 2) GO TO 9000
      IF (KTRC .EQ. 1) NHAVE=0
C
      NHAVE=NHAVE+1
C
      IF (NHAVE .LE. KNTR/3) THEN
      CALL RAOU(RAN,1,NHAVE,GLTRC,KNSAMP,ISTAT)
      KSTATE=1
      RETURN
      ENDIF
C - - - - - - - - - - - - - - - - - - - - - - - - - - - - - - - - - - - - - - - - - - - - - - - - - - - - - - - - - -
C PASS THROUGH VERTICAL TRACES
C - - - - - - - - - - - - - - - - - - - - - - - - - - - - - - - - - - - - - - - - - - - - - - - - - - - - - - - - - -
         IF (NHAVE.GE.((KNTR/3))+1.AND.NHAVE.LE.(KNTR*2)/3) THEN
      KSTATE=1
      RETURN
      ENDIF
C - - - - - - - - - - - - - - - - - - - - - - - - - - - - - - - - - - - - - - - - - - - - - - - - - - - - - - - - - -
C CAPTURE INLINE TRACES
```

```
C - - - - - - - - - - - - - - - - - - - - - - - - - - - - - - - - - - - - - - - - - - - - - - - - - - - -
      NGET = KTRC - (KNTR*2)/3
     CALL MPCVMV(GLTRC,WORK1,KNSAMP)
     CALL RAIN (RAN,1,NGET,WORK2,KNSAMP,ISTAT)
C - - - - - - - - - - - - - - - - - - - - - - - - - - - - - - - - - - - - - - - - - - - - - - - - - - - -
C CALCULATE COVARIENCE MATRIX OF SHIFTED DATA BY LENGTH OFMOVING WINDOW
C - - - - - - - - - - - - - - - - - - - - - - - - - - - - - - - - - - - - - - - - - - - - - - - - - - - -
      KNLEN = KNSAMP+LEN-1
C
      CALL VPVCLR (WORK3,1,1,KNLEN)
      CALL VPVCLR (WORK4,1,1,KNLEN)
      CALL VPVMOV (WORK1,1,1,WORK3,LEN,1,KNSAMP)
      CALL VPVMOV (WORK2,1,1,WORK4,LEN,1,KNSAMP)
     CALL VPOUT (WORK3,1,WORK3,KNLEN)
     CALL VPOUT (WORK4,1,WORK4,KNLEN)
     CALL VPSTAT (STATUS,HARDST)
C - - - - - - - - - - - - - - - - - - - - - - - - - - - - - - - - - - - - - - - - - - - - - - - - - - - -
C START CALCULATION
C - - - - - - - - - - - - - - - - - - - - - - - - - - - - - - - - - - - - - - - - - - - - - - - - - - - -
     DO 20 K = 1, KNSAMP
C
      CALL VPVCLR (WORK5, 1, 1, LEN)
      CALL VPVCLR (WORK6, 1, 1, LEN)
      CALL VPVMOV (WORK3, K, 1, WORK5,1,1, LEN)
      CALL VPVMOV (WORK4, K, 1, WORK6,1,1, LEN)
      CALL VPSVE  (WORK5, 1, 1, WORK7(1), LEN)
      CALL VPSVE  (WORK6, 1, 1, WORK7(2), LEN)
      CALL VPOUT  (WORK7, 1, WORK7, 2)
     CALL VPSTAT (STATUS,HARDST)
C
        XBAR = -WORK7(1)/LEN
C
      CALL VPSADD (WORK3,K,1,XBAR, WORK3,K,1,LEN)
      CALL VPSADD (WORK4,K,1,YBAR, WORK4,K,1,LEN)
```

```
      CALL VPVMUL (WORK3,K,1,WORK3,K,1,WORK8,1,1,LEN)
      CALL VPVMUL (WORK4,K,1,WORK4,K,1,WORK9,1,1,LEN)
      CALL VPVMUL (WORK3,K,1,WORK4,K,1,WORK10,1,1,LEN)
      CALL VPSVE (WORK8,1,1,A(1),LEN)
      CALL VPSVE (WORK9,1,1,A(2),LEN)
      CALL VPSVE (WORK10,1,1,A(3),LEN)
     CALL VPOUT (A,1,A,3)
    CALL VPSTAT (STATUS,HARDST)
C ------------------------------------------------------------
C DEFINE THE COVARIENCE MATRIX
C ------------------------------------------------------------
       AR(1,1) = (A(1)/LEN)
       AR(2,2) = (A(2)/LEN)
       AR(1,2) = (A(3)/LEN)
       AR(2,1) = (A(3)/LEN)
C
    CALL JACOBI(AR,NSIZE,NP,D,V,NROT)
    CALL EIGSRT(D,V,NSIZE,NP)
C         WORK11(K) = SQRT((D(1)-D(2))/D(1))
C
      IF ((V(1,1).GT.0.0 .AND. V(2,1).GT.0.0) .OR. (V(1,1).LT.0.0
   &   .AND. V(2,1).LT.0.0)) THEN
         WORK12(K) = PI - ATAN(V(2,1)/V(1,1))
    ELSE
         WORK12(K) = PI/2 + ABS(ATAN(V(2,1)/V(1,1)))
    ENDIF
C
 20 CONTINUE
C
    CALL VPVCOS (WORK12,1,1, WORK13,1,1, KNSAMP)
    CALL VPVSIN (WORK12,1,1, WORK14,1,1, KNSAMP)
C     CALL VPVMUL (WORK13,1,1, WORK11,1,1, WORK15,1,1, KNSAMP)
C     CALL VPVMUL (WORK14,1,1, WORK11,1,1, WORK16,1,1, KNSAMP)
     CALL VPVMUL (WORK1,1,1, WORK14,1,1, WORK16,1,1, KNSAMP)
```

```
      CALL VPVMUL (WORK2,1,1, WORK13,1,1, WORK15,1,1, KNSAMP)
C
      CALL VPVMOV (WORK15,1,1,WORK15,1,1,KNSAMP)
      CALL VPVMOV (WORK16,1,1,WORK16,1,1,KNSAMP)
     CALL VPOUT (WORK15,1, WORK15,KNSAMP)
     CALL VPOUT (WORK16,1, WORK16,KNSAMP)
    CALL VPSTAT (STATUS,HARDST)
C
      CALL VPVSUB (WORK15,1,1, WORK16,1,1, WORK,1,1, KNSAMP)
    CALL VPOUT (WORK,1,GLTRC,KNSAMP)
    CALL VPSTAT (STATUS,HARDST)
C
    KNSHOT = 1
      KNTR = KNTR/3
     KTRC = NGET
     KTRECS = (NHAVE/3)
    KTRTYP = 1
     CALL MPMVCM (1,GLTRC(KNSAMP+1))
    KSTATE = 2
C - - - - - - - - - - - - - - - - - - - - - - - - - - - - - - - - - - - - - - - - - - - - - - - - - - - - - - - - - - - -
C END OF SUBPROGRAM ENGA21.F
C - - - - - - - - - - - - - - - - - - - - - - - - - - - - - - - - - - - - - - - - - - - - - - - - - - - - - - - - - - - -
9000 RETURN
    END
```